Musculoskeletal Adaptation to Partial Weight Suspension: Studies of Lunar and Mars Loading

by

Erika Brown Wagner

B.E., Vanderbilt University
S.M., Massachusetts Institute of Technology

Submitted to the
Harvard-MIT Division of Health Sciences and Technology
in partial fulfillment of the requirements for the degree of

Doctor of Philosophy in Medical Engineering and Bioastronautics

at the

MASSACHUSETTS INSTITUTE OF TECHNOLOGY

September 2007

Author .....
Harvard-MIT Division of Health Sciences and Technology
July 17, 2007

Certified by .....
Dava J. Newman, Ph.D.
Professor, MacVicar Faculty Fellow, HST Affiliate
MIT Department of Aeronautics & Astronautics,
and Engineering Systems Division
Thesis Supervisor

Accepted by .....
Martha L. Gray, Ph.D.
Edward Hood Taplin Professor of Medical and Electrical Engineering
Director, Harvard-MIT Division of Health Sciences and Technology

Musculoskeletal Adaptation to Partial Weight Suspension: Studies of Lunar and Mars Loading

by

Erika Brown Wagner

B.E., Vanderbilt University

S.M., Massachusetts Institute of Technology

Submitted to the
Harvard-MIT Division of Health Sciences and Technology
on July 17, 2007, in partial fulfillment of the
requirements for the degree of
Doctor of Philosophy in Medical Engineering and Bioastronautics

Abstract

As human spaceflight extends in both duration and scope, it is critical to better understand the physiologic effects of this novel environment. In the weightbearing structures of the body, bone loss and muscle atrophy far in excess of age-related declines are hallmarks of microgravity adaptation. However, while the physiological effects of such disuse unloading are well-described, the effects of partial weightbearing, such as expected on the moon (16% of Earth's gravity) and Mars (38% of Earth's gravity), have yet to be quantified. In these environments, the risks of musculoskeletal atrophy and accompanying orthopedic injury are uncertain, and a means of further investigation is needed.

To address this need, we developed a novel model of Partial Weight Suspension (PWS) that supports investigation of the physiologic effects of chronically reduced quadrupedal loading in mice. Validation of the PWS system was conducted using a gait analysis treadmill and high-precision force platform. These studies showed that peak ground reaction forces were significantly reduced under conditions of partial weightbearing, and changes in gait dynamics were consistent with previous studies of human locomotion.

Using the PWS system, we conducted the first known studies of chronic musculoskeletal adaptation to Mars and lunar levels of weightbearing. Adult female BALB/cByJ mice underwent 21 days of partial weightbearing or control treatment. Relative to controls, suspended animals showed significant bone and muscle loss. In particular, bone formation rate was decreased, leading to deterioration of both cortical and trabecular bone structure in mice exposed to partial weightbearing. Although

material properties of the bone were largely unaffected, structural and geometric changes resulted in lower bone strength. Reduced weightbearing at Mars and lunar levels led to similar losses of muscle and bone relative to controls.

Comparison with previous literature suggests that adaptation to partial weightbearing associated with both Mars and lunar loading provided some protection relative to the deconditioning seen in full unloading. Although additional studies are needed, the data also indicated that the musculoskeletal deterioration was not linearly related to the degree of unloading. Altogether, this model provides a validated, controlled system for investigating effects of partial weightbearing and countermeasures on musculoskeletal deconditioning. Our initial findings have practical applications for bioastronautics, suggesting that physiological investigations on the surface of the moon may not be fully predictive for future Mars exploration.

Thesis Supervisor: Dava J. Newman, Ph.D.
Title: Professor, MacVicar Faculty Fellow, HST Affiliate
MIT Department of Aeronautics & Astronautics, and Engineering Systems Division

Thesis Committee

Dava J. Newman, Ph.D. (Chair/Thesis Supervisor)
MacVicar Faculty Fellow; Director, Technology and Policy Program
Professor, MIT Department of Aeronautics & Astronautics and Engineering Systems
Affiliate Faculty, Harvard-MIT Division of Health Sciences and Technology

Mary L. Bouxsein, Ph.D.
Senior Research Associate, Beth Israel Deaconess Medical Center
Assistant Professor, Harvard Medical School

Laurence R. Young, Sc.D.
Apollo Program Professor of Astronautics
MIT Department of Aeronautics & Astronautics
Professor, Harvard-MIT Division of Health Sciences and Technology

Emily R. Morey-Holton, Ph.D. (Reader)
Emeritus Staff Scientist for the Life Science Division
NASA Ames Research Center

Acknowledgments

In an effort that spans so many years, milestones, and inch pebbles, there are many to be thanked. This document would be nothing were it not for those who stood by me, encouraged me, cajoled me, inspired me, helped me, and guided me throughout the process.

To my advisors: for granting unusual amounts of freedom to chase after my dreams.

Dava Newman: If I had tried to imagine an advisor who would support crazy ideas, encourage interdisciplinary adventures, and foster the balance so badly needed in graduate school, I could not have done better. Thank you for being a mentor, a role model, an advocate, and an inspiration. I hope to have at least half your courage to dream and live large.

Mary Bouxsein: I could not have known when I first walked into your lab to find help for Mars Gravity that I would leave with such an amazing advisor. Thank you for all of your well-founded advice, support inside the lab and out, and indefatigable spunk.

Larry Young: From day one, you have kept an eye on my professional development, guiding and encouraging me through two degrees. Thank you for sticking by me and for challenging me to reach higher.

Emily Holton: This thesis would never have happened without the strong foundation you have laid over the years, and my own career will always be shaped by the direct mentorship and support you have provided. Thank you for taking the time to share your wisdom with a newcomer.

To my funding sources: the Whitaker Biomedical Foundation Graduate Fellowship Program, NASA Graduate Student Research Program (NNG 04-GN71H), and NSBRI Bioastronautics Graduate Program (EO01001).

To my UROPs: for many hours of hands-on assistance and service as a sounding board throughout this process. I am indebted to each of you:

Carlos Barreiro, Aaron Bell, Amy Brazin, Betsy Eames, Travis Samuel, Viviana Serra, Mike Shields, Wen Hui Tan, and Adam Yock

With special thanks to Matt Theis, Kachina Gosselin, and Aaron Harmon for your instrumental work in developing and testing the Partial Weight Suspension hardware and for dedication above and beyond the call of duty.

To Nic Granzella: for six months of living and breathing the challenge. Your blend of attention to both detail and humor is missed around here! Your contributions to this work—from small screwholes to big ideas—are evident and appreciated.

To Stefan Judex and Russell Garman at SUNY Stony Brook: for taking the time to be true colleagues, sharing your techniques and ideas for *in vivo* strain gaging.

To Mouse Specifics, Inc.: for generous donation of time on the DigiGait treadmill.

To Ann Zumwalt: for lending your AMTI force plate to a complete stranger and providing support in its use.

To the Beth Israel Deaconess Orthopedic Biomechanics Lab: Vaida Glatt, Esther Cory, John Muller, Paula Cohen, and others—thank you for making me feel at home in your lab and for all your assistance with my endless questions, oddball research, and unorthodox requests.

To Alan Natapoff: for guidance in all things statistical, trivial, and profound.

To Todd Billings, John Kane, Dave Robertson, and Paul Bauer: for being masters of mechanical and electrical wizardry, and true teachers to boot.

To the MIT Man-Vehicle Lab: for being my home for nearly seven years. Through theses, papers, classes, quals, travels near and far, and countless other adventures, this lab has been the one constant in my MIT life. Extra special thanks to JJ, JJM, and Kristen for helping put the "W" in MVL, and for countless sanity checks and laughs over the years. To Chris Carr for leading by example and always helping those following behind.

To the Mars Gravity Team: for being my primary source of joy, frustration, energy, inspiration, madness, and education since 2001. This thesis is for you.

John Keesee: Our program exists because faculty like you have faith that it can. Thank you for caring enough to help us succeed.

Thaddeus Fulford-Jones: Thank you for putting up with my American accent, disaster area of a desk, and the 240 science requirements levied on your design.

Dan Judnick: Thanks for two years of good cheer, incredibly hard work, and constant reassurance that I had learned a couple things along the way.

Biff Deems: JPL will soon learn how lucky they are to have you. Thanks for being such a stalwart and a friend.

Rosie Combs-Bachmann: I'm still not sure you believe me when I say this, but Mars Gravity would be in shambles without you. You are a consummate juggler and a source of joy.

Paul Wooster: Thanks for the years you spent steering the ship, and more importantly, for the bike rides, chats, and trips that cemented it all together.

And to our countless advisors: on behalf of myself and the 570 other students that have come through the program, thank you for believing in us.

To my friends and family: for not only putting up with me through all of this, but supporting me all the way. From Dad's advice to Mom's phone calls, Emily's cooking to Greg's handiwork, Jen and Susannah's examples of balance to the HUCA sense of adventure—thanks for keeping me in touch with the real world!

And last here, but first in my heart:

To Andy: for being my rock, my best friend, the love of my life, and the captain of our tandem. I can't wait to see where the next roads take us.

Biographical Note

Erika Brown Wagner was born in Boulder, Colorado and raised in Marietta, Georgia. From 1996 until 2000, she attended Vanderbilt University, earning a Bachelor's degree in Biomedical Engineering. For her Master's education, Erika joined the Department of Aeronautics and Astronautics at MIT, investigating visual-vestibular interactions during short-radius centrifugation with Dr. Laurence Young of the Man-Vehicle Laboratory. She is also a proud alumna of the International Space University.

In the fall of 2001, Erika accepted the challenge of serving as Science Director for the Mars Gravity Biosatellite, a multi-university initiative to design, launch, and recover a novel uncrewed research spacecraft. The mission is designed improve understanding of the effects of Martian gravity levels (0.38-g) on mammalian physiology, paving the way for humans living and working on the surface of the Red Planet.

In 2002, Erika began her doctoral studies in the Harvard-MIT Division of Health Sciences and Technology, where she has held fellowships from the Whitaker Biomedical Foundation, NASA, and the National Space Biomedical Research Institute.

"MAN MUST RISE ABOVE EARTH
TO THE TOP OF THE ATMOSPHERE
AND BEYOND, FOR ONLY THEN WILL HE
FULLY UNDERSTAND THE WORLD
IN WHICH HE LIVES."

~ SOCRATES

Contents

List of Figures

List of Tables

Chapter 1

Introduction

Whereas NASA's human exploration agenda over the last thirty years has been confined exclusively to low Earth orbit, and largely to flights of less than six months, the new Vision for Space Exploration once again sets the agency's sights beyond the Van Allen belts (NASA, 2004). While new vehicle development is well underway, the human element of the system remains both the greatest unknown and the greatest source of risk.

Microgravity experiments and ground models of unloading have proven that musculoskeletal atrophy, neurovestibular adaptation, cardiovascular deconditioning, and radiation effects pose real challenges to mission success (Nicogossian, 2003; Buckey, 2006). Although most physiological systems settle into a new homeostasis appropriate for the novel environment, studies of up to a year show that bone loss does not yet reach that plateau (NASA, 1989). Furthermore, there is no body of literature, or even an established research model, yet available to answer the question of how skeletal adaptation will proceed on the surface of the moon and Mars. This thesis provides a first look at these questions and establishes a new model for supporting future investigations.

1.1 Background

Following a developmental period of genetically determined growth, skeletal structure at both the micro- and macroscopic levels adapts, within hormonal constraints, to accommodate the strains placed on it. Mechanotransduction pathways signal osteoblasts and osteoclasts to work together, providing local increases in structural and/or material strength in regions of greater loading. Similarly, skeletal structure that is more robust than necessary for the peak dynamic loads it supports is subject to resorption and remodeling. Research in a variety of models of skeletal unloading has shown that when bones are relieved of the loads to which they have become adapted, there is a significant decrease in bone mineral density and other metrics of skeletal strength.

Despite the fact that such adaptive processes are appropriate to the loads supported by a skeletal member, these losses can be troubling. The resulting weaker bones are poorly suited for a return to a previous state of loading, and even less well prepared to support the extreme loads of falls, trauma, or other impacts.

While these concerns are present in bed-ridden clinical patients and individuals healing from fractures, perhaps the most extreme case of chronic unloading for active individuals is that experienced in the microgravity environment of spaceflight. Significant bone loss in spacefaring humans has been noted since the early days of the Gemini program. Despite rigorous exercise protocols and other countermeasures, negative calcium balance ($\sim$0.5% per month) and bone loss in weightbearing bones (1.0–1.6% per month) are still the hallmarks of microgravity flight (LeBlanc, 1996; Turner, 1998). The increased fracture risk that accompanies these losses is difficult to precisely quantify, but is likely substantial. The loss of 20% of femoral neck bone mineral density (BMD), as seen during a year of spaceflight, corresponds to 30 years of age-related bone loss in a postmenopausal woman, leading to a 20–40% increase in fracture risk (Looker, 1998).

However, due to small sample sizes, restricted experimental capabilities on orbit, and the inherent limitations of invasive techniques with human subjects, data on

the mechanisms of these responses is limited and often contradictory (LeBlanc, 1996; Turner, 1998; Vico, 1998; Zérath, 1998).

1.2 Significance

Under NASA's current plan, initial journeys back to the moon will be short sorties of around a week, building up to stays of up to 180 days at a lunar base with exposure to 0.16-g (Lavoie, 2006). With such moderate flight durations and emergency medical care only a few days away, clinical risk management has been downplayed relative to other concerns.

On the other hand, the conjunction-class Mars Design Reference Mission utilized in NASA's Exploration Systems Architecture Study couples approximately 12 months in transit with 500 days on the Martian surface in 0.38-g (NASA, 2005b). If bone loss continues at microgravity rates for the entire mission duration, astronauts might experience average bone density losses in weightbearing skeletal components of 36%, with individual variability peaking even higher. At the other extreme, after a long journey in microgravity, Mars gravity may be anabolic, allowing for recovery of the bone mineral lost during the outbound flight. This uncertainty translates to poor understanding of fracture risk for the exploration class astronaut population, with anywhere from a 1-fold to 6-fold increased risk of hip fracture over the course of the flight compared to an age-matched population on Earth (De Laet, 1997).

Based on the currently accepted view that mechanical loading provides the primary stimulus for skeletal maintenance (Frost, 1987; Rubin, 1987; Judex, 1997; Turner, 1998; Judex, 2002), it is likely that partial loading regimes will provide partial prophylaxis against the deconditioning seen in microgravity. One must then ask how these adaptive processes scale with changes in gravitational loading. Does a given decrease in gravitational acceleration lead to a proportionate decrease in bone density? Is this response curve nonlinear? Perhaps there is a threshold below which deconditioning is much more severe?

It is a critical issue of due diligence that the spaceflight community gains a more

thorough understanding of the magnitudes of this musculoskeletal atrophy and the mechanisms that underlie it before placing astronauts at increased risk of such extensive deconditioning.

To date, NASA's charge to understand aerospace physiology has been addressed by a host of experiments in microgravity and a broad range of investigations in varying degrees of hypergravity. However, knowledge of the physiologic responses to gravitational loading between 10^{-4}-g and 1-g is not well understood (Figure 1-1). Of particular relevance to this work, the musculoskeletal response to partial weightbearing is almost wholly unexplored. The basic questions of how well partial gravity counteracts deconditioning and how long-duration exposure to partial gravity affects basic physiological processes remain to be answered.

1.3 Hypotheses and Research Objectives

This research and development effort characterizes the musculoskeletal responses to reduced loading conditions. It serves as novel scientific inquiry in its own right, and also provides preliminary data and ground control hardware for the Mars Gravity Biosatellite program (Wagner, 2004; Wagner, 2006a). The student-designed Mars Gravity research satellite will return the first rodent flight data on adaptation to a partial gravity environment. More details are included in Appendix A.

Five primary hypotheses were explored in this work:

Hypothesis 1: *A partial weight suspension simulation can be used to support chronic studies of reduced weightbearing in adult mice, with loads titrated as desired.*

Hypothesis 2: *Reductions in weightbearing by means of partial weight suspension will result in significantly reduced peak skeletal strains.*

Hypothesis 3: *Adaptation to a suspension harness and habitat prior to unloading will provide sufficient opportunity for animals to adjust to the novel housing environment, and partial weight suspension will not further increase systemic stress.*

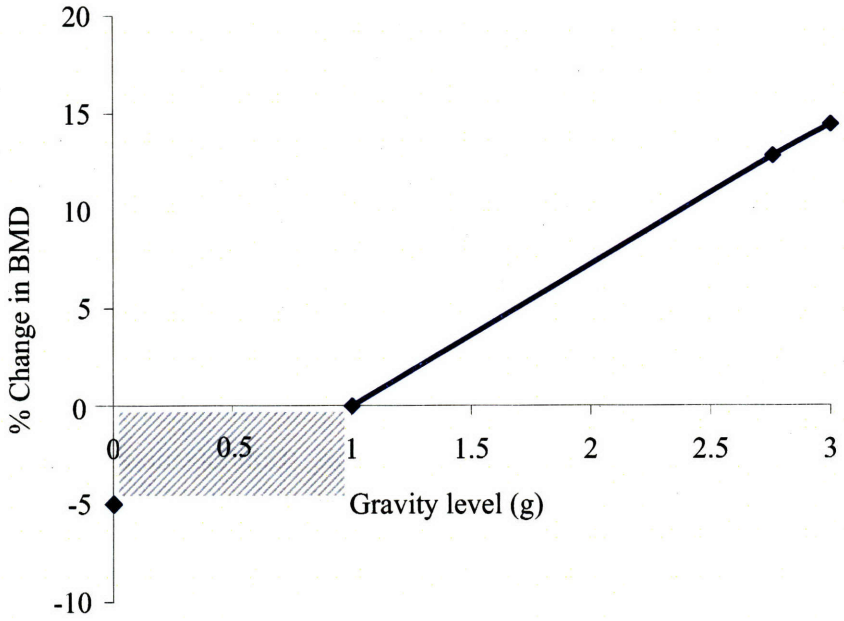

Figure 1-1: The Hypogravity Gap. While there is a wealth of data on mammalian adaptation to both microgravity and hypergravity (> 1-g), there are no established methods for describing the physiological responses in the partial gravity domain between the two. Data points represent bone mineral density changes in the rat femur from previous spaceflight and hypergravity investigations (Fosse, 1971; Amtmann, 1979; LaFage-Proust, 1998). The shaded box represents the region of uncertainty. While these data points are just a suggestive sampling, and are based on different experimental methods, the demonstrated need is a real one.

Hypothesis 4: *Reductions in the dynamic loading environment will cause decrements in osteoblastic activity, resulting in a decrease in bone mass, material, and structural properties.*

Hypothesis 5: *The patterns of response to partial unloading will be similar to those seen in previous research with full hindlimb unloading, but the magnitude of change will be related to the strain magnitudes of the partial loading environment.*

In order to test these hypotheses, a new suspension system (referred to herein as Partial Weight Suspension, or PWS) was developed, capable of supporting adult mice in a variety of partial weightbearing environments. The effects of titrated unloading (16% and 38%) on musculoskeletal tissues were broadly characterized to help elucidate the continuum of responses to dynamic stresses and strains. Validation of the PWS system included quantifying the static and dynamic load environments supported by the system, as well as examining the propagation of these loads by measuring *in vivo* periosteal strains in the proximal tibia. Finally, the PWS habitat was utilized to support two chronic studies of the musculoskeletal response to Mars-analog and lunar-analog weightbearing. Ten-week old female BALB/cByJ mice underwent 21 days of suspension or control treatment. Body mass, hindlimb musculature, and long bones were analyzed to provide a detailed portrait of the responses to reduced gravity loading at the cellular, material and structural levels.

This research has broad applicability to fundamental gravitational biology and countermeasure development, as well as to age-related bone loss and associated skeletal fragility. It can help inform design of future experiments and provide a novel ground control model for musculoskeletal studies aboard a variety of space research platforms. Additionally, the results of the proposed experiments will begin to answer some of the critical questions about sending life from Earth to Mars and beyond.

This thesis makes a key contribution to clarifying the effects of partial gravity loading, focusing on bone loss, which has repeatedly been identified as one of the largest potential obstacles to human exploration of space (NRC, 1998; NASA, 2005a).

The novel PWS habitat stands poised to provide a new perspective on the incremental role of loading in bone and muscle adaptation. The results of these studies offer unique insights into the musculoskeletal risks and benefits of reduced gravity environments, as well as the potential efficacy of artificial gravity countermeasures using partial gravity accelerations.

1.4 Thesis Outline

Bringing together established models of human partial-weightbearing locomotion studies and rodent tail suspension, this thesis describes a new ground model for partial weightbearing in adult mice, enabling critical studies on the musculoskeletal effects of such loads.

Chapter two provides a review of the relevant literature in skeletal biomechanics and spaceflight physiology, examining the patterns and physiology of bone loss due to unloading. Human and rodent data are compared and contrasted to contextualize the mouse studies later in the thesis.

Chapter three examines the limited existing data on physiological responses to loads between weightlessness and normal Earth gravity. Physical and mathematical models of bone loss due to hypogravity are examined, highlighting the current uncertainty regarding skeletal adaptation to partial weightbearing.

Chapter four describes the Partial Weight Suspension hardware designed to support experiments in adult mice and presents validation studies quantifying the associated static and dynamic loading environment.

Chapter five describes the methods used to study the musculoskeletal adaptive effects of lunar and Mars weightbearing and presents evidence from histology, histomorphometry, imaging, and biomechanics to provide a comprehensive portrait of the adaptive skeletal processes at the cellular, material and structural levels.

Chapter six synthesizes the data from the Mars and lunar-analog studies outlined in Chapter four and examines the overarching trends to provide insight into mechanisms of these changes.

Chapter seven concludes this thesis, examining the responses to the hypotheses put forward above, offering directions for future work, and summarizing the broader implications of this effort.

Chapter 2

Response to Skeletal Unloading

2.1 Physiology of Mechanotransduction

Despite its static appearance, bone is a metabolically and functionally active tissue. Throughout the skeleton, it serves such diverse roles as support structure, lever arm for muscular action, protector of vital organs, mineral storehouse, site for hematopoesis, and even, in the case of the middle ear, mechanotransducer.

Early work by Roux and Wolff suggested that bone responds to mechanical loads by adjusting its architecture to best support the stresses placed upon it (Wolff, 1892; Roux, 1895). Examination of cortical bone distribution and trabecular orientation upholds this observation, insofar as the dominant orientation of the mineralized tissue is well-aligned with the primary axes of stresses within the bone. Changes in the magnitude and/or orientation of these stresses lead to an adaptive remodeling, aimed at bringing the structure into alignment with its new mechanical demands.

A compelling example is seen in athletes with a history of playing racquet sports, where a significant increase has been shown in bone mineral content, bone mineral density, cross-sectional area, and structural strength of the dominant playing arm as compared with the contralateral arm (Huddleston, 1980; Kannus, 1994). Conversely, reductions in limb loading associated with anterior cruciate ligament surgery lead to asymmetrical skeletal weakening for both the proximal tibia and femur of the involved leg (Reiman, 2006; Zerahn, 2006).

In addition to this large scale architectural reorganization, bone also undergoes a continuous process of renewal. As with any material undergoing repeated stresses, bone accumulates microfractures due to overloading and cyclical fatigue damage. Unlike steel beams in bridge trusses, however, bone has tremendous capacity for self-repair, known also as remodeling. This dynamic process involves the coordinated recruitment and activation of both osteoblasts and osteoclasts.

Osteoblasts, the key cells in bone formation, are derived from a mesenchymal lineage. They are most often found along bone surfaces, where they secrete new osteoid matrix for later mineralization. This organic phase of the bone consists of approximately 90% type I collagen, and 10% assorted glycoproteins and glucosaminoglycans. To support the high levels of protein production needed for bone formation, osteoblasts contain an extensive rough endoplasmic reticulum and Golgi apparatus. Squamous bone lining cells that cover inactive skeletal surfaces are also thought to be in the osteoblast family (Figure 2-1).

Upon "retirement", these once-active osteoblasts are encased within a lacuna of osteoid, where they become osteocytes, the purported mechanosensors of the bone (Cowin, 1989). Far from being isolated within the bone, osteocytes are subject to fluid flow within the lacuno-canalicular network, which provides nutrients, removes waste, and may signal larger scale deformations of the bone. The cells are able to communicate with neighboring osteocytes and surface osteoblasts via long tendril-like branches that stretch through the canaliculi. Messages within this syncitium are passed between cells via gap junctions.

Osteoclasts, on the other hand, are highly active, large multi-nucleate cells that lead the process of bone resorption. They are derived from a macrophage lineage and feature numerous mitochondria and a substantial Golgi apparatus for the production of highly acidic lysosomes. The ruffled border of the osteoclast seals around sites of bone resorption and the contents of these lysosomes are released into the site to reduce the local pH, activating proteolytic enzymes within the bone. Products of this dissolution are trafficked across the cell, leaving behind a scalloped-out region known as a Howship's lacuna.

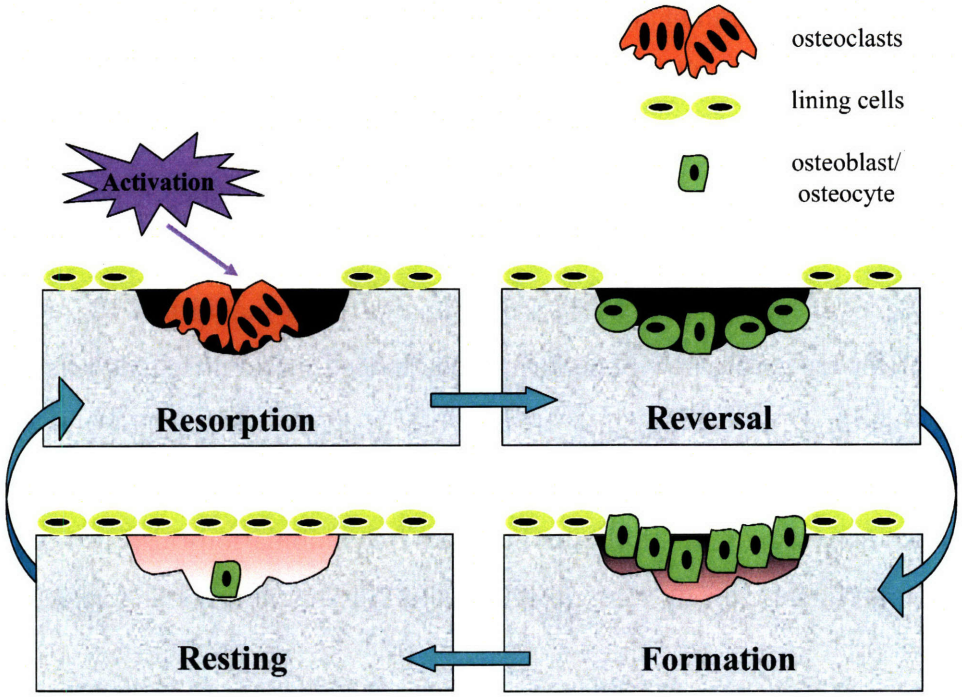

Figure 2-1: Remodeling process of normal bone. Pursuant to an activating signaling cascade, multi-nucleate osteoclasts begin to hollow out a scalloped region along the bone surface. Osteoblasts fill the resulting hole with osteoid matrix, which is later mineralized. Some fraction of this osteoblast population is left embedded in the new bone, becoming osteocytes. These buried cells are thought to serve as the mechanosensors of the skeletal structure, initializing the next remodeling cycle in response to local strains. *(Image from Mary Bouxsein, with permission)*

Under normal circumstances, healthy adults maintain a delicate balance between the processes of resorption and formation, which tips towards net bone losses in situations of unloading. Such losses may occur due to any combination of increased resorption and/or decreased formation.

Although the precise signal(s) that control this remodeling process are unknown, multiple features of mechanical loads have been proposed, including strain magnitude, strain rate, strain gradients, and strain history (Rubin, 1987; Judex, 1997, 2000; Mosley, 1997; Turner, 1998; Robling, 2002).

It seems certain that dynamic loads, rather than static loads, play a key role in this process of skeletal maintenance (Kodama, 1999). In fact, while it was long believed that high intensity impact loading was required for bone formation (Judex, 2000), new evidence is emerging that the strain stimulus of low magnitude vibrations may be sufficient for triggering new bone formation. Indeed, in adult female rats undergoing 28-day hindlimb unloading, just 10 min/day (5 days/wk) of 90 Hz 0.25-g (peak-to-peak) vibrations restored bone formation rates to the level seen in age-matched controls. Interestingly, the forces induced by free ambulation (also 10 min/day) in a second experimental group were insufficient to fully maintain bone formation (Rubin, 2001).

Based on the available evidence, it seems likely that multiple features of the strain stimulus described above contribute to the osteogenic stimulus provided by mechanical loading. Whether the induced bone deformations are themselves the root cause or the end effector, however, remains to be determined. Interstitial fluid shears, streaming potentials, and piezoelectric currents caused by these dynamic strains are also potential candidates for the proximal osteogenic stimulus (Anderson, 1970; Turner, 1994; Colleran, 2000; Cherian, 2003).

The fluid shear hypothesis, in particular, explains a wide variety of details regarding the adaptation process. In this model, osteocytes within their lacunae of mineralized bone are deformed by interstitial fluid shears in the interconnected canaliculi networks. By some mechanism, they transduce this mechanical signal into a chemical or chemoelectrical stimulus for osteogenesis. This provides a putative mechanism by

which the relatively stiff skeletal structure can sufficiently amplify mechanical loads to create the cellular strains necessary for osteocyte activation.

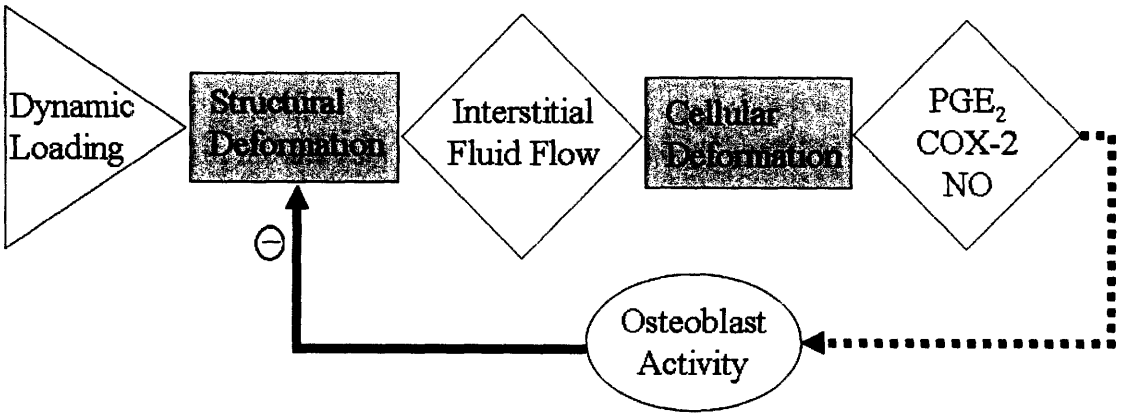

Figure 2-2: Hypothesized mechanotransduction pathways for bone formation. Dynamic loading leads to bone deformation, which turn moves fluid throughout the porous lacuno-canalicular network. Fluid shear deforms osteocytes, leading to a cascade of autocrine and paracrine cytokines that activate osteoblasts for bone formation. Newly formed bone stiffens the structure locally, reducing future deformations.

Supporting this theory, circumferential strain gradients, which have been shown to correlate with areas of new periosteal bone formation, are proportional to fluid flow within the lacuno-canalicular network of long bones (Judex, 1997). Similarly, whereas bending moments induce high levels of fluid flow and osteoblastic activity, torsional loads stimulate both significantly less flow and less osteogenesis (Rubin, 1996; Gross, 1997). *In vitro* experiments with osteocytes have demonstrated an increased release of nitric oxide and prostaglandin E2 (PGE2) in response to pulsatile fluid flow, as well as upregulation of cyclooxygenase 2 (COX-2) expression (Figure 2-2). It is believed that PGE2 acts in an autocrine manner to regulate gap junction function between osteocytes. This intracellular communication chain is mediated via PGE2 receptor activation of the cyclic AMP-dependent protein kinase A (PKA) signaling chain (Cherian, 2003). However, the mechanisms by which this communication induces downstream regulation of osteoblastic activity are as yet undefined.

The means by which such mechanotransduction can lead to resorption in the case of disuse are less clear. Burger and Klein-Nulend (1999) hypothesized that the

reduction of transport through the lacuno-canalicular network due to disuse could lead to waste buildup, nutritional deficiencies, and reduced osteocyte viability. In this framework, either osteocyte apoptosis could directly signal osteoclast recruitment, or conversely, shear-stimulated osteocytes could actively inhibit such recruitment, with disuse, in turn, removing this inhibition. A model of disuse which does not adversely affect bone perfusion would provide a useful context for exploring these theories.

2.2 Musculoskeletal Effects of Unloading

2.2.1 Human Studies

As described in the Introduction, perhaps the most extreme case of disuse in healthy individuals occurs in the microgravity environment of spaceflight, wherein the tonic loads to which Earth organisms have become evolutionarily accustomed are removed.

As early as the initial Soyuz and Gemini flights, research began examining bone density in astronauts (Mack, 1967; Rambaut, 1975). Despite the methodological flaws of evaluating skeletal losses with early plain film x-rays, the evidence of microgravity-induced bone loss at multiple skeletal sites was enough to warrant further research. Short duration studies during Apollo (Rambaut, 1975) led to a robust investigation in calcium balance and bone demineralization during the long-duration Skylab flights of 1973 and 1974. Comparing dietary intake with fecal, urine, and serum mineral levels, the team of investigators showed a negative calcium and phosphorous balance over 28–84 day missions, even in the presence of exercise countermeasures. Losses averaged -50 mg/day at the end of a week in flight and peaked around -300 mg/day by the end of the 12 week mission (Rambaut, 1979; Smith, 1999).

More recently, Smith et al. (1998) revived some of the frozen urine samples from these studies and applied modern immunoassay techniques (ELISA) to examine collagen cross-links (N-telopeptide, pyridinoline, and deoxypyridinoline) as sensitive and specific markers of bone resorption. During the first four weeks of flight, cross-link concentrations doubled on average over pre-flight levels, remaining high until 1–3

weeks post-flight and indicating a persistent increase in osteoclast activity for up to 12 weeks in flight.

The case for spaceflight-induced changes in astronaut bone formation is less clear. As reviewed by Turner (2000), human flight data are simply not resolved as to "whether the bone loss is associated with increased bone remodeling, reduced bone remodeling, or an uncoupling between bone formation and resorption." He suggests that discrepancies may be due to the timing of measurements, with a need for more extensive longitudinal sampling in flight. Furthermore, biomarker measurements from serum and urine samples necessarily represent a systemic picture of adaptation, integrating the balance of resorption and formation throughout the whole body. Therefore, such measurements may not accurately reflect local bone remodeling that varies from site to site.

What is clear, however, is that the balance of formation and resorption, at least in some regions of the skeleton, is sharply tilted in favor of bone loss. While no flight studies have taken biopsies to allow for histological evaluation of the astronaut skeleton, numerous imaging studies have examined the degree and distribution of bone loss across the human skeleton, evolving from simple plain film x-ray to higher precision quantitative absorptiometry techniques such as dual-energy x-ray absorptiometry (DXA), and most recently, to quantitative computerized tomography (QCT) which combines true volumetric density measurements with an ability to distinguish between cortical and trabecular compartments. QCT is considered the current best practice in spaceflight studies because of its unique ability to render high-resolution images in three dimensions, to tease apart compartmental differences, and to measure bone geometry.

DXA measurements before and after long duration flights (4–14.4 mo) showed that bone mineral losses occur predominantly in weightbearing bones (Figure 2-3). Areal bone mineral density (aBMD) declined significantly in the femur, pelvis, and lumbar spine by approximately 1 to 1.6%/mo (Schneider, 1992; Leblanc, 2000; McCarthy, 2004; Oganov, 2004). Depending on the study, either slight losses or minimal gains were reported for the arms and ribs, and more than one study reported significant

gains ($\sim$ 0.7%/mo) in the cranium (Schneider, 1992; McCarthy, 2004; Oganov, 2004). This pattern of changes, with greater losses in the weightbearing bones in the lower body, is not only consistent with changes in weightbearing in microgravity, but also with gravity-dependent changes in fluid distribution. According to the canalicular fluid flow model postulated above, changes in bone perfusion brought about by this cephalic fluid shift may be partially responsible for the observed losses.

Lang et al. (2004) examined compartment-specific patterns of bone loss with QCT measurements in fourteen Space Station crew members who had flown for missions of 4–6 months. Integral volumetric bone mineral density (vBMD) in the spine declined 0.9%/mo, with trabecular vBMD losses of 0.7%/mo. Measurements from the proximal femur showed significantly greater percentage losses of volumetric BMD in the trabecular compartment than the cortical (Trab: -2.3%/mo; Ct: -0.4%/mo). Impressively, such changes in vBMD for small astronaut populations (n =1–2) have been observed in flights as short as 1–2 months (Vico, 2000).

One year after spaceflight, recovery of vBMD varied with skeletal site and compartment (Lang, 2006b, 2007). No significant recovery occurred in the spinal trabecular or femoral neck cortical vBMD. However, recovery was noted in the trabecular vBMD of the femoral neck and whole femur. Cortical volume of the femoral neck decreased in flight, then recovered in the 12 months that followed (+8% relative to post-flight means). On the other hand, the neck's cross-sectional area grew slightly due to flight, and continued to enlarge postflight (+2.5% relative to post-flight means). This suggests that the in-flight mechanism of cortical thinning was primarily endosteal resorption, while post-flight recovery was due to a mix of periosteal and endosteal expansion. The periosteal expansion is particularly useful biomechanically, as it leads to a greater section modulus and resistance to bending for the same cortical thickness.

Inter-individual variability in both periods of adaptation is quite high, and thus far, no correlation has been found between bone loss in the load-bearing skeleton and factors such as age, height, weight, or duration of previous flight experience (Vico, 2000). Indeed, in one analysis, the cosmonaut with the most flight experience (460 days) showed no cortical losses in the proximal tibia, and only moderate (6–7%)

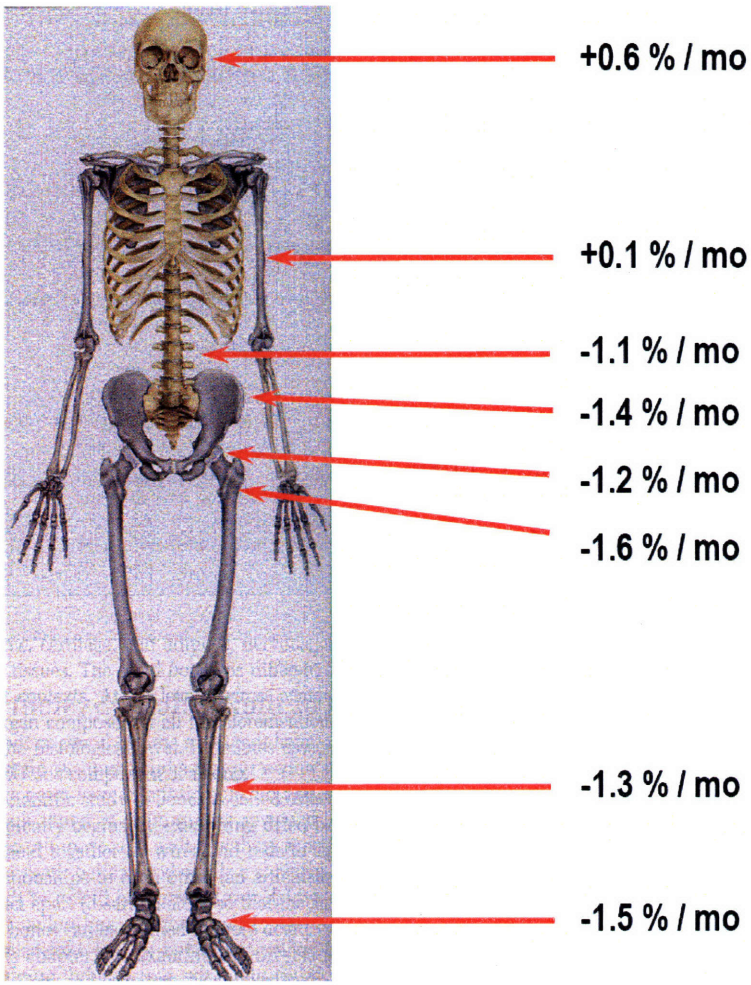

Figure 2-3: Site-specificity of microgravity bone loss. DXA and QCT measurements taken before and after long duration spaceflights indicate that bone loss occurs largely in the weightbearing bones of the lower body, with small but interesting increases in BMD in the humerus and cranium. (Data from LeBlanc, 1996; Lang, 2004. *Image from Jim Pawelczyk, with permission.*)

trabecular losses in the distal tibia.

Recovery, from both short and long-duration missions, is nearly always incomplete after a time equal to the length of flight (Vico, 2000; Lang, 2006b, 2007), suggesting that readaptation to 1-g is a slower process than the initial response to microgravity.

The mechanostat theory, presented by Carter, Frost, and others (Carter, 1984; Frost, 1987; Turner, 1991), proposes that bone adapts in response to stress stimuli which are significantly different from habitual loading. Outside of a "lazy zone", where loads are sufficiently similar to expected values, higher stresses and strains cause the formation of new bone to increase structural rigidity and reduce deformation. Stresses and strains below the "lazy zone" indicate strength in excess of physiological needs and trigger resorption.

Consistent with spaceflight recovery data, the threshold for resorption in this model is smaller than the threshold for formation. This leads to a differential efficacy of remodeling whereby small reductions in skeletal strains cause greater structural changes than small increases in strain.

While this thesis is focused largely on skeletal changes, it is important to note that spaceflight and other models of unloading also cause significant atrophy of skeletal muscles. Muscles act through inefficient lever arms to move the limbs and stabilize the body, exerting bending moments as large or larger than those caused by joint and ground reaction forces (Rittweger, 1999). Decreased muscle tone has been shown to modify bone strength independently of changes in axial loading due to locomotion (Warner, 2006), and resistance training which preserves muscle mass also prevents trabecular bone loss in hindlimb unloaded rats (Fluckey, 2002).

Without the loads imposed by gravity and 1-g locomotion, muscles atrophy significantly in spaceflight. Because of their normal anti-gravity role in 1-g physiology, lower-body extensors are subject to the earliest changes (Fitts, 2001). Microgravity exposures of 8–17 days causes reductions in astronaut muscle size as high as 10% in the gastrocnemius and 15% in the quadriceps (Adams, 2003). Consistent with these losses, maximal voluntary contractile strength in the triceps suriae also decreases greatly, particularly during longer missions (-42% over 6 months; Koryak,

2001). Presumably because of the reduced need for tonic and postural muscle tone, the balance of protein synthesis shifts with unloading, increasing the percentage of fast-type myosin isozymes over slow-type, and thereby increasing peak contraction velocity (Belozerova, 2002). Due to these changes, muscle atrophy is a key factor in fully deciphering results from flight and ground experiments of reduced weightbearing.

Given the high levels of musculoskeletal atrophy described in this section, it is worth a reminder that all of the data reported above is for astronauts serving as experimental subjects in the midst of their other flight responsibilities; results are not necessarily representative of controlled experimental conditions. Exercise is a key part of life on an orbital station, with sessions on the order of 1–2 hrs/day. Food intake is variable, sleep/wake cycles are only moderately controlled, and pharmacologic treatments (which may or may not have effects on musculoskeletal health) are common. Due to these confounds, as well as small sample sizes and restricted experimental capabilities on orbit, a variety of human ground models have been developed to support investigations (Table 2.1). Thorough reviews of the similarities and differences between these models and flight data are available from other authors (Giangregorio, 2002; Adams, 2003; LeBlanc, 2007).

Even in these human simulations, however, invasive investigational techniques are necessarily limited. The use of animal models opens the door to a wider variety of experimental techniques and endpoints, enables the use of genetically modified strains for targeted investigation of mechanisms, and facilitates much larger studies under a variety of well-controlled experimental conditions.

2.2.2 Animal Studies

Over the last four decades, young rats have been the mammalian model of choice for spaceflight experiments, due to their relatively small body masses, speed of breeding, and ease of handling. A recent review by Morey-Holton, Hill, and Souza (2007) highlighted the key space missions for musculoskeletal studies in rodent models: "the unmanned Russian Cosmos series (782, 936, 1129, 2044 missions lasting 14-19.5d), multiple Shuttle Spacelab missions including Spacelab 3 (STS-51B, 7d), Space Life

Table 2.1: Human models of chronic musculoskeletal unloading (Koryak, 1996; Giangregorio, 2002; Adams, 2003; LeBlanc, 2007)

Unloading Model	*Description*	*Features and constraints*
Spaceflight	Individuals are exposued to extended periods of microgravity, with flights to date up to 437.7 days (Mir LD-4).	Systemic model, characterized by bone loss, muscle atrophy, cephalic fluid shift, cardiovascular deconditioning, neuromotor adaptation, and radiation exposure. Offers uniquely reduced otolith inputs. Extremely limited subject pool, with numerous practical constraints.
Bedrest	Subjects are maintained in bed, either horizontally or with 6° head-down tilt.	Full-body unloading model. Head-down tilt produces cephalic fluid shift. Expensive, with particularly large challenges maintaining compliance in long studies.
Dry immersion	Subjects are neutrally buoyant in a tank of water and typically supine. Rubber sheets maintain a dry state of immersion.	Full-body unloading model. Reduces proprioceptive feedback, consistent with spaceflight. Expensive, with particularly large challenges maintaining compliance over long studies
Limb immobilization	Limb is immobilized, typically with a cast, to force reductions in movement and loading. Gait is assisted with crutches.	Localized model, limited practically to long bones. Muscle activity is sharply constrained.
Unilateral lower limb suspension	Subject's leg is placed in a sling to prevent locomotor loads. Gait is assisted with crutches.	Localized model. Highly affordable and easy to set up/maintain.
Spinal cord injury	Clinical model of chronic reductions in regional neuromuscular tone and daily loading.	Leads to bone and muscle losses consistent with long-duration spaceflight. Denervation also affects other local systems, including vascular control. Challenging experimental design.

Sciences 1 (STS-40, 9d), Space Life Sciences 2 (STS-58, 14d), Life and Microgravity Mission (STS-78, 17d), Neurolab (STS-90, 16d), and Shuttle mid-deck flights including adult male rats on STS-29 (5d) and female mice on STS-108 (12d)." It is clear from this listing that the observed changes thus far have largely been due to acute exposures of less than three weeks.

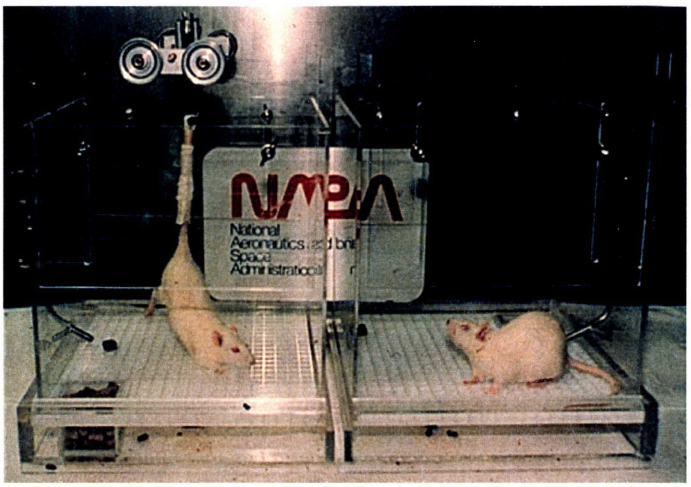

Figure 2-4: Rodent model of hindlimb unloading by tail suspension, with similarly housed full-weightbearing control. *(Image from Wronski, 1987, with permission.)*

Like spaceflight, ground-based techniques of cast immobilization, sciatic nerve crush, and others have also been shown to result in significant osteopenia (Table 2.2). However, hindlimb suspension, first introduced by Morey in 1979 to provide NASA with a rodent ground-based model comparable to the human bedrest and chimpanzee chair immobilization (Figure 2-4), has become the rodent ground model of choice for investigating the musculoskeletal effects of microgravity. Hindlimb suspension is unique among existing rodent models in that it requires no surgical intervention and, while it does result in reduced muscle loading, it does not unduly constrain or prohibit contraction of the limb musculature. Due to the integrated nature of muscle and bone adaptation, the maintenance of this function is highly desirable in studies that are attempting to replicate the effects of spaceflight. Moreover, the model also replicates the characteristic cephalic fluid shift experienced by astronauts, enabling its application to cardiovascular studies as well.

Table 2.2: Physical rodent models of chronic musculoskeletal unloading (Mussachia, 1992; Jee, 1999; Morey-Holton, 2002; Simske, 2003; Warner, 2006). Genetic variants, pharmacological treatments, ovariectomy, and dietary restrictions which replicate features of musculoskeletal atrophy without changing chronic loading patterns, are not included (i.e. osteoprotegrin knockouts with increased bone resorption, reduced-calcium diets with decreased mineralization).

Unloading Model	*Description*	*Features and constraints*
Spaceflight	Extended microgravity exposure, with flights to date up to 21.5 days (Cosmos 605)	Systemic model, characterized by bone loss, muscle atrophy, cardiovascular deconditioning, neuromotor adaptation, and radiation exposure. Only model with reduced otolith inputs. Numerous practical constraints.
Hindlimb suspension	Hindquarters are elevated to provide full unloading on hindlimbs. Most studies are conducted with tail suspension, although some have used full-body harnessing.	Non-surgical model with localized unloading. Fully recoverable. Head-down tilt causes cephalic fluid shift.
Limb immobilization	Limb is immoblized via casting, bandaging, or pinning of a joint, forcing reductions in movement and loading	Except for pinning variants, a non-surgical model of localized unloading. Fully recoverable. Limb position determines passive muscle tone.
Sciatic nerve crush	Pressure is applied to the nerve within its neural sheath, causing functional immoblization	Minimally invasive surgical model of localized skeletal unloading and muscle hypotonus. Recoverable with time. Denervation also affects other local systems, including vascular control.
Neurectomy	Sciatic and/or femoral nerve are fully transected, causing permanent denervation of elements of the lower leg. May be extended to full spinal cord transection to immobilize the full leg and hip	Surgical model of localized skeletal unloading and muscle hypotonus. Non-recoverable. Denervation also affects other local systems, including vascular control.
Tenotomy	Tendons, typically of the knee joint, are fully transected, causing permanent impairments to mobility of that joint	Surgical model of localized skeletal unloading and muscle hypotonus. Non-recoverable. Muscle length may be below resting length.
Botulinum toxin	Injections of neurotoxin inhibit acetylcholine release and inhibit muscle contraction	Non-invasive model of localized skeletal unloading and muscle hypotonus. Some systemic effects. Fully recoverable.

Early versions of the model used epoxy to bond a hexcelite brace to the animal's back to support suspension. This unfortunately induced high stress responses and, consequently, systemic loss of bone density even in the normally loaded humerus.

Current tail suspension paradigms do not result in significantly elevated of stress hormones or other indications of systemic stress response (Wronksi, 1987). In this model, traction tape is applied along the base of the tail to provide a stable point for load application. The animal's hindquarters are elevated by approximately 30°, fully removing the dynamic loads associated with normal locomotion and rearing. (Specifically, whereas normal ambulation induces strains of approximately 1300 microstrain in rat hindlimbs, gage recordings during suspension measure less than 50 microstrain, even during active muscle contractions (Schultheis, 1999).)

With much of the animal's weight supported by this tail suspension, the forelimbs continue to bear weight at approximately normal levels, providing an internal control for musculoskeletal studies. A tether with a swivel to allow free rotation is run from the tail tape to the top of the cage, and is typically connected to either a slider on a guide wire or a pulley/wheel on a rod, providing the rodent access to the majority of the cage floor. Stops are typically installed to prevent the animals from bearing weight against the walls. More detailed technical notes on this protocol may be found in (Morey-Holton, 2002).

Under such hypodynamic and hypokinetic unloading, mice and rats show flight-like musculoskeletal deconditioning, resulting in reduced bone mineral density and strength. Over 1000 tail suspension studies in a variety of physiological systems have been published since the model's inception (Morey-Holton, 2005), and extensive reviews of rodent skeletal adaptation to spaceflight and suspension are available elsewhere (Vico, 1998; Zérath, 1998; Turner, 2000; Carmeliet, 2001; Giangregorio, 2002).

While variations are seen with species, strain, sex, age, housing, feeding strategy, and duration of study, some of the most consistent findings are highlighted below:

- Bone loss accrues predominantly in the unloaded bones.

- Trabecular bone deteriorates more than cortical, though most studies see losses in both compartments.
- Bone formation and mineral apposition are inhibited.
- Mineralized matrix matures more slowly, but there is no significant change in the proportions of the various mineral fractions.
- Muscle atrophy occurs, with preferential losses in slow twitch muscles and extensors.
- Fluid shifts cephalically with an accompanying diuresis.

Of particular note on this last item, a 30° head-down suspension in rodents was selected to provide normal loads to the forelimbs without excessive tension on the tail (Hargens, 1984). However, while notable cephalic fluid shift and the diuresis it engenders are typical of human flight responses, the magnitude is excessive relative to actual flight responses in the small quadrupeds. Unlike humans who tend to retain fluids postflight, rats exposed to microgravity for 14 days showed a diuresis immediately post-flight (Wade, 1998). This suggests that rodents may have different patterns of fluid handling than humans in response to spaceflight, maybe even retaining water during flight.

Furthermore, in anesthetized rats flown in a horizontal position under conditions of parabolic flight, no changes were seen in jugular venous pressure, carotid arterial pressure, aortic pressure, cerebrocortical blood flow, or muscle blood flow in the temporal muscle during the low-g portion of the parabola ($\sim 0.4-$g; Tanaka, 2005).

Models that do not cause fluid shift may, in fact, more accurately represent rodent spaceflight changes.

2.2.3 Comparison of Human and Rodent Studies

Comparing astronaut and rodent adaptation is instructive both for the interpretation of animal results and for clarifying physiological differences in the models. Table 2.3

summarizes overarching trends across the two species, as well as specific data from two investigators. What becomes clear from this evidence is that perhaps the biggest difference between human and rodent data is the evidence implicating increases in bone resorption (human) versus decreases in bone formation (rodents).

Table 2.3: Comparison of dominant patterns of bone loss seen in the femurs of human astronauts and tail suspended 16 week BALB/cByJ mice. Human data is from QCT after 4–6 mo flight (n = 14; Lang, 2004, 2006b). Rodent data is from μCT and histology after 3 week tail suspension (n = 10; Judex, 2004).

	Astronaut Flight Data	*Rodent Tail Suspension*
Pattern of loss	Greatest in weightbearing bones, with higher percentage losses in trabecular compartment	Greatest in weightbearing bones, with higher percentage losses in trabecular compartment
Changes in Formation	Unclear evidence	Significant reductions in bone formation, mineral apposition, and double-labeled surfaces
Changes in Resorption	Urinary biomarkers consistent with high, sustained resorption	Unclear evidence
Periosteal Apposition	No significant change	No significant change
Endosteal Resorption	Significant in-flight expansion at femoral neck	Significant expansion in proximal metaphysis and mid-diaphysis
Magnitude of Cortical Losses	0.3-0.5%/mo vBMD from hip	18% Ct.BA from proximal metaphysis in 3 weeks
Magnitude of Trabecular Losses	2.2-2.7%/mo vBMD from hip	59.5% BV/TV from proximal metaphysis in 3 weeks

In two studies of 6 month male rats, Dehority (1999) and Bloomfield (2002) demonstrated time-course evidence that full unloading in mature animals led to sharp declines in periosteal bone formation rate (BFR) and decreased numbers of osteoblasts per bone surface area (Ob.BS) in the cancellous portion of the metaphysis, sustained

throughout up to 5 weeks of suspension. The greatest structural changes in both young and old animals here and in many other studies were in the more metabolically active cancellous compartment, with smaller effects on cortical bone. While resorptive changes were predicted at the cortical endosteal border, low turnover rates in these mature animals minimized changes on that surface (Bloomfield, 2002).

Overall, the balance of formation and resorption was clearly disrupted in the direction of suppressed bone formation.

For rodents, such decrements in bone structure and formation rates are largely consistent across age (Globus, 1986; Morey-Holton, 1998), sex (Hefferan, 2003), spaceflight/suspension (Wronski, 1983; Morey-Holton, 2005), and rodent species (Judex, 2002; Bateman, 2000). Importantly, work by Globus et al. (1986) using radioisotope incorporation and histomorphometry suggests that while young, growing rats do show initial evidence of suppressed formation in the first week of tail suspension, these declines rebound to control levels by the end of a two week suspension period.

While decreased formation with no change in resorption is generally considered the dominant mechanism in disuse osteopenia in rodents, the evidence is not wholly conclusive. Selected studies have shown significant increases in osteoclasts relative to controls (Sakai, 2001), as well as differential changes in resorption on the basis of sex (males > females; David, 2006), and age (older > younger; Hefferan, 2003).

Data for human studies is significantly more limited, as samples are not typically collected for histology. Nearly all evidence comes from systemic markers of resorption and formation, which cannot accurately reflect local changes. Iliac biopsies taken before and after 120 days of bedrest showed clear evidence of decreased formation due to disuse (Vico, 1987), but systemic serum and urine markers of bone formation are largely unchanged by spaceflight or bed rest (Smith, 2005; LeBlanc, 2007). Additional research is needed to clarify these effects.

In summary, rodent tail suspension largely succeeds as a model of spaceflight musculoskeletal losses in humans, although further investigations are necessary to clarify the relative roles of formation and resorption in humans and animals. Additionally, while patterns of bone loss are similar between the two species, the absolute mag-

nitude of changes cannot be compared, nor is it appropriate to think they should be. High levels of genetic homology and evolutionary commonality suggest similar mechanisms should be responsible for adaptation in both species, but different body sizes, growth patterns, and life spans modify the relative phenotypes.

2.3 Choice of Animals

Historically, both flight and ground unloading experiments in animals used predominantly young male rats to focus on the specific effects of unloading during growth (NASA, 2006), hypothesizing that these effects would be greater in animals with higher rates of bone turnover. However, the use of young animals correlates poorly with astronaut physiology, where the average candidate is selected around 35 years of age and has reached skeletal maturity (Looker, 1998). In particular, skeletally mature animals typically have structural changes driven less by bone growth or modeling and more by remodeling.

Unexpectedly, however, tail suspension in mature male rats has been shown to cause a more pronounced and persistent decrease in bone formation than in young, growing rats (Dehority, 1999). Moreover, whereas it was long-believed that the bone changes in response to unloading were confined predominantly to cancellous bone, recent hindlimb unloading studies report that female retired breeders show decrements in the cortical compartments of the weightbearing skeleton as well (Bloomfield, 2002; Allen, 2006). Taken together, these findings suggest that adult rodents respond differently than growing ones to altered mechanical loading, and therefore may be better matches for the astronaut population in terms of relative skeletal maturity. Additionally, because larger effects were observed in the adult animals, statistical power may be improved relative to studies in juvenile rodents.

Recently, the large and rapidly growing knowledge base of mouse/human genetic homology has opened up a valuable tool for extrapolation to human physiology. As early as 1998, the National Research Council Space Studies Board recommended that spaceflight rodent models "should include mice, given their smaller size and the

availability of genetic variants and transgenic animals" (NRC, 1998). Thus far, two Space Shuttle flights—STS-90 and STS-108—have flown mice, and in both cases, the cohort was comprised of growing young animals (~6-8 weeks). Even as rat flights become more infrequent, a third mouse flight is scheduled for 2007 aboard STS-118, and ground studies are moving towards mice as the primary spaceflight model, often to take advantage of genetically altered strains.

In selecting an appropriate experimental cohort, the underlying milieu of growth and resorption due to age should also be taken into account. Peak trabecular bone volume fraction (BV/TV) in C57Bl/6J (B6) mice occurs around 2 months of age in both the distal femur and the L5 vertebra (Glatt, 2007a), whereas cortical thickness peaks around 3 months of age. Femoral epiphyses close nearer to 6 months and would represent a more fully mature state; however, the paucity of trabecular bone volume at this age, particularly in females, may make it more difficult to detect bone loss. Therefore, 3 to 5 month animals are recommended for such studies, except where research objectives explicitly necessitate rapid growth or senescence.

The literature on the effect of sex on responses to unloading is equivocal, with studies showing no difference between males and females (Simske, 1994), significantly higher losses in females (Simske, 2004), and different patterns but similar magnitudes of change (Bateman, 1997). More research is necessary to determine whether the patterns of bone loss in male or female rodents is more consistent with findings in the astronaut population.

2.4 Spaceflight Fractures

While the changes due to spaceflight and tail suspension are theoretically interesting and offer a unique window on the role of gravity and loading in Earth-bound physiology, they also have an important operational consequence for spaceflight. NASA's Bioastronautics Roadmap (NASA, 2005a) calls out Accelerated Bone Loss and Fracture Risk as a Level 2 priority, meaning that it is associated with a "risk of serious health or performance consequences, and there is no mitigation strategy that has

been validated in space."

Examining the patterns of fracture incidence in similar Earth-bound populations, one sees that fractures in young, healthy adults occur most frequently in long bones and predominantly cortical structures. In osteoporotic populations, on the other hand, fractures are most common in the hip, spine, and wrist, in areas of higher trabecular content. Given that bone loss in spaceflight tends to be in the weightbearing skeleton, vertebral and hip fractures pose the greatest additional risk to a flight crew.

The vast majority of hip fractures in the normal adult population ($\sim$ 90%) are sustained in falls from standing height or less (Youm, 1999), with a significant percentage (17.7%) occurring from seated or lying positions (Goh, 1996). Even in young healthy populations, such falls can result in fracture (Kannus, 1996, 2006). This is all the more relevant to the astronaut corps, who have been shown to be more susceptible to orthopedic injuries than an age-matched population, due at least in part to their active and competitive lifestyle (Jennings, 1996).

Following spaceflight exposure, astronauts have multiple risk factors for such fractures, including decreased BMD, gait instability due to neuromotor deconditioning, orthostatic intolerance, and weight loss. Furthermore, extraterrestrial locomotion is likely to take place on loosely packed regolith, under conditions of poor visual contrast, in spacesuits that significantly restrict motion and add substantial inertia to both gait and falls (Carr, 2007).

Compounding this risk, the role of loading in the fracture healing process is still poorly understood. The key study in this area was conducted aboard Cosmos-2044, using a rat model of fibular osteotomy (Kaplansky, 1991). Microgravity exposure on days 3–16 post-osteotomy resulted in poor callus development and bone fragment consolidation, as well as poor mineralization of newly formed bone. Similar results were observed in hindlimb suspension controls. Slight refinements were achieved by Kirchen et al. (1995) also using adult male rats, this time exposed to microgravity or suspension on post-fracture days 5–9. They found similar periosteal osteogenesis to that observed in weightbearing controls, but reduced chondrogenesis. Observed reductions in angiogenesis in flight animals relative to suspension controls suggested

that the spaceflight environment, per se, may influence fracture healing. Whether this was an effect of flight stresses, radiation, impacts of the floating animals with cage walls, or other environmental conditions remains to be determined.

Ovariectomized animals have been shown to have decrements in bone quality and strength after fracture, and reductions in initial fracture stability and callus strength have been demonstrated in osteoporotic bone. It is still unclear, however, whether osteoporosis and osteopenia significantly and independently impair the fracture healing process (as reviewed in Augat, 2005), or whether this effect is strictly hormonal. Because fracture healing is most rapid in young, growing animals with active bone modeling processes, there is significant concern that the altered balance of remodeling in response to reduced loading may lead to an imbalance between formation and resorption that can inhibit fracture healing.

Thus, the risk of astronaut fracture is an important one due not only to its immediate impact on mission operations, but also its longer-term consequences. With reduced rates of bone healing, decrements in immune status, and logistical challenges in wound management, the chances of secondary morbidity, and even mortality, due to sequelae are not insignificant. As NASA's focus shifts from the highly constrained and subdued environment of the Space Shuttle and Space Station towards more intensive surface operations on the Moon and Mars, these risks are likely to increase sharply. Not only is time spent in extravehicular activities (EVA) predicted to increase markedly (Figure 2-5), but the types of activities to be conducted — including field geology, establishment and maintenance of a lunar/Mars base, and exploratory excursions — are also likely to carry higher risk of falls and other trauma.

Schaffner (1999) used finite element and multi-link dynamic modeling to assess the factor of risk (applied force divided by failure load) for hip fracture in case of an astronaut fall. Estimation of femoral neck strength after a 12 month stay in microgravity was paired with gait and falling dynamics representative of the moon, Mars, and Earth. He noted that post-flight risk was highest for falling in Earth-gravity conditions, due to the proportionately higher impact loads. For "typical" 50th percentile males, the factor of risk for hip fracture during a post-flight fall in

Figure 2-5: Historical and predicted levels of extravehicular activity (EVA) for the American and Russian space programs through completion of Space Station, as of 2000. Estimates of Mars surface activity (in red) are based on a single 600-day surface stay with 10 EVAs per crew-week. The sharp rise predicted with these exploration-class surface operations carries substantial additional risk of musculoskeletal trauma and fracture. *(Image from Carr, 2001, with permission)*

Earth gravity was 1.75. While this only represented a 10% increase of fracture risk compared to a similar fall pre-flight, any factor of risk greater than one suggests that the proposed loads exceed the maximum predicted strength of the bone structure.

For Mars simulations, suit mass increased impact loads, but padding compliance added a 20% margin of safety to impact stiffness. Taken together, these two factors resulted in similar risks for suited and unsuited falls in 0.38-g. Compared to typical pre-flight falls on Earth, the model actually suggested a 30% lower fracture risk for falls on the Martian surface after skeletal weakening. However, the factor of risk was still 1.11, indicating a significant likelihood of hip fracture in the event of such an impact. Benefiting from recent advances in bone imaging and finite element modeling, Lang and Keyak (Lang, 2006a) are evolving a patient-specific approach to this same problem, using voxel-based CT data to automatically generate individual models and predict fracture risk.

While these unique models provide a valuable level of initial insight into fracture risk after a long microgravity journey, however, they cannot accurately predict the fracture risk associated with a Mars surface stay. Again, NASA's Exploration Systems Architecture Study recommends a baseline Mars mission with 6–9 months of microgravity transit each way, coupled with 500 days on the Martian surface (NASA, 2005b). This "long-stay" design necessitates a more fundamental understanding of the effects of partial weightbearing (i.e., between 0 and 100%) on skeletal adaptation.

Chapter 3

Review of Partial Gravity Physiology

As NASA looks forward to exploration-class missions to the moon (0.16-g), Mars (0.38-g), and beyond, it is vital to consider the physiological effects of reduced loading. Called alternatively subgravity, hypogravity, reduced gravity, or fractional-g, the partial gravity domain between free fall and 1-g remains one of the unexplored arenas of gravitational physiology. To date, extended periods of true partial gravity exposure have been experienced only by the twelve Apollo moonwalkers, for periods not exceeding 75 hours. Parabolic flights, artificial gravity, head-up tilt bedrest, and ground-based suspension studies have offered limited additional insights, as described below.

3.1 Flight and Ground Data

3.1.1 Apollo Lunar Data

During the six Apollo moon landings, twelve male astronauts each spent between 22 and 75 hours on the lunar surface. Unfortunately for science, biomedical data collection during the exposure was minimal, and much of the changes seen post-flight reflect the days spent traveling in microgravity to and from the moon.

In *Biomedical Results of Apollo*, Rambaut et al. (1975) demonstrated that the reduced gravity environment of the Apollo 17 lunar flight (12.6 days, with 75 hours on the lunar surface) resulted in increased urinary and fecal phosphorus excretion and increased fecal calcium. These changes resulted in negative mineral balance, averaging -0.2% of estimated total body calcium and -0.7% of estimated total body phosphorus. This suggested both skeletal and soft tissue losses as well as decreased calcium absorption, possibly due to low levels of the active form of vitamin D.

A small but particularly interesting control cohort exists in the Command Module Pilots, who spent their entire flights in microgravity without the benefit of either lunar loading or extensive EVA exercise. Data from Apollo 8, 10, and 13, which approached the lunar surface but did not land may also provide an instructive contrast. While Apollo 14 and 16 astronauts showed no bone mineral losses from the os calcis or radius, both the Apollo 15 Commander and Command Module pilot experienced approximately 7% losses in the os calcis, as measured by photon absorptiometry. However, the Commander, who walked on the lunar surface, experienced more rapid post-flight recovery (Rambaut, 1975).

Given the inter-individual variability of both flight and recovery adaptation, as well as the poor imaging techniques of the era (Vose, 1974), this small sample may be merely anecdotal. However, the suggestion that exercise helped compensate for reduced-gravity osteopenia is a reasonable one. Future missions to the moon should prioritize additional biomedical research in the 0.16-g environment to bolster this limited data set.

3.1.2 Parabolic Flight

By flying an aircraft in large parabolic trajectories, a pilot can place untethered crew and cargo into a temporary state of free fall as the plane crests the top of its arc and begins to rapidly descend. Such flights are currently operated aboard NASA's C-9, Novespace's A-300, the ATLAS Aerospace IL-76MDK, and ZERO-G Corporation's 727-200. Passengers on these flights experience a series of 10 to 40 parabolas consisting of 20–25 seconds of free fall, alternating with longer "pull outs"

with peak loads around 1.8-g. These trajectories can also be made more shallow, enabling longer periods of partial gravity in lieu of free fall. While the g-level is not entirely stable, due to flight disturbances and aircraft dynamics, these short exposures are truly partial gravity, without the confounds of rotating environments or ground simulations.

A number of human studies in parabolic flight have examined gait kinematics and energetics. The classic inverted pendulum model of walking describes an arc-shaped motion of the body's center of gravity during forward locomotion, exchanging kinetic for potential energy throughout the gait cycle. The ratio of these two energies defines the Froude number, and is inversely proportional to gravitational accelerations. This non-dimensional Froude number can be used to predict optimal walking speeds for a given environment, as well as the run-walk transition.

In accordance with this model, data from parabolic flight (and other simulations, e.g., Section 3.1.5) shows that optimal walking velocities are lower for lower g-levels and that the range of available walking speeds that are energetically efficient is smaller (Minetti, 2001). Energy expenditures are also lower at these reduced accelerations, such that in parabolic flight at 0.4-g, external work due to walking is about half that on Earth (Cavagna, 2000).

Yuganov and Yemelyanov (1975, 1972) and Yuganov (1972) examined vestibular, motor, and electromyographic data from humans and animals aboard parabolic aircraft. Based on their observations, they suggested that 0.28 to 0.31-g was "adequate to orient the human body in space, to preserve movement coordination, as well as to maintain the necessary level of certain physiological indices." Similarly, Shipov et al. (1981) observed that no atrophic muscular changes were seen in turtles under 0.3-g parabolic flight conditions, presumably from electromyographic readings. These minimum accelerations were presumed adequate for basic neuromuscular activation and coordination, at least during short exposures to the stimulus. Insufficient data, however, was available to draw conclusions about chronic musculoskeletal maintenance.

3.1.3 Flight Centrifuge Data

The next nearest simulation to "true" partial gravity comes from centrifuge studies in spaceflight. Through the removal of tonic 1-g loads characteristic of ground centrifuges, it is possible to simulate intermediate gravity levels with a rotating environment. At very large radii and low rates of rotation, such artificial gravity environments approach "true" partial gravity. However, as practical constraints reduce the size of these systems, gravity gradients, cross-coupled accelerations, and Coriolis forces play a larger role in experiment outcomes (Graybiel, 1973; Young, 1999, 2003). To date, however, only single cellular organisms, fruit flies, Fundulus embryos, and plants have been subjected to such a partial-g artificial gravity environment for any extended length of time.

Hemmersbach et al. (1998) and Hader et al. (1996) examined gravitactic behaviors, whereby simple organisms aligned themselves in accordance with the local gravity vector. Despite different receptor mechanisms, *Loxodes striatus*, *Paramecium biaurelia*, and *Euglena gracilis* demonstrated clear sensing thresholds in the range of 0.15–0.3-g. Persistence of such thresholds was confirmed in *Paramecium* throughout a 15-day flight, and in *Euglena* throughout a 12-day flight (Hemmersbach, 1996; Hader, 1995). These experiments suggest that even the simplest organisms have a minimum level of gravitational stimulation necessary to evoke evolved responses. (Perception of gravitational loads in rotating vehicles and in-flight centrifuges has been shown to arise between 0.2 and 0.5-g in humans (Clément, 2004).)

As part of the Soviet/Russian Cosmos biosatellite program, Cosmos 782 included a 52-rpm centrifuge providing either 0.6-g or 1.0-g to fruit flies, *Fundulus* embryos, carrot tissue, and cultured carrot cells. Ilyin's 1983 review of the Cosmos flights also sums up an experiment on *Drosophila* and meal worm centrifugation on Cosmos 1129, which "indicated that the distribution of pupae and larvae about the zones with different levels of artificial gravity (0G, 0.3G, 0.6G, and 1G) was equal."

Multiple papers on artificial gravity system design (Grigorev, 1981; Shipov, 1981; Clément, 2004) suggest a minimum useful level of artificial gravity around 0.3-g,

based largely on Soviet centrifuge and parabolic flight findings with rodents, dogs, and humans. However, review of these studies shows that periods of exposure were typically brief (seconds to minutes), and utilized imprecise behavioral metrics as their primary outcomes, including the choice of rats to walk on the floor rather than the walls.

Together, however, these diverse studies suggest gravitational thresholds for both perception and physiological adaptation, which must be further explored. There is no *a priori* reason to believe that these thresholds should be the same across organisms or physiological systems, and investigations at a variety of g-levels are needed. While a number of space station experiments have been designed by the Russians, Americans, and others to more explicitly test animals across the gravitational continuum, none has been seen through to completion (Bonting, 1992; Katovich, 1998; Clément, 2004). Most recently, the International Space Station Centrifuge Accommodation Module, or CAM, was designed to provide a 2.5-meter radius flight facility for supporting plants and animals at accelerations from 0.001-g to 2-g. Unfortunately, after multiple delays, this module was removed from the flight manifest in 2005.

The Mars Gravity Biosatellite, currently under development at MIT, aims to provide an uncrewed research platform for future partial gravity flight studies (detailed in Appendix A). Artificial gravity will be provided by rotation of the full satellite, and can be adjusted to desired levels. The configuration for the first flight of this new platform supports 15 adult mice for a 35-day mission at 0.38-g. Post-flight recovery will enable extensive physiological characterization of the flight specimens.

For now, however, it remains necessary to rely on ground models for this data.

3.1.4 Head-up Tilt Bedrest

In contrast to the traditional 6-degree head-down tilt used to mimic microgravity fluid shifts and hypokinesia, some researchers have also explored a novel head-up tilt model for partial gravity physiology.

Pavy-Le Traon et al. (1997) utilized a 10-degree head-up tilt bedrest model to explore the cardiovascular and hormonal changes that accompany a 14 day lunar

mission. They treated six male subjects with four days at 6-degree head-down tilt as a "microgravity trans-lunar flight", followed by six days of head-up tilt with 40 minutes daily of ergometer-based "EVA" exercise, and capped with a final four days of head-down tilt to represent the flight back to Earth. Similar to spaceflight and other bedrest simulations, 67% of subjects demonstrated orthostatic arterial hypotension in response to a post-experiment tilt test. A drop in plasma volume was coupled with a significant decrease in atrial natriuretic peptide and an increase in plasma renin activity during head-up tilt, consistent with a caudal fluid shift relative to head-down steady-state. While this study provided interesting data on the effects of fluid shift and hypokinesia, no specific data was gathered on the musculoskeletal results of the treatment, and the hypodynamic stimulus induced by bedrest challenges such investigations.

3.1.5 Human Partial Weight Simulations

Although none have been used for chronic musculoskeletal studies, multiple systems have been developed for investigating the locomotor changes in humans in partial gravity.

Underwater treadmills, as used by Newman, et al. (1992, 1993, 1994), allow for limbs to be independently weighted to achieve appropriate levels of neutral buoyancy. While fluid drag and hydrodynamic damping substantially modifies rapid movements, the model provides reasonable fidelity at low speeds (Newman, 1993).

Vertical cable suspension, as used in the MIT "Moonwalker" offers simpler operations (Wu, 1999; Jackson, 2000). In this system, a subject is harnessed and springs or other elastic elements provide a vertical force to reduce ground reaction forces to the desired level. The goal is to provide a constant or near-constant harness tension, so as to accurately simulate the gravitational environment of choice. Because spring tension necessarily changes with vertical excursions of the subject's center of mass, some more advanced systems have aimed to improve performance with hydraulic and pneumatic designs using force feedback control loops.

The upward forces exerted by the suspension system reduce the load-bearing re-

quirements placed on the legs in a rough approximation of the effects of reduced gravity. However, while the harness applies a local upward force, gravitational forces on the distributed mass of the body segments remain unchanged. As reviewed by Davis and Cavanagh (1993), investigators have approached this challenge in a number of ways, including numerous variations on horizontal subject position. Although unwieldy, cables can be added to each limb to provide independent suspension.

To date, the primary foci of this research community have been the biomechanics and energetics of locomotion and work in such an environment (Duddy, 1969; He, 1991; Newman, 1992; Jackson, 2000). The data of He et al. agrees with results attained during Apollo lunar simulation studies (Roberts, 1963; Duddy, 1969; Hewes, 1969) and suggests a change in the mechanics of partial gravity locomotion, which may play an interesting role in determining skeletal stresses. Ground reaction forces in these human simulations vary directly with loading level (Flynn, 1997; Griffin, 1999), with average peak vertical forces deviating less than 10% from predicted values for loads from 5–100% of body weight (Ivanenko, 2002). Because the skeletal strain environment is directly related to these ground reaction forces (Peterman, 2001), similar variations may be expected for the osteogenic stimulus of partial weightbearing.

Experiments in the MIT Man-Vehicle Laboratory have tested the hypothesis that the mechanics and energetics of human locomotion in simulated partial gravity environments found on other planetary bodies differ from typical 1-g Earth-normal locomotion (Newman, 1992, 1993, 1994, 1996, 1997; Wu, 1999; Jackson, 2000; Carr, 2007; Rader, 2007). Both gait and energetics have been assessed to further the understanding of the mechanics and physiological requirements of partial gravity locomotion. Energy requirements were found to be significantly lower for partial gravity locomotion than for Earth-normal 1-g locomotion at the same speeds (Newman, 1994). Partial gravity simulation by suspension was found to reduce the load-bearing demands on the legs and to increase the body's inverted pendulum time constant across the continuum of gravitational acceleration (Jackson, 2000).

In a variation on horizontal suspension, Hargens et al. have developed a treadmill for supine exercise with lower-body negative pressure (LBNP) applied to create

appropriate ground reaction forces (Murthy, 1994). The system is an ideal one for supporting exercise during bedrest studies, and has been shown to protect cardiovascular fitness similar to normal upright exercise (Watenpaugh, 2000) and to partially mitigate the bone loss associated with disuse (Smith, 2003). Such a system could be used to investigate the effects of daily loading at partial-g levels, particularly in association with the head-up bedrest model described in Section 3.1.4.

3.1.6 Clinically Reduced Loading

While not explicitly designed to test the effects of reduced loading for aerospace applications, multiple clinical conditions also provide insight into locomotion under conditions of partial weightbearing. Patients utilizing assistive devices for walking may alter loading in one or both legs. Those with hemiparesis or hip osteoarthritis may have pathological gaits that favor one limb at the loading expense of the other. Other patients with cerebral palsy or Down's Syndrome, as well as those recovering from surgery, may benefit from gait training at partial weightbearing levels to improve neuromuscular control.

Jorgensen et al. (2000) examined hemiparetic stroke patients relearning how to walk and found that the degree of asymmetrical weight bearing correlated with BMD losses in the lower femoral neck of the paretic leg. Because peak external joint moments at the hip during walking and jogging can explain up to 40% of the variance in BMD for normal healthy adults (Moisio, 2004), these asymmetries are likely candidates for bone loss investigations.

Similarly, patients with osteoarthritis tend to adjust their gait so as to minimize rotational moments at the diseased joint, showing decrements in dynamic hip range of motion, peak adduction, and peak external rotation moments, as well as BMD losses in the greater trochanter (Hurwitz, 1998). Quantifying these loads may provide a point of comparison for partial gravity environments.

With training, patients may even be able to reproducibly match target loading levels with assistive devices. Kotajarvi (2003) and Youdas et al. (2005) examined ground reaction forces in healthy volunteers under three-point partial weight bearing

locomotion using conventional assistive devices, and found that training loads were best reproduced with axillary and forearm crutches, with underestimation of actual loads using wheeled walkers and canes. Reproducing vertical ground reaction forces in crutch walking is most accurate at intermediate levels of support ($\sim$ 50%; Li, 2001), suggesting that Mars simulation of this parameter may be possible.

While complicated by disease states and other factors, some human studies of chronic partial weightbearing might be accomplished in a more typical clinical setting. Load calibration and measurement pose the greatest technical challenges.

3.1.7 Animal Partial Weight Suspension

To the best of our knowledge, Schultheis et al. were the first, and thus far only, to attempt prolonged partial weightbearing experiments in mammals (Schultheis, 2000b, 2001). They exposed 3-month-old female rats to a combination of full hindlimb suspension and active feedback control of forelimb loading, such that the loads borne by the front paws were maintained at 50% of normal for 5 weeks.

These investigations showed significant decreases in forelimb trabecular bone density, collagen, and proteoglycan concentrations; as well as a significant increase in serum osteocalcin; but no changes in histomorphometric or mechanical properties, serum vitamin D levels, or urine catecholamine levels. Interventions with the bisphosphonate ibandronate, or passive mechanical loading applied at 3 Hz for 2 hrs/day were sufficient to maintain all parameters near the level of control (i.e., fully loaded) animals.

Interestingly, in more mature female rats (5 months), 50% weightbearing was sufficient to preserve cortical bone, but not trabecular bone. The efficacy of both ibandronate and 3-Hz countermeasures in maintaining trabecular structure and strength was reduced in this group (Schultheis, 2000a). These results are consistent with reduced levels of turnover, but require further investigation.

Interestingly, while the loads provided to the forelimbs in this model were half of that expected in 1-g, the hindlimbs were fully suspended. It has been suggested that models of limb unloading lead to an underestimation of bone loss, due to the prevailing

systemic trends of normal loading (Jee, 1991). Likewise, the Schultheis model may overestimate load-dependent changes in the forelimbs, due to the extensive unloading elsewhere in the rat. Certainly, quantitative analysis of systemic markers is challenged by such a mixed milieu. A more ideal model would provide for consistent changes in loading across the animal's body.

These first chronic studies conducted at partial weightbearing suggest that 50% is insufficient to wholly prevent bone losses. Comparisons with other weightbearing regimes are necessary to develop a more comprehensive understanding of the relationship between loading and skeletal adaptation. Importantly, the active control mechanisms used to enable frequency-tuned partial loading in these investigations significantly complicated the design, manufacture, operation and maintenance of the suspension system. Future work would benefit greatly from a simplified, passive suspension mechanism.

3.1.8 Conclusions from Existing Data

Ultimately, every data set across the gravitational continuum has its own limitations when making predictions of actual adaptation to partial gravity. Microgravity studies couple the extreme effects of complete unloading with the stresses of spaceflight. Tail suspension models are likewise imperfect and limit animal mobility and activity. Hypergravity studies induce changes in metabolic rate and endocrine function that couple to affect musculoskeletal metrics. In all cases, muscle atrophy and hypertrophy will affect skeletal loading, as will changes in neuromuscular activation, soft tissue characteristics, gait, activity levels, etc.. From this body of research, no clear recommendations spring forth; however, a few overarching statements appear worthy of consideration:

1. The longest true partial gravity experiments to date in humans, or any other mammalian model, are the 1–3 day stays on the lunar surface made by the Apollo astronauts. Unfortunately, there is a paucity of relevant musculoskeletal data available from these flights, due at least in part to the incredibly short

duration of their stay and its close proximity on either end of the missions to longer periods of microgravity transit. The comparison of data from those astronauts who walked on the lunar surface with that of the command module pilot may be instructive.

2. Multiple papers suggest a minimal gravitational level of around 0.3-g for supporting normal behavioral patterns and functional activity in a variety of physiological systems. Most of the evidence supporting this claim, however, is qualitative or anecdotal. Additional quantitative physiological studies of adaptation to extended exposures are still required to support such claims.

3. While chronic flight centrifuges offer a versatile platform for multi-acceleration studies, they have yet to be put to significant use in the service of physiology research beyond single cellular organisms, plants, and fruit flies. In these simpler models, however, there is a clear threshold effect between 0.1- and 0.3-g, below which responses to gravitational accelerations are not evident. It is reasonable to postulate that a similar type of threshold may well exist in the more complex musculoskeletal systems of mammals.

4. Head-up tilt bedrest provides a useful model for examining the fluid shifts expected in partial gravity, and the accompanying cardiovascular and endocrine responses to such shifts. The exact form of hypodynamia, however, does not provide an accurate representation of partial gravity loads on the musculoskeletal system.

5. Partial weight suspension in rodents offers a promising window on both skeletal adaptation to partial weight bearing and countermeasure development. Initial studies suggest that 50% loading helps maintain molecular and tissue level bone properties as compared to complete unloading, but that such loads will be insufficient to wholly prevent bone losses.

6. Partial weight bearing has salient clinical importance both in acute gait rehabilitation and in the more chronic implications of various pathologic or assisted

gait dynamics. The reduction in peak vertical GRF that accompanies these gaits have been shown to reduce BMD, and further analysis of a chronic cohort may yield some valuable insights.

3.2 Modeling Skeletal Adaptation Across the Gravitational Continuum

Given these scattered data points, multiple conflicting theories have been put forth in the literature regarding the nature of physiological responses expected between microgravity and 1-g. Data from extended bed rest studies suggests that reductions in bone density following full unloading should not exceed -40% (Jiang, 2006). Each of the models below describes a different curve for steady state BMD, relative to g-level, as seen in Figure 3-1.

1. Phillips (2002) and Pace et al. (1985) suggested an approximate linear relationship along the heart of the continuum, citing morphological, biochemical, and functional evidence from microgravity and hypergravity studies at 2–3-g in a variety of physiological systems. While there are indeed strong relationships in hypergravity, however, it seems unlikely that mechanosensors will behave linearly all the way down to zero input, especially as other physiological sensors, such as retinal photosensors, olfactory bulbs, and tactile pressure sensors, display definite threshold effects.

   Motufar-Solis and Duke (1999) examined tibial growth plates from Spacelab-3, Cosmos 1887 and 2044, tail suspension, and 2-g ground centrifuge studies and observed that chondrocytes responded to accelerations in accordance with Hert's curve, whereby small increases in loading lead to greater growth and small decrements lead to decreased growth, but large changes away from the baseline loading profile in either direction lead to reduced growth plate activity. Based on the accumulated evidence, a linear change seems unlikely, at least at very low g-levels.

2. Schultheis (1991) drew predominantly on the mechanostat theory described in Section 2.2 to suggest a relationship driven by the error between physiological exposure and a given mechanical setpoint. Consistent with the theory, extraphysiologic strains in this model had to be above an upper setpoint ($> 2,500\mu$strain) to cause modeling and below a lower setpoint ($< 200\mu$strain) to trigger remodeling activity.

   Peterman et al. (2001) measured tibial strains during simulated partial-g walking and showed that maximal principal strains in a given location on the bone were linearly related to the simulated gravity level. Because strains due to bending are negligible near the neutral axis of the bone, greatest variation and remodeling would be expected orthogonal to this axis. Experimental evidence suggested maximum principal strains (ϵ) on the anterior tibial crest at the peak generation of stance forces would be:

$$\epsilon = 850g + 238 \tag{3.1}$$

   With mean values of:

$$\epsilon = 390g + 213 \tag{3.2}$$

   Given that peak strains on Mars in this model are predicted to be within 7% of mean strains experienced on Earth, it is possible that this mechanical environment would not be pro-resorptive at the periosteal surface of the bone. However, in accordance with beam bending theory, strain varies linearly with distance from the neutral axis of bending. This axis is perpendicular to the applied loads and passes through the object's centroid, leading to maximum (tensional) strains on one surface of the beam, and minimum (compressional) strains on the opposing surface. Thus, the magnitude of the strain stimulus at the endosteal surface of a bone would be substantially reduced relative to the periosteal surface.

   Schultheis assumed that remodeling in any bone is induced below 200 μstrain.

If this prediction holds at the endosteal surface, the model predicts regional bone losses at Mars loading of approximately 5% and suggests a minimum g-level of 0.43-g to prevent losses. Clearly these numbers are highly sensitive to the assumed resorptive threshold, and further experimental evidence would be necessary to select a more appropriate local threshold value.

3. Keller and Strauss (1993) used non-parametric modeling based on existing literature to predict the relationship between gravity and bone mineral density. They worked with four key assumptions: (1) Young's modulus is proportional to density cubed, (2) activity levels are related to bone mineral content within certain limits, (3) even weakened bone structures retain of margin of safety, and (4) bone strength is proportional to density squared.

   These assumptions resulted in a model that predicted equilibrium bone mineral density proportional to the level of gravitational acceleration, g, raised to the 2/7 power:

$$\Delta BMD \propto \left(1 - g^{2/7}\right) \tag{3.3}$$

   This suggests limits as g approaches zero. For $g = 0.38$, bone loss at equilibrium is predicted to be about 10% of Earth values.

4. Whalen (1993) similarly modeled changes in bone mineral density as related to musculoskeletal loading, such that

$$BMD \propto \sqrt[8]{\sum (GRFz_i^4)} \tag{3.4}$$

   where GRFz_i represents the individual peak forces acting on bone throughout its daily loading, and the summation integrates across this history. Estimates are given for Earth as 4000 cycles at 1.2 times body weight (BW), 1800 cycles at 2.42 BW. Given the Peterman data above, Mars loads might be anticipated as 0.38 times Earth normal.

   Interestingly, Whalen also estimated the loads anticipated from treadmill exercise with 70% gravity replacement loads, as used on Space Station: 1600 cycles

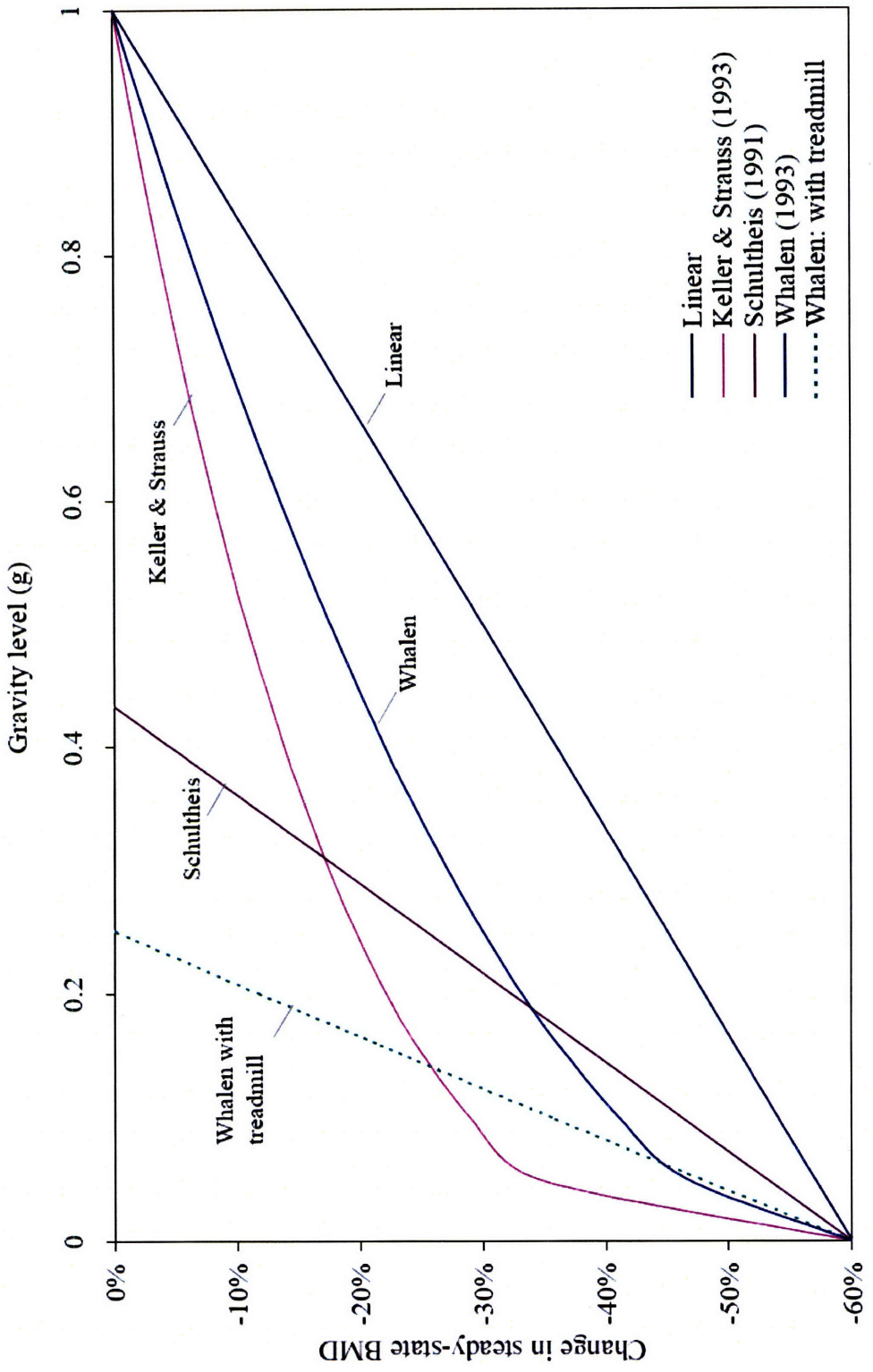

Figure 3-1: Models of skeletal adaptation to partial gravity. Steady-state losses of femoral BMD at varying g-levels are predicted by a variety of models in the literature.

at 0.85 BW and 3200 cycles at 1.84 BW. If such a treadmill were taken to Mars, the bungee loading would enable astronauts to achieve true Earth-like exercise loads. Substituting these for the same fraction of daily loading as seen on Space Station (Peterman, 2001), one can predict full preservation of BMD. In a similar lunar mission, use of such a treadmill would prevent 40% of expected bone losses in the same model.

More recent data coming from Space Station better quantified lower body loading during treadmill exercise using a novel force measuring shoe insole (pre-publication data from Cavanagh, 2006). Walking loads peaked around 0.89 body weight (BW), compared to 1.20 BW on Earth. Running loads showed an even steeper reduction of 1.30 BW versus 2.36 BW in Earth running. Pushing the current hardware to its limits of comfort provided a 29% increase relative to these typical loads, reaching 1.73 BW during running. These numbers suggest overestimation by Whalen.

However, a new shoulder-and-waist harness designed to provide more Earth-like ground reaction forces on the Space Station treadmill was recently demonstrated (Genc, 2006). Running on a ground-based microgravity simulator showed peak forces and rate of change of forces comparable to normal 1-g loads, and the level of comfort was reasonably well tolerated. Such an advance could enable full gravity replacement loads for lunar exercise and even greater preservation at low g-levels than proposed in Figure 3-1.

Together, these models span a wide range of predicted values. Mars adaptation may equilibrate at values from -5 to -25% of Earth-normal, as compared with 40% losses in microgravity. With bungee-assisted treadmill exercise, bone density may even be fully preserved. Lunar adaptation may reach steady-state losses anywhere from -16 to -34% of Earth BMD, without gravity replacement.

Compared to predicted microgravity bone losses, these boundaries predicted by models of partial gravity adaptation represent a more promising future for astronaut explorers. However, without any significant ground or flight data upon which to verify

these predictions, the level of uncertainty is still substantial. Chapter 4 describes a novel passive partial weight suspension system designed to support rodent ground studies of adaptation and countermeasure development for such environments.

Chapter 4

Partial Weight Suspension Hardware and Validation

As described in the last chapter, various passive models of partial weightbearing have been used in human locomotion and energetics research. The habitats designed for this thesis draw on the design elements developed in that field, coupling them with lessons learned over three decades of rodent suspension. This chapter describes the Partial Weight Suspension (PWS) hardware and tests used to validate its function. All protocols for these studies were approved by the Institutional Animal Care and Use Committee (IACUC) at MIT. The 2006 renewal of Protocol 0906-104-09 is included in Appendix B. Hardware design details are included in Appendix C.

4.1 Partial Weight Suspension Design Considerations

Design goals for the PWS system were to:

- Support adult mice (16–36g) in hypodynamic loading for periods of up to 5 weeks;
- Be tunable to within ±5% of a desired hypodynamic load level between 10% and 80% weightbearing;

- Provide an environment that is not more stressful than controls;
- Support normal movement, cleaning, and feeding; and
- Allow for full recovery to facilitate reloading studies.

4.1.1 PWS Habitat

Mice are singly housed in specially developed habitats derived from designs of NASA Ames Research Center and Cornell University (Morey-Holton, 2002). The living volumes, as illustrated in Figure 4-1, are polycarbonate open cubes, with four 12" x 12" (30.5 cm x 30.5 cm) walls joined at the corners using acrylic solvent. Triangular wooden feet with grooves for the walls support the box as well as a removable perforated PVC floor (92985T22 PVC Perforated Sheet, 3/16" (4.8 mm) thick, 3/16" hole diameter (4.8 mm), 32% open area, McMaster-Carr, Princeton, NJ), which passively minimizes waste buildup. An absorbent paper wipe is situated below the floor and exchanged weekly for sanitation purposes.

The habitat ceilings are made of the same perforated PVC material as the floor and are attached with plastic hinges (1588A721 Harsh Environment Plastic Piano Hinge, McMaster-Carr). A central aluminum channel supported by cutouts in the side walls provides a rigid base for suspension hardware (Figure 1). Hanging from this aluminum channel, a 1/8" (3.2 mm) steel rod supports a custom-milled nylon wheel with a 1/8" (3.2 mm) diameter groove and a low-friction bearing (R144 miniature ball bearing, ESI Bearing Distribution, Tujunga, CA) to provide one linear degree of freedom for the suspended animals. Axles are made from 1/8" (3.2 mm) steel rod sanded on a lathe for appropriate slip-fit with the bearing.

4.1.2 Suspension

A full-body suspension design was developed around the traditional tail suspension model used in hindlimb unloading. While back suspension with attached aluminum braces have been shown to be stressful for growing rats (Wronski, 1987), Musacchia

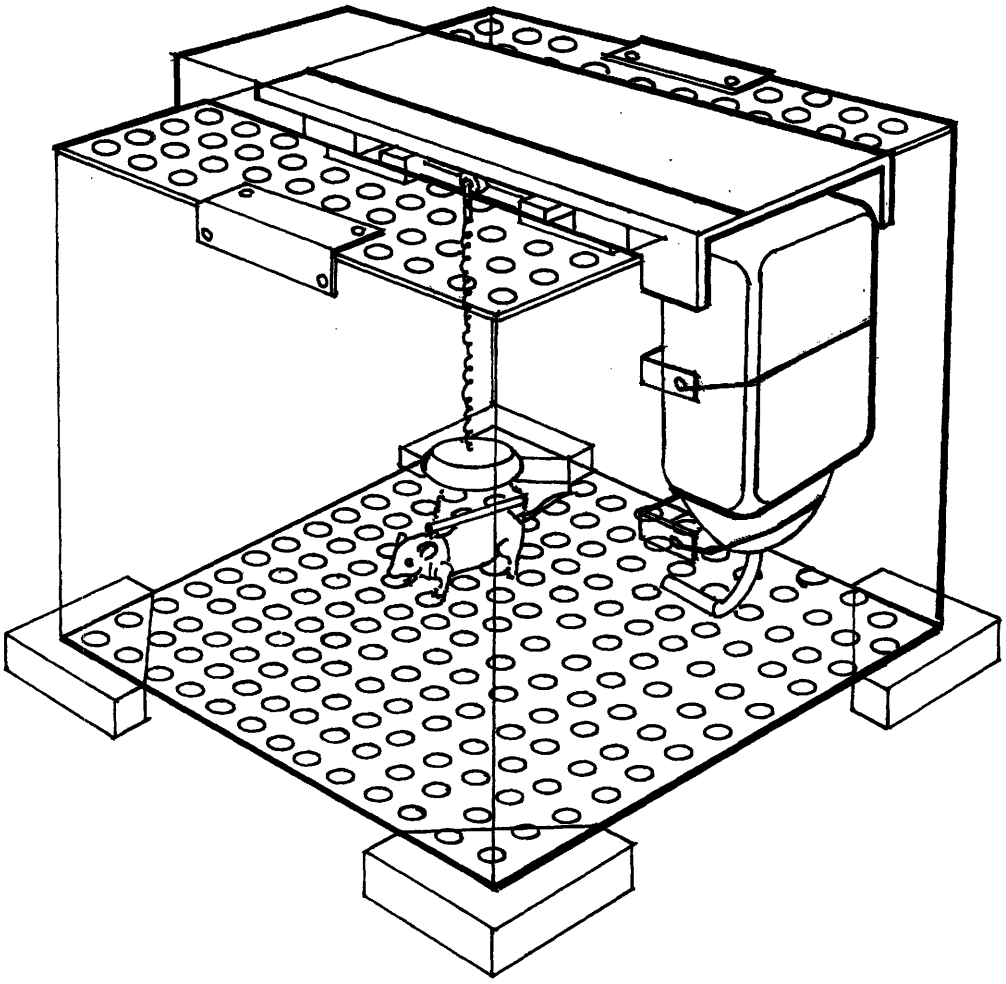

Figure 4-1: Partial Weight Suspension habitat with polycarbonate walls, perforated PVC floor and lid, and aluminum channel supporting suspension hardware. Note that holes in this drawing are oversized. Actual openings are 4.8 mm in diameter and allow for passive passage of waste without risk of injury to the animals. *(Image Credit: Shaun Modi)*

and colleagues made repeated successful use of a fabric body harness in their studies of muscular hypokinesia and hypodynamia in growing rats (Musacchia, 1980, 1992; Steffen, 1987). Supporting mice in full-body suspension with all four paws on the ground helps preserve normal gait characteristics and loading patterns.

Hindlimb support is provided by a tail wrap based on those used in previous tail suspension studies. The tail is prepared with 70% isopropyl alcohol and tincture of benzoin spray. A "second-skin" bandage of Tegaderm or SteriStrip (3M, St. Paul, MN) is loosely wrapped at the base of the tail to prevent irritation, and a small piece of athletic tape (Johnson & Johnson, New Brunswick, NJ) is wrapped around this layer and secured to the harness.

The forelimbs are supported by a flexible, breathable "jacket." The two-piece jacket, made of athletic tape and soft moleskin, is secured by velcro under isoflurane anesthesia. Several pilot studies resulted in the optimization of the jacket design, allowing the jacketed mice movement and flexibility comparable to that of unjacketed control animals. A two-piece velcro-fit design allows for adjustments to accommodate small body mass differences between mice. As seen in Figure 4-2, the harness and tail wrap are connected by an adjustable bead chain and spaced by a hollow metal rod to distribute loading.

Titrated suspension is accomplished with a low-modulus plastic-coated spring (k$\approx$ 1.6 N/m; S0101 coil cord, Statico, San Carlos, CA). Twisting the spring through its support engages a variable number of coils, N, thereby changing the spring constant proportional to $1/N$. Small swivels (Laker Fishing Tackle Co., Camdenton, MO) prevent spring bind-up, and a plastic lid secured above the animal inhibits climbing. A small orthodontic rubber band (JAW Products, Cinnaminson, NJ) wrapped around the spring where it connects to the top-running wheel minimizes overnight deviations in spring length and tension by preventing slipping.

4.1.3 Animal Care

Free access to water is provided for all animals, using standard laboratory bottles mounted to the outside of the habitat with bent sipper tubes protruding through a

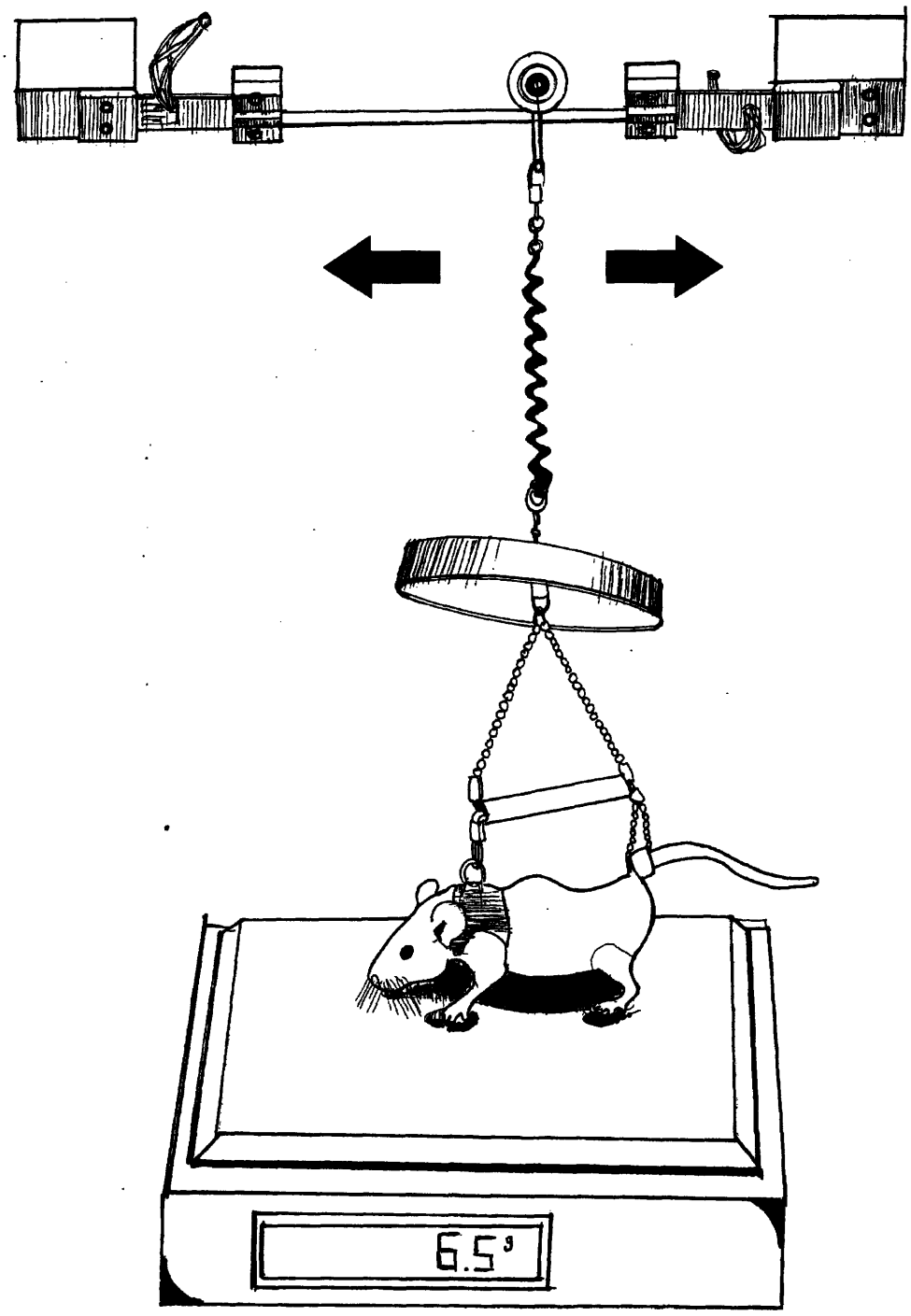

Figure 4-2: System for measuring effective body mass. Animals are suspended above a scale and spring tension is adjusted to provide the desired level of partial weight-bearing. *(Image Credit: Shaun Modi)*

hole in the side wall (Figure 4-1). Food pellets (LabDiet 5P00 Prolab RMH 3000, PMI Nutrition, Richmond, IN) are weighed daily and provided on the floor of the habitat. Any residual stock remaining in the habitat the next day is weighed and discarded.

Daily weighing of suspended animals quantifies the static loads experienced during quiet standing. Full body masses are first obtained by briefly hanging the animal on a rig positioned over a lab animal scale, so as to avoid full weightbearing. Titrated weightbearing, expressed throughout as *effective* body mass, is then measured with the animal standing in suspension on the same scale (Figure 4-2). Adjustments to spring tension are made as necessary to accommodate changes in body mass and spring stiffness.

Large fluctuations in daily mass ($\geq$ 1 gram) usually suggest some degree of illness or poor adaptation of the mice. To minimize discomfort, animals are checked daily for tail irritation around the site of the wrap, chafing around the jacket armholes, and signs of proper hydration (skin flexibility, water bottle function, etc.). Mice are removed from the studies if persistent wounds are noted, or if discomfort significantly alters movement or inhibits normal behavior. Tail wraps are removed and replaced if their integrity becomes compromised by animal chewing or other wear.

The 10–13 week old mice used in these investigation do not present problems of rapid growth, which would necessitate the refitting of harnesses throughout the experiment. A variety of pilot studies have demonstrated that the habitat, feeding, water delivery, and animal care methods provide sufficient standard of care for daily animal activities. Mice have been maintained in harnesses for up to six weeks at full weightbearing, and at 16–38% weightbearing suspension for up to four weeks, with no significant visible adverse effects.

4.1.4 Components of Tension Force

Given that tension developed by the spring element of the suspension tether is linear with displacement, deviation from the central transit rod results in greater total spring force. Contours of equivalent tension exist throughout the cage area, equidistant from

the rod. Resolving this force into horizontal and vertical components, the variation in spring force incurred as the animal moves about the cage may be mapped (Figures 4-3 and 4-4).

Observation indicated that animals spent the vast majority of their time along the center axis of the cage, and rarely ventured more than about 7 cm from this zone.

4.2 Validation Studies

4.2.1 Basic Care and Feeding

Pilot studies of jacketed animals in the PWS habitats were conducted for periods of up to six weeks to observe reactions to the hardware. Multiple studies from one day to four weeks were run with animals in suspension at 16–70% weightbearing levels. Based on observations, animal escape rates, and wear patterns, at least nine different jacket configurations were tested before settling on the current design for the tests described in Chapter 5.

Ad libitum access to food pellets above a perforated floor does not allow for true quantification of food consumption, but rather what is termed *food usage.* All animals evidence patterns of significant wasted food, which falls through the perforated floor. Due to mixing with fecal and nesting materials, such losses were not quantified in this study. However, no large differences in crumbling patterns were noticeable between experimental groups.

Partial weightbearing SUSPENSION animals were found to consume less food on average than their full weightbearing JACKET controls, at least for the first week of the experiment. In an attempt to minimize differences in body mass between SUSPENSION and JACKET groups, JACKET animals were fed according to the SUSPENSION group's mean food usage from the previous day. Due to the caloric restriction caused by lower consumption in the SUSPENSION group, JACKET animals nearly always consumed the full ration of food provided to them.

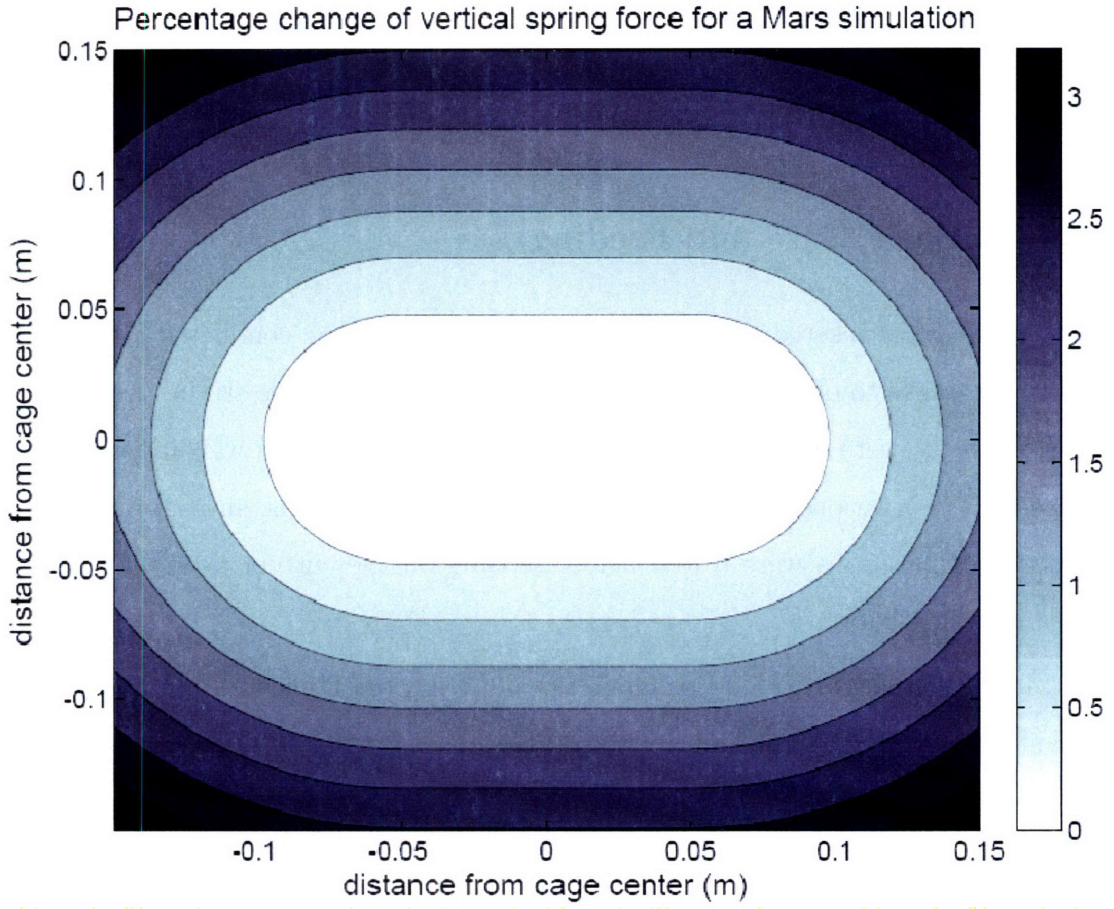

Figure 4-3: Percent change in vertical suspension force due to mouse position in the cage. Due to the low friction wheels and bearing used, motion along the central rod is assumed to support no significant horizontal loads.

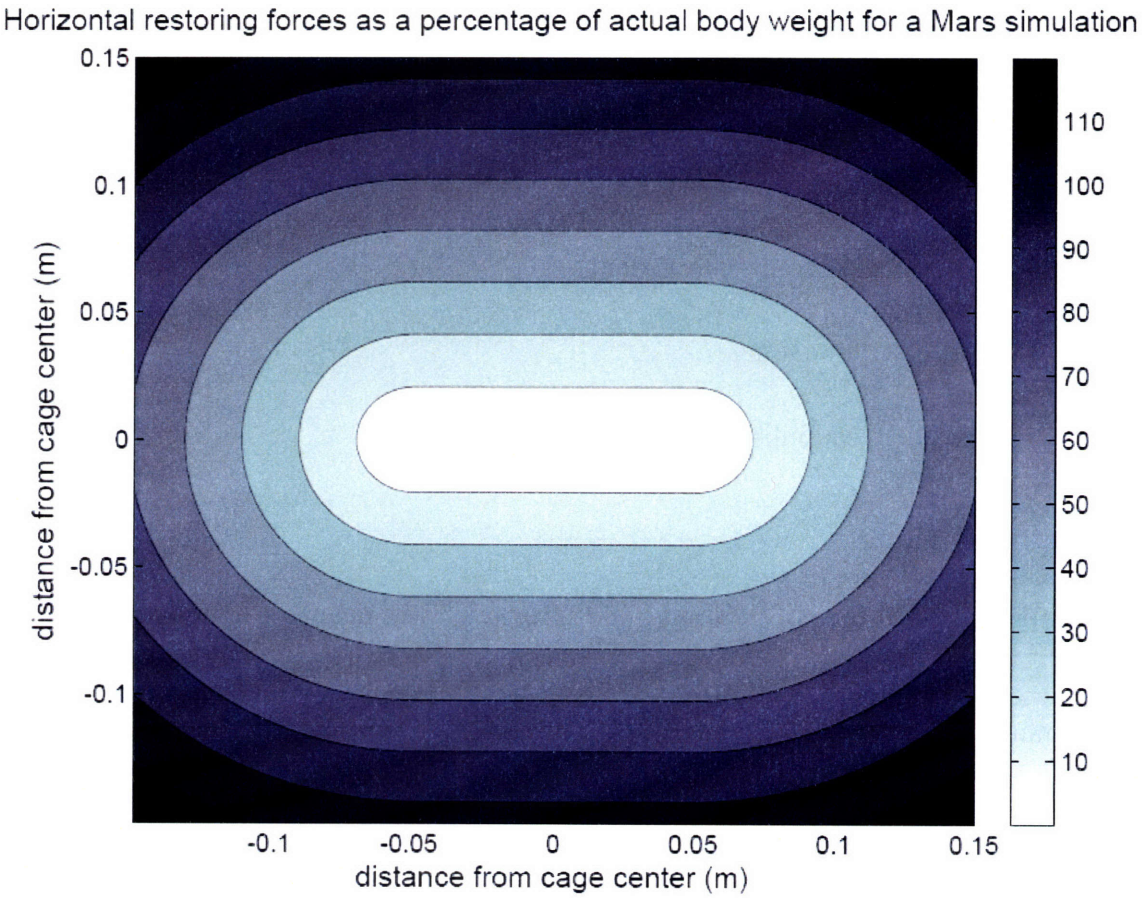

Figure 4-4: Horizontal restoring forces acting on the mouse due to position in the cage, given as a function of true body weight.

4.2.2 Load Measurement

A model for examining the effects of partial gravity exposure must replicate the key mechanical features of the expected dynamic loading, including reductions in peak loads and loading rates. Our unique quadrupedal unloading model allows for these stresses and strains to be measured during normal locomotion.

That the mechanical loading environment actually provides expected reductions in ground reaction forces and *in vivo* tibial strains has been confirmed through the following methods:

- Daily weighing
- Suspension force measurement
- *In vivo* strain gaging
- DigiGait treadmill-based gait analysis

Daily weighing

As described above, both actual and effective body masses were examined daily in each of our studies. Effective masses were set within ± 0.5 grams of the desired stimulus by adjusting suspension tension, giving a variability approximately 2.5% of total body mass. Between subsequent daily measures, there was often a small change in effective body mass, due primarily to changes in actual body mass, animal posture changes, or creep and slippage of the spring element. Small rubber bands were added along the spring to minimize this latter effect.

Together with the variations outlined above due to animal motion around the habitat, these sources of error — static mass errors, overnight changes in spring tension, and mouse position within the habitat — suggest an average deviation of $\pm 4.5\%$ body mass, which is within the system design specifications outlined above.

Instrumented flexures were originally designed to measure changes in suspension forces using strain gages on steel shim stock in a double cantilever configuration (Figure 4-5). Due to calibration difficulties, the system was never used; however,

as the eventual implementation of the habitat was dependent on the design of this system, the design constraints highlighted in Figure 4-5 are summarized briefly in Table 4.1.

Treadmill Gait Analysis Pilot

In order to evaluate changes in gait due to the forelimb jackets and suspension, a pilot study was run on a DigiGait treadmill (MouseSpecifics Inc., Boston, MA; Hampton, 2004). Briefly, the system utilized a high-speed (80 fps) digital video camera mounted underneath a transparent treadmill belt. The mouse was placed in a 5 cm wide running compartment atop the treadmill, providing a ventral view to the camera. Lighting both underneath the treadmill and above the compartment illuminated the animal for video capture. Thresholding algorithms identified each paw as it hit the treadmill belt and calculated the area applied on a frame by frame basis, providing an estimate of force application versus time. Stride, stance, and swing duration were calculated from this signal. Braking phase was defined as the period of increasing paw area, and propulsion phase as the period of decreasing paw area. Treadmill speed divided by stride frequency yielded stride length.

Eleven mice were assigned randomly to one of three trial conditions:

- **NORMAL (n=3):** untreated animals
- **JACKETED (n=4):** animals acclimated to forelimb jackets as described above for a minimum of two days.
- **SUSPENSION (n=4):** jacketed animals under partial weight suspension, at a level of approximately 50% weight bearing.

Prior to treadmill testing, mice were acclimated to forelimb jackets or partial weight suspension for a minimum of two days. On the day of testing, animals were exposed to the treadmill compartment, then to increasing belt speeds, until they were able to sustain consecutive running strides at 14 cm/s for periods of at least 5 seconds. Gentle nudges with a plastic prod were used to keep the animal in the center of the

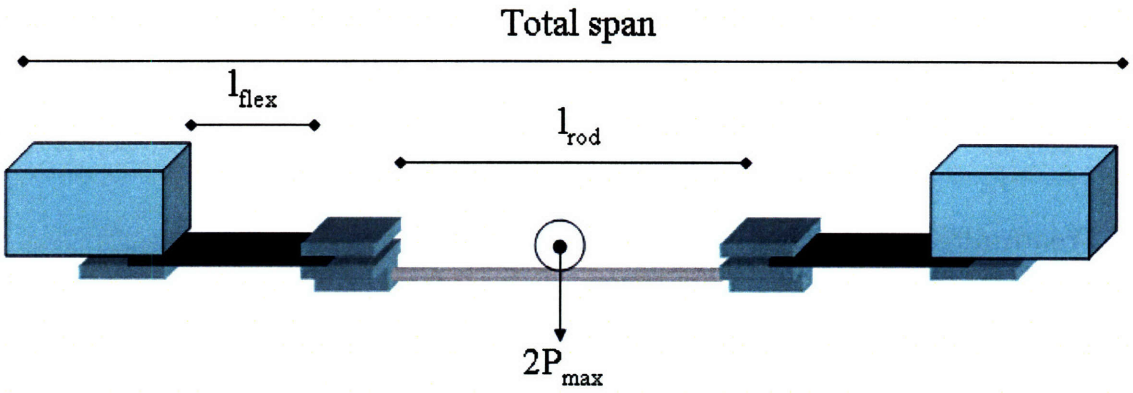

Figure 4-5: Cage-top transit rod and flexures. System design parameters were selected to balance animal freedom of motion, registration of strains in the region of the flexures, and overall system stiffness.

Table 4.1: Design parameters for the transit rod and flexure system. Calculations from Heglund, 1981 and Biewener, 1992. Young's modulus for both steel rod and flexures is taken as 200 GPa.

Parameter	Value	Justification
Total span	30.5 cm	Constrained by habitat volume
Transit rod size, d_{rod}, l_{rod}	3.2 mm diameter, 10 cm long	Allows maximal use of cage width while restricting weightbearing on end walls and assuring that bending occurs primarily in the flexures Spring constant, $k_{rod} = 0.75\pi E d^4 / l_{rod}^3 = 4940$ kN/m
Flexure length, l_flex	32 mm	Constrained by cage size, transit rod, and connector hardware Spring constant, $k_{flex} = 0.5 E b h^3 / l_{flex}^3 = 2.42$ kN/m
Flexure breadth, b	12.7 mm	Accommodates two side-by-side strain gages, and constrains bending primarily to the plane of interest $b/h > 7$
Flexure thickness, h	0.25 mm	Prevents yielding at max loads while constraining bending primarily to the plane of interest and enabling measurement of minimum expected strains $h \geq \sqrt{6 P_{max} l / b \sigma_y}$
Maximum load, $2P_{max}$	1.66 N	Driven by yield strength of steel flexures, $\sigma_y \approx 200$ MPa $P_{max} = h^2 b \sigma_y / 6 l_{flex}$

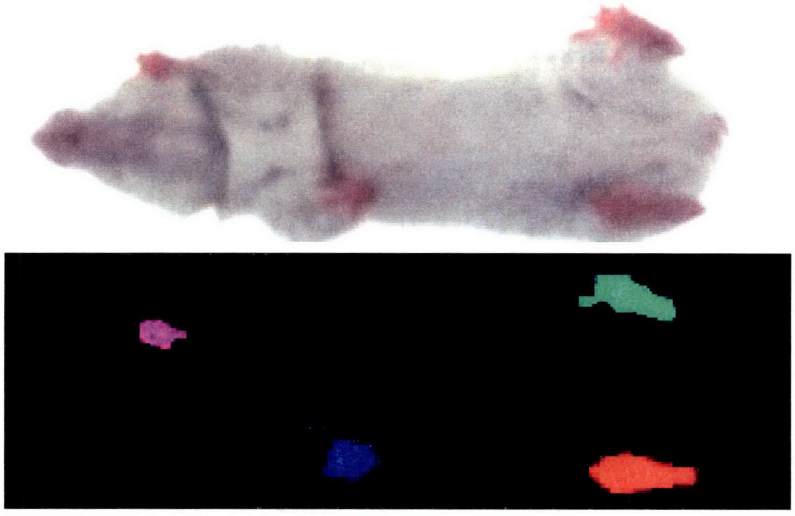

Figure 4-6: Ventral view of a mouse through the clear DigiGait treadmill belt and paw images as extracted by image thresholding software. Paw area in contact with the belt was calculated on a frame-by-frame basis to determine basic gait parameters.

filming chamber. A minimum of seven sequential strides, including both forelimb and hindlimb footfalls, were collected for processing from each animal.

Pairwise differences between groups were evaluated using a two-tailed Student's t-test with assumption of equal variance. Significant differences were taken as $p < 0.05$.

Force Platform

As discussed earlier, dynamic forces, rather than static ones, are key to skeletal maintenance. While daily weighing quantified average static loads under suspension, a more advanced measure was needed to quantify the dynamic load environment. A high-precision force plate (HE-6x6-1 AccuSway Force Plate, AMTI Measurements Inc., Watertown, MA) was used to measure ground reaction forces (GRF) during active locomotion.

The AccuSway plate uses Hall-effect sensors to quantify forces and moments along 3-axes. The system can measure vertical loads up to 4.9 N, and loads in the horizontal plane up to 2.45 N, with a nominal resolution of 0.0025 N. To minimize transmission of disturbances, the plate was mounted to a thick aluminum base (15.2 x 45.8 x 1.3 cm) with foam foot pads to help isolate the system.

Forces in the three dimensions (GRFx, GRFy, GRFz) were collected at an acquisition rate of 200 Hz using AMTI's proprietary NetForce software. Calibration of GRFz was accomplished with static masses from 1–50 grams. Measurements of 5 seconds duration were made in triplicate, with a "hardware zero" and software tare between each acquisition. Data from all three runs for each mass were averaged in Excel and a best fit linear trendline was added. R^2 values were typically better than 0.99, suggesting a high degree of linearity and precision. Variations were consistent with previous findings (Zumwalt, 2006), with standard deviations between 2 and 5% from the mean across the range of interest.

Power spectral density for these static signals was analyzed in MATLAB (The Mathworks, Inc., Natick, MA). As expected, the majority of signal was below 1 Hz. Given that mouse locomotor signals are typically composed of frequencies below 25 Hz (Zumwalt, 2006), signals from gait tests were filtered with a two-pole, low-pass Butterworth filter with a corner frequency of 25 Hz (MATLAB *filter* routine).

For collection of locomotor loads, a plywood platform was built over the plate to provide a level walking surface, with a 2 cm wide strip of plywood atop the force plate as a local load sensor, as described by Zumwalt et al. (2006). The plywood was covered with cloth tape to improve traction, and the mice were allowed to locomote freely over the surface (Figure 4-7).

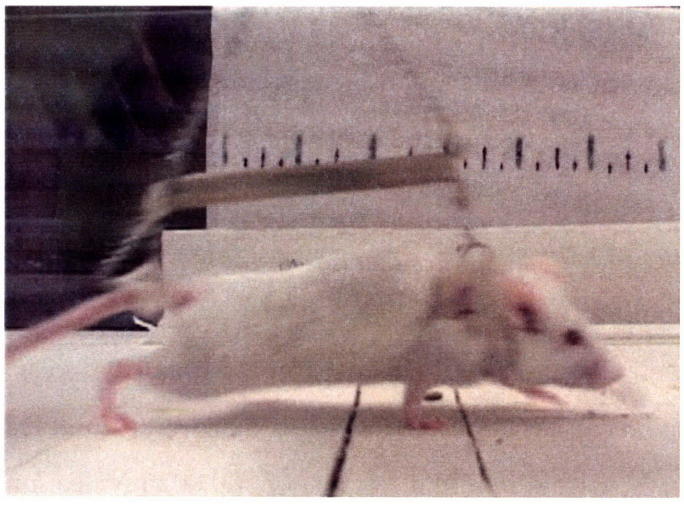

Figure 4-7: Mouse at 38% weightbearing making footfall on the AMTI force plate.

For validation, adult female BALB mice were walked across the plate with and without forelimb jackets, and under partial weight suspension at 16%, 38%, and/or 60% weightbearing.

Sequential recordings were made, each up to 3 minutes at a time. Traces were selected for analysis whenever a single forelimb made unobstructed contact with the local load sensor strip. In most cases, this first forelimb footfall was immediately followed by the ipsilateral hindlimb. Hardware zero and software tare were applied between runs, at least once every 3 minutes to reduce error due to drift.

All evaluated impacts were confirmed with video footage. The data in Section 4.3.3 below was gathered from a single animal for internal consistency, and included pairs of footfalls from normal gait ($n = 4$), jacketed gait ($n = 5$), 60% weightbearing suspension ($n = 4$), and 38% weightbearing suspension ($n = 4$).

Peak forces were obtained in the X (nose-to-tail), Y (medio-lateral), and Z (vertical) directions. Ratios of the peak transverse forces to forces in the vertical direction were also calculated. The rate of force onset was estimated as the slope of the initial portion of the GRF rise. Stance duration and area under the curve were also calculated.

In Vivo Strain Gaging

Regardless of ground reaction forces, if gait kinematics of propagation of loads change substantially, the strain environment of the long bones is unlikely to remain the same. Given that material deformation is believed to be the proximal stimulus to osteogenesis and remodeling, *in vivo* strains were measured at the tibial periosteal surface, under a variety of loading conditions.

Axial strain gages were mounted to the tibial surface, as described below. Deformation of the bone to which these gages were bonded caused a corresponding change in gage resistance, ΔR. Measuring a simple voltage drop across such a gage would yield a change in voltage, ΔV, directly proportional to ΔR. For the small changes associated with small strains, however, this output is better amplified using a Wheatstone bridge configuration.

Assuming a similar change in resistance for gages under similar degrees of tension and compression, the output voltage, V_o, for a bridge with three static resistors of resistance, R, and one active gage with resistance R$\pm\Delta$R, would scale with input voltage, V_i, as:

$$\frac{V_o}{V_i} = \frac{(\Delta R)}{(4R + 2\Delta R)} \tag{4.1}$$

Which for ΔR $\ll$ R, equals approximately:

$$V_o = V_i \frac{\Delta R}{4R} \tag{4.2}$$

Briefly, UFLK-1-11-1L single element strain gages (1 mm x 0.7 mm gage element, 120 Ω, TML Gages, Japan) with Teflon-coated lead wires (36 AWG CZ-1174, Cooner Wire, Chatsworth, CA) and silicone waterproofing (M-COAT C, Vishay Micro-Measurements, Malvern, PA) were implanted on the anterior-medial surface of the left tibia, using a procedure modified from Judex (1997) and learned in his laboratory. Data collection during both suspended and un-suspended locomotion quantified tibial surface strains.

Buprenorphine (0.1–0.2 mg/kg, SC) was administered before the procedure for analgesia. Mice were anesthetized with isoflurane using a precision vaporizer (1–4% to effect). Ointment was applied to the eyes (Puralube, Pharmaderm Animal Health, Melville, NY) to prevent them from drying under anesthesia.

The hindlimb was shaved and cleansed with betadine scrub, isopropyl alcohol, and betadine wash. Under aseptic conditions, the anterio-medial aspect of the proximal tibia was exposed with minimal musculoskeletal disruption. A scalpel blade was used to remove residual tissues and periosteal surface to prepare for gage seating. A cotton swab with $<$ 0.5 ml of chloroform was used to cleanse the site and the back of the gage of fatty acids, and a second swab of water followed to prevent local desiccation or unnecessary exposure. A suture was advanced behind the posterior surface of the tibia, taking care to minimize damage to surrounding musculature. The suture was tied off to two flanking supports to provide a reaction force behind the bone during

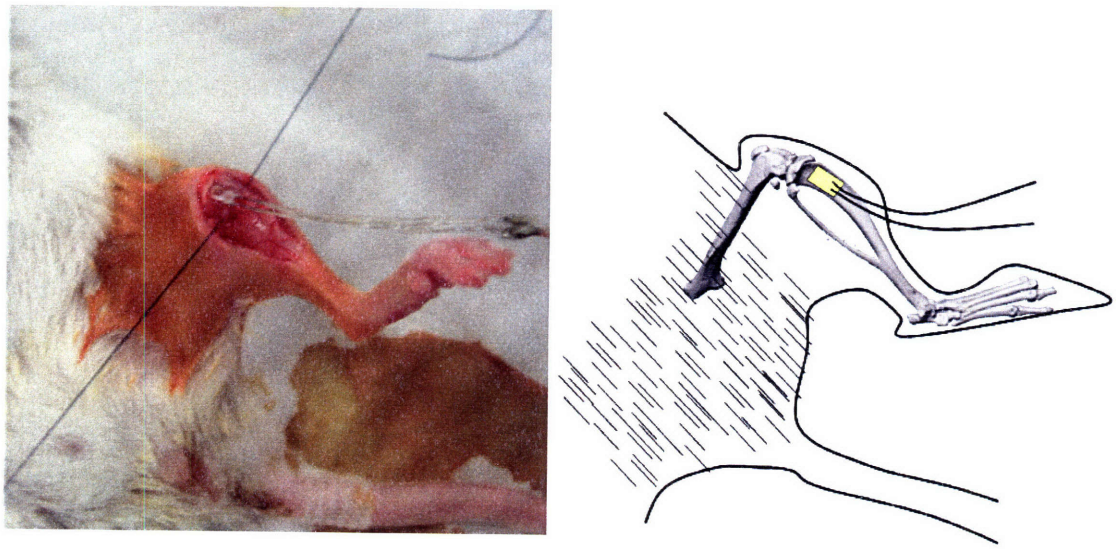

Figure 4-8: Surgical implantation of an *in vivo* strain gage on the left hindlimb. After local sterilization with betadine, a single element gage was applied to the anterio-medial aspect of the proximal tibia. Strains were measured under a variety of standing and locomotor conditions.

gage placement. Cyanoacrylate adhesive and 20–30 seconds of steady pressure were used to secure the sensor in place (Figure 4-8), and the wound was closed with a short run of continuous sutures.

To prevent animal disruption of the lead wires, small incisions were made at the posterior hip and nape of the neck. Wires were tunneled under the loose skin of the back with the aid of a sterilized plastic tube (5553K24 Tygon Tubing, McMaster-Carr), and exteriorized out of reach of chewing by the animals. The small inlet and outlet incisions were closed with cyanoacrylate adhesive, and a hot-bead sterilizer was used to sterilize instruments between animals.

The gage was connected via a shielded three-conductor cable (Mogami W2754-08, Marshall Electronics, El Segundo, CA) to a full Wheatstone bridge configuration with three 120Ω bridge completion resistors. Data collection and signal conditioning (gain=600) was provided by a DBK43A 8-Channel Strain Gage Module, with a Daqbook/216 16-bit Data Acquisition System (IOtech, Cleveland, OH).

Output from such a single-element bridge configuration is equal to $0.25 V_i GF * \epsilon$; thus, for a bridge excitation, V_i, of 5V, gage factor (GF) of 2.11 $[\frac{\Delta R/R}{\epsilon}]$, and V_{in} of 5 V, expected bridge output voltages were equal to 2.64 times the measured strain.

With 600-fold gain as applied by the data acquisition system, the final system output was 1583 times the measured strain.

The full procedure typically took approximately 40 minutes, and animals were usually fully ambulatory within 20 minutes after removal of anesthesia. Personal communication with Stefan Judex suggested that data should be collected within 48 hours of surgery, to ensure gage stability. Here, recordings took place under buprenorphine analgesic (0.1–0.2 mg/kg, sc) within 6 hours, followed by euthanasia via carbon dioxide immersion.

For the data presented in Section 4.3.4, one animal was adapted to suspension for two days before gage implantation. Bridge output was measured during locomotion under conditions of jacketed and unjacketed full-weightbearing, and with suspension at 16, 38, and 60% weightbearing. Zero load normalization was collected by lifting the animal's hindpaws fully off the ground. A series of measurements was also made during walking over the AccuSway force platformed described above. Video footage was used to align gage output with GRFz correlating with impacts of the instrumented hindpaw.

Multiple confirmed footfalls were acquired for each weightbearing condition (16% $n = 5$; 38% $n = 8$, 60% $n = 12$, JACK $n = 11$), along with quiet standing data. The loss of a leadwire prior to the completion of testing precluded data collection in unjacketed conditions.

For each footfall, peak to trough differences in strain and GRFz were calculated. Because the system was not "zeroed" between runs, these peaks represent changes in strain, rather than absolute strain values. The slope of the linear portion of the strain profile on each footfall was also calculated to estimate strain rate.

4.3 Validation Results

4.3.1 Basic Care

Following the first 4–6 hours of harness acclimation, no significant discomfort or distress were typically observed. Minor weight loss (typically $< 10\%$) was most likely to occur during the first 2–4 days of harness adjustment in control animals, so all JACKET and SUSPENSION animals were acclimated to the harness for 2 days prior to the start of the study. Pilot studies of up to one week at a variety of loads showed no evidence of sores, lesions, or other indicators of poor animal health. Animals readily consumed normal food pellets and water, with no need for wet, powdered food. After pilot studies of three weeks, a slight dermal thickening and redness was noticed where the arm contacted the top edge of the animal jacket, but no open wounds or noticeable gait abnormalities were typically observed. Arm holes were opened more widely, which improved the condition, but full resolution of the contact appears incompatible with jacket designs that prevent escape.

Minimal rectal bleeding was seen on occasion in some animals during the first 48 hours of suspension, but was self-resolving and non-repeating. Somewhat more troublesome was a tendency of some animals to scratch and chew at their tail wraps, causing superficial bleeding and abrasions. If necessary, this could be addressed in future studies with protector derived from a syringe barrel as described by Morey-Holton, et al. (2005).

The ability to set loads as desired was demonstrated, and stability of those regimes on a day-to-day basis was confirmed. In early pilot studies, the mean value of this deviation was 1.68 grams, or 6.3% of total body mass. Once rubber bands were added along the spring to prevent slippage, the average daily deviation in later studies was reduced to only 0.4 grams, or 2.0% of total body mass (Figure 4-9). Mice did occasionally chew through their tail wraps, resulting in periods of full weightbearing for the hindlimbs. These were always limited to less than 24 hours in length, but could be a significant stimulus for bone formation.

PVC tunnels with a central cut-out to allow passage of the suspension tether were

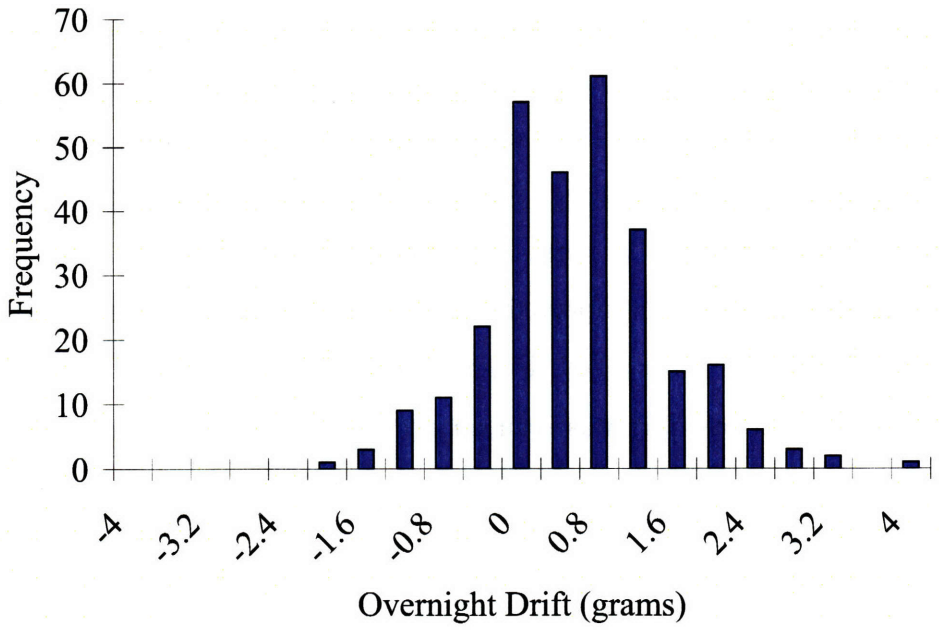

Figure 4-9: Histogram of overnight drift in effective body mass (mean=0.410 ± 0.937 grams). Two outliers caused by a hardware failure, which was remedied, have been removed.

initially added to the habitats as environmental enrichment for the animals. The mice repeatedly wedged themselves under the ledges for additional weightbearing, so this enhancement was replaced with cotton bedding squares.

4.3.2 Treadmill Gait Pilot Results

Data collected on the DigiGait treadmill (Table 4.2) suggests that jackets caused no significant changes in the percentage of time spent in swing and stance phases of locomotion, but did significantly shorten the duration and length of the gait cycle ($p < 0.05$). Adding suspension significantly lengthened the swing phase of gait in both the forelimbs and hindlimbs ($p < 0.05$) but did not significantly alter the total duration or length of the cycle compared to the jacket alone. Maximum paw area during stance phase was somewhat reduced in suspension, relative to controls ($p = 0.085$), but jackets also tended to reduce this value. Given that true ground reaction forces were not measured in this study, it is difficult to say what causes this effect. Visual inspection of the video suggests that the mice were still using all aspects of their paws for locomotion and not simply walking on their toes, as is seen in very low g-level human suspension simulations (Ivanenko, 2002).

Table 4.2: Kinematic data from treadmill pilot study locomotion analysis. Values are given as mean (std dev).

	NORMAL (n=3)	JACKET (n=4)	SUSPENSION (n=4)
Swing/Stride (%)	24.150 (2.975)	24.263 (2.995)	31.600 (8.107) [b]
Brake/Stride (%)	24.383 (11.429)	27.581 (8.697)	24.129 (9.044)
Propel/Stride (%)	51.458 (10.503)	48.144 (9.540)	44.257 (10.942)
Stance/Stride (%)	75.850 (2.975)	75.738 (2.995)	68.400 (8.107) [b]
Stride (s)	0.345 (0.038)	0.310 (0.031) [a]	0.329 (0.044)
Stance/Swing (%)	3.192 (0.574)	3.188 (0.554)	2.314 (0.704) [b]
Stride Length (@ 14.00cm/s)	4.842 (0.537)	4.331 (0.419) [a]	4.607 (0.602)
Stride Frequency (Hz)	3.017 (0.364)	3.319 (0.323) [a]	3.143 (0.407)
Absolute Paw Angle (deg)	11.433 (5.190)	10.419 (8.551)	7.979 (5.825)
Stance Width (cm)	1.783 (0.264)	1.775 (0.465)	1.686 (0.380)
Stride Length CV (%)	29.588 (12.156)	23.732 (9.402)	28.998 (8.647)
Stance Width CV (%)	26.216 (14.043)	27.902 (13.934)	31.403 (16.043)

[a] JACKET significantly different than NORMAL ($p < 0.05$);
[b] SUSPENSION significantly different than NORMAL ($p < 0.05$)

Six "clean" footfalls from each forelimb and hindlimb were visually selected from

one animal's data in each group for further analysis (Table 4.3). The ratio of peak paw area between the forelimb and the hindlimb in this subset was decreased by 16.9% for JACKET animals versus NORMAL, and 28.1% for SUSPENSION animals versus NORMAL, suggesting that suspension (and harnessing to a lesser degree) caused mice to preferentially shift their weight towards the rear during locomotion.

As seen in Figure 4-10, SUSPENSION mice demonstrated a slightly slower rate of onset of paw area, relative to NORMAL, with similar rates of withdrawal, suggesting lower strain rates in addition to lower peak strains.

Total area under the curve was significantly greater for NORMAL animals, due to both higher peak values and longer stance times. SUSPENSION animals had the smallest integrated area, with greater discrepancy from JACKET animals in the hindlimbs than forelimbs.

While faster speeds are typical for other published mouse locomotion studies (Amende, 2005), suspension animals were reluctant to walk or run at increased velocities. While some portion of this reduction in speed was likely a matter of discomfort, studies of human gait in suspension conditions have also noted that the optimal walking speed for maximum exchange of potential and kinetic energy is slower at lower simulated g-levels (Minetti, 2001).

Given the small number of animals in this pilot study, the results must be considered preliminary. However, coupled with other sources of data presented here, they provide some useful insight into the mechanics acting in the studies outlined in the next chapter.

4.3.3 Force Platform Results

Data collection with the AMTI AccuSway force plate confirmed that peak ground reaction forces were reduced by application of the forelimb jacket, approximately -24.6% in the forelimbs and -13.9% in the hindlimbs (Table 4.4). As with the DigiGait data, this suggested a relative unweighting of the forelimbs due to the mechanics of the jacket.

Compared to NORMAL data, MARS weightbearing reduced mean peak GRFz

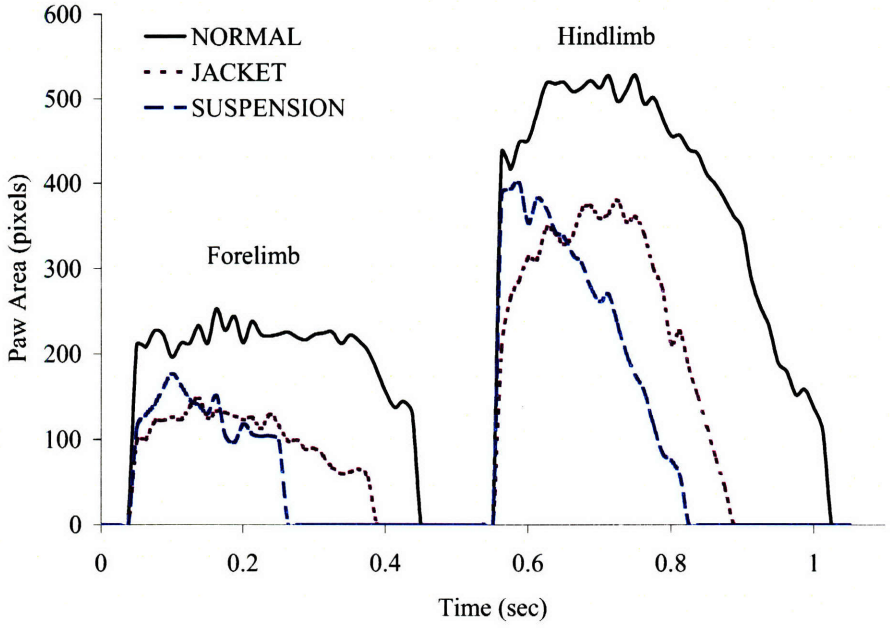

Figure 4-10: Paw area versus time for representative footfalls from animal locomotion on a DigiGait treadmill. Figure shows single footfalls as paw area in contact with the treadmill at a given time, based on threshold analysis of pixel intensity. Onset of footfalls have been aligned for convenience of comparison.

Table 4.3: Characteristic metrics of paw area versus time for locomotion on the DigiGait treadmill. Six clean footfalls were visually selected from each forelimb and hindlimb for analysis. In all forelimb and hindlimb parameters, JACKET and SUSPENSION differ significantly from NORMAL ($p < 0.05$).

	NORMAL (n=1)	JACKET (n=1)	SUSPENSION (n=1)
Forelimbs			
Average paw area (pixels)	203.23 (16.13)	107.28 (14.19)	121.39 (24.50)
Peak paw area (pixels)	259.31 (13.07)	151.85 (59.89)	140.88 (27.97)
Integrated paw area (pixels*sec)	69.37 (9.02)	27.24 (10.18)	26.20 (10.27)
Hindlimbs			
Average paw area (pixels)	366.89 (53.98)	258.47 (33.31)	239.36 (39.94)
Peak paw area (pixels)	516.60 (31.58)	364.24 (25.94)	390.51 (42.44)
Integrated paw area (pixels*sec)	149.77 (32.16)	99.27 (36.19)	76.71 (12.96)
Forelimb to hindlimb ratios			
Average paw area ratio	55.39 %	41.51 %	50.71 %
Peak paw areas ratio	50.20 %	41.69 %	36.07 %
Integrated paw areas ratio	46.32 %	27.44 %	34.15 %

by -63.7% in the forelimbs and -85.3% in the hindlimbs, while LUNAR weightbearing reduced mean peak GRFz by -50.0% in the forelimbs and -70.7% in the hindlimbs. Interestingly, while jackets alone led to more equal weight-sharing between the forelimbs and hindlimbs, suspension tended to redistribute mass towards the normal forelimb-dominated balance.

Suspension also sharply reduced the rate of onset of forces in both the forelimbs and the hindlimbs, with MARS gait showing a -73.3% change in forelimb onset rates, and a -91.8% change in hindlimb onset rates, relative to NORMAL gait.

The biggest analytical challenge was posed by the inconstancy of locomotor speeds under the different weightbearing conditions. Contrary to the DigiGait data, mean stance duration was increased with suspension (Figure 4-11). However, the force plate data were not velocity-controlled; therefore, the degree to which this change in stance was caused by an observable slowing of the gaits selected by these populations is unclear. Across trials, suspended animals had a significantly lower average speed per stride (10.98 ± 4.77 cm/s) than non-suspended animals (38.69 ± 17.22 cm/s, $p < 0.0001$).

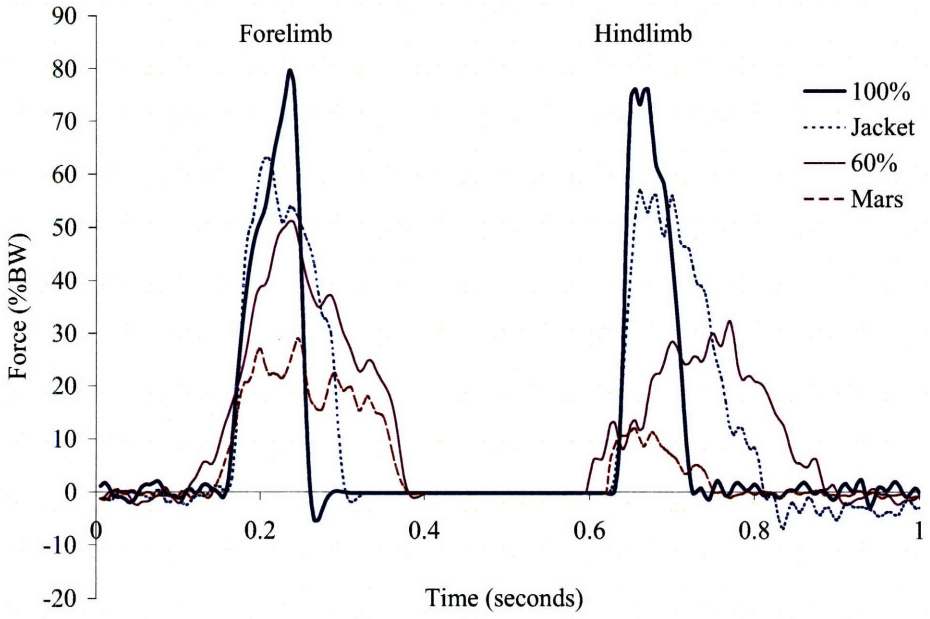

Figure 4-11: Vertical ground reaction forces (GRFz) from representative single footfalls on a AccuSway force platform. Traces are presented as a percentage of full body weight versus time for one forelimb, followed by the contralateral hindlimb. Data has been filtered with a two-pole, 25 Hz low-pass Butterworth filter, and the onset of each footfall has been aligned for convenience of comparison.

Furthermore, peak force is known to increase with decreasing stance time (approximately +5% body weight for a 50 msec reduction in stance time; Clarke, 2001). Therefore, it is likely that Table 4.4 and Figure 4-11 below underestimate the degree of reduction that might be expected in a speed-matched trial. However, the data are representative of free gait for each of the conditions, and should be characteristic of the actual peak forces observed during daily living for each group.

Examination of transverse ground reaction forces in the plane of the force plate (GRFx and GRFy) shows that these components played a much larger role in suspended than non-suspended gaits, particularly in the hindlimb. Although the absolute

le 4.4: Ground reaction force data from AccuSway platform. All measurements came from a single mouse and footfalls firmed by video prior to analysis.

		NORMAL n=4	JACKET n=5	60% n=5	MARS n=4	LUNAR n=11 fore n=3 hind
Peak $\|GRFz\|$ (%BW)	Fore	78.85 (13.66)	59.48 (12.93)	41.93 (8.45)	28.63 (2.92)	20.09 (5.06)
	Hind	70.93 (11.53)	61.10 (3.65)	32.43 (5.80)	10.44 (2.99)	10.92 (1.21)
Peak $\|GRFx\|$ (%BW)	Fore	18.25 (14.11)	11.23 (7.87)	15.06 (4.90)	10.04 (2.72)	6.21 (2.67)
	Hind	16.42 (7.42)	13.65 (7.92)	15.57 (6.65)	5.00 (3.80)	3.96 (3.75)
Peak $\|GRFy\|$ (%BW)	Fore	15.83 (7.46)	13.44 (5.84)	10.18 (7.73)	11.44 (6.69)	4.08 (2.28)
	Hind	15.18 (8.81)	12.99 (6.22)	9.55 (8.43)	5.37 (6.25)	2.17 (2.24)
Area under GRFz (%BW*sec)	Fore	4.14 (0.81)	4.53 (1.06)	6.71 (1.17)	3.86 (1.42)	2.30 (1.03)
	Hind	3.60 (1.09)	4.07 (1.12)	5.50 (1.86)	1.29 (1.11)	1.91 (0.05)
GRFz onset (%BW/sec)	Fore	2239.86 (1009.89)	1928.42 (572.65)	565.32 (89.02)	566.54 (190.96)	318.98 (145.13)
	Hind	2782.23 (1185.03)	2323.04 (757.37)	600.89 (281.43)	210.48 (163.60)	192.28 (106.44)
Stance Duration (sec)	Fore	0.10 (0.02)	0.14 (0.04)	0.30 (0.03)	0.33 (0.08)	0.26 (0.11)
	Hind	0.11 (0.01)	0.13 (0.04)	0.32 (0.05)	0.23 (0.12)	0.37 (0.13)

magnitude of these forces was lower in suspension, the ratio of each in-plane force to vertical GRFz was larger, suggesting a greater relative need for stabilization, despite the moderating presence of harness forces (Figure 4-12).

4.3.4 *In Vivo* Strain Gaging Results

Walking causes medio-lateral bending in the mouse tibia, such that the anterio-medial gage site experiences compressional stresses (i.e., negative strains; DeSouza, 2005). We collected 62 trials of individually resolvable footfalls, based on strain gage data. Representative footfalls from each loading regime are shown in Figure 4-14. At all levels of loading, footfalls were marked by a characteristic double peak, previously reported in the literature (Rabkin, 2001).

Across 36 footfalls (LUNAR $n = 5$; MARS $n = 8$, 60% $n = 12$, JACKET $n = 11$), selected for clarity of start/finish and characteristic shape, there was no significant difference across groups for peak compressive strains (Figure 4-13). Strain rate in the linear portion of the compressive phase tended to be lower in suspension animals, with LUNAR rates 52.5% lower than JACKET ($p = 0.0095$). (As above, at least a portion of this decrease is consistent with the lower walking velocities observed in the suspended mice.)

Animals were also allowed to stand quietly for multiple runs to quantify static strains due to unloading. Mean output during half a second of quiet standing is given in Table 4.5. Bridge output voltages during hindlimb elevation were significantly less than jacketed standing (p=0.043), but the other conditions did not differ significantly.

Notably, lower bridge output voltages were seen in hindlimb unloading relative to quiet standing and locomotor swing phases, indicating relatively greater compressive loads on the medial tibial surface during this maneuver. Such a change could be due to any combination of reduced tensile loading from axial compression, changing patterns of muscle activation, or gravitational loading of the hindlimb during tail lift. Further investigation is necessary.

The addition of the AMTI force plate described above enabled co-registration of tibial strain gage data with measured ground reaction forces (Figure 4-15). Changes

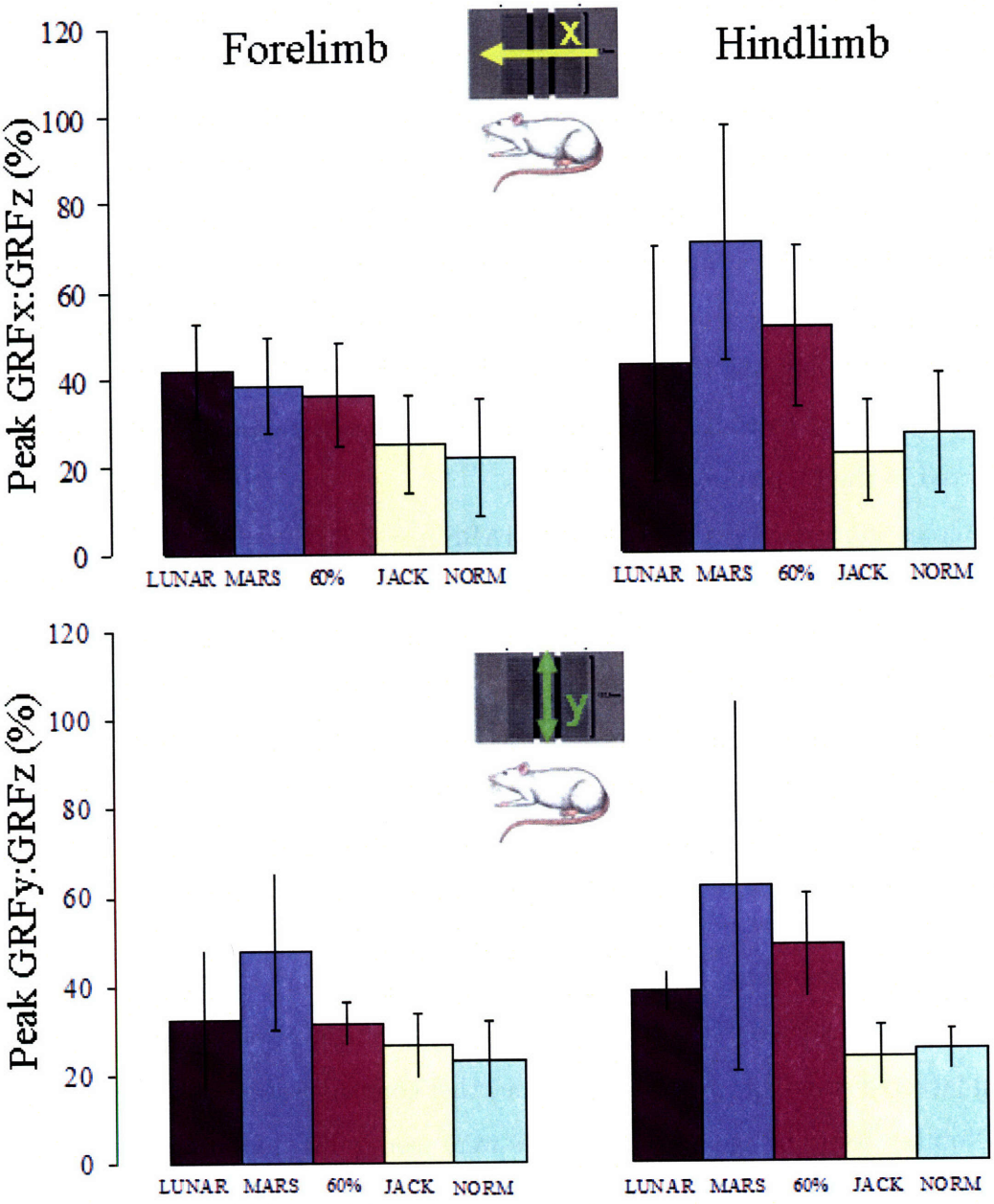

Figure 4-12: Ratios of peak ground reaction forces in the (a) x- and z-directions, and (b) y-and z-directions, for different experimental conditions on a AccuSway force platform. Particularly in the hindlimb, in-plane forces, while reduced in absolute magnitude by suspension, composed a larger percentage of total GRF.

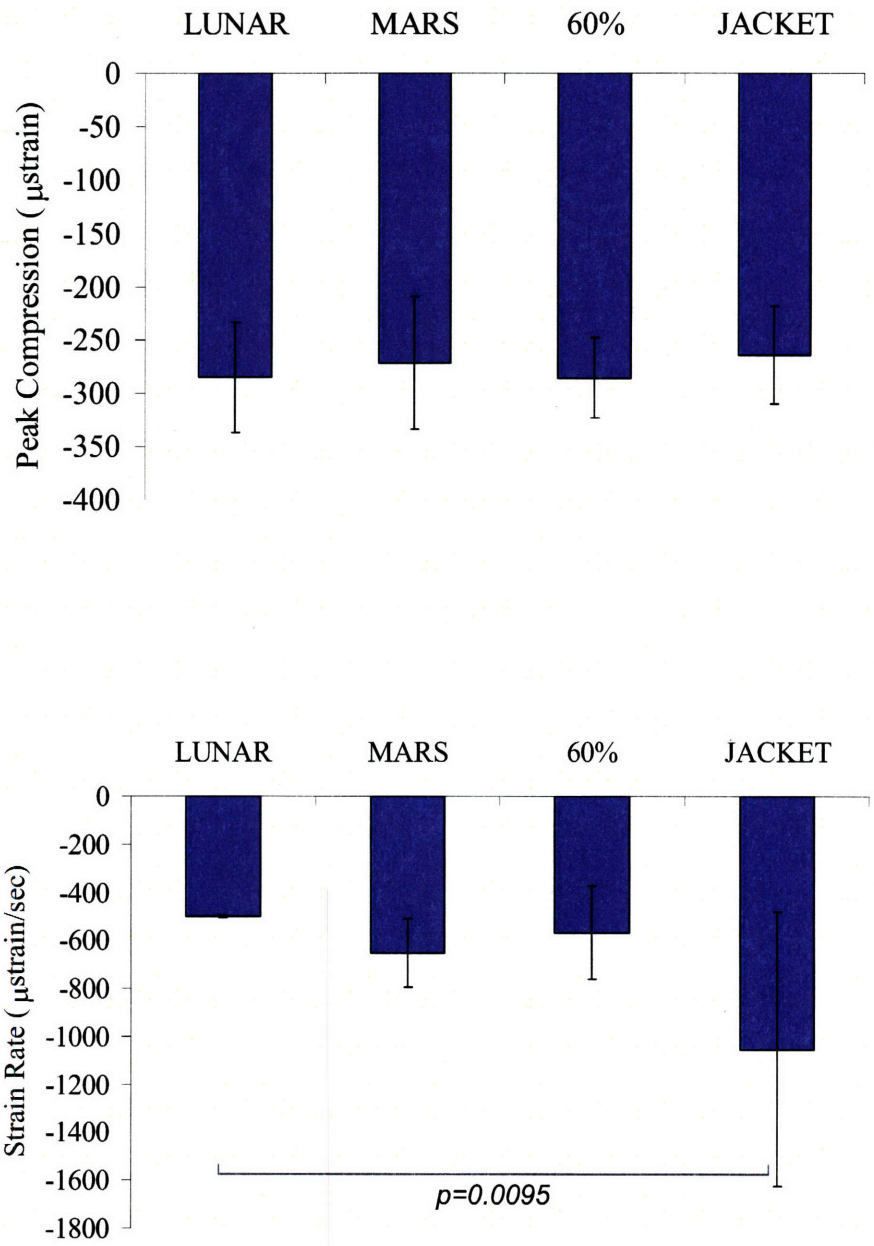

Figure 4-13: Minimum compressive strains and strain rates during the onset of compression for LUNAR, MARS, 60%, and JACKET loading. There were no significant differences in strain among the groups, but a strong suggestion of lower strain rates in the suspension animals, reaching significance in the comparison between LUNAR and JACKET animals.

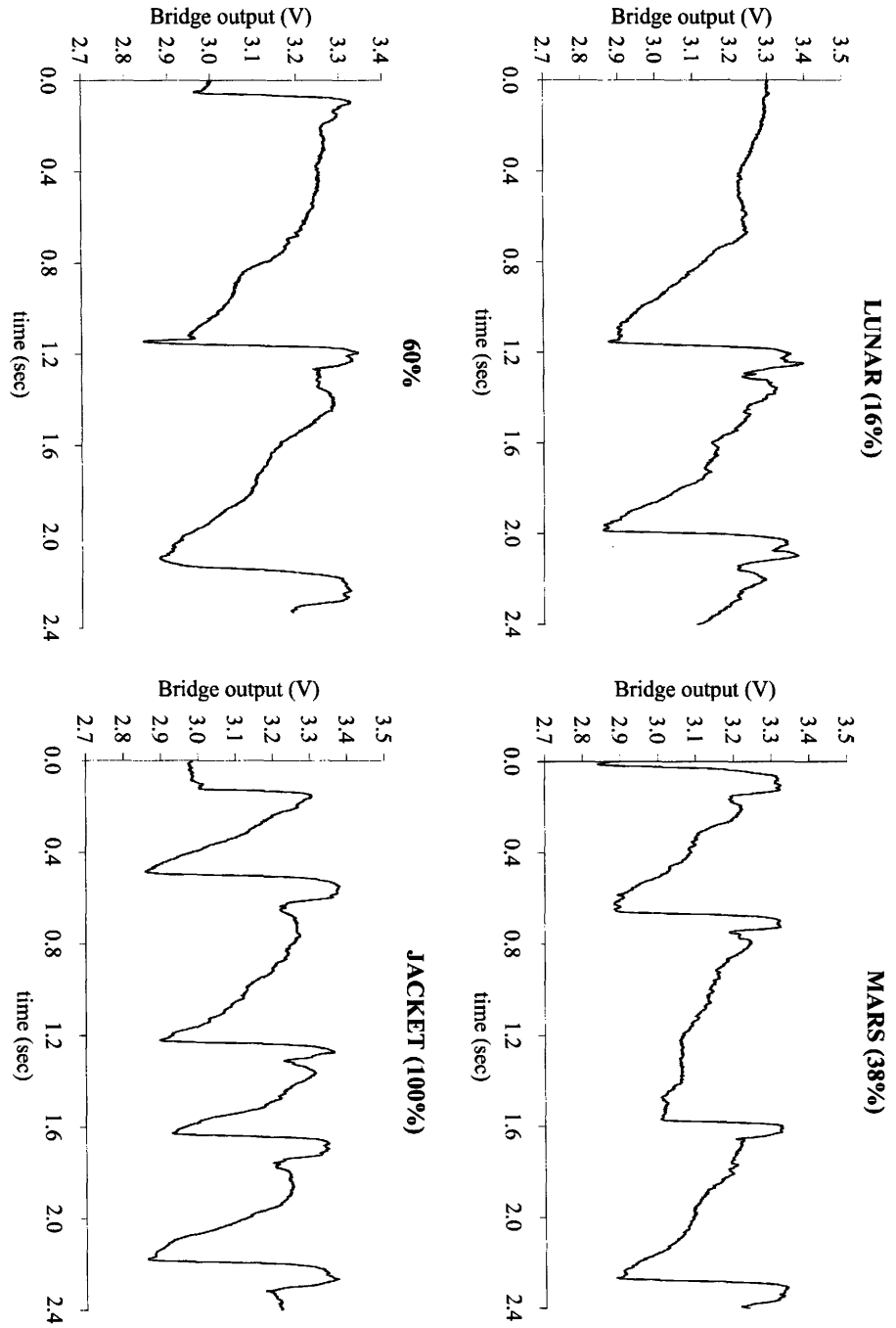

Figure 4-14: Tibial strain gage output for representative footfalls during unpaced locomotion under LUNAR, MARS, 60%, and JACKET weightbearing. A 100 mV drop equates to 63.17 microstrain in compression. There are no significant differences in the magnitude of either peaks or troughs across groups.

in the two measures were well correlated in time, but not in value. Surprisingly, across a four-fold range of vertical ground reaction forces, there was no significant difference in the magnitude of observed *in vivo* strains.

4.4 Discussion

4.4.1 Gait Kinematics

Human studies of partial weight suspension have demonstrated a characteristic shift in bipedal gait kinematics and dynamics at lower g-levels. Changing the level of statically supported load typically has a direct impact on peak dynamic loads, with average peak vertical forces deviating less than 10% from predicted values for a given walking speed (Ivanenko, 2002). For self-paced walking, there appears to be a further reduction in GRFz for simulations below 0.4-g (Davis, 1993). The most efficient exchange between kinetic and potential energy when walking occurs at lower speeds for lower g-levels, leading to lower optimal velocities and lower velocities for the transition from walking to running (Griffin, 1999; Minetti, 2001). It is likely that some of the reduction in GRFz seen at lower g-levels is due to slower walking speeds with lower peak kinetic and potential energies.

Down to approximately 0.2-g, partial gravity locomotion typically does not modify stance time, but does increase the length of the aerial swing phase, leading to less

Table 4.5: Mean bridge output during quiet standing at a variety of loading levels. Hindlimb unloading was accomplished by elevating the animal's hindquarters by the tail and waiting for strain values to stabilize. Values are given as mean (std dev).

Condition	*Mean bridge output (V)*
Hindlimb Unloaded	3.074 (0.003)*
LUNAR	3.239 (0.002)
MARS	3.231 (0.002)
60%	3.307 (0.002)
JACKET	3.254 (0.004)

** Significantly different than JACKET, $p < 0.05$*

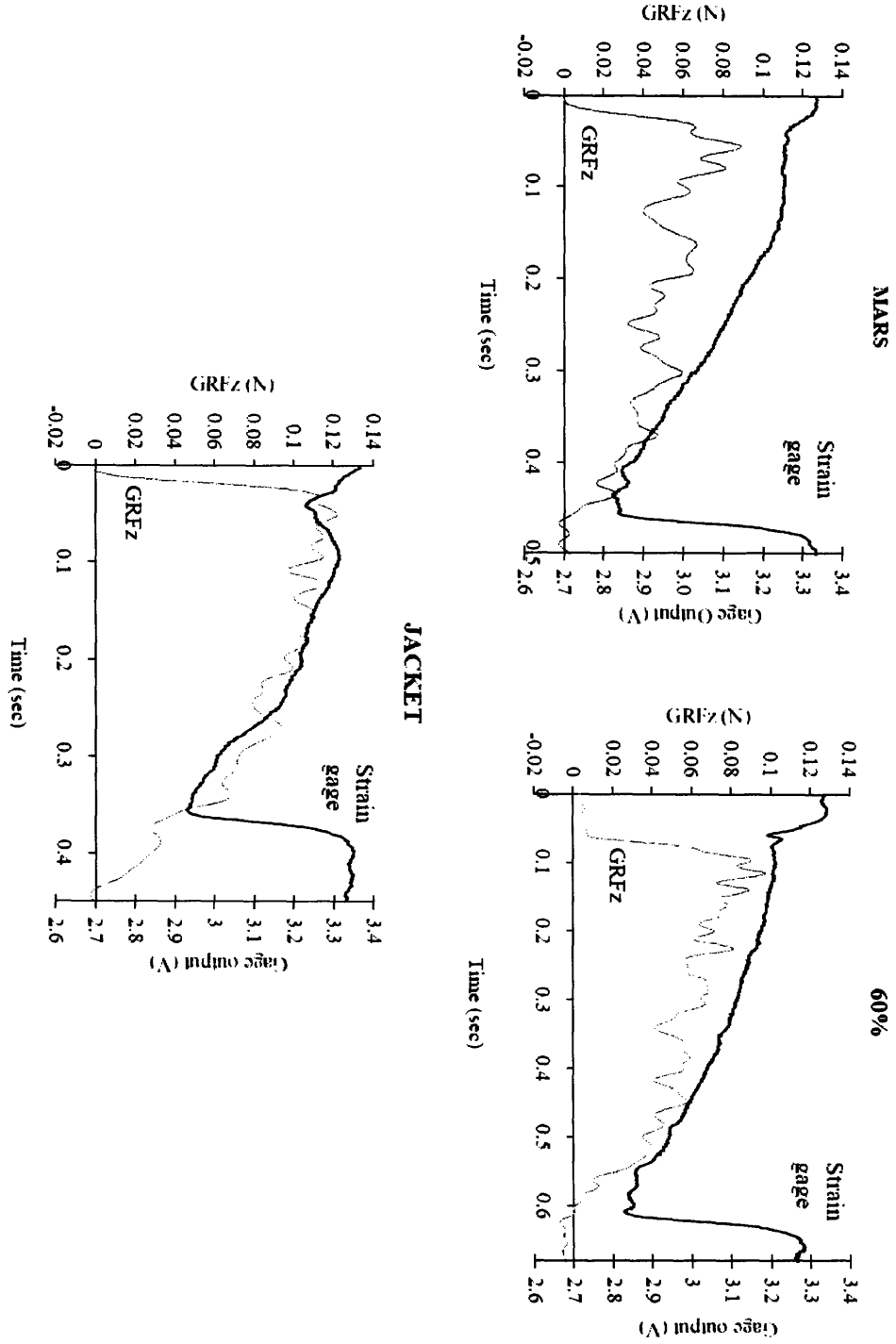

Figure 4-15: Co-registerd outputs from tibial strain gages and AccuSway GRFz data. Footfalls were acquired during unpaced locomotion under MARS, 60%, and JACKET weightbearing. (No appropriately co-registered data was detected from LUNAR trials.) A 100 mV drop in bridge output equates to 63.17 microstrain in compression. Scaling on both y-axes is maintained across trials, but the x-axis has been stretched to accommodate variation in walking speed (MARS=7.88 cm/s, 60%=7.00 cm/s, JACKET=12.60 cm/s).

frequent footfalls for a given speed (Newman, 1994). At very low g-levels ($< 0.2-$g), however, support time in bipedal gait does increase, and cadence falls off more sharply (Davis, 1993). Partial weight simulations also lead to greater reductions in vertical ground reaction forces than in the transverse components, which may reduce traction at critical gait phases, including heelstrike and toe-off (Davis, 1993).

Table 4.6: Comparison of gait parameters for partial weightbearing locomotion relative to normal 1-g locomotion. Bipedal human data drawn from the literature is compared with our initial studies using either a treadmill or a force plate to quantify gait parameters.

	Human studies	*DigiGait treadmill*	*AccuSway force plate*
Peak vertical GRF	$\Downarrow$, with $\Downarrow\Downarrow$ at self-paced low-g walking	N/A	$\Downarrow\Downarrow$ at self-paced low-g walking
Onset of vertical GRF	$\Downarrow$	$\Downarrow$	$\Downarrow$
Walking speed	$\Downarrow$	N/A	$\Downarrow$
Transverse GRF	absolute, $\Downarrow$, w.r.t. GRFz, $\Uparrow$	N/A	absolute, $\Downarrow$, w.r.t. GRFz, $\Uparrow$
Stance:Swing ratio	$\Downarrow$	$\Downarrow$	N/A

This is the first study to examine quadrupedal gait under partial weightbearing, and one of very few to measure locomotor loads in a freely walking mouse (Srinivasan, 2003; DeSouza, 2005). The low number of confirmed and registered steps means that additional future studies are certainly needed. A larger database of footfalls would allow for more robust statistical comparisons between groups, and would also enable a more reliable quantification of the full range of "normal" behaviors in mice, including walking, running, scratching, feeding, grooming, and rearing.

The preliminary evidence, however, strongly suggests that the reductions in static loads, as measured daily in our experiments, are representative of the peak ground reaction forces during locomotion. Gait patterns changed in ways consistent with the existing human literature on partial weightbearing locomotion.

4.4.2 Hardware Validation Across g-Levels

The design of our hardware and experimental methods ensured that average static loads were proportionally reduced. Daily weighing and titration of effective weight

allowed for tight control of these chronic loads, generally to well within ±0.01 N, approximately ±5% of full body weight.

It is well-established, however, that osteogenesis is driven by dynamic, rather than static loads (Lanyon, 1984; Turner, 1998; Robling, 2001), and that peak strains and strain rates are key drivers in skeletal maintenance (Lanyon, 1984; Judex, 2000). The use of daily static weighing, force platform measurements of locomotor ground reaction forces demonstrated that peak ground reaction forces and force onset (i.e., strain rate) were lower for suspension animals than controls. The evidence presented above suggests that reductions in peak force are somewhat larger than predicted by the level of suspension, perhaps due to the independent effects of forelimb harnessing (Figure 4-16).

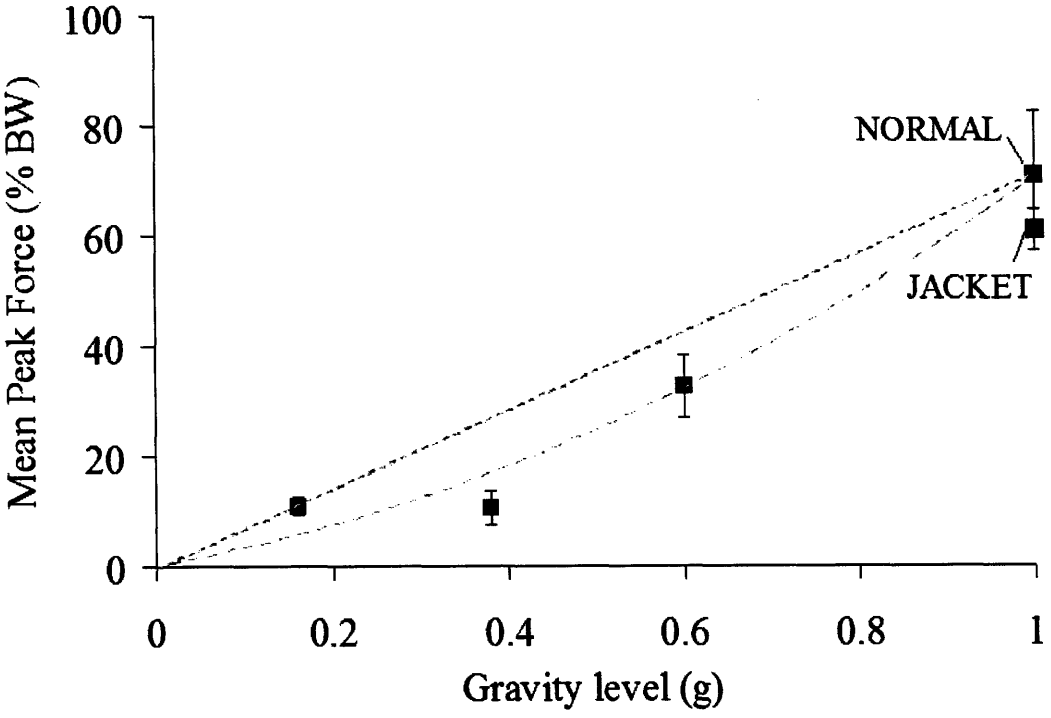

Figure 4-16: Relationship between peak vertical ground reaction forces and simulated g-level. Dotted trendline represents a hypothesized linear relationship between the two variables. Dashed trendline is a second-order fit for data, excluding JACKET ($R^2 = 0.97$).

4.4.3 Lack of Correlation between Tibial Strains and Ground Reaction Forces

Surprisingly, the addition of *in vivo* tibial strain gaging showed no correlation between peak ground reaction forces and peak strains or strain rates. Throughout all conditions, compression at the anterio-medial tibial surface was consistent with values from the literature acquired under normal locomotion (approximately -300μstrain; DeSouza, 2005).

For internal consistency, data was compared from multiple consecutive trials using the same mouse. Therefore, differential effects of muscle atrophy did not contribute to the observed measurements. Data was collected within 6 hours post-surgery, and no degradation in signal quality was noted until a leadwire broke, ending the study.

Assuming similar patterns of gait kinematics, one would anticipate that a reduction in applied forces at the foot would lead to changes in the propagated loads at the tibial surface. Indeed, across any single gait cycle, this seems to hold true, as the timing of compressional strains correlated well with individual footfalls. However, examining aligned traces of GRFz and tibial strain (Figure 4-15), the peak vertical ground reaction force and maximally compressive strain did not correlate in time. Indeed, in most trials, peak forces in the hindlimb occured approximately 15% through the stance phase of the gait cycle, while peak strains occured at around 90% of the same cycle.

This misalignment between ground reaction forces and strains suggests that the primary source of tibial deformation, at least along the axis of the strain gage on the anterio-medial surface, is not ground reaction loading. Muscles are known to apply very large moments to skeletal members, due to their inefficient insertion patterns which minimize joint size at the cost of bone stresses (Rittweger, 1999). It seems reasonable, therefore, that the patterns of strain observed during locomotion may be due largely to muscle activation.

Previously reported electromyographic (EMG) studies of the mouse hindlimb reported high levels of extensor tone, particularly in the vastus lateralis, during the

stance phase of locomotion (Leblond, 2003). This activation has been hypothesized to "prevent flexion above a certain limit caused by gravity and to resist higher torques in the knee joint" (Scholle, 2005). Peak activation of the vastus lateralis occurs mid-stance, and the muscle contracts eccentrically, lengthening throughout the stance phase (Gillis, 2002; Schumann, 2006).

The biceps femoris is also active during stance, playing a role both knee flexion and joint stabilization (Gillis, 2002; Scholle, 2005). While biceps electrical activity peaks early in stance, however, muscle shortening continues throughout the stance phase (Gillis, 2002).

In rodents, both the vastus lateralis and the biceps femoris wrap around the lateral aspect of the leg to insert on the proximal tibia. Contraction of these muscles would therefore be expected to cause medio-lateral bending, consistent with the compressive strains seen in the tibia during walking. Correlation of bone strain and EMG activity with ground reaction forces would provide confirmation of the relative timing of these signals.

Strain gaging is non-ideal for investigating the effects of musculoskeletal interactions. While application of the gage to the anteromedial tibial surface is consistent with numerous previous investigations and anatomically convenient, it does not provide optimal measurements of muscle strain. Unfortunately, placing a gage at the attachment site of an atrophying muscle is impossible without disrupting the muscle itself. Furthermore, mathematical predictions made with simple beam models are insufficient to accurately elucidate the tibial surface strains expected at a given site due to the complexity of the bone shape and the additional support provided by the fibula. Finite element modeling could be used to supplement this work.

4.5 Limitations of the Model

All ground-based models of partial weightbearing are subject to some limitations, due to the tonic presence of Earth's gravity. Some physical limitations for this model include:

- Earth-level gravitational forces acting on distributed body segment masses;
- Variation of upward force across the gait cycle due to small displacements of the center of mass of the animal during normal locomotion;
- Localized harness forces;
- Non-representative altered gait dynamics;
- Neurovestibular inputs consistent with 1-g;
- No substantive cephalic fluid shift;
- Stress of chronic restraint.

However, if the musculoskeletal effects of chronic reductions in dynamic loads are the primary goal of such a model, the simulation should be sufficient.

Chapter 5

Musculoskeletal Studies: Design and Results

This chapter describes the design and results of two 21-day studies utilizing PWS to characterize the responses of bone to titrated loading. An extensive Mars-analog investigation is discussed first, followed by a study of complementary lunar-analog weightbearing.

5.1 Mars-Analog Investigations

Despite NASA's focus on Mars as a primary destination for both science and exploration, there has yet to be a study examining the effects of chronic 38% loading in any mammalian model. The study described in this section uses the PWS system to support mice at Mars-analog levels of weightbearing for the first ever study on musculoskeletal adaptation to such an environment.

5.1.1 Experimental Design

Animal Selection

The choice of mouse strain and duration for these studies were selected based on findings by Judex et al. (2002). Compared with age-matched controls, 16-week old

BALB/cByJ (BALB) mice undergoing 21 days of tail suspension showed significant suppression of bone formation in the proximal tibial metaphysis (BFR/BS: -55%). This led to a highly significant reduction in trabecular bone volume fraction (BV/TV: -43%). A follow-on study in mice of the same age and strain (Judex, 2004) showed even larger mean BV/TV losses in the distal femoral metaphysis, (−59.5% relative to controls). These results confirmed that three weeks of unloading was sufficient to elicit significant histological and structural changes in mice past their peak growth phase.

Furthermore, the changes in BALB trabecular remodeling were significantly larger than those seen in either C57Bl/6J or C3H/HeJ mice in the same study, allowing for more powerful statistical analyses. BALB/c and BALB/c-derived mice are also among the most commonly used inbred research strains, making them a valuable data for future comparisons with both wild-type and genetically modified cohorts. For these reasons, BALB/cByJ animals were used for both this Mars study and the lunar investigation described below.

Animals at the beginning of our studies were 10 weeks old to take advantage of the plateau in longitudinal femoral growth, which is more representative of the adult human skeleton, and a near-maximum in trabecular fraction, which improves the chance of visualizing changes in this compartment.

Characterization of age-related changes to the distal femoral metaphysis in female BALB mice (Glatt, 2007b) suggests that compared to the 16-week-old animals used in the study above, trabecular parameters in the distal femur are largely unchanged. In the femoral midshaft, cortical thickness is increasing at a slow rate. Overall, the period between 10 and 16 weeks is not a time of rapid change, and the prevailing growth patterns are similar between the two populations.

Experiment Cohorts

In order to investigate the effects of Mars-analog weightbearing on musculoskeletal physiology, 10-week-old female BALB/cByJ mice were assigned to one of four groups for a 21-day study. (Numbers of animals represent starting populations.)

- **MARS:** jacketed animals suspended at 38% weightbearing, individually housed, with *ad libitum* food and water, n=10

- **JACK-M:** fully weightbearing jacketed controls, identically housed to suspension animals and pair-fed according to MARS group daily means, n=13

- **AGE:** unjacketed age-matched, group-housed vivarium controls with *ad libitum* food and water, n=21

- **BASE:** baseline cohort, age-matched to animals at study day 1 (single timepoint only), n=8

This effort was conducted in a series of three-week experiments, as outlined in Appendix D. For greater statistical power, data from AGE animals were shared between the Mars-analog studies presented here and the lunar-analog studies described below. Of the 127 parameters measured for both groups in these studies, there were no statistically significant differences between the two cohorts for any parameters except cortical bone area in the distal femur ($A_{MARS} = 0.873 \pm 0.057$, $A_{LUNAR} = 0.929 \pm 0.036$), bending moment at yield ($A_{MARS} = 14.894 \pm 3.862$, $A_{LUNAR} = 19.517 \pm 4.000$), and estimated BMD of the femoral mid-shaft ($A_{MARS} = 1260.277 \pm 13.229$, $A_{LUNAR} = 1277.583 \pm 10.134$).

5.1.2 Methods

As described in Section 4.1.3, animals were adapted to forelimb jackets for two days prior to the start of the study. Daily care included measurement of real and effective body masses, and adjustment of suspension tethers to ensure appropriate weightbearing. JACK-M animals were pair-fed according to the previous daily mean of the MARS group's food usage.

Two intraperitoneal injections of calcein (0.05 ml) were given to label newly forming bone (Suzuki, 1966). Solutions were prepared with 12 mg calcein powder per ml of 2% $NaHCO_3$ in 0.15 M saline, filtered, and kept in cold storage. For animals older

than 10 weeks, injections were given at 10 and 2 days prior to sacrifice. For animals 10 weeks of age or younger, injections were given at 8 and 2 days prior to sacrifice.

Following sacrifice by carbon dioxide immersion, gastrocnemii, femurs, tibiae and humerii were harvested bilaterally from all study animals. Muscles were weighed and discarded. Left side bones were prepared for imaging and biomechanical testing in gauze soaked in normal saline (0.9%), then stored at -20 °C. Right side bones were prepared for histology in 10% neutral buffered formalin at 4 °C for 48–72 hours, then transferred to 70% ethanol and returned to refrigeration.

Microcomputed Tomography (μCT)

As previously described (Alexander, 2001; Bouxsein, 2002), structural imaging was performed with high-resolution microcomputed tomography (μCT40, Scanco Medical, Basserdorf, Switzerland) using a 10-mm focal spot microfocus X-ray tube. The distal femoral metaphysis was scanned using a 12-μm slice increment. 204 transverse slices were acquired, beginning 240 μm above the growth plate and proceeding distally (Figure 5-1a). Images were reconstructed, filtered, and thresholded using a specimen-specific adaptive-iterative threshold algorithm (Meinel, 2005). The images were stored in 3D arrays with an isotropic voxel size of 12 μm. Morphometric parameters were computed using a direct 3D approach that does not rely on any assumptions about the underlying structure. For the cancellous bone region we assessed the following variables: bone volume fraction (BV/TV, %), trabecular thickness (Tb.Th, μm), trabecular separation (Tb.Sp, μm), trabecular number (Tb.N, mm^{-1}), connectivity density (Conn.D, mm^{-3}), and structure model index (SMI). For the cortical region, the total cross-sectional area, cortical bone area and medullary area were measured (TA, BA and MA, mm^2). From this, bone area fractions (BA/TA, %) and cortical thickness (Ct.Th μm) were calculated. To assess structural rigidity, the maximum, minimum, and polar ((I_{max}), (I_{min}), pMOI, mm^4) moments of inertia were also calculated.

Transverse CT slices (50 per specimen) were similarly acquired at the femoral mid-shaft, beginning 55% of the distance down the length of the bone and proceeding

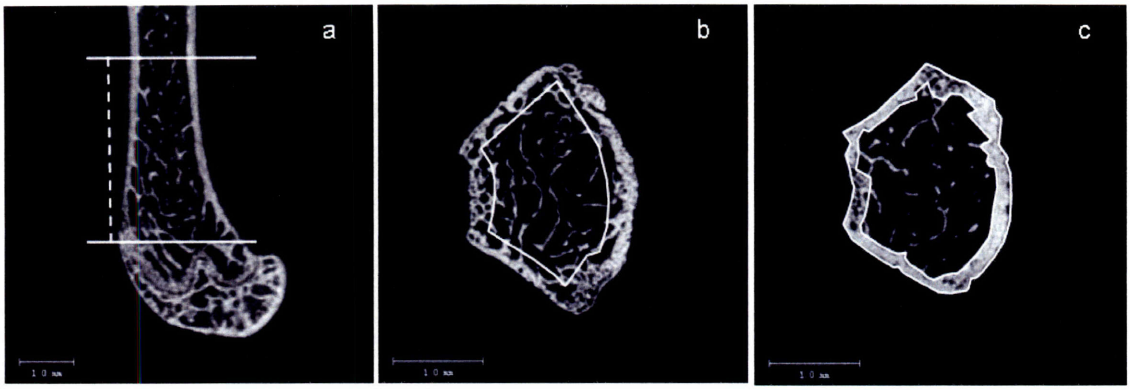

Figure 5-1: Location of μCT slice acquisition and contour preparation. Morphological data was gathered in the femur at both the mid-diaphysis and distal metaphysis, as well as from the proximal tibial metaphysis. (*Image from Glatt, 2007b, with permission*)

distally. Cortical parameters were measured as above.

Finally, 70 sagittal CT slices were acquired from the proximal tibial metaphysis for further trabecular analysis. Trabecular contours were evaluated from immediately below the primary spongiosa for 3 mm distally.

Digital contouring of each region of interest was done manually. A single operator contoured all of the samples for a given region to ensure consistency.

Biomechanical Testing

Following μCT scanning, the strength of the femoral mid-shaft was assessed by threee-point bending, as previously described (Turner, 1993). Briefly, specimens were thawed to room temperature in physiological saline for a minimum of 3 hours to ensure adequate hydration and tested in random order to prevent effects of thaw duration. The length from the proximal tip of the greater trochanter to the distal edge of the lateral condyle was measured with digital calipers, and the femur was placed dorsal surface downward across a 6.0 mm span. A low force mechanical testing system (MTS Bionix 200, with 100 N load cell, MTS Systems Corporation, Eden Prairie, MN) was used to apply a flexion moment to the midpoint of the ventral diaphysis. A pre-load of 1–2 N was applied, followed by a constant displacement rate of 0.03 mm/sec. Force-displacement data were acquired at 100 Hz, using the MTS TestWorks4 software. A

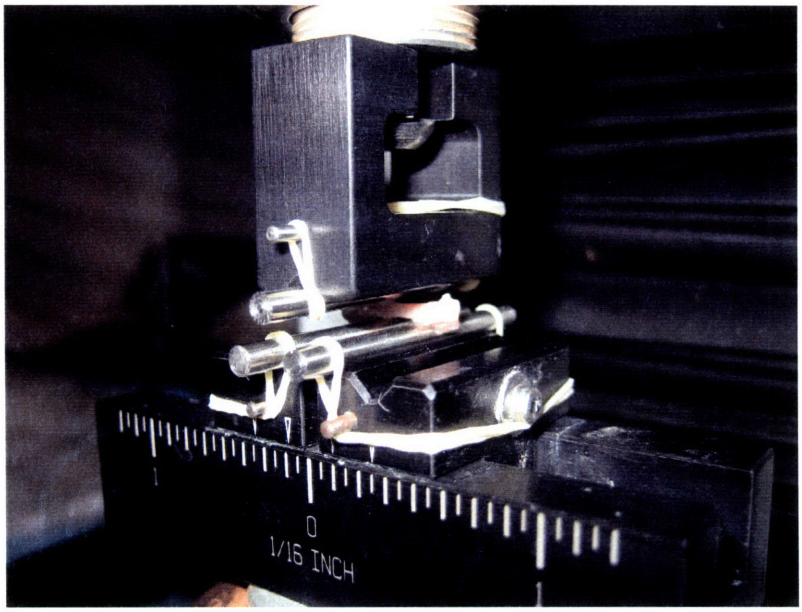

Figure 5-2: Three-point bending test setup. Femurs were placed dorsally on a 6.0 mm span formed by two 3.0 mm rods. Flexion was applied by a third rod at the midshaft of the bone. Orthodontic rubber bands secured the rods to the jig.

custom MATLAB routine (Appendix E) was used to determine structural properties.

As displayed in Figure 5-3, extrinsic Stiffness was taken as the slope of the secant to the initial linear portion of the force-displacement curve, selected manually. A second line, with the same x-intercept and slope equal to 95% of Stiffness, was calculated, and yield was defined at its intersection with the force-displacement curve. Failure was selected manually as the point at which applied force sharply decreased. Energy to yield and failure were calculated from the areas under the force-displacement curve.

Data for each specimen was then adjusted for the appropriate femoral mid-shaft area moment of inertia (I_{min}), as measured on the μCT scans, to derive estimated Young's modulus, E^*, at this location (Equation 5.1; Turner, 1993). Here, F and d are the applied force and crosshead displacement at yield, and L is the distance between the two lower supports:

$$E^* = \frac{FL^3}{48dI_{min}} \tag{5.1}$$

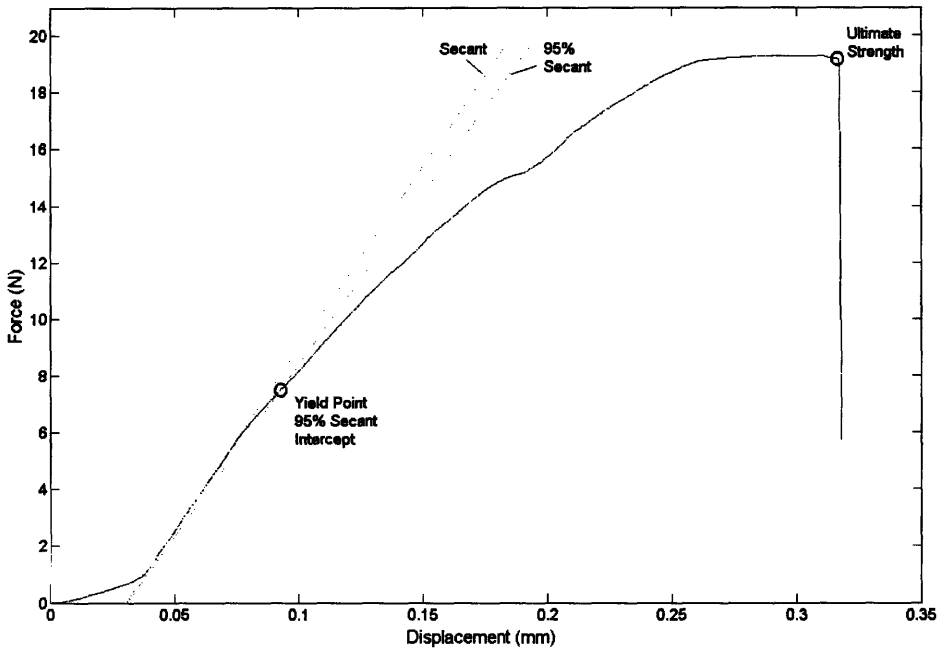

Figure 5-3: Representative output for three-point pending test. Initial slope of the force-displacement version of this curve was estimated to determine stiffness, and a second line, with the same x-intercept and 95% the slope was constructed to determine yield.

Histology

Following μCT, the five median tibiae from each group in terms of trabecular bone volume fraction were selected for histomorphometry. Dr. Hiroaki Saito (Department of Orthopaedics and Cell Biology, School of Medicine, Yale University) conducted this portion of the study per the following methods (Saito, personal communication):

> The removed tibiae were infiltrated with a mixture of 90% methyl methacrylate (Sigma), 10% dibutyl phthalate (Sigma), and 0.15% benzoyl peroxide (Polyscience) at 4 °C, then embedded in a mixture composed of 85% methyl methacrylate (Sigma), 15% dibutyl phthalate (Sigma), and 5% benzoyl peroxide (Polyscience). Polymerization was performed at 37 °C. Standard undecalcified sections (4μm) were prepared using a Reichert-Jung microtome (Cambridge Instrument, Heidelberger, Switzerland), and were stained with toluidine blue or without. A standard histomorphometric analysis of the tibial metaphysis was performed (Parfitt, 1987), using the OsteoMeasure analyzing system (OsteoMetrics, Inc., Decatur, GA). The measurements were performed in a $1.28mm^2$ area [eight $0.16mm^2$ regions] starting 0.3 mm from the proximal growth plate.

Muscle Mass

Immediately following sacrifice, the animal's skin was removed and both legs were separated from the carcass for sample collection. The quadriceps muscle group was loosened with a single cut along the posterior side of the femur, then retracted distally with tweezers and removed, exposing the gastrocnemius along the posterior lower limb. The Achilles tendon was released at the calcaneus, and the calf musculature was retracted proximally. The two heads of the gastrocnemius were released from the femur, and the thin red soleus was resected from the posterior belly of the muscle. Both right and left gastrocnemii were weighed to assess atrophy (ProScale Gemological 10, 10 x 0.001 grams, My Weigh, Phoenix, AZ).

Serum Collection

Blood collection was conducted by retro-orbital bleeding or terminal cardiac puncture. Samples were centrifuged at 12,000 rpm for 10 minutes to obtain at least two 20 μliter aliquots of serum, which were stored at -80 °C for future analysis. Samples gathered in the November study (Appendix D) were unfortunately lost due to excessive chilling prior to centrifugation.

Data Analysis

Statistical analysis of μCT and three-point testing data utilized a combination of Microsoft Excel and SYSTAT 11 (Systat Software, Inc., San Jose, CA). To examine the effect of GROUP on Mars-analog and lunar-analog findings, an omnibus least-squares linear regression was used. For variables demonstrating a significant effect of GROUP ($p < 0.05$), pairwise comparisons between groups were made using a two-tailed Student's t-test with an assumption of unequal variance. Because the experimental design called for comparison between MARS and AGE, and MARS and JACK-M, no post-hoc correction was necessary for these analyses. Differences were considered significant for $p < 0.05$.

For histology and histomorphometry, where group sizes were smaller (n=5), a Kruskall Wallis non-parametric test was utilized. These results are noted in the text with a p_{KW}, and differences were considered significant for values less than 0.05.

In order to adequately display the variability of data within individual groups, box-and-whisker plots are used throughout the remainder of this chapter. In these plots, the box represents the central 50% of data for the group, and a short horizontal bar marks the median. The distance from the first to the third quartile, outlined by the box, is considered the central spread. Whiskers extend to demarcate all the data that falls up to an additional 1.5 times the spread away from the central quartiles. Outliers between one and two whisker lengths are marked with an asterix, and far outliers that fall outside this range are marked with an open circle.

5.2 Mars-Analog Results

5.2.1 Mars *In Vivo* Outcomes

Of the 10 animals suspended at the beginning of the study, 2 MARS animals were removed before the study was completed due to significant losses of body mass and signs of poor health. Of the 13 pair-fed jacketed animals, 5 JACK-M animals were removed. This attrition rate was significantly higher than seen in pilot (and later) studies in part because of ocular inflammation secondary to retro-orbital bleeds taken at the start of the experiment (Appendix D). Changes from these initial populations in the tables reported below typically represent samples lost to fracture or other handling errors during processing.

Across all studies, there were no significant differences in initial body mass (mean across groups $= 20.54 \pm 1.21$ grams).

Food usage for MARS animals decreased sharply at the time of suspension, stabilizing between days 6 and 7 (Figure 5-4). Consistent with this, MARS animals lost 6.6% of their body mass on average during the first week ($p < 0.0001$ relative to AGE controls). In weeks 2 and 3, there were no significant differences in growth rate between AGE and MARS groups, suggesting that stress levels had normalized (Figure 5-4).

Unexpected patterns of weight gain were seen for jacketed control animals (JACK-M), which experienced caloric restriction in the first week of the study while being pair fed to match their suspension cohorts (Figure 5-4). (A previous pilot study suggested that unrestricted food usage for well-adapted JACKET animals averages $7.5 \pm$ 1.39 grams/day.) After an initial decline in both consumption and body mass, the JACK-M animals experienced a rapid increase in body mass, showing significantly higher weight gain in weeks 2 and 3 than AGE or MARS animals ($p < 0.001$), resulting in a final JACK-M mean body mass significantly higher than both MARS and AGE controls. Femoral length was similar between AGE and JACK-M animals, suggesting that this weight gain was not due to true animal growth (Table 5.2).

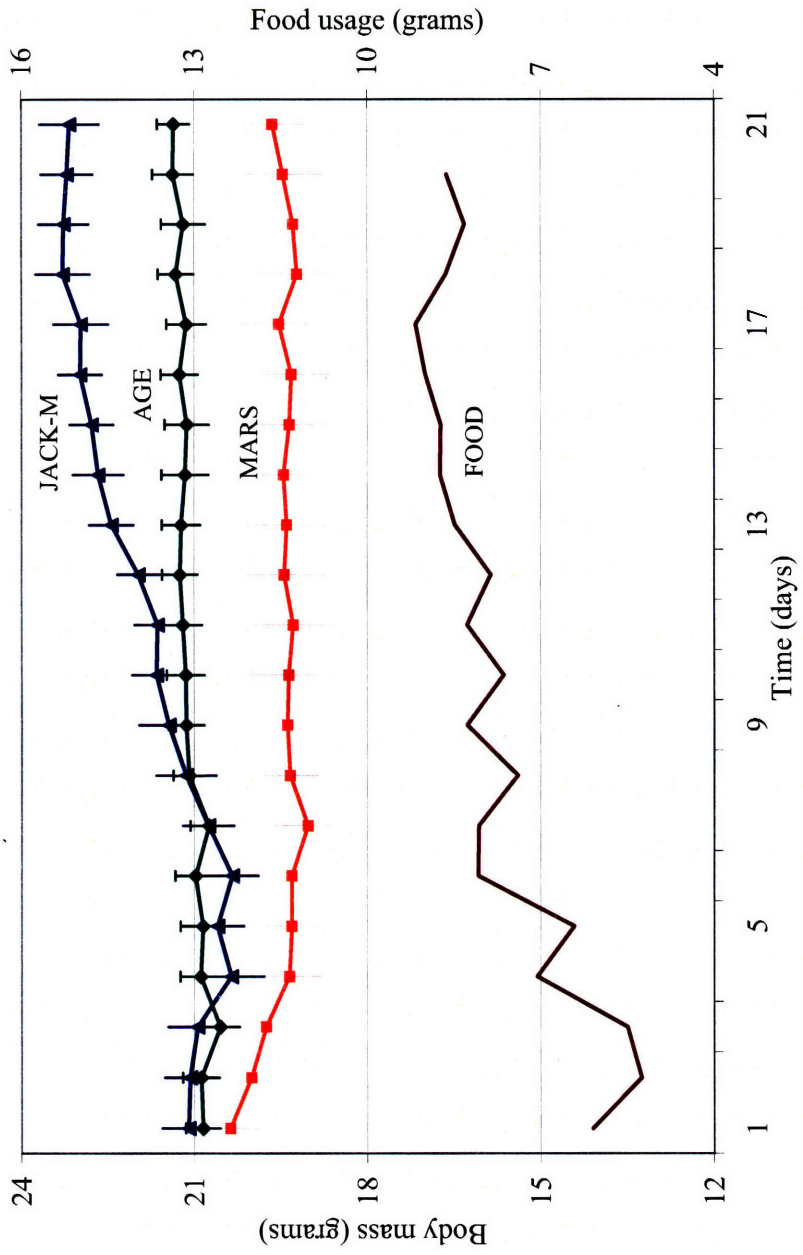

Figure 5-4: Body mass and food usage for Mars-analog study animals. Error bars represent ± standard error of the mean (SEM).

5.2.2 Mars *Ex Vivo* Outcomes

Bone Microarchitecture by μCT: Mars Results

MARS animals demonstrated significant thinner cortical bone in the femoral diaphysis relative to both AGE and JACKET controls (Figure 5-7). The size of the medullary cavity was similar in MARS, JACK-M, and AGE groups. However, MARS animals showed significant decrements in cortical bone area (BA) and cross-sectional tissue area (TA) relative to both control groups, suggesting that cortical thinning was due to relative reductions in bone formation on the periosteal surface (Figure 5-5). Similarly, in the distal femoral metaphysis, MARS animals also demonstrated significant cortical thinning and reductions in cross-sectional tissue area relative to both control groups.

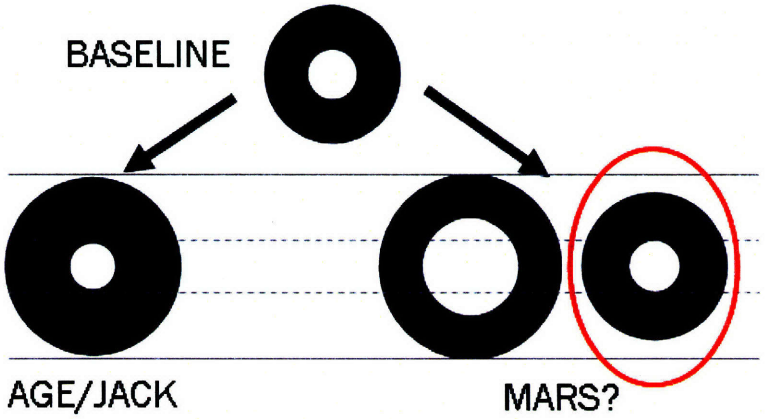

Figure 5-5: During phases of cortical growth, relative cortical thinning can be caused either by endosteal resorption from the inside out, or by a reduction in periosteal apposition. MARS animals showed no significant changes in the size of their marrow cavities, but did have significantly smaller cross-sectional areas in the femoral mid-shaft than controls, suggesting periosteal changes were responsible for the observed cortical thinning. (Dimensions in this illustration are exaggerated for clarity.)

In the trabecular compartment of the distal femoral metaphysis, BV/TV was decreased in MARS animals relative to controls (-20.6% vs AGE, $p < 0.005$, Table 5.1). There was no difference in trabecular number or spacing in the distal femur (Figure 5-9). Rather, BV/TV losses were driven by a significant trabecular thinning, above and beyond that expected due to age-related changes. JACK-M animals had

Table 5.1: Trabecular and cortical bone architecture, and muscle mass following 3 weeks of MARS-analog loading in adult female mice. Variation in sample numbers were due to bones broken during dissection or handling. Values are given as mean (std dev).

	BASE (n=7–8)	AGE (n=19–20)	JACK-M (n=8)	MARS (n=8–9)
Trabecular bone architecture (distal femur)				
Bone volume fraction (%)	23.51 (3.03)	18.07 (2.37)	18.06 (1.60)	14.34 (3.18) [a,b]
Trab. Thickness (μm)	54.97 (0.00)	53.56 (1.48)	53.26 (2.82)	47.65 (1.85) [a,b]
Trab. Number (mm^{-1})	5.24 (0.29)	4.39 (0.28)	4.47 (0.18)	4.37 (0.29)
Trab. Spacing (μm)	182.84 (12.34)	222.28 (18.24)	216.65 (9.61)	222.46 (15.06)
Connectivity Density (mm^{-3})	207.12 (23.89)	134.35 (20.29)	145.84 (18.73)	124.29 (26.29)
Structural Model Index	1.31 (0.30)	1.69 (0.24)	1.79 (0.22)	2.14 (0.40) [a]
*Trabecular bone architecture (proximal tibia) **				
Bone volume fraction (%)	0.13 (0.03)	0.11 (0.02)	0.12 (0.02)	0.10 (0.02)
Trab. Thickness (μm)	47.46 (4.74)	47.71 (5.07)	48.22 (1.89)	45.77 (2.29)
Trab. Number (mm^{-1})	4.38 (0.35)	3.91 (0.30)	4.11 (0.36)	3.56 (0.23)
Trab. Spacing (μm)	233.34 (21.90)	259.74 (20.55)	245.12 (22.14)	250.44 (13.67)
Connectivity Density (mm^{-3})	121.10 (13.86)	78.77 (36.08)	83.71 (22.75)	59.31 (19.68)
Structural Model Index	2.32 (0.19)	2.62 (0.27)	2.58 (0.24)	2.69 (0.22)
*Cortical bone architecture (distal femur) ***				
Cross-sectional area (mm^2)	3.64 (0.33)	3.69 (0.22)	3.58 (0.25)	3.04 (0.21) [a,b]
Cortical thickness (μm)	166.57 (9.66)	167.10 (8.06)	158.60 (7.47)	134.00 (6.46) [a,b]
Cortical bone architecture (femoral midshaft)				
Cross-sectional area (mm^2)	1.55 (0.09)	1.54 (0.10)	1.55 (0.09)	1.46 (0.10) [a]
Cortical bone area (mm^2)	0.87 (0.08)	0.87 (0.06)	0.87 (0.05)	0.79 (0.05) [a,b]
Medullary area (mm^2)	0.68 (0.08)	0.67 (0.07)	0.68 (0.06)	0.68 (0.07)
Cortical thickness (μm)	223.75 (16.46)	233.20 (11.75)	230.75 (5.31)	212.44 (8.92) [a,b]
*Gastrocnemius muscle wet mass ****				
Average mass (mg)	107.88 (7.26)	116.17 (10.20)	113.50 (9.19)	90.88 (9.38) [a]
Normalized to body mass (%)	0.55 (0.02)	0.55 (0.06)	0.51 (0.01)	0.48 (0.04) [a]

[a] MARS significantly different than AGE ($p < 0.05$);
[b] MARS significantly different than JACK-M ($p < 0.05$);
* n=9 for AGE
** n=10 for AGE
*** n=8 for BASE, n=13 for AGE, n=2 for JACK-M, n=4 for MARS

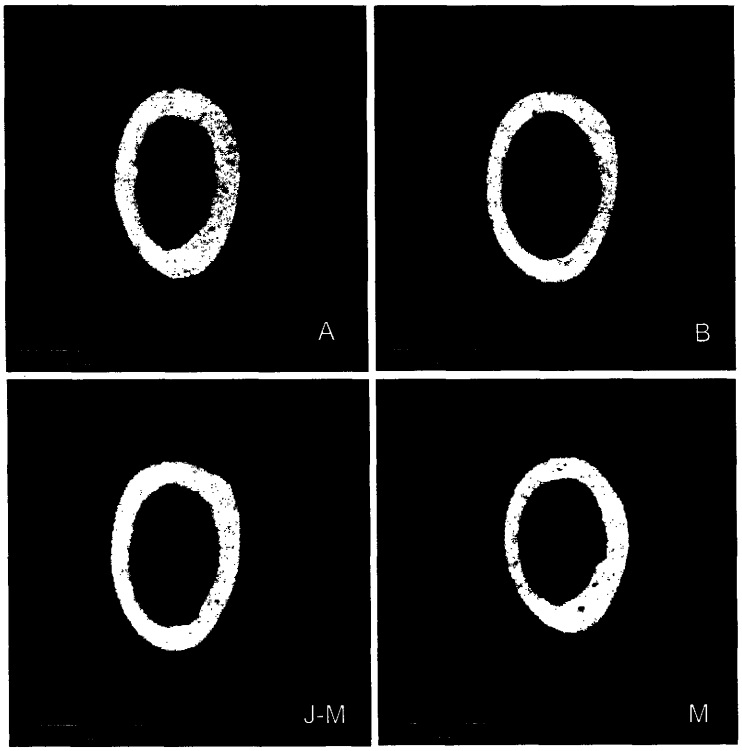

Figure 5-6: Representative μCT images of the distal femoral mid-diaphysis for the Mars-analog study.
A=AGE, B=BASE, J-M=JACK-M, M=MARS

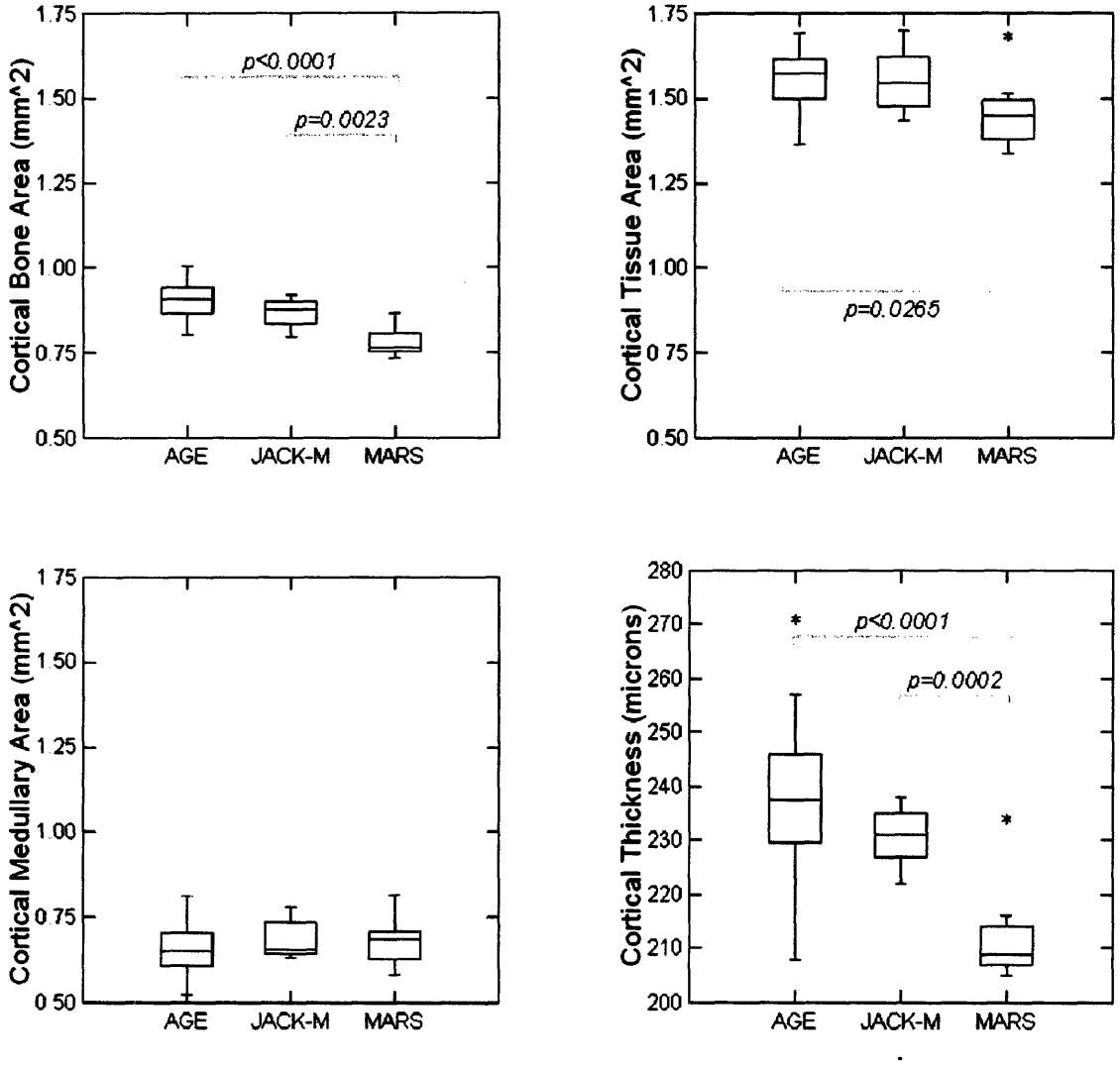

Figure 5-7: Effect of group on cortical parameters of the femoral mid-diaphysis in Mars-analog study animals. MARS suspension resulted in significant cortical thinning, due to reduced periosteal apposition. Significant differences between MARS animals and controls are marked with p-values.

somewhat greater trabecular connectivity (Conn.D) than AGE controls, but MARS animals showed significantly sparser connections than these jacketed animals.

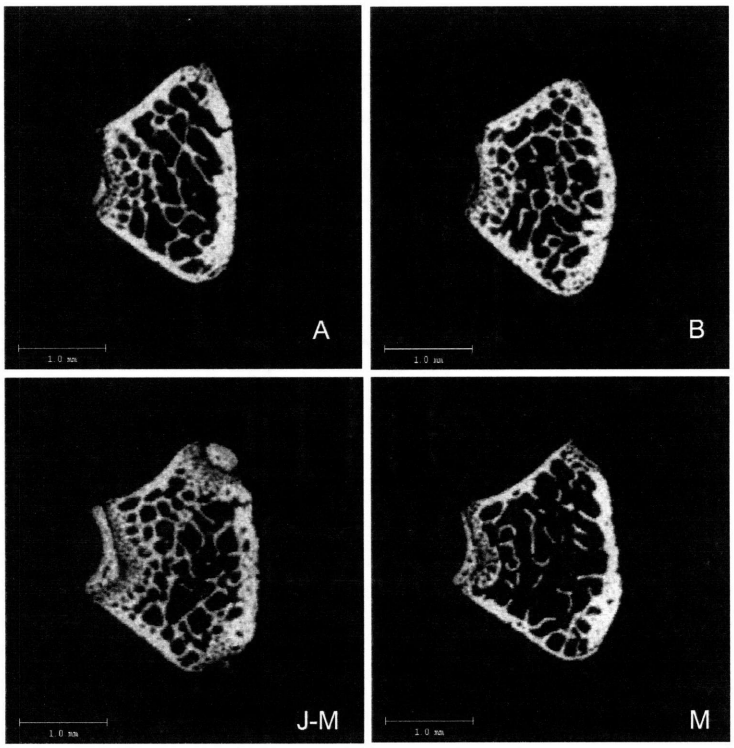

Figure 5-8: Representative μCT images of the distal femoral metaphysis for the Mars-analog study. Additional structures outside the main femoral compartment are associated sesamoid bones.
A=AGE, B=BASE, J-M=JACK-M, M=MARS

In keeping with the trabecular thinning just described, there was also a significant shift in the structural model index (SMI) of MARS femurs. Whereas all groups had intermediate values of SMI, suggesting a mix of both plate-like (SMI=0) and rod-like (SMI=3) structures, MARS animals demonstrated a shift towards rod-like geometry.

Data from the proximal tibia also showed reductions in BV/TV ($p = 0.1688$ vs AGE). There was, again, noticeable trabecular thinning versus controls (vs AGE, vs JACK-M), with no clear difference in trabecular number. However, the magnitude

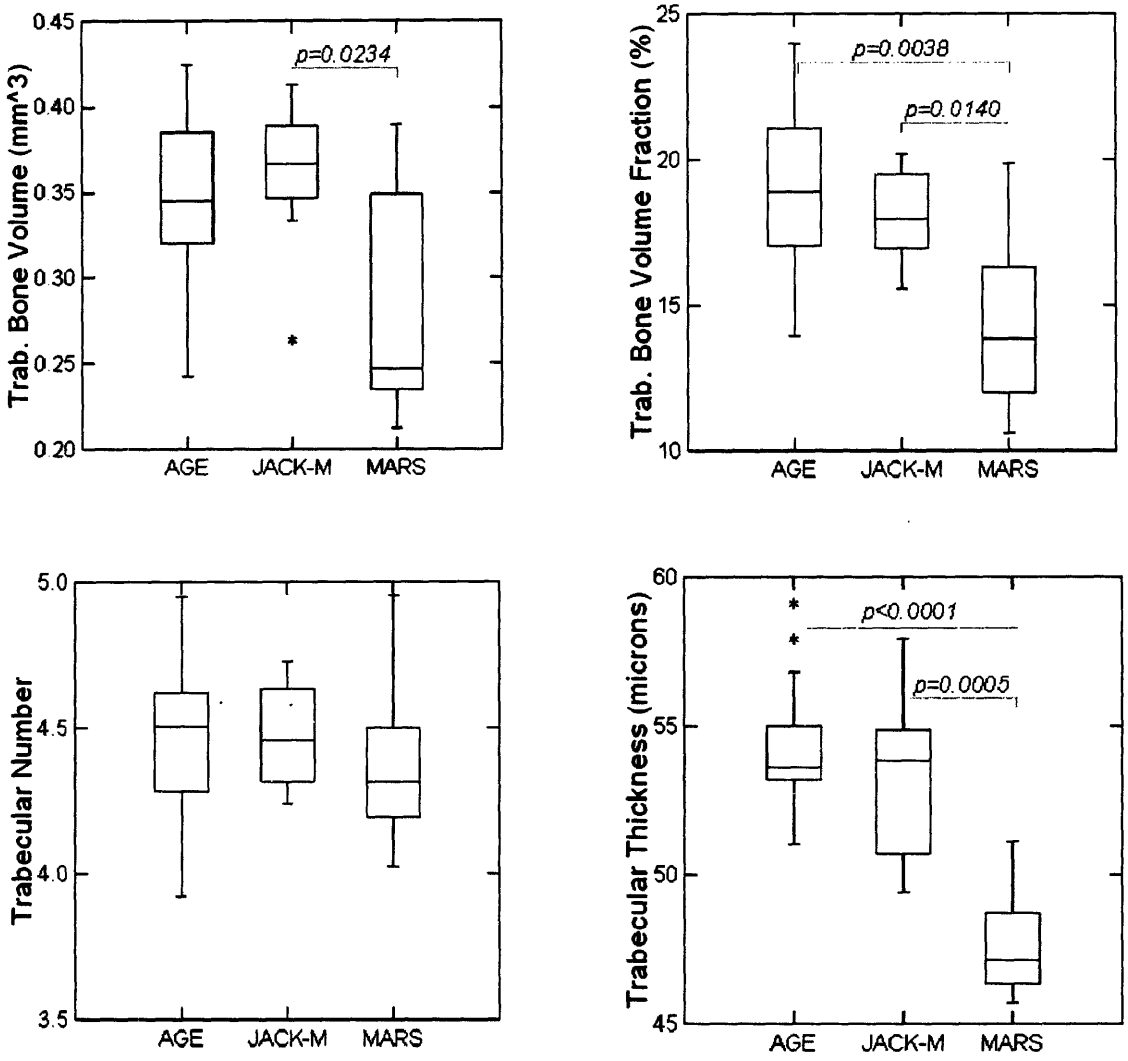

Figure 5-9: Effect of group on trabecular parameters of the distal femoral metaphysis in Mars-analog study animals. MARS suspension resulted in a significant reduction in trabecular bone volume, due to trabecular thinning. Significant differences between MARS animals and controls are marked with p-values.

of the effect was much smaller in the tibia (-6.8% Tb.Th vs AGE) than in the distal femur (-11% Tb.Th vs AGE).

Femoral Biomechanics: Mars Results

One AGE and one MARS specimen that broke incompletely due to interference between the MTS jig and condyles were removed from this analysis. One additional specimen (Case 50, OCT M3), was removed due to atypical post-yield behavior that caused inappropriately large values of post-yield bending energy and displacement.

Ultimate strength was reduced by 22.4% in MARS samples relative to AGE controls ($p = 0.0003$) and by 17.4% relative to JACK-M ($p = 0.0315$)(Table 5.2, Figure 5-10). Yield strength was significantly reduced by 12.4% for MARS animals relative to AGE controls ($p = 0.001$). There were no significant difference in displacement at yield, and this combination revealed significant reductions in extrinsic stiffness relative to AGE controls. Unlike the μCT data above, many of these significant differences in biomechanical behavior between MARS and AGE groups were not seen for MARS vs JACK-M comparisons, though trends were in the same direction.

Bending energy to failure and post-yield bending energy were similar across groups, suggesting that specimens did not become noticeably more brittle or ductile in the 3-week study.

When extrinsic stiffness was normalized to area moments of inertia (I_{min}) in order to examine intrinsic stiffness, effective Young's modulus (E^*) was not significantly different between groups, suggesting that changes in biomechanical performance were not due to material properties, but rather to geometric changes (Figure 5-10). This was consistent with the significantly lower values of moments of inertia in MARS specimens relative to AGE controls ($p = 0.0007$). Interestingly, despite the lack of effect in effective Young's modulus, there *were* reductions in a measure of bone mineral density in the femoral mid-shaft for MARS relative to AGE, suggesting a possible increased bending stiffness in non-mineral components.

Surprisingly, JACK-M animals showed significant reductions in effective Youngs modulus relative to AGE controls ($p = 0.0005$), with no significant decrease in esti-

Table 5.2: Structural and derived material properties for the Mars-analog study. Values are given as mean (std dev).

	BASE (n=8)	AGE (n=19)	JACK-M (n=7–8)	MARS (n=7–9)
Femur Length (mm)	14.23 (0.46)	14.89 (0.33)	14.97 (0.28)	14.56 (0.45) [b]
Minimum Moment of Inertia (mm^4)	0.10 (0.01)	0.11 (0.01)	0.11 (0.01)	0.09 (0.01) [a,b]
Maximum Moment of Inertia (mm^4)	0.21 (0.03)	0.21 (0.03)	0.21 (0.03)	0.18 (0.03) [a]
Polar Moment of Inertia (mm^4)	0.31 (0.04)	0.32 (0.04)	0.32 (0.04)	0.28 (0.04) [a,b]
Displacement at Yield (mm)	0.12 (0.03)	0.10 (0.02)	0.10 (0.02)	0.10 (0.02)
Moment at Yield (N*mm)	15.69 (5.56)	14.89 (3.86)	13.16 (2.03)	13.05 (1.21) [a]
Stiffness (N/mm)	125.85 (12.10)	134.04 (7.23)	124.35 (7.58)	114.70 (13.86) [a]
Bending Rigidity (N*mm^2)	566.35 (54.46)	603.16 (32.52)	559.57 (34.11)	516.14 (62.38) [a]
Ultimate Moment (N*mm)	26.10 (3.59)	27.31 (3.28)	25.67 (2.77)	21.20 (3.38) [a,b]
Crosshead Displacement At Failure (mm)	0.30 (0.05)	0.28 (0.02)	0.30 (0.03)	0.27 (0.04)
Bending Energy To Failure (N*mm^2)	6.23 (1.90)	6.46 (1.42)	6.87 (1.94)	6.22 (2.24)
Post-Yield Crosshead Displacement (mm)	0.25 (0.11)	0.25 (0.06)	0.28 (0.09)	0.29 (0.10)
Post-Yield Bending Energy (N*mm^2)	5.45 (2.16)	5.82 (1.40)	6.35 (1.95)	5.67 (2.22)
Est. Young's Modulus (N/mm^2)	5611.95 (598.13)	5720.97 (662.78)	4933.61 (192.55)	5480.99 (702.87)
Est. BMD (Mean2, g/cm^2)	1231.20 (20.52)	1260.28 (13.23)	1261.88 (13.03)	1251.25 (11.99) [a]

[a] MARS significantly different than AGE ($p < 0.05$);
[b] MARS significantly different than JACK-M ($p < 0.05$)

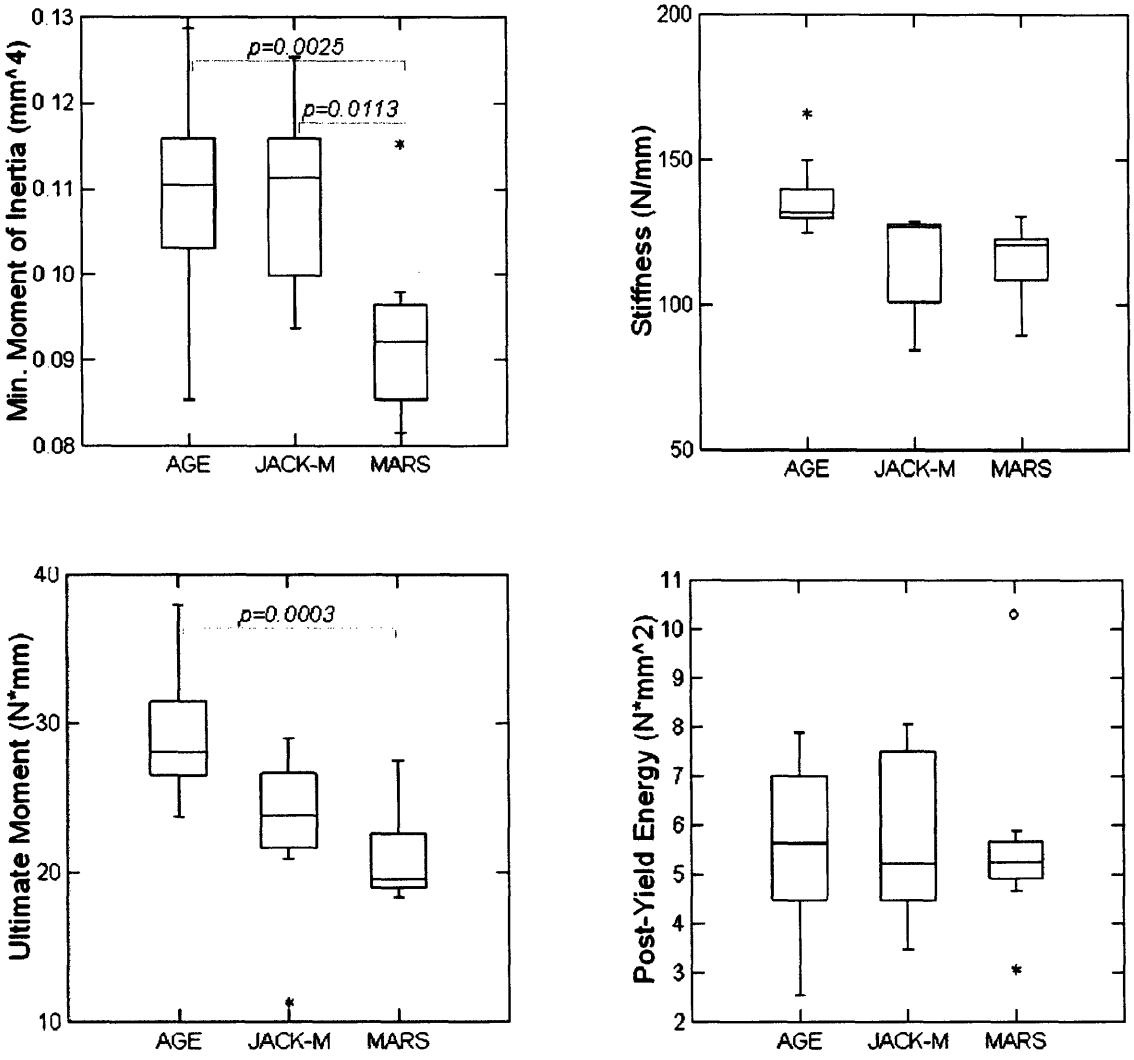

Figure 5-10: Effect of group on three-point bending of the whole femur in Mars-analog study animals. MARS suspension resulted in a significant reduction in ultimate moment and extrinsic stiffness, as compared with AGE controls, due to changes in mid-shaft geometry. Significant differences between MARS animals and controls are marked with p-values.

mated bone mineral density for the femoral mid-shaft.

In summary, MARS bones were significantly weakened in bending relative to AGE controls, due largely to geometric changes, and not intrinsic material stiffness.

Histology: Mars Results

Compared to AGE matched controls, MARS animals had significantly less mineralizing surface (MS/BS) and lower bone formation rates (BFR/BS) in the proximal tibial metaphysis (Table 5.3). Furthermore, MARS animals also had significant less osteoid surface (OS/BS), consistent with reduced BFR.

Interestingly, while age-related trends suggested increasing numbers of osteoclasts in this timeframe, MARS animals had significantly lower areas of osteoclast surface (Oc.S/BS) and no change in erosion surface (ES/BS), with trends towards lower osteoclast numbers ($p_{KW} = 0.117$). This suggests unchanged or slightly lower rates of resorption in MARS animals.

Despite the reductions in BFR, there were no differences in osteoblast numbers or surface area between groups.

In summary, despite unexpected reductions in osteoclasts and no clear changes in osteoblasts, MARS animals demonstrated reduced rates of bone formation and no clear changes in resorption, compared to AGE controls.

Muscle Mass: Mars Results

MARS animals had significantly lower average gastrocnemius muscle wet mass than AGE controls ($-21.8\%, p = 0.0062$). Normalizing gastrocnemius mass to final body mass, MARS animals continued to show significantly reduced muscle relative to AGE controls ($-14.2\%, p = 0.0232$). There was no significant difference for MARS animals vs JACK-M for either raw or normalized muscle mass.

Interestingly, despite their high rate of growth, JACK-M animals showed significant decreases in normalized gastrocnemius wet mass relative to AGE controls ($p = 0.0034$).

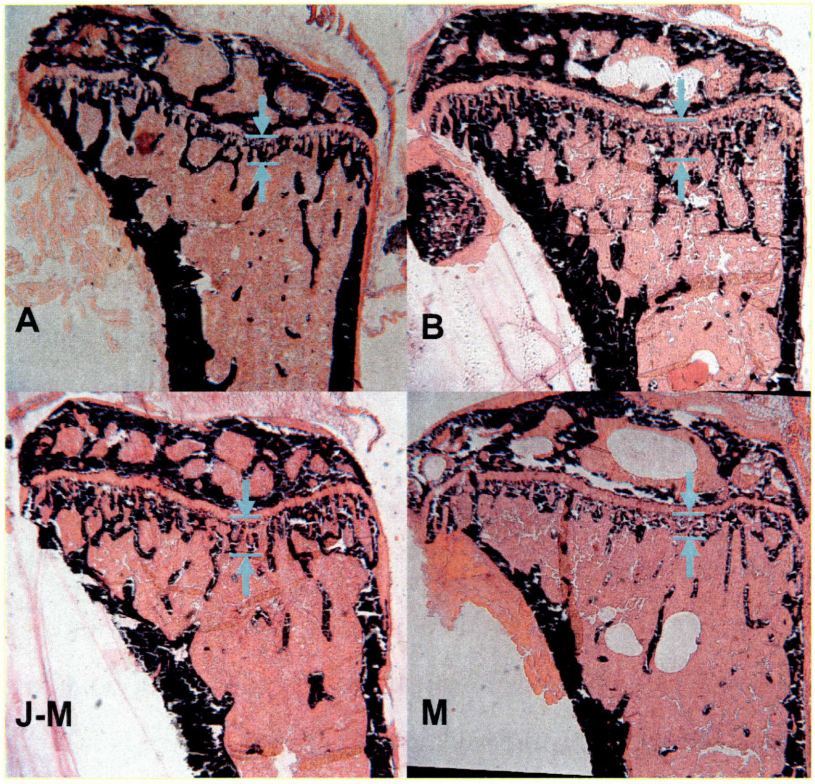

Figure 5-11: Selected histological slices of proximal tibia, treated with von Kossa stain. Black silver stain accumulates in the presence of calcium in mineralized bone. Arrows delineate the width of the primary spongiosa, highlighting a reduction in thickness, particularly related to JACK-M controls.
A=AGE, B=BASE, J-M=JACK-M, M=MARS

Table 5.3: Histological and histomorphometric data from the Mars-analog study. Values are given as mean (std dev).

	BASE (n=5)	AGE (n=5)	JACK-M (n=5)	MARS (n=5)
MS/BS (%)	18.58 (4.10)	17.72 (6.80)	10.62 (4.28)	11.19 (2.91) [a]
BFR/BS ($\mu m^3/\mu m^2/day$)	169.72 (62.13)	105.50 (88.16)	46.91 (44.55)	43.38 (16.69) [a]
BFR/BV ($\mu m^3/\mu m^3/day^{-1}$)	731.54 (217.83)	441.21 (356.50)	200.54 (168.55)	263.09 (98.46)
MAR ($\mu m/day$)	2.49 (0.57)	1.42 (0.63)	1.03 (0.58)	1.10 (0.23)
OS/BS (%)	3.19 (1.60)	2.08 (0.29)	2.09 (0.58)	1.4832 (0.42) [a]
Ob.S/BS (%)	24.166 (5.425)	12.922 (4.710)	9.842 (0.668)	10.762 (2.208)
ES/BS (%)	1.10 (0.55)	0.95 (0.20)	1.12 (0.28)	0.95 (0.18)
Oc.S/BS (%)	0.65 (0.30)	0.82 (0.08)	0.69 (0.24)	0.58 (0.19) [a]
O.Th (μm)	6.78 (1.04)	4.73 (0.60)	3.73 (0.52)	4.47 (1.48)
N.Ob/BS (μm^{-2})	14.71 (4.72)	7.29 (2.86)	5.43 (0.11)	6.00 (1.05)
N.Oc/BS (μm^{-2})	0.48 (0.21)	0.59 (0.07)	0.63 (0.11)	0.46 (0.17)

[a] MARS significantly different than AGE by Kruskall-Wallis test ($p_{KW} < 0.05$)

MS: mineralized surface, BFR: bone formation rate, OS: osteoid surface, Ob.S: osteoblast surface, ES: erosion surface, Oc.S: osteoclast surface, O.Th: osteoid thickness, N.Ob: number of osteoblasts, N.Oc: number of osteoclasts, BS: bone surface, BV:bone volume

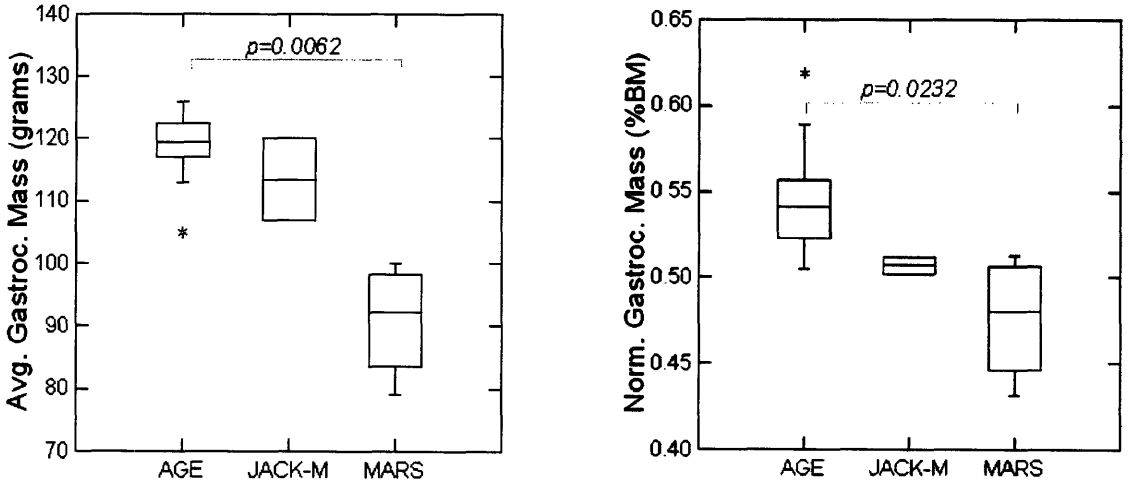

Figure 5-12: Effect of group on gastrocnemius wet mass in Mars-analog study animals. MARS suspension resulted in a significant reduction in muscle wet mass, independent of body mass changes. Significant differences between MARS animals and controls are marked with p-values.

5.3 Lunar-Analog Investigations

5.3.1 Experimental Design

Following the Mars investigations described above, a second study was conducted to further explore the continuum of partial weightbearing effects, focusing on the operationally relevant domain of lunar exploration. Experimental design mirrored that used in the Mars study, with a target weightbearing condition of 16%.

Ten week old female BALB/cByJ mice were assigned to one of three conditions for periods of 0 (baseline) or 21 days. Numbers of animals represent starting populations.

- **LUNAR:** jacketed animals suspended at 16% weightbearing, individually housed, with *ad libitum* food and water, n=10

- **JACK-L:** fully weightbearing jacketed controls, identically housed to suspension animals and pair-fed according to LUNAR group daily means, n=11

- **AGE:** unjacketed age-matched, group-housed vivarium controls with *ad libitum* food and water, n=21

As mentioned earlier, for greater statistical power, data from AGE animals were shared between the Mars- and lunar-analog studies.

5.3.2 Lunar-Analog Methods

Experimental methods for the lunar-analog studies were identical to the Mars-analog methods described above. Left femurs were preserved in cold storage and subjected to microCT imaging and three-point bending, as described. While animals were administered calcein labels, no histology was undertaken at this time.

5.4 Lunar-Analog Results

5.4.1 Lunar *In Vivo* Outcomes

Of the 10 animals that started in lunar suspension, one was removed before the study was completed due to significant losses of body mass and signs of poor health. None of the 11 pair-fed jacketed animals were removed. Changes from these initial populations in the tables reported below typically represent samples lost to fracture or other handling errors during processing.

As in the Mars study above, LUNAR animals had significant decreases in body mass during the first week, relative to AGE controls ($p < 0.0001$, Figure 5-13). There were no significant differences in weight gain between AGE and LUNAR groups during weeks 2 and 3, suggesting that stress levels had normalized.

Food usage for LUNAR animals also followed a similar pattern to the MARS animals, decreasing sharply at the time of suspension, but stabilizing around day 7 (Figure 5-13). Mirroring the JACK-M findings, in the first 8 days of the lunar study, JACK-L controls lost 2.4 grams of body mass, commensurate with increased stress and caloric restriction. After this initial decline, however, JACK-L animals showed significantly higher weight gain in weeks 2 and 3 than AGE or LUNAR animals ($p < 0.0001$), resulting in final mass values nearly identical to AGE controls.

5.4.2 Lunar *Ex Vivo* Outcomes

Bone Microarchitecture by μCT: Lunar Results

LUNAR animals demonstrated significant cortical thinning in the femoral diaphysis relative to AGE controls, with no significant changes in the medullary area and only slightly decreased cross sectional tissue area (Table 5.4, Figure 5-15). Interestingly, there were significant decrements in cortical bone area (BA), suggesting minimal inhibition of bone formation on the periosteal surface. Cortical properties of the distal femur were not analyzed for this cohort.

In the distal femoral metaphysis, LUNAR animals had a significant reduction in

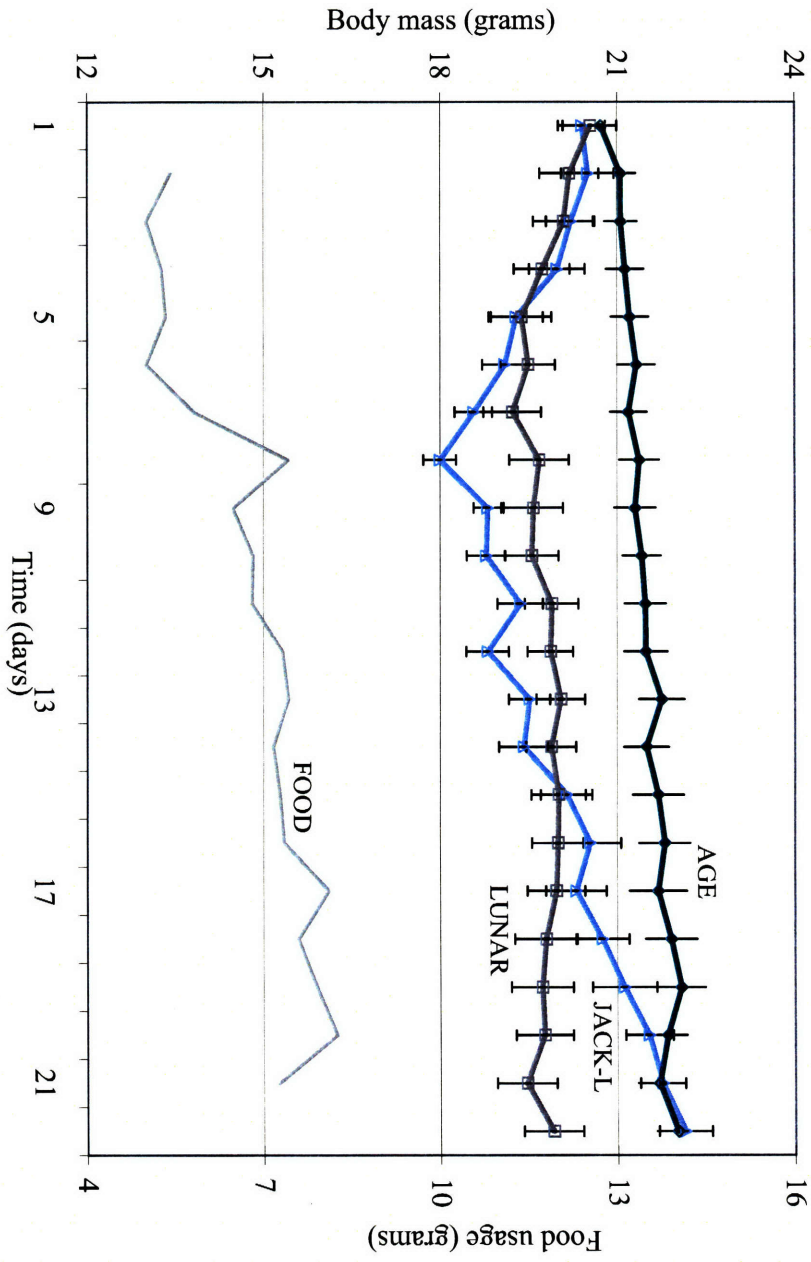

Figure 5-13: Body mass and food usage for lunar-analog study animals. Error bars represent ± standard error of the mean (SEM).

Table 5.4: Muscle weight, trabecular and cortical bone architecture and bone strength following 3 weeks of LUNAR-analog loading in adult female mice. Values are given as mean (std dev).

	AGE (n=19–20)	JACK-L (n=10–11)	LUNAR (n=7–8)
Trabecular bone architecture (distal femur)			
Bone volume fraction (BV/TV, %)	18.07 (2.37)	18.02 (1.90)	16.50 (2.48) [a]
Trab. Thickness (μm)	53.56 (1.48)	52.36 (2.10)	49.29 (1.62) [a,b]
Trab. Number (mm^{-1})	4.39 (0.28)	4.46 (0.23)	4.50 (0.23)
Trab. Spacing (μm)	222.28 (18.24)	218.09 (12.89)	213.34 (12.75)
Connectivity Density (connections/mm^{-3})	134.35 (20.29)	143.33 (22.76)	143.33 (20.48)
Structural Model Index	1.69 (0.24)	1.79 (0.22)	1.92 (0.34) [a]
Cortical bone architecture (femoral midshaft)			
Cross-sectional tissue area (mm^2)	1.54 (0.10)	1.54 (0.10)	1.51 (0.11)
Cortical bone area (mm^2)	0.87 (0.06)	0.85 (0.05)	0.83 (0.07) [a]
Medullary area (mm^2)	0.67 (0.07)	0.68 (0.07)	0.68 (0.08)
Cortical thickness (μm)	233.20 (11.75)	225.82 (8.42)	216.88 (12.29) [a]
Gastrocnemius muscle wet mass *			
Average gastrocnemius mass (mg)	116.17 (10.20)	115.50 (6.79)	102.50 (12.10) [a,b]
Normalized to body mass (%)	0.55 (0.06)	0.51 (0.03)	0.52 (0.09)

[a] LUNAR significantly different than AGE ($p < 0.05$);
[b] LUNAR significantly different than JACK-L ($p < 0.05$);
* n=13 for AGE, n=7 for JACK-L, n=8 for LUNAR

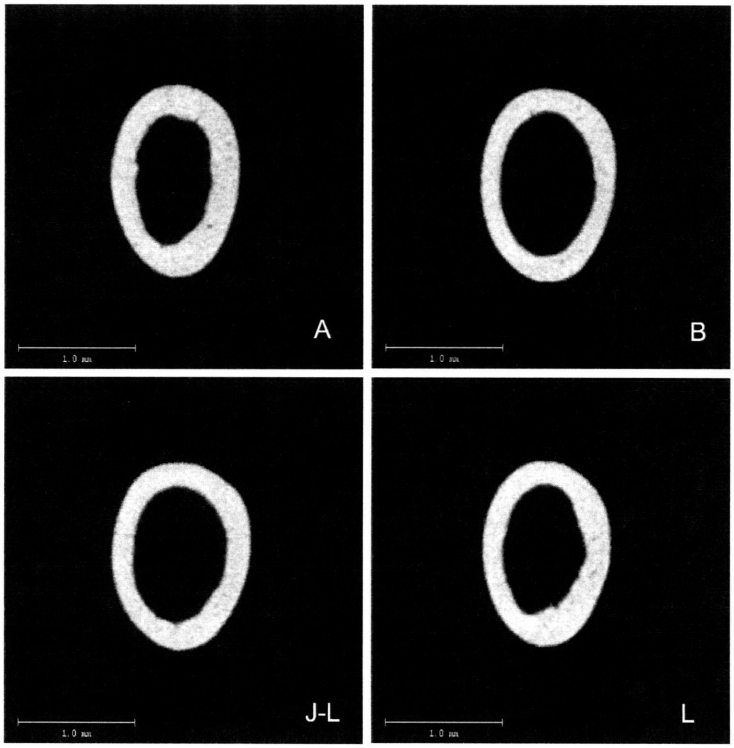

Figure 5-14: Representative μCT images of the distal femoral mid-diaphysis for the lunar-analog study.
A=AGE, B=BASE, J-L=JACK-L, L=LUNAR

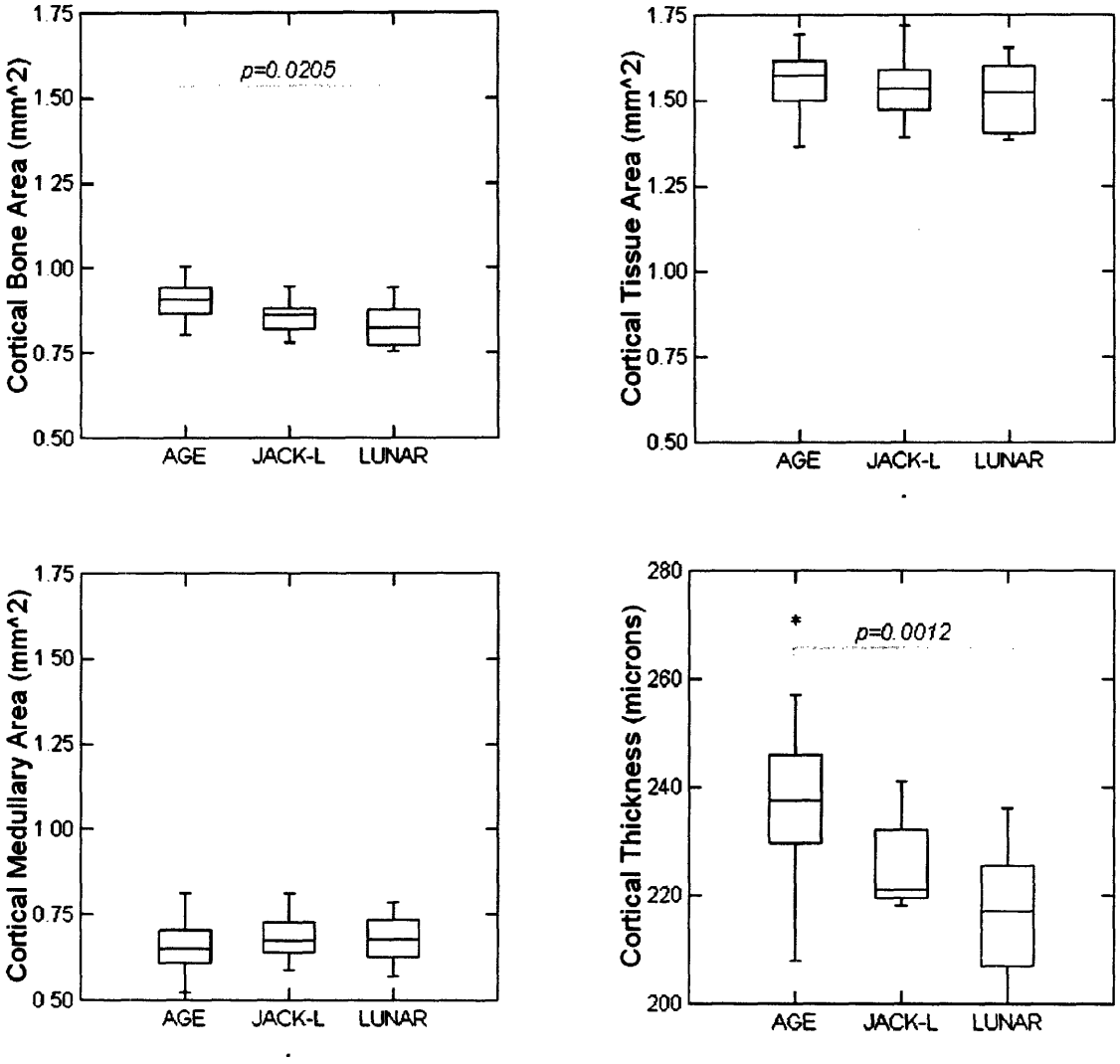

Figure 5-15: Effect of group on cortical parameters of the femoral mid-diaphysis in Lunar-analog study animals. LUNAR suspension results in significant cortical thinning, due to periosteal resorption. Significant differences between LUNAR animals and controls are marked with p-values.

bone volume fraction, relative to AGE controls (Table 5.4, Figure 5-17). As in the Mars study, no changes in trabecular number, spacing, or connectivity density were evident in this region. Rather, trabecular bone losses on the order of -8.7% were driven by a significant trabecular thinning, as reflected by a significant increase in SMI towards a more rod-like geometry.

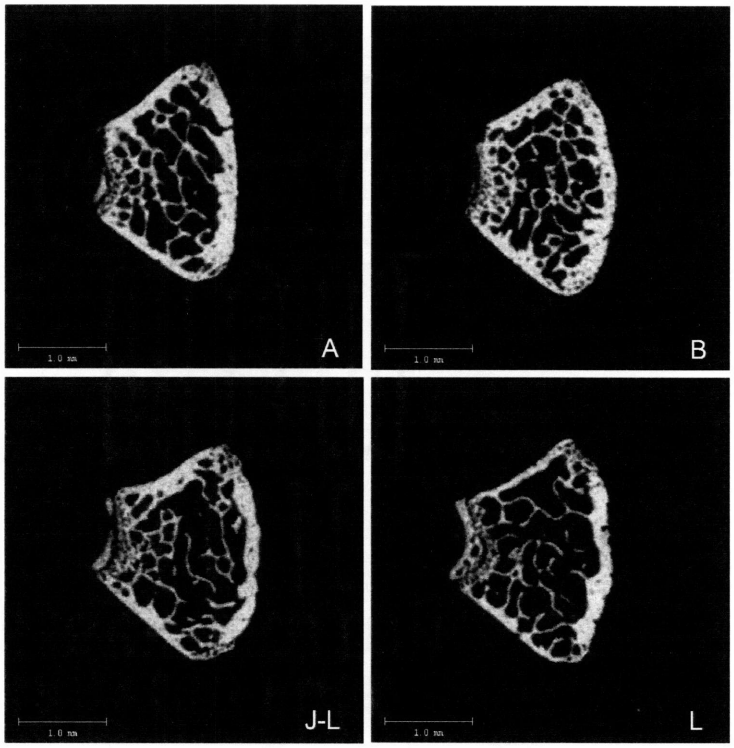

Figure 5-16: Representative μCT images of the distal femoral metaphysis for the lunar-analog study.
A=AGE, B=BASE, J-L=JACK-L, L=LUNAR

Femoral Biomechanics: Lunar Results

One LUNAR specimen that broke incompletely, due to interference between the testing jig and the bone condyles, was removed from this analysis.

LUNAR samples showed significant reductions in ultimate moment relative to

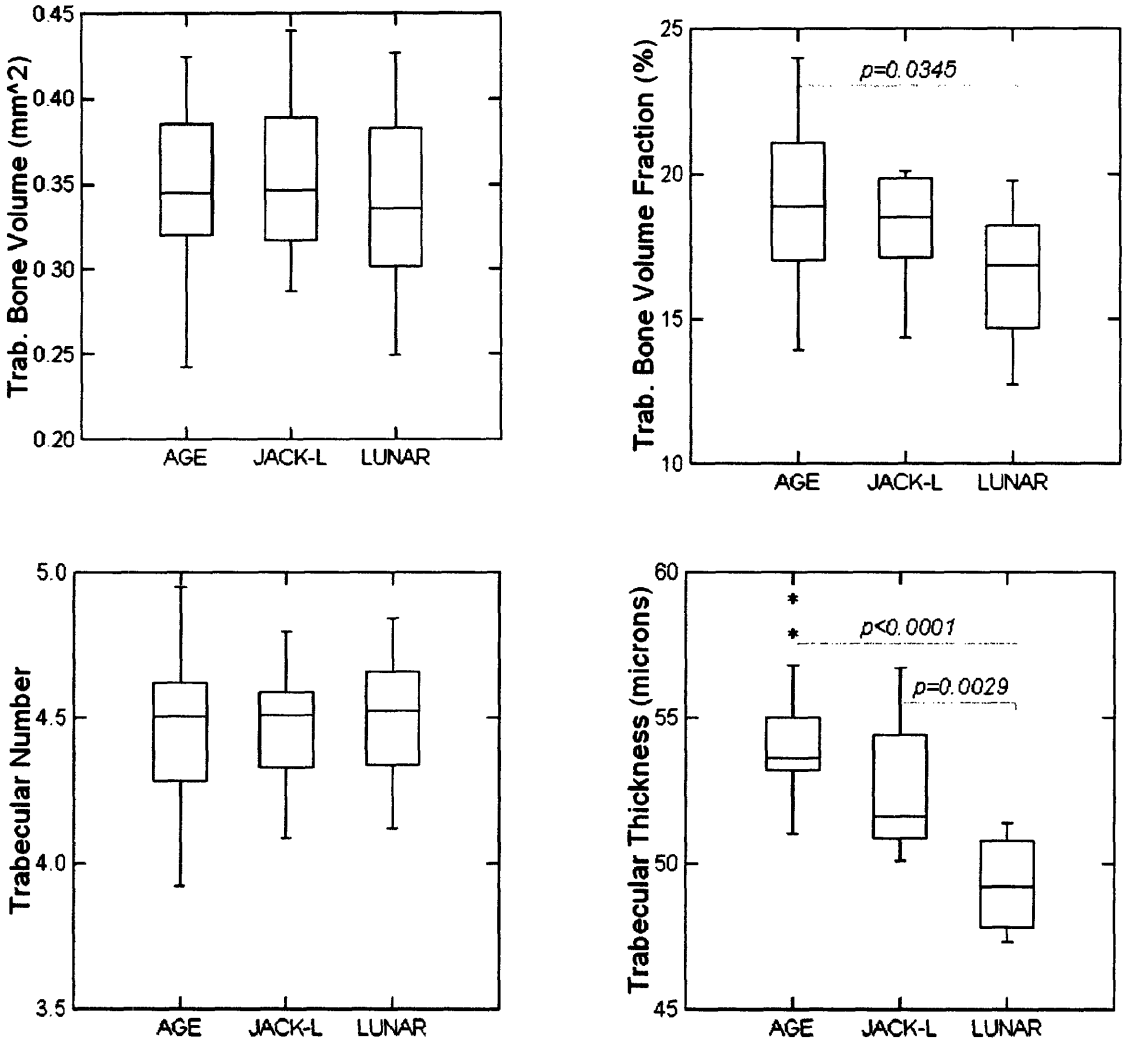

Figure 5-17: Effect of group on trabecular parameters of the distal femoral metaphysis in Lunar-analog study animals. LUNAR suspension results in a significant reduction in trabecular bone volume, due to trabecular thinning. Significant differences between LUNAR animals and controls are marked with p-values.

AGE controls, but no significant changes in bending energy (Table 5.5). Ultimate displacement was lower in LUNAR animals relative to AGE due to decreases in displacement at yield. There were no significant differences in extrinsic stiffness between groups.

When extrinsic stiffness was normalized to area moments of inertia (I_{min}), effective Young's modulus (E*) was not significantly different between groups, suggesting that changes in biomechanical performance were not due to material properties, but rather to geometric changes (Figure 5-18). This was consistent with the strong trend towards lower moments of inertia in LUNAR specimens relative to AGE controls (Figure 5-18, I_{min} vs NORM, $p = 0.0770$).

No significant changes were noted in post-yield behavior, suggesting that specimens did not become noticeably more brittle or ductile in the 3-week study.

In summary, like the MARS study described above, LUNAR bones were also significantly weakened relative to AGE controls, due largely to geometric changes, and not intrinsic material stiffness.

Table 5.5: Structural and derived material properties for the lunar-analog study. Values are given as mean (std dev).

	AGE (n=19)	JACK-L (n=10–11)	LUNAR (n=7–8)
Femur Length (mm)	14.89 (0.33)	14.73 (0.44)	14.98 (0.50)
Polar Moment of Inertia (mm^4)	0.32 (0.04)	0.31 (0.04)	0.30 (0.04)
Minimum Moment of Inertia (mm^4)	0.11 (0.01)	0.11 (0.01)	0.10 (0.01)
Maximum Moment of Inertia (mm^4)	0.21 (0.03)	0.21 (0.03)	0.20 (0.03)
Displacement at Yield (mm)	0.10 (0.02)	0.10 (0.04)	0.09 (0.02) [a]
Moment at Yield (N*mm)	14.89 (3.86)	13.59 (3.56)	14.11 (3.74)
Stiffness (N/mm)	134.04 (7.23)	133.03 (14.38)	129.89 (11.55)
Bending Rigidity (N*mm^2)	603.16 (32.52)	598.64 (64.71)	584.52 (51.96)
Ultimate Moment (N*mm)	27.31 (3.28)	27.37 (3.20)	24.67 (4.19) [a]
Crosshead Displacement At Failure (mm)	0.28 (0.02)	0.27 (0.05)	0.24 (0.03) [a]
Bending Energy To Failure (N*mm^2)	6.46 (1.42)	7.21 (2.00)	5.78 (1.52)
Post-Yield Crosshead Displacement (mm)	0.25 (0.06)	0.30 (0.13)	0.24 (0.08)
Post-Yield Bending Energy (N*mm^2)	5.82 (1.40)	6.68 (2.14)	5.20 (1.67)
Est.Young's Modulus (N/mm^2)	5720.97 (662.78)	5689.70 (708.38)	5870.17 (825.42)
Est. BMD (Mean2, g/cm^2)	1261.88 (13.03)	1269.43 (11.20)	1264.46 (15.42)

[a] LUNAR significantly different than AGE ($p < 0.05$);
[b] LUNAR significantly different than JACK-L ($p < 0.05$)

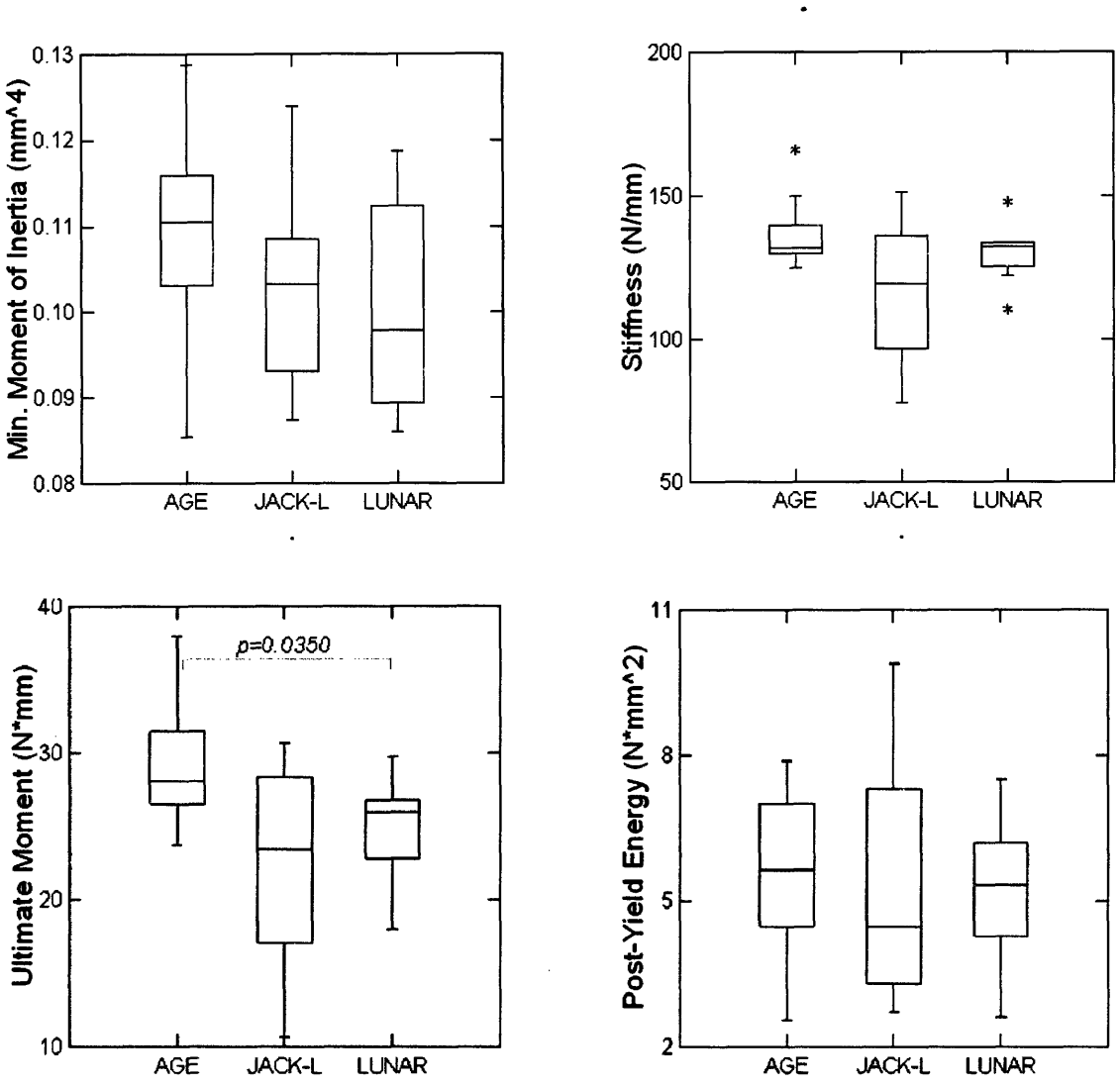

Figure 5-18: Effect of lunar suspension on femoral biomechanics. Lunar-analog loading resulted in a significant reduction in ultimate moment and displacement at yield, as compared with AGE controls, due to small changes in mid-shaft geometry. Significant differences between LUNAR animals and controls are marked with p-values.

Muscle Mass: Lunar Results

Average gastrocnemius muscle mass in LUNAR animals was 11.8% lower than AGE controls, while JACK-L animals showed no significant loss. When normalized to final body mass, LUNAR muscle mass was only 6.3% lower than AGE (Figure 5-19). As in the Mars study, JACK-L animals showed significant decreases in normalized gastrocnemius wet mass relative to AGE controls.

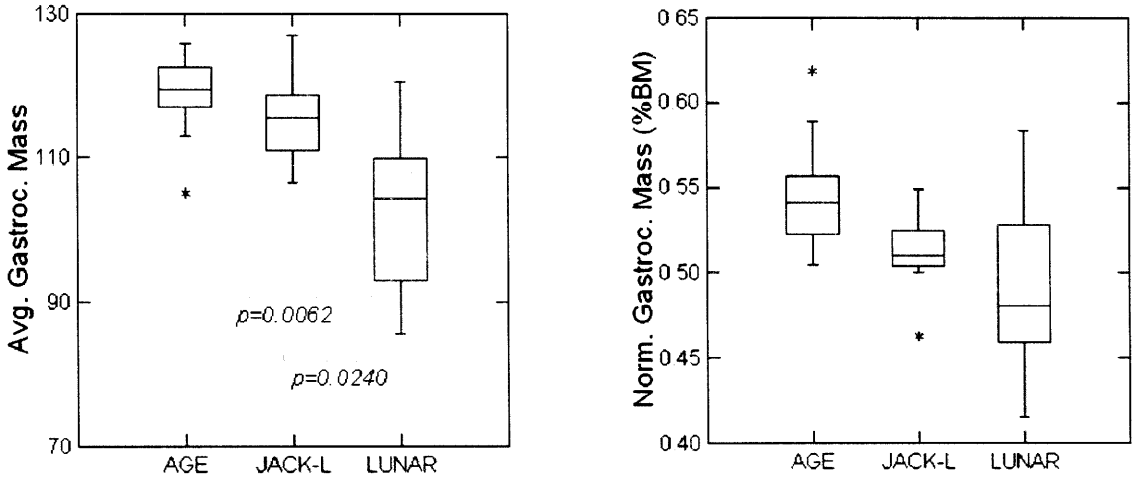

Figure 5-19: Effect of group on gastrocnemius wet mass in Lunar-analog study animals. LUNAR suspension resulted in a significant reduction in muscle wet mass, which was somewhat dependent on body mass changes. Significant differences between LUNAR animals and controls are marked with p-values.

Chapter 6

Discussion

This chapter synthesizes the data presented in the last chapter, exploring it in light of the existing literature. The underlying animal growth upon which our studies are overlaid is first explored. Next, emergent trends in the data are discussed, highlighting the imbalance between formation and resorption which drives bone loss in our model, anatomical site-specificity of such changes, and the observed trends in material strength. Finally, the lunar-analog results are compared and contrasted with Mars-analog findings, and possible reasons for the differences between the two studies are explored.

6.1 Musculoskeletal Studies

6.1.1 Baseline Context

In order to understand the changes brought about due to suspension, it is first imperative to understand the background upon which these changes are overlaid. These studies utilized BALB/cByJ female mice, 10 weeks old at start, and 13 weeks old at study completion. Previous work suggests that this interval occurs near the peak of trabecular maturity (Glatt, 2007a, 2007b), meaning that the transition between predominantly anabolic and predominantly catabolic states begins to take place at about this time, particularly in the trabecular compartment.

Comparison of BASELINE and AGE control animals further clarifies the age-related changes taking place in our specific population:

- Body mass is increasing at decreasing rates of growth, with minimal changes ($< 1\%$) in week three.
- Significant but slow longitudinal bone growth is still taking place, as seen in measures of total femoral length.
- Cortical thickness is increasing significantly in the femoral diaphysis, but no significant thickening is evident in the distal femoral metaphysis.
- Trabecular compartment changes, however, are distinctly catabolic, as seen in the femoral metaphysis.
- Osteoblast numbers and bone formation rates are clearly on the decline.
- Osteoclast numbers are trending higher, but erosion surfaces remain largely unchanged, suggesting little change in resorption activity.
- Furthermore, there is a significant decrease in osteoid thickness and mineralization, which suggests that turnover rates are low.

In summary, for normal female BALB/cByJ mice, the time between 10 and 13 weeks is one of slowing growth in the cortical compartment, and increasing losses in the trabecular compartment, driven largely by decreases in formation paired with a relatively constant rate of resorption.

It is worth noting that, in contrast to previously reported trends (Glatt, 2007b) suggesting slow but persistent expansion of the cortical cross-sectional area in the femoral midshaft, we saw no periosteal expansion in this timeframe. Given the small size of our cohort, this is likely an effect of undersampling, and points to the limitations of a study design that does not use repeated longitudinal measures in the same population of animals.

6.1.2 Systemic Stress

Corticosterone and other systemic stress hormones are known to be catabolic to both muscle and bone. In the early days of hindlimb unloading, Wronski and Morey-Holton (1987) determined that harness design and poor experimental protocols can have a significant effect on systemic stress, and thereby, on musculoskeletal markers. The tail suspension model that was generated to improve upon these problems is now established as a non-significant stressor when well executed (Morey-Holton, 2005).

While we did not measure corticosterone levels or adrenal/thymus masses to explicitly track stress, body mass changes are typically accepted as a surrogate marker for chronic systemic stress in tail suspension models (Morey-Holton, 1998). The significant body mass losses in MARS and LUNAR animals during the first week of suspension suggest a brief period of increased stress and adaptation to the experimental environment. The similar losses noted in both the SUSPENSION (i.e., MARS and LUNAR) and JACKET (i.e., JACK-M and JACK-L) groups relative to AGE controls would seem to indicate that this change is due primarily to some combination of the forelimb vest, alternative single housing arrangement, and reduced caloric intake, rather than simply the state of suspension.

The return of normal growth rates in suspended MARS and LUNAR animals in weeks 2 and 3, and the accompanying stabilization of food usage, suggest that systemic stress due to the experimental treatment is negligible after an initial adaptive period. Similar results have been seen in centrifuge studies (Wade, 1997; Warren, 2001) and tail suspension experiments (Wronski, 1987).

As noted, following an initial period of adaptation, both JACK-M and JACK-L control groups experienced a rapid increase in body mass, showing significantly higher growth rates in weeks 2 and 3 than AGE or MARS animals. These higher growth rates, however, were not correlated with significant additional longitudinal bone growth or proportional muscle gain in the gastrocnemius, suggesting a shift in body composition towards higher fat content. It is also possible that gastrocnemius atrophy was not fully representative of other muscles, and that there was accompanying

hypertrophy elsewhere in the body. Body composition scans are recommended for future studies to resolve this open question.

Caloric restriction in mice has been shown to result in significantly decreased resting metabolic rate and reductions in energy expenditures from exercise (Hambly, 2005). Weight gain in calorically restricted animals is largely due to increases in adipose body fraction, while lean mass changes are curtailed relative to controls. If the JACKET animals adopted a reduced metabolic rate in study week 1, then were provided more food as the SUSPENSION mice adapted to their treatment, weight gain and increasing body fat would be expected.

Interestingly, as reviewed by Morey-Holton (1998), pair-fed controls typically gain weight at similar rates to tail suspended rats in similar caging. Thus, it seems likely that behavioral modification in our JACKET animals due to the forelimb vests may be an important factor in the observed differential growth rates. Future quantification of this activity could be achieved with a video, infrared, or mechanical monitoring system.

Forelimb jackets in this cohort could have also contributed to weight gain simply by requiring animals to carry their added mass. At 0.6–0.7 grams, however, a jacket represents an extra burden of only about 3% of initial body weight. The carriage of this small additional mass is unlikely fully account for the 7 to 10% changes in total body mass in the two studies.

While the experimental design for this work was originally intended to support comparisons between SUSPENSION and JACKET animals, similarly housed and fed, this unexpected weight gain in the JACKET groups challenges the validity of such a comparison. Given the degree to which musculoskeletal strength is typically dependent on body mass (Felson, 1993), the comparison between more similarly matched SUSPENSION and AGE animals will be the point of focus for subsequent discussions herein. This choice is further bolstered by a strong positive relationship between femoral length and final body mass in AGE and MARS animals, but not JACK-M animals (Figure 6-1), suggesting weight gain without significant growth in the latter group.

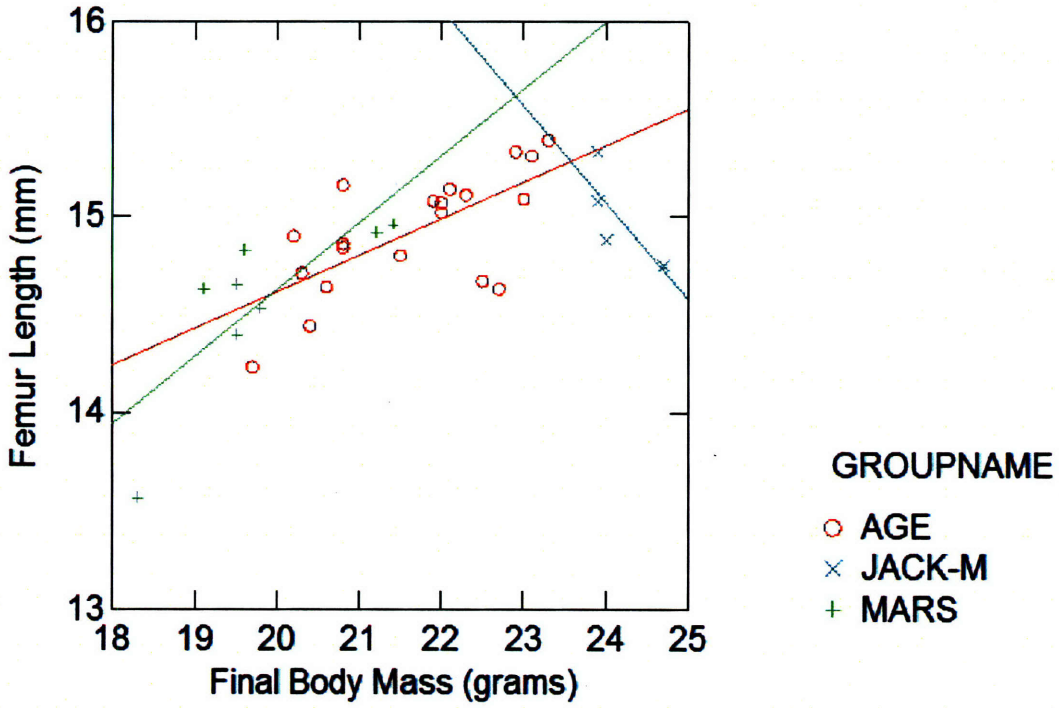

Figure 6-1: Correlation between femoral length and final body mass for the Mars-analog study. JACK-M animals show distinctly different patterns of growth, consistent with their unexpected weight gain.

To recap, given the disparity in JACKET animal growth, the primary comparisons presented throughout are between MARS and AGE, or LUNAR and AGE, animals. Care has been taken to note areas in which JACKET animals demonstrate noticeably different behavior than AGE controls.

Interestingly, when kept in identical habitats, singly housed mice have been shown to exhibit lower growth rates, BMC, and BMD than group housed animals. They also show less variability in body composition parameters, presumably because genetic effects have the opportunity to dominate over more highly variable environmental and behavioral effects (Nagy, 2002). Similarly, spaceflight reductions in periosteal bone formation and bone mass of growing rats were blunted by as much as 80% in group-housing habitats, relative to experiments with singly housed rats (Morey-Holton, 2000). While the effects were not as clear in spaceflight studies of mature rats, singly housed animals, in the same habitats, with better-matched growth rates would be the ideal control for future partial weight suspension experiments. These studies should also examine whether jacketed control animals that are not calorically restricted may demonstrate more comparable rates of growth to AGE and SUSPENSION groups. A final study of pair fed, non-jacketed controls could then more conclusively differentiate between the stressors of caloric restriction, single housing, and forelimb vests.

6.1.3 Mars-Analog Discussion

Histology

Compared to AGE matched controls, MARS animals showed a significant decrease in MS/BS and BFR/BS in the proximal tibial metaphysis. While there was a trend suggesting reduced mineral apposition rates in MARS animals (Kruskall Wallis (KW), $p_{KW} = 0.295$), the much larger effect here was clearly a reduction in bone formation. Furthermore, MARS animals also demonstrated significant decreases in OS/BS, suggesting reductions in turnover rate.

Interestingly, while age-related trends suggest increasing numbers of osteoclasts in this timeframe, MARS animals demonstrated a significant reduction in Oc.S/BS

with trends towards lower osteoclast numbers ($p_{KW} = 0.117$), which suggested lower rates of resorption in MARS animals. However, despite the enhanced reductions in BFR, there were no demonstrable changes due to suspension in osteoblast numbers or surface area. This could be due to reduced osteoblastic activity from a stable population of cells. Alternatively, as bone formation rates are a dynamic metric, examining accumulated bone over time, and osteoblast numbers are a static metric, providing data from only a single timepoint, it is possible that formation was reduced but recovering. Serum metrics of formation or longitudinal assessment of bone will be required to clarify this uncertainty.

In summary, despite unexpected reductions in osteoclasts and no clear changes in osteoblasts, MARS animals demonstrated lower rates of bone formation and no clear changes in resorption. As described in Section 2.2.2, this is consistent with numerous animal studies across the spaceflight canon.

Examination of the selected histological slices presented in Figure 5-11 also reveals interesting morphometric trends that were not evident in the earlier data because that selected region of interest explicitly excluded the growth plate. The Mars animals (M, lower right) showed a visible reduction in thickness of the primary spongiosa, relative to the other groups, suggesting a suppression of longitudinal growth. This was corroborated by caliper measurements of total femoral length, where MARS femurs were shorter than controls ($p = 0.06$ vs AGE, $p = 0.02$ vs JACK-M, Table 5.1). The effects of unloading on longitudinal growth are controversial (Morey-Holton, 1998): such inhibition is consistent with the reduction in primary spongiosa thickness seen after one week of both spaceflight and tail-suspension in the tibiae of 12–13 week old male Wistar rats (Vico, 1991), but may also be indicative of increased systemic stress (Sibonga, 2000). Further study, including analysis of serum and/or urine corticosterone, is required.

Site Specificity of Changes

MARS and LUNAR femurs were weaker in three-point bending than AGE controls, due largely to changes in geometric rather than material properties. Partial weight

bearing caused a significant reduction in area moments of inertia in the femoral mid-shaft. Contrary to intuition, despite the age-related background of cortical thickening due to periosteal apposition, and no histological signs of increased resorption in the proximal tibia, the reductions in periosteal bone formation rate caused significant cortical thinning in the femoral mid-shaft.

It is possible that the histological picture of the femoral midshaft is poorly correlated to that which was obtained from the proximal tibial metaphysis. Bone loss in cortical compartments was predicted and confirmed to be smaller than trabecular compartments. Even in the same compartment, there was site-specificity: cortical thinning in the distal femoral metaphysis was more extensive than in the femoral mid-shaft (MARS v AGE, Ct.Th metaphysis: -19.81%, diaphysis -8.90%), and trabecular thinning was greater in the distal femur than the proximal tibial metaphysis (MARS v AGE, BV/TV femur: -20.62%, tibia -12.25%).

As highlighted by Judex (2004a, 2004b), there is a great deal of strain- and site-specificity in both bone morphology and responses to disuse osteoporosis: Bone loss in the femurs of 16 week-old female BALB mice subjected to 21 days of tail suspension varied from -59% in the metaphysis to -3% in the proximal diaphysis, and was well-correlated to variations in baseline bone morphology ($R^2 = 0.94$).

This is consistent with our own trabecular findings for MARS weightbearing vs AGE controls. Both baseline BV/TV and losses in this parameter relative to controls were higher in the distal femur than the proximal tibia.

Interestingly, percentage bone losses from the femoral cortex were greater in our model for the thinner distal metaphysis than in the thicker mid-diaphysis. This may be due to the different functional roles of the cortical compartment at the two sites. Whereas the midshaft is subject to high bending loads and must carry the full burden of these stresses with cortical structure, the metaphysis is subject to relatively larger axial loads. Furthermore, loads are shared with the trabecular network, and skeletal maintenance is active over a greater surface area.

Material Strength

Interestingly, despite the lack of effect of treatment on effective Young's modulus in three-point bending of the femur, and the absence of any significant difference in mineral apposition rate in the proximal tibia, there *were* significant reductions in estimated bone mineral density in the femoral mid-shaft, distal femoral metaphysis, and proximal tibial metaphysis for MARS specimens relative to AGE. Such reductions in mineral content were also consistent with the images from histology, showing reductions in von Kossa staining in the proximal tibia (Figure 5-11). In future experiments, bone composition could be more precisely evaluated with ashing to determine bone mineralization, and high performance liquid chromatography (HPLC) or gel electrophoresis techniques to quantify collagen composition (e.g. Komsa-Penkova, 1996; Puustjarvi, 1999).

JACK-M animals showed unexpected significant reductions in estimated Young's modulus, resulting in significantly lower extrinsic stiffness relative to AGE controls. Such losses were not seen for JACK-L animals, but were consistent across samples from both batches of Mars experiments. No obvious abnormalities were evident in the force-displacement curves or best fit lines of the JACK-M bones. Samples were subjected to bending in random order, and there was no effect of order on estimated Young's modulus. It is unlikely that the change in JACK-M bones was due to inadvertent differences in handling or freeze-thaw cycles, as other bones collected in the same sample group did not show such low intrinsic stiffness. The small sample size precludes more in-depth analysis.

While material strength was not investigated in trabecular bone samples, in both the distal femur and proximal tibia, bone volume losses were due to trabecular thinning, not significant changes in trabecular number. For a given bone volume loss, this pattern suggests as much as two to five times smaller changes in modulus and strength than if the same loss was mediated by changes in the number of trabeculae (Silva, 1997). While longer experiments might lead to eventual "break-through" and loss of trabeculae, this initial pattern of thinning is notable because therapies

that lead to trabecular apposition are significantly more effective prior to losses of trabecular connectivity (Guo, 2002).

6.1.4 Lunar-Analog Discussion

Comparison with Mars Results

Like the Mars-analog studies described above, lunar-analog suspension caused similar reductions in skeletal structure and strength. Relative to AGE controls, 16% weightbearing caused significant reductions in cortical thickness at the femoral mid-diaphysis due to limited periosteal expansion with no significant changes in medullary area. Moments of inertia in the femoral midshaft (polar, max, and min) showed strong trends ($p < 0.10$) of decline relative to AGE controls, and as a consequence, LUNAR samples were significantly weaker in three-point bending. Trabecular bone volume fraction in the distal femoral metaphysis was significantly decreased, with a dominant effect of trabecular thinning rather than loss. Average gastrocnemius wet mass was significantly less in the LUNAR animals.

Interestingly, while data trends for LUNAR samples were nearly always in the same direction as those for MARS samples, the magnitude of the effect was not significantly different, but typically smaller for LUNAR animals. Based on the hypothesis that changes in bone structure and strength should be proportional to the reduction in weight borne by the animals, this result was unexpected.

One possible explanation for this trend stems from behavioral differences in the two groups. It is reasonable to believe that suspension causes somewhat greater discomfort for the LUNAR mice than MARS. It is the experience of the author that this is true for human partial weight locomotion simulations, due to greater localized harness forces. Furthermore, when ground reaction forces are reduced, proprioceptive feedback during locomotion is reduced, impairing normal gait. As GRFz declines, slipping becomes a greater problem, and horizontal forces take on a proportionately larger effect on locomotor stability.

While we observed no clear visual evidence of such instability, high speed videog-

raphy may provide additional insights. Ivanenko et al. (2002) also demonstrated changes in the pattern and strength of muscle activation for human treadmill locomotion under increasing suspension. Further evidence may be gathered in future studies through electromyographic or histological analysis of the musculature supporting postural stability.

Another suggestion of relative inefficiencies at low ground reaction forces is given by Griffin et al. (1999). Using a partial weightbearing human treadmill, they explored the validity of the inverted pendulum model for conditions of simulated reduced gravity. Down to simulations of 0.5-g, the percent recovery of potential to kinetic energy was not significantly changed. At 0.25-g, however, there was a significant reduction, suggesting a threshold effect in walking efficiency at lower g-levels. A 1993 review of partial gravity simulators by Davis and Cavanagh suggests that the ballistic model of limb movement is most accurate for simulations down to 0.4-g. Below this point, there is increasing error due to "greater muscular effort during the swing phase."

Perhaps most tellingly, Newman and Alexander (1993) found significant nonlinearity in metabolic expenditure for slow speed walking (0.5 m/s) at simulated lunar g-levels. Using a novel underwater treadmill, they found an increase in heart rate and oxygen uptake ($\dot{V}_{O_2}$) for lunar-g performance relative to Mars-g in more than half the subjects tested. Newman and Alexander hypothesized that this relative inefficiency at low g-levels may be due to subjects "wasting energy for stability and posture control." Likewise, a more recent study using the MIT Moonwalker showed that at constant Froude number, there was a similar local minimum at Mars loading levels for cost of transport in both suited and unsuited locomotion (Rader, 2007).

These studies suggest a threshold effect for metabolic efficiency between 0.25- and 0.5-g. In longer simulations below this threshold, it is reasonable to hypothesize that these inefficiencies might lead to changes in gait or other adaptive behaviors. Because osteogenesis and resorption are driven largely by deviations from expected patterns of bone stress and strain, any behavioral changes that led to different patterns of musculoskeletal loading could stimulate significant changes in bone growth and loss.

Furthermore, beyond some threshold, increasing numbers of high intensity loads have diminishing returns in stimulating bone formation (Turner, 1998). In an isolated rooster ulna, Rubin and Lanyon (1984) showed that merely four cycles a day of physiologically relevant strains (2050 μstrain at 0.010–0.012 strain/s) were necessary to prevent disuse osteoporosis. Srinivasan et al. (2002) used axial tibial loading in 10 week B6 mice to demonstrate that, by inserting 10 second rest periods between cycles, even 10 low magnitude (650 μstrain at 0.010 strain/s) cycles a day could cause a significant increase in periosteal bone formation rate.

In both true and simulated partial gravity environments, loads due to most non-locomotor behaviors, such as scratching and feeding, are unchanged relative to 1-g. Therefore, if the skeletal strains induced by such activities are high relative to the dominant mechanical loads, it is possible that they will be protective of bone mechanical properties. Observation of our LUNAR mice suggests that the additional discomfort due to higher suspension loads may lead to more scratching and other escape behaviors, and thereby, more of this type of stimulus. While we were unable to capture tibial strain gage readings during these sorts of behaviors, such quantification would improve understanding of such gravity-independent loading.

In summary, our lunar-analog bones exhibited patterns of structural and strength loss similar to the previously described Mars-analog results, but with consistent trends towards smaller effect sizes. I believe this is consistent with increases in muscle activation and changes in gait adopted to help control for reduced stability of locomotion at these lower g-levels, and may be further accentuated by the increased role of loading due to gravity-independent behaviors.

6.1.5 Trends Across g-Levels

Compared to an earlier tail suspension study in 16–19 week old female BALB/cByJ mice under full hindlimb unloading (Judex, 2002), we show relative preservation of both cortical and trabecular bone in both MARS and LUNAR animals. Indeed, relative to a linear relationship between bone loss and g-level, we show greater than predicted preservation for key trabecular bone metrics (Figure 6-2). This suggests

that trabecular bone loss does not have a direct linear relationship with reductions in weightbearing. Rather, limited loading provides some level of prophylaxis compared to a linear model. Such preservation is a boon for human exploration of the Moon and Mars, enabling longer mission durations or substantial risk reduction relative to current microgravity missions.

Interestingly, changes in midshaft cortical bone area were not significantly different than previous tail suspension findings. While there were strong trends suggestive of preservation, MARS cortical thickness was actually slightly below that predicted by a linear model of bone loss versus g-level. Given that adaptation to reduced loading was greater in the trabecular compartment than the cortical, and that recovery occurs more rapidly along the periosteal margin (Lang, 2007), this lack of effect is probably less critical to mission success.

Perhaps the most surprising finding, however, was the non-monotonic decrease in skeletal properties with respect to effective g-level. As discussed above, while there were no significant differences between MARS and LUNAR animals for key metrics like BV/TV and Ct.Th, in 95% of morphometric variables, the change in MARS animals relative to controls was larger than the change for LUNAR animals.

It is possible that this difference may simply be an idiosyncratic outcome of the partial weight suspension model. However, as discussed above, it is also possible that the difference is a real one, driven by a threshold effect and the inefficiencies due to gait instability at low g-levels. In this case, while bone structure may be relatively preserved on the lunar surface, it could come at an increased risk of falls and connective tissue injuries. As astronauts adopted adaptive locomotor strategies appropriate for the altered environment, altered strain patterns throughout the skeleton would be expected to result in local areas of both increased resorption and increased formation.

It is important to note that the smaller losses seen in LUNAR animals relative to MARS suggest that future human missions to Mars may not wish to rely on evidence from precursor lunar expeditions to place limits on expected adaptation. While a monotonic trend would suggest that changes due to the lunar environment would bound the needs for countermeasures and rehabilitation on Mars missions, our

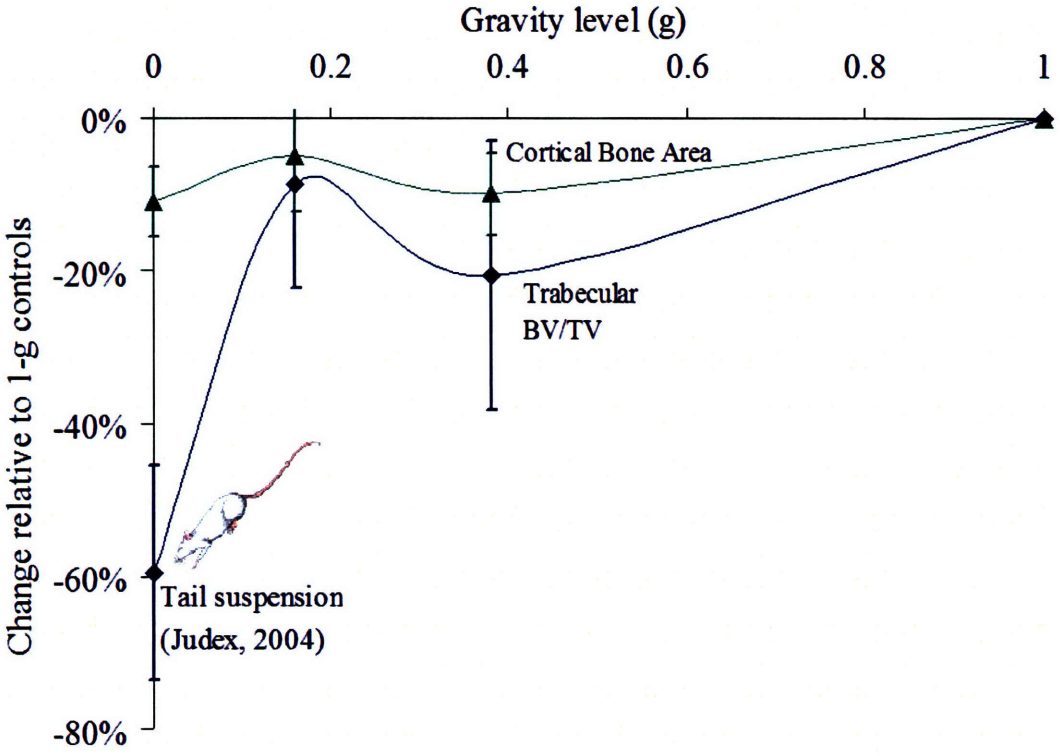

Figure 6-2: Trends for key femur skeletal parameters across the simulated gravitational continuum. "0-g" data comes from 3-week tail suspension by Judex, et al. (2004a). MARS trabecular variables performed better than a linear relationship between 1-g and 0-g, suggesting relative preservation with partial loading. Cortical variables exhibited changes much nearer to those seen in full unloading. LUNAR variables demonstrated even greater preservation relative to MARS, possibly due to compensation for postural instability.

evidence suggests that more research is needed to understand the differences between the two missions.

6.1.6 Relationship of Bone Loss to *In Vivo* Strains

Contrary to our initial hypothesis, no reduction in *in vivo* tibial strains accompanied the bone loss seen at MARS and LUNAR levels of weight-bearing (Section 4.3.4). Indeed, across a 6.5-fold range in ground rection forces, there were no significant differences in the observed peak compressional strains. As discussed earlier, the lack of observed differences is likely due to the larger role of muscle activation than GRF in producing these strains. The questions remains, however, why bone loss occurred despite a lack of altered strain stimulus.

One possibility is that the observed effects are due less to reductions in peak strain and more to inactivity. However, as explored above, peak bone strains are osteogenic at low numbers of repetitions. Furthermore, non-locomotor activities would also contribute to this strain history.

Second, it is possible that the surface strains observed in this region of the tibia are not representative of the patterns of strain in the metaphyseal and diaphyseal regions of the hindlimb where bone loss was evaluated. Finite element analysis incorporating both reaction forces and major muscle groups (Duda, 1998) could help resolve this question.

A third alternative is that the role of muscle atrophy in these *in vivo* strains was not explored. If bone deformations were due largely to muscle activation, the atrophy demonstrated in LUNAR and MARS mice could be an important covariate. Comparison of results between mice with and without muscle atrophy would be instructive.

Interestingly, however, studies of muscle fatigue have shown that transmitted loads are actually higher when muscle forces are lower, i.e., muscles stabilize bones during normal activities, reducing peak strains (Yoshikawa, 1994; Milgrom 2007). Furthermore, fatigue can also shift gait patterns so as to rotate the neutral axis of bending and expose different areas of bone to greater strains. With preferential atrophy of

extensor muscles due to unloading, the role of muscle tension in bone bending is likely to change significantly throughout the course of an PWS study.

6.2 Limitations

With its narrow scope of data collected largely at a single timepoint within the study, this effort is inherently limited in the claims that may be made regarding longitudinal changes. While comparison with a baseline sacrifice group is instructive, future studies should aim to apply appropriate longitudinal techniques of *in vivo* imaging and biomarker analysis to more accurately describe temporal changes.

The use of only two data points (16% and 38%) to suggest the full domain of hypogravity adaptation is clearly incomplete. More data points are needed to understand the nature of the apparent musculoskeletal threshold at low g-levels, and to flesh out the continuum at intermediate levels of weightbearing. Furthermore, relying on comparisons with tail suspension experiments run in another lab with different protocols and procedures can merely suggest conclusions about the relative preservation of musculoskeletal form and function relative to full unloading. The use of tail suspension controls run in parallel with PWS experiments would provide more robust grounds for comparison.

As noted in Chapter 2, one of the largest differences between ground and flight models of unloading is the omnipresent signal of gravity present on the ground. The otolith organs play an important role in postural control, as evidenced, e.g., by lower limb muscle activation during neck retroflexion (Zangemeister, 1991). In true partial gravity environments, vestibulospinal changes due to reduced otolith inputs may play an important secondary role in gait control.

Evidence from hypergravity experiments in labyrinthine-defective rodents also strongly suggests a role for otolith signaling in autonomic and metabolic pathways (Fuller, 2002; Murakami, 2002). While these pathways were not historically considered inputs to skeletal maintenance, leptin, a hormone involved in regulation of obesity, was recently shown to centrally influence bone formation via hypothalamic

inputs to the adrenergic signaling pathways (Pogoda, 2005). Knowing that autonomic signaling can affect bone, modulation of the otoliths inputs to these pathways should be examined more closely to determine their role in musculoskeletal adaptation to reduced gravity.

Chapter 7

Summary and Conclusions

7.1 Summary of Hypotheses

As outlined in Section 1.3, these investigations were designed to explore four primary hypotheses.

Hypothesis 1: *A partial weight suspension simulation can be used to support chronic studies of reduced weightbearing in adult mice, with loads titrated as desired.*

As described in Chapter 4, the PWS habitat, a novel model of quadrupedal partial weightbearing, was developed and validated for multi-week studies of partial weightbearing in adult mice. Design features were drawn from both rodent tail suspension and human full-body suspension systems. A tunable spring was used to adjust the loads to within $\pm 10\%$ of a desired stimulus.

Using a high-precision force plate, we demonstrated that peak dynamic ground reaction forces were substantially reduced under suspension, consistent with the reductions in static loading.

Hypothesis 2: *Reductions in weightbearing by means of partial weight suspension will result in significantly reduced peak skeletal strains.*

Unexpectedly, peak compressional strains at the anterio-medial surface of the proximal tibia did not show significant reductions with changes in suspension level

and vertical ground reaction forces. We postulate that these strains were heavily influenced by muscle activation, and that locomotion in the presence of significant atrophy may yield differences in strain levels and patterns.

Hypothesis 3: *Adaptation to a suspension harness and habitat prior to unloading will provide sufficient opportunity for animals to adjust to the novel housing environment, and partial weight suspension will not further increase systemic stress.*

We did not measure corticosterone levels or adrenal/thymus masses to explicitly quantify stress, so this hypothesis remains formally untested. However, two days of adaptation to suspension harnesses was subjectively observed to be sufficient for animals to acclimate and return to normal patterns of activity. While the significant body mass losses in MARS and LUNAR animals during the first week of suspension suggest a brief period of increased stress, the similar losses noted in both the SUSPENSION and JACKET groups relative to AGE controls would seem to indicate that this change is due primarily to some combination environmental or feeding effects, rather than simply suspension.

The return of normal growth rates in suspended MARS and LUNAR animals in weeks 2 and 3, and the accompanying stabilization of food consumption, suggest that systemic stress due to the experimental treatment was negligible after the initial adaptive period.

Hypothesis 4: *Reductions in the dynamic loading environment will cause decrements in osteoblastic activity, resulting in a decrease in bone mass, material and structural properties.*

This hypothesis was fully confirmed in MARS animals relative to AGE controls. As measured by dynamic histomorphometry, MARS mice showed significant decreases in bone formation indices. There was no accompanying reduction in osteoblast number, suggesting that either cellular activity was reduced for a relatively constant population or that an earlier decline in cell number was recovered by the time of sampling.

In both MARS and LUNAR femurs, there was a significant deterioration in cortical and trabecular bone, with greater effects in the trabecular compartment. These changes were accompanied by reductions in femoral diaphyseal bending strength and extrinsic stiffness. No significant changes due to treatment were seen in estimated material properties.

Hypothesis 5: *The patterns of response to partial unloading will be similar to those seen in previous research with full hindlimb unloading, but the magnitude of change will be related to the strain magnitudes of the partial loading environment.*

Patterns of bone loss were consistent with previous reports in tail suspension, with greater losses in the femur than the tibia, trabecular compartment than cortical, and formation than resorption. Compared with earlier tail suspension work by Judex et al. (2004a), we showed relative preservation of both cortical and trabecular markers in both MARS and LUNAR animals. Indeed, examining our results against a linear relationship between bone loss and g-level, we showed greater than predicted preservation for key trabecular metrics (Figure 6-2). This suggests that trabecular bone loss does not have a direct relationship with reductions in weightbearing. Rather, limited loading provides some level of prophylaxis compared to a linear model. Such preservation would be a boon for human exploration of the Moon and Mars, enabling longer mission durations or substantial risk reduction relative to current microgravity missions.

Interestingly, changes in midshaft cortical bone area trended in the same direction but did not differ significantly from tail suspension values. Given that bone loss due to reduced loading was greater in the trabecular compartment than the cortical, and that recovery occurs more rapidly along the periosteal margin, trabecular preservation will probably play a greater role in risk reduction.

The non-monotonic behavior of both cortical and trabecular parameters in response to low loads was particularly curious. Despite more than a two-fold difference in loading levels, there were no significant differences between loss in Mars and lunar

simulations. Whether this was purely an effect of the suspension model design, or representative of the actual dynamics of low-g behavior is a fascinating subject for future work.

7.2 Future Work

Various additional opportunities for building upon the work herein are suggested. Indeed, a majority of the more than 1000 tail suspension studies published to date could be run in partial weightbearing. A variety of loading regimes, numerous genetically modified strains, and many additional outcome assessments could be envisioned to further explore the degree and mechanisms of adaptation.

However, a few areas stand out as promising early research targets. First, the preliminary evidence suggests that both static and dynamic forces can be tuned to provide a desired level of partial weight suspension. Additional development of techniques is needed for measuring these forces, particularly *in vivo*, over long durations and a variety of animal behaviors. This data will both characterize the model in more depth and also provide further insight into the mechanisms by which lunar adaptation differs from Mars.

Second, whereas the studies presented here provide compelling data on the effects of three weeks of musculoskeletal unloading, future effort should be applied to examining the time course over which this adaptation occurs. At a minimum, serum markers of bone formation and resorption and longitudinal *in vivo* imaging techniques might be applied. A more thorough study could provide cohorts of animals for sacrifice at multiple time points, enabling full characterization of changes with exposure duration.

With an established model for examining musculoskeletal changes due to partial weightbearing, the next step to prepare for human exploration is formulating and proving the efficacy of appropriate countermeasures. The differential adaptation associated with partial loading may also translate to differential countermeasure efficacy and appropriate reductions in recovery timelines upon reloading. A number of

pharmacological interventions have been shown to reduce fracture risk in large-scale randomized clinical trials, either by antiresorptive or anabolic activity. As the mechanisms of partial weight adaptation are elucidated in future studies, the selection of an appropriate agent may be targeted for trials.

Perhaps the ultimate application of this model would be a simulation of a Mars mission, beginning with a period of full unloading under tail suspension, then measuring the changes associated with the transition from this state to Mars loading. A second period of tail suspension could mimic the return transit, and a return to full weightbearing would round out the simulation. The timelines for such a comprehensive simulation would have to be considered carefully due to the relatively compressed rodent lifecycle, but the potential exists to offer unprecedented predictive value for an exploration-class journey.

Beyond exploration, PWS also offers a unique platform upon which to explore fundamental science, providing a novel stimulus for examining mechanisms of musculoskeletal mechanotransduction.

7.3 Conclusions

NASA has committed to a return to the moon, the first trips to Mars, and a vision beyond the inner solar system. Enterprising companies are actively engaged in creating a future in space for private explorers, including trips to other lunar and planetary surfaces. More so now than ever before, the relevancy of partial gravity physiology is at hand.

The studies detailed in this thesis offer some of the first glimpses at musculoskeletal adaptation to extended stays in such environments. They demonstrate that partial weightbearing triggers adaptive processes consistent with that seen in full unloading. Structural deterioration brought about by reduced loading is seen in both the cortical and trabecular compartments of the hindlimb, with greater percentage losses in the more metabolically active spongy bone. Bone formation is suppressed, with minimal effect on bone resorption. Thinning of the cortex and trabeculae leads to reductions

in bone strength, and presumably, increased risk of fracture. Muscles atrophy.

However, the studies also begin to confirm the hypothesis that partial weight-bearing will confer some degree of protection against the atrophy and osteopenia that characterize microgravity deconditioning. Unexpectedly, they suggest that such protection may not be directly proportional to local gravity levels. Due to changing control strategies, inefficiencies, and/or altered sensory feedback, low g-levels may lead to fundamentally different patterns of adaptation. Results of physiological studies undertaken on the lunar surface may not be predictive of changes expected on the surface of Mars.

This unexpected finding points clearly to a need for further investigations. Magnitudes and patterns of adaptation must be quantified with larger numbers of samples. Countermeasures and recovery protocols must be tested for their interactions with partial weightbearing. The danger of fracture and concerns about bone healing under reduced loads must be better understood.

In summary, this thesis not only delivers new information about musculoskeletal adaptation across the hypogravity continuum, but also provides a flexible platform for the next generation of rodent studies into spaceflight adaptation and mechanotransduction. If we are to send humans to experience partial gravity — planetary, centrifugal, or otherwise — these studies must not be the last to investigate this gap in our understanding.

Chapter 8

Bibliography

Adams, G. R., V. J. Caiozzo, et al. (2003). "Skeletal muscle unweighting: spaceflight and ground-based models." J Appl Physiol **95**(6): 2185-201.
Alexander, J. M., I. Bab, et al. (2001). "Human parathyroid hormone 1-34 reverses bone loss in ovariectomized mice." J Bone Miner Res **16**(9): 1665-73.
Allen, M. R., H. A. Hogan, et al. (2006). "Differential bone and muscle recovery following hindlimb unloading in skeletally mature male rats." J Musculoskelet Neuronal Interact **6**(3): 217-25.
Amende, I., A. Kale, et al. (2005). "Gait dynamics in mouse models of Parkinson's disease and Huntington's disease." J Neuroengineering Rehabil **2**: 20.
Amtmann, E., T. Kimura, et al. (1979). "Maximum likelihood factor analysis of the effects of chronic centrifugation on the structural development of the musculoskeletal system of the rat." Anat Embryol (Berl) **156**(1): 89-101.
Anderson, J. C. and C. Eriksson (1970). "Piezoelectric properties of dry and wet bone." Nature **227**(5257): 491-2.
Augat, P., U. Simon, et al. (2005). "Mechanics and mechano-biology of fracture healing in normal and osteoporotic bone." Osteoporos Int **16 Suppl 2**: S36-43.
Bateman, T. A., J. J. Broz, et al. (1997). "Differing effects of two-week suspension on male and female mouse bone metabolism." Biomed Sci Instrum **34**: 374-9.
Bateman, T. A., C. R. Dunstan, et al. (2000). "Osteoprotegerin mitigates tail suspension-induced osteopenia." Bone **26**(5): 443-9.
Beamer, W. G., L. R. Donahue, et al. (1996). "Genetic variability in adult bone density among inbred strains of mice." Bone **18**(5): 397-403.
Belozerova, I. N., T. L. Nemirovskaya, et al. (2002). "Structural and metabolic characteristics of human soleus fibers after long duration spaceflight." J Gravit Physiol **9**(1): P125-6.
Biewener, A. A. and R. J. Full (1992). Force platform and kinematic analysis. Biomechanics Structures and Systems: A Practical Approach. A. A. Biewener. New York, Oxford Univeristy Press**:** 45-74.
Bloomfield, S. A., M. R. Allen, et al. (2002). "Site- and compartment-specific changes in bone with hindlimb unloading in mature adult rats." Bone **31**(1): 149-57.
Bonting, S. L. (1992). "Animal research facility for Space Station Freedom." Adv Space Res **12**(1): 253-7.
Bouxsein, M. L., D. D. Pierroz, et al. (2005). "beta-Arrestin2 regulates the differential response of cortical and trabecular bone to intermittent PTH in female mice." J Bone Miner Res **20**(4): 635-43.
Bouxsein, M. L., C. J. Rosen, et al. (2002). "Generation of a new congenic mouse strain to test the relationships among serum insulin-like growth factor I, bone mineral density, and skeletal morphology in vivo." J Bone Miner Res **17**(4): 570-9.
Bouxsein, M. L., P. Szulc, et al. (2007). "Contribution of trochanteric soft tissues to fall force estimates, the factor of risk, and prediction of hip fracture risk." J Bone Miner Res **22**(6): 825-31.
Buckey, J. C. (2006). Space Physiology. New York, NY, Oxford University Press.
Burger, E. H. and J. Klein-Nulend (1999). "Mechanotransduction in bone--role of the lacuno-canalicular network." Faseb J **13 Suppl**: S101-12.
Carmeliet, G., L. Vico, et al. (2001). "Space flight: a challenge for normal bone homeostasis." Crit Rev Eukaryot Gene Expr **11**(1-3): 131-44.

Carr, C. (2001). Distributed Architectures for Mars Surface Exploration. Aeronautics and Astronautics. Cambridge, MA, Massachusetts Institute of Technology. **S.M.**

Carr, C. E. and D. J. Newman (2007 (submitted)). "Bioenergetics of Unsuited and Space Suited Activity: Framework and Review. ." Aviat Space Environ Med.

Carter, D. R. (1984). "Mechanical loading histories and cortical bone remodeling." Calcif Tissue Int **36 Suppl 1**: S19-24.

Cavagna, G. A., P. A. Willems, et al. (2000). "The role of gravity in human walking: pendular energy exchange, external work and optimal speed." J Physiol **528**(Pt 3): 657-68.

Cavanagh, P. R., A; Gopalakrishnan, R; Kuklis, M; Genc, K; Samorezov, J (2006 (pre-publication)). Exercise on the International Space Station: Exercise Bout Duration and Lower Extremity Loading During Increments 6-12, A Preliminary Report. Cleveland, OH, The Center for Space Medicine, The Cleveland Clinic.

Cherian, P. P., B. Cheng, et al. (2003). "Effects of mechanical strain on the function of Gap junctions in osteocytes are mediated through the prostaglandin EP2 receptor." J Biol Chem **278**(44): 43146-56.

Clarke, K. A., L. Smart, et al. (2001). "Ground reaction force and spatiotemporal measurements of the gait of the mouse." Behav Res Methods Instrum Comput **33**(3): 422-6.

Clement, G. and A. Pavy-Le Traon (2004). "Centrifugation as a countermeasure during actual and simulated microgravity: a review." Eur J Appl Physiol **92**(3): 235-48.

Colleran, P. N., M. K. Wilkerson, et al. (2000). "Alterations in skeletal perfusion with simulated microgravity: a possible mechanism for bone remodeling." J Appl Physiol **89**(3): 1046-54.

Cowin, S., Ed. (1989). Bone Mechanics. Boca Raton, FL, CRC Press.

David, V., M. H. Lafage-Proust, et al. (2006). "Two-week longitudinal survey of bone architecture alteration in the hindlimb-unloaded rat model of bone loss: sex differences." Am J Physiol Endocrinol Metab **290**(3): E440-7.

Davis, B. L. and P. R. Cavanagh (1993). "Simulating reduced gravity: a review of biomechanical issues pertaining to human locomotion." Aviat Space Environ Med **64**(6): 557-66.

De Laet, C. E., B. A. van Hout, et al. (1997). "Bone density and risk of hip fracture in men and women: cross sectional analysis." Bmj **315**(7102): 221-5.

De Souza, R. L., M. Matsuura, et al. (2005). "Non-invasive axial loading of mouse tibiae increases cortical bone formation and modifies trabecular organization: a new model to study cortical and cancellous compartments in a single loaded element." Bone **37**(6): 810-8.

Dehority, W., B. P. Halloran, et al. (1999). "Bone and hormonal changes induced by skeletal unloading in the mature male rat." Am J Physiol **276**(1 Pt 1): E62-9.

Duda, G. N., M. Heller, et al. (1998). "Influence of muscle forces on femoral strain distribution." J Biomech **31**(9): 841-6.

Duddy, J. H. (1969). "The simulation of weightlessness using water immersion techniques: an annotated bibliography." Hum Factors **11**(5): 507-40.

Farley, C. T. and T. A. McMahon (1992). "Energetics of walking and running: insights from simulated reduced-gravity experiments." J Appl Physiol **73**(6): 2709-12.

Felson, D. T., Y. Zhang, et al. (1993). "Effects of weight and body mass index on bone mineral density in men and women: the Framingham study." J Bone Miner Res **8**(5): 567-73.
Fitts, R. H., D. R. Riley, et al. (2001). "Functional and structural adaptations of skeletal muscle to microgravity." J Exp Biol **204**(Pt 18): 3201-8.
Fluckey, J. D., E. E. Dupont-Versteegden, et al. (2002). "A rat resistance exercise regimen attenuates losses of musculoskeletal mass during hindlimb suspension." Acta Physiol Scand **176**(4): 293-300.
Flynn, T. W., P. K. Canavan, et al. (1997). "Plantar pressure reduction in an incremental weight-bearing system." Phys Ther **77**(4): 410-6.
Fosse, G. (1971). "The radiodensity of skeletal parts in animals growing and living in a constant artificially increased gravitational field." Growth **35**(1): 33-53.
Frost, H. M. (1987). "Bone "mass" and the "mechanostat": a proposal." Anat Rec **219**(1): 1-9.
Fuller, P. M., T. A. Jones, et al. (2002). "Neurovestibular modulation of circadian and homeostatic regulation: vestibulohypothalamic connection?" Proc Natl Acad Sci U S A **99**(24): 15723-8.
Genc, K. O., V. E. Mandes, et al. (2006). "Gravity replacement during running in simulated microgravity." Aviat Space Environ Med **77**(11): 1117-24.
Giangregorio, L. and C. J. Blimkie (2002). "Skeletal adaptations to alterations in weight-bearing activity: a comparison of models of disuse osteoporosis." Sports Med **32**(7): 459-76.
Gillis, G. B. and A. A. Biewener (2002). "Effects of surface grade on proximal hindlimb muscle strain and activation during rat locomotion." J Appl Physiol **93**(5): 1731-43.
Glatt, V., E. Canalis, et al. (2007a). "Age-Related Changes in Trabecular Architecture Differ in Female and Male C57BL/6J Mice." J Bone Miner Res **22**(8): 1197-207.
Glatt, V., K. L. Shultz, et al. (2007b). "Age-related changes in bone architecture vary among inbred strains of mice." Bone **40**: S194.
Globus, R. K., D. D. Bikle, et al. (1986). "The temporal response of bone to unloading." Endocrinology **118**(2): 733-42.
Goh, J. C., K. Bose, et al. (1996). "Pattern of fall and bone mineral density measurement in hip fractures." Ann Acad Med Singapore **25**(6): 820-3.
Graybiel, A. (1973). "Space missions involving the generation of artificial gravity." Environ Biol Med **2**(2): 91-138.
Griffin, T. M., N. A. Tolani, et al. (1999). "Walking in simulated reduced gravity: mechanical energy fluctuations and exchange." J Appl Physiol **86**(1): 383-90.
Grigoriev, Y. G. (1981). "Experimental biology and medicine in space." Endeavour **5**(4): 147-51.
Gross, T. S., J. L. Edwards, et al. (1997). "Strain gradients correlate with sites of periosteal bone formation." J Bone Miner Res **12**(6): 982-8.
Guo, X. E. and C. H. Kim (2002). "Mechanical consequence of trabecular bone loss and its treatment: a three-dimensional model simulation." Bone **30**(2): 404-11.
Hader, D. P., A. Rosum, et al. (1995). "Gravitaxis in the flagellate Euglena gracilis is controlled by an active gravireceptor." J Plant Physiol **146**(4): 474-80.

Hader, D. P., A. Rosum, et al. (1996). "Graviperception in the flagellate Euglena gracilis during a shuttle space flight." J Biotechnol **47**(2-3): 261-9.
Hambly, C. and J. R. Speakman (2005). "Contribution of different mechanisms to compensation for energy restriction in the mouse." Obes Res **13**(9): 1548-57.
Hampton, T. G., M. R. Stasko, et al. (2004). "Gait dynamics in trisomic mice: quantitative neurological traits of Down syndrome." Physiol Behav **82**(2-3): 381-9.
Hargens, A. R., J. Steskal, et al. (1984). "Tissue fluid shift, forelimb loading, and tail tension in tail-suspended rats." Physiologist **27**: S37–S38.
He, J. P., R. Kram, et al. (1991). "Mechanics of running under simulated low gravity." J Appl Physiol **71**(3): 863-70.
Hefferan, T. E., G. L. Evans, et al. (2003). "Effect of gender on bone turnover in adult rats during simulated weightlessness." J Appl Physiol **95**(5): 1775-80.
Heglund, N. C. (1981). "A simple design for a force-plate to measure ground reaction forces." J Exp Biol **93**: 333-338.
Hemmersbach, R., R. Voormanns, et al. (1998). "Comparative studies of the graviresponses of Paramecium and Loxodes." Adv Space Res **21**(8-9): 1285-9.
Hemmersbach, R., R. Voormanns, et al. (1996). "Graviresponses in Paramecium biaurelia under different accelerations: studies on the ground and in space." J Exp Biol **199**(Pt 10): 2199-205.
Hewes, D. E. (1969). "Reduced-gravity simulators for studies of man's mobility in space and on the moon." Hum Factors **11**(5): 419-31.
Huddleston, A. L., D. Rockwell, et al. (1980). "Bone mass in lifetime tennis athletes." Jama **244**(10): 1107-9.
Hurwitz, D. E., K. C. Foucher, et al. (1998). "Hip motion and moments during gait relate directly to proximal femoral bone mineral density in patients with hip osteoarthritis." J Biomech **31**(10): 919-25.
Ilyin, E. A. (1983). "Investigations on biosatellites of the Cosmos series." Aviat Space Environ Med **54**(12 Pt 2): S9-15.
Ivanenko, Y. P., R. Grasso, et al. (2002). "Control of foot trajectory in human locomotion: role of ground contact forces in simulated reduced gravity." J Neurophysiol **87**(6): 3070-89.
Jackson, D. K. and D. J. Newman (2000). "Adaptive effects of spaceflight as revealed by short-term partial weight suspension." Aviat Space Environ Med **71**(9 Suppl): A151-60.
Jee, W. S. and Y. Ma (1999). "Animal models of immobilization osteopenia." Morphologie **83**(261): 25-34.
Jee, W. S. S., X. J. Li, et al. (1991). "The skeletal adaptation to mechanical usage in the rat." Cells and Materials **Suppl 1**: 131-142.
Jennings, R. T. and J. P. Bagian (1996). "Musculoskeletal injury review in the U.S. space program." Aviat Space Environ Med **67**(8): 762-6.
Jiang, S. D., L. Y. Dai, et al. (2006). "Osteoporosis after spinal cord injury." Osteoporos Int **17**(2): 180-92.
Johnston, R. S., L. F. Dietlein, et al., Eds. (1975). Biomedical Results of Apollo. Houston, Texas, Lyndon B. Johnson Space Center.

Jorgensen, L., N. J. Crabtree, et al. (2000). "Ambulatory level and asymmetrical weight bearing after stroke affects bone loss in the upper and lower part of the femoral neck differently: bone adaptation after decreased mechanical loading." Bone **27**(5): 701-7.

Judex, S., L. R. Donahue, et al. (2002). "Genetic predisposition to low bone mass is paralleled by an enhanced sensitivity to signals anabolic to the skeleton." Faseb J **16**(10): 1280-2.

Judex, S., R. Garman, et al. (2004a). "Genetically linked site-specificity of disuse osteoporosis." J Bone Miner Res **19**(4): 607-13.

Judex, S., R. Garman, et al. (2004b). "Genetically based influences on the site-specific regulation of trabecular and cortical bone morphology." J Bone Miner Res **19**(4): 600-6.

Judex, S., T. S. Gross, et al. (1997). "Strain gradients correlate with sites of exercise-induced bone-forming surfaces in the adult skeleton." J Bone Miner Res **12**(10): 1737-45.

Judex, S. and R. F. Zernicke (2000). "High-impact exercise and growing bone: relation between high strain rates and enhanced bone formation." J Appl Physiol **88**(6): 2183-91.

Kannus, P., H. Haapasalo, et al. (1994). "The site-specific effects of long-term unilateral activity on bone mineral density and content." Bone **15**(3): 279-84.

Kannus, P., P. Leiponen, et al. (2006). "A sideways fall and hip fracture." Bone **39**(2): 383-4.

Kaplansky, A. S., G. N. Durnova, et al. (1991). "The effect of microgravity on bone fracture healing in rats flown on Cosmos-2044." Physiologist **34**(1 Suppl): S196-9.

Katovich, M. J. (1998). "Gravitational biology opportunities planned for the International Space Station." J Gravit Physiol **5**(1): P189-92.

Keller, T. S. and A. M. Strauss (1993). "Predicting skeletal adaptation in altered gravity environments." J Br Interplanet Soc **46**(3): 87-96.

Kirchen, M. E., K. M. O'Connor, et al. (1995). "Effects of microgravity on bone healing in a rat fibular osteotomy model." Clin Orthop Relat Res(318): 231-42.

Kodama, Y., H. P. Dimai, et al. (1999). "Cortical tibial bone volume in two strains of mice: effects of sciatic neurectomy and genetic regulation of bone response to mechanical loading." Bone **25**(2): 183-90.

Komsa-Penkova, R., R. Spirova, et al. (1996). "Modification of Lowry's method for collagen concentration measurement." J Biochem Biophys Methods **32**(1): 33-43.

Koryak, Y. (1996). "Mechanical and electrical changes in human muscle after dry immersion." Eur J Appl Physiol Occup Physiol **74**(1-2): 133-40.

Koryak, Y. U. (2001). "Electrically evoked and voluntary properties of the human triceps surae muscle: effects of long-term spaceflights." Acta Physiol Pharmacol Bulg **26**(1-2): 21-7.

Kotajarvi, B. (2003). "Ground Reaction Forces During Partial Weight Bearing Gait Using Conventional Assistive Devices: A Feasibility Study." Retrieved June 2004, from http://mayoresearch.mayo.edu/mayo/research/biomechanics/gait1.cfm.

Lafage-Proust, M. H., P. Collet, et al. (1998). "Space-related bone mineral redistribution and lack of bone mass recovery after reambulation in young rats." Am J Physiol **274**(2 Pt 2): R324-34.

Lang, T., A. LeBlanc, et al. (2004). "Cortical and trabecular bone mineral loss from the spine and hip in long-duration spaceflight." J Bone Miner Res **19**(6): 1006-12.
Lang, T. F. (2006a). "What do we know about fracture risk in long-duration spaceflight?" J Musculoskelet Neuronal Interact **6**(4): 319-21.
Lang, T. F. (2007). Skeletal Atrophy and Long-Term Recovery in Long-Duration Spaceflight. 16th Humans in Space Symposium of the International Academy of Astronautics. Beijing, China.
Lang, T. F., A. D. Leblanc, et al. (2006b). "Adaptation of the proximal femur to skeletal reloading after long-duration spaceflight." J Bone Miner Res **21**(8): 1224-30.
Lanyon, L. E. and C. T. Rubin (1984). "Static vs dynamic loads as an influence on bone remodelling." J Biomech **17**(12): 897-905.
Lavoie, T. (2006). Lunar Architecture Overview. Implementing the Vision: 2nd Space Exploration Conference. Houston, TX.
LeBlanc, A., V. Schneider, et al. (2000). "Bone mineral and lean tissue loss after long duration space flight." J Musculoskelet Neuronal Interact **1**(2): 157-60.
LeBlanc, A., V. Schneider, et al. (1996). "Bone mineral and lean tissue loss after long duration spaceflight." J Bone Miner Res **11**(Suppl 1): S323.
LeBlanc, A. D., E. R. Spector, et al. (2007). "Skeletal responses to space flight and the bed rest analog: a review." J Musculoskelet Neuronal Interact **7**(1): 33-47.
Leblond, H., M. L'Esperance, et al. (2003). "Treadmill locomotion in the intact and spinal mouse." J Neurosci **23**(36): 11411-9.
Li, S., C. W. Armstrong, et al. (2001). "Three-point gait crutch walking: variability in ground reaction force during weight bearing." Arch Phys Med Rehabil **82**(1): 86-92.
Looker, A. C., H. W. Wahner, et al. (1998). "Updated data on proximal femur bone mineral levels of US adults." Osteoporos Int **8**(5): 468-89.
Mack, P. B., P. A. LaChance, et al. (1967). "Bone demineralization of foot and hand of gemini-titan IV, V and VII astronauts during orbital flight." Am J Roentgenol Radium Ther Nucl Med **100**(3): 503-11.
McCarthy, I., A. Goodship, et al. (2000). "Investigation of bone changes in microgravity during long and short duration space flight: comparison of techniques." Eur J Clin Invest **30**(12): 1044-54.
Meinel, L., R. Fajardo, et al. (2005). "Silk implants for the healing of critical size bone defects." Bone **37**(5): 688-98.
Milgrom, C., D. R. Radeva-Petrova, et al. (2007). "The effect of muscle fatigue on in vivo tibial strains." J Biomech **40**(4): 845-50.
Minetti, A. E. (2001). "Walking on other planets." Nature **409**(6819): 467, 469.
Moisio, K. C., D. E. Hurwitz, et al. (2004). "Dynamic loads are determinants of peak bone mass." J Orthop Res **22**(2): 339-45.
Montufar-Solis, D. and P. J. Duke (1999). "Gravitational changes affect tibial growth plates according to Hert's curve." Aviat Space Environ Med **70**(3 Pt 1): 245-9.
Morey-Holton, E., R. K. Globus, et al. (2005). The Hindlimb Unloading Rat Model: Literature Overview, Technique Update and Comparison with Space Flight Data. Experimentation with Animal Models in Space. G. Sonnenfeld, Elsevier B.V.

Morey-Holton, E. R. and R. K. Globus (1998). "Hindlimb unloading of growing rats: a model for predicting skeletal changes during space flight." Bone **22**(5 Suppl): 83S-88S.
Morey-Holton, E. R. and R. K. Globus (2002). "Hindlimb unloading rodent model: technical aspects." J Appl Physiol **92**(4): 1367-77.
Morey-Holton, E. R., E. L. Hill, et al. (2007). "Animals and spaceflight: From survival to understanding." J Musculoskelet Neuronal Interact **7**(1): 17-25.
Morey, E. R. (1979). "Space flight and bone turnover: correlation with a new rat model of weightlessness." BioScience **29**: 168-172.
Mosley, J. R., B. M. March, et al. (1997). "Strain magnitude related changes in whole bone architecture in growing rats." Bone **20**(3): 191-8.
Murakami, D. M., L. Erkman, et al. (2002). "Evidence for vestibular regulation of autonomic functions in a mouse genetic model." Proc Natl Acad Sci U S A **99**(26): 17078-82.
Murthy, G., D. E. Watenpaugh, et al. (1994). "Supine exercise during lower body negative pressure effectively simulates upright exercise in normal gravity." J Appl Physiol **76**(6): 2742-8.
Musacchia, X. J. (1992). "An assessment of suspension systems: models that reproduce responses to weightlessness." Physiologist **35**(1 Suppl): S92-5.
Musacchia, X. J. and D. R. Deavers (1980). "A new rat model for studies of hypokinesia and antiorthostasis." Physiologist **23**(Suppl 6): S91-2.
Nagy, T. R., D. Krzywanski, et al. (2002). "Effect of group vs. single housing on phenotypic variance in C57BL/6J mice." Obes Res **10**(5): 412-5.
NASA. (November 2, 2006). "Life Sciences Data Archive." Retrieved April, 2007, from http://lsda.jsc.nasa.gov/.
NASA (1989). Spacelab Life Sciences 1: First Space Laboratory Dedicated to Life Sciences Research. L. B. J. S. Center, National Aeronautics and Space Administration.
NASA (2004). The Vision for Space Exploration. Washington, DC.
NASA (2005a). Bioastronautics Roadmap Baseline Document: A Risk Reduction Strategy for Human Space Exploration.
NASA (2005b). Exploration Systems Architecture Study: Final Report.
National Research Council, S. S. B. (1998). A Strategy for Research in Space Biology and Medicine in the New Century. Washington, DC, National Academy Press.
Newman, D. J. (1992). Human locomotion and energetics in simulated partial gravity. Aeronautics and Astronautics. Cambridge, MA, Massachusetts Institute of Technology. **PhD**.
Newman, D. J. and H. L. Alexander (1993). "Human locomotion and workload for simulated lunar and Martian environments." Acta Astronaut **29**(8): 613-20.
Newman, D. J., H. L. Alexander, et al. (1994). "Energetics and mechanics for partial gravity locomotion." Aviat Space Environ Med **65**(9): 815-23.
Newman, D. J., D. K. Jackson, et al. (1997). "Altered astronaut lower limb and mass center kinematics in downward jumping following space flight." Exp Brain Res **117**(1): 30-42.

Newman, D. J., G. Schaffner, et al. (1998). Finite Element Modeling of Strength Changes in the Proximal Femur following Long–Term Spaceflight. National Space Biomedical Research Institute Symposium. Houston, TX.

Newman, D. J., K. U. Schultz, et al. (1996). "Closed-loop, estimator-based model of human posture following reduced gravity exposure." J Guid Control Dyn **19**(5): 1102-8.

Nicogossian, A. P., SL (2003). Space Physiology and Medicine. Philadelphia, Lippincott Williams & Wilkins.

Oganov, V. S. (2004). "Modern analysis of bone loss mechanisms in microgravity." J Gravit Physiol **11**(2): P143-6.

Pace, N., A. H. Smith, et al. (1985). "Skeletal mass change as a function of gravitational loading." Physiologist **28**(6 Suppl): S17-20.

Parfitt, A. M., M. K. Drezner, et al. (1987). "Bone histomorphometry: standardization of nomenclature, symbols, and units. Report of the ASBMR Histomorphometry Nomenclature Committee." J Bone Miner Res **2**(6): 595-610.

Pavy-Le Traon, A., A. M. Allevard, et al. (1997). "Cardiovascular and hormonal changes induced by a simulation of a lunar mission." Aviat Space Environ Med **68**(9): 829-37.

Peterman, M. M., A. J. Hamel, et al. (2001). "In vitro modeling of human tibial strains during exercise in micro-gravity." J Biomech **34**(5): 693-8.

Phillips, R. W. (2002). "Gravity: It's the law." J Gravit Physiol **9**(1): P15-6.

Pogoda, P., M. Priemel, et al. (2005). "Bone remodeling: new aspects of a key process that controls skeletal maintenance and repair." Osteoporos Int **16 Suppl 2**: S18-24.

Puustjarvi, K., J. Nieminen, et al. (1999). "Do more highly organized collagen fibrils increase bone mechanical strength in loss of mineral density after one-year running training?" J Bone Miner Res **14**(3): 321-9.

Rabkin, B. A., J. A. Szivek, et al. (2001). "Long-term measurement of bone strain in vivo: the rat tibia." J Biomed Mater Res **58**(3): 277-81.

Rader, A., D. Newman, et al. (2007). Loping: A Strategy for reduced gravity human locomotion? International Conference on Environmental Systems (ICES) Chicago, IL.

Rambaut, P. C. and R. S. Johnston (1979). "Prolonged weightlessness and calcium loss in man." Acta Astronaut **6**(9): 1113-22.

Rambaut, P. C., C. S. Leach, et al. (1975). "Calcium and phosphorus change of the Apollo 17 crew members." Nutr Metab **18**(2): 62-9.

Reiman, M. P., M. E. Rogers, et al. (2006). "Interlimb differences in lower extremity bone mineral density following anterior cruciate ligament reconstruction." J Orthop Sports Phys Ther **36**(11): 837-44.

Rittweger, J., H. C. Gunga, et al. (1999). "Muscle and bone-aging and space." J Gravit Physiol **6**(1): P133-6.

Roberts, J. F. (1963). Walking Responses under Lunar and Low Gravity Conditions. Amrl Tr**:** 1-117.

Robling, A. G. and C. H. Turner (2002). "Mechanotransduction in bone: genetic effects on mechanosensitivity in mice." Bone **31**(5): 562-9.

Roux, W. (1895). Gesammelte Abhandlungen. Leipzig, Engelmann.

Rubin, C., G. Xu, et al. (2001). "The anabolic activity of bone tissue, suppressed by disuse, is normalized by brief exposure to extremely low-magnitude mechanical stimuli." Faseb J **15**(12): 2225-9.

Rubin, C. G., TS; Guilak, F; Qin, Y-X; Fritton, S; McLeod, KJ (1996). "Differentiation of the bone tissue remodeling response to dilatational and deviatoric strain." J Bone Joint Surg **78A**: 1523-33.

Rubin, C. T. and L. E. Lanyon (1984). "Regulation of bone formation by applied dynamic loads." J Bone Joint Surg Am **66**(3): 397-402.

Rubin, C. T. and L. E. Lanyon (1987). "Kappa Delta Award paper. Osteoregulatory nature of mechanical stimuli: function as a determinant for adaptive remodeling in bone." J Orthop Res **5**(2): 300-10.

Sakai, A. and T. Nakamura (2001). "Changes in trabecular bone turnover and bone marrow cell development in tail-suspended mice." J Musculoskelet Neuronal Interact **1**(4): 387-92.

Schaffner, G. (1999). Assessment of Hip Fracture Risk in Astronauts Exposed to Long-Term Weightlessness. Aeronautics & Astronautics. Cambridge, MA, Massachusetts Institute of Technology. **PhD**.

Schneider, V. O., V; LeBlanc, A; Rakhmanov, A; Bakulin, A; Grigoriev, A; Varonin, L (1992). "Space flight bone loss and change in fat and lean body mass." J Bone Miner Res **S122**: abstract 117.

Scholle, H. C., F. Biedermann, et al. (2005). "A surface EMG multi-electrode technique for characterizing muscle activation patterns in mice during treadmill locomotion." J Neurosci Methods **146**(2): 174-82.

Schultheis, L. (1991). "The mechanical control system of bone in weightless spaceflight and in aging." Exp Gerontol **26**(2-3): 203-14.

Schultheis, L. (2000a). The Effects of Partial Mechanical Loading and Ibandronate on Skeletal Tissues in the Adult Rat Hindquarter Suspension Model of Microgravity. NASA Life Sciences Taskbook.

Schultheis, L., M. Daphtary, et al. (2001). The effects of partial weightbearing, mechanical loading and ibandronate on skeletal tissues in the adult rat hindquarter suspension model of microgravity. NSBRI**:** 27.

Schultheis, L., C. B. Ruff, et al. (2000b). "Disuse bone loss in hindquarter suspended rats: partial weightbearing, exercise and ibandronate treatment as countermeasures." J Gravit Physiol **7**(2): P13-4.

Schultheis, L. L., J; Annand, J; Gilka, P; Schultheis, A (1999). High pass mechanical filtering of the forelimb in the hindquarter suspended rat. 45th Annual Meeting of the Orthopaedic Research Society, Anaheim, CA.

Schumann, N. P., F. H. Biedermann, et al. (2006). "Treadmill locomotion in normal mice-Step related multi-channel EMG profiles of thigh muscles." Pathophysiology **13**(4): 245-55.

Shipov, A. A., A. R. Kotovskaya, et al. (1981). "Biomedical aspects of artificial gravity." Acta Astronaut **8**(9-10): 1117-21.

Sibonga, J. D., M. Zhang, et al. (2000). "Effects of spaceflight and simulated weightlessness on longitudinal bone growth." Bone **27**(4): 535-40.

Silva, M. J. (1996). Predicting the Failure Behavior of the Human Vertebral Body. Cambridge, MA, Massachusetts Institute of Technology **PhD**.

Silva, M. J. and L. J. Gibson (1997). "Modeling the mechanical behavior of vertebral trabecular bone: effects of age-related changes in microstructure." Bone **21**(2): 191-9.

Simske, S. F., VL; Bateman, TA (2003). Mice and osteoporosis research. Recent Research Developments in Biotechnology and Bioengineering S. Pandalai. Kerala, India, Research Signpost. **5:** 97-127.

Simske, S. J., M. W. Luttges, et al. (1994). "The role of sex and genotype on antiorthostatic suspension effects on the mouse peripheral skeleton." Aviat Space Environ Med **65**(2): 123-33.

Smith, S. M., J. E. Davis-Street, et al. (2003). "Evaluation of treadmill exercise in a lower body negative pressure chamber as a countermeasure for weightlessness-induced bone loss: a bed rest study with identical twins." J Bone Miner Res **18**(12): 2223-30.

Smith, S. M., J. L. Nillen, et al. (1998). "Collagen cross-link excretion during space flight and bed rest." J Clin Endocrinol Metab **83**(10): 3584-91.

Smith, S. M., M. E. Wastney, et al. (1999). "Calcium metabolism before, during, and after a 3-mo spaceflight: kinetic and biochemical changes." Am J Physiol **277**(1 Pt 2): R1-10.

Smith, S. M., M. E. Wastney, et al. (2005). "Bone markers, calcium metabolism, and calcium kinetics during extended-duration space flight on the Mir space station." J Bone Miner Res **20**(2): 208-18.

Srinivasan, S., S. C. Agans, et al. (2003). "Enabling bone formation in the aged skeleton via rest-inserted mechanical loading." Bone **33**(6): 946-55.

Srinivasan, S., D. A. Weimer, et al. (2002). "Low-magnitude mechanical loading becomes osteogenic when rest is inserted between each load cycle." J Bone Miner Res **17**(9): 1613-20.

Steffen, J. M., R. D. Fell, et al. (1987). "Physiological responses during whole body suspension of adult rats." Physiologist **30**(1 Suppl): S94-5.

Suzuki, H. K. and A. Mathews (1966). "Two-color fluorescent labeling of mineralizing tissues with tetracycline and 2,4-bis[N,N'-di-(carbomethyl)aminomethyl] fluorescein." Stain Technol **41**(1): 57-60.

Tanaka, K., T. M. Gotoh, et al. (2005). "Regional difference of blood flow in anesthetized rats during reduced gravity induced by parabolic flight." J Appl Physiol **99**(6): 2144-8.

Turner, C. H. (1991). "Homeostatic control of bone structure: an application of feedback theory." Bone **12**(3): 203-17.

Turner, C. H. (1998). "Three rules for bone adaptation to mechanical stimuli." Bone **23**(5): 399-407.

Turner, C. H. and D. B. Burr (1993). "Basic biomechanical measurements of bone: a tutorial." Bone **14**(4): 595-608.

Turner, C. H., M. R. Forwood, et al. (1994). "Mechanotransduction in bone: do bone cells act as sensors of fluid flow?" Faseb J **8**(11): 875-8.

Turner, R. T. (2000). "Invited review: what do we know about the effects of spaceflight on bone?" J Appl Physiol **89**(2): 840-7.

Vico, L., D. Chappard, et al. (1987). "Effects of a 120 day period of bed-rest on bone mass and bone cell activities in man: attempts at countermeasure." Bone Miner **2**(5): 383-94.
Vico, L., P. Collet, et al. (2000). "Effects of long-term microgravity exposure on cancellous and cortical weight-bearing bones of cosmonauts." Lancet **355**(9215): 1607-11.
Vico, L., M. H. Lafage-Proust, et al. (1998). "Effects of gravitational changes on the bone system in vitro and in vivo." Bone **22**(5 Suppl): 95S-100S.
Vico, L., V. E. Novikov, et al. (1991). "Bone histomorphometric comparison of rat tibial metaphysis after 7-day tail suspension vs. 7-day spaceflight." Aviat Space Environ Med **62**(1): 26-31.
Vose, G. P. (1974). "Review of roentgenographic bone demineralization studies of the Gemini space flights." Am J Roentgenol Radium Ther Nucl Med **121**(1): 1-4.
Wade, C. E., J. S. Harper, et al. (1997). "Body mass change during altered gravity: spaceflight, centrifugation, and return to 1 G." J Gravit Physiol **4**(3): 43-8.
Wade, C. E. and E. Morey-Holton (1998). "Alteration of renal function of rats following spaceflight." Am J Physiol **275**(4 Pt 2): R1058-65.
Wagner, E. B. and T. R. Fulford-Jones (2006a). "Sensorimotor investigations for the Mars Gravity Biosatellite: a rotating spacecraft for partial gravity research." Brain Res **1091**(1): 75-8.
Wagner, E. G., NP (2006b). The Musculoskeletal Effects of Partial Weightbearing in Mice (poster). Annual Meeting of the American Society for Gravitational and Space Biology. Arlington, VA.
Wagner, E. G., NP; Bouxsein, ML (2007). Musculoskeletal Adaptation to Mars-Analog Loading in Female Mice (poster). 28th Annual International Gravitational Physiology Meeting. San Antonio, TX.
Wagner, E. W., PD; Keesee, JE; Kubert, H; Schaffer, A (2004). Mars Gravity Biosatellite: International Student Training and Public Outreach. SAE International Conference on Environmental Systems. Colorado Springs, CO.
Warner, S. E., D. A. Sanford, et al. (2006). "Botox induced muscle paralysis rapidly degrades bone." Bone **38**(2): 257-64.
Warren, L. E., B. A. Horwitz, et al. (2001). "Effects of 2 G on adiposity, leptin, lipoprotein lipase, and uncoupling protein-1 in lean and obese Zucker rats." J Appl Physiol **90**(2): 606-14.
Watenpaugh, D. E., R. E. Ballard, et al. (2000). "Supine lower body negative pressure exercise during bed rest maintains upright exercise capacity." J Appl Physiol **89**(1): 218-27.
Whalen, R. (1993). "Musculoskeletal adaptation to mechanical forces on Earth and in space." Physiologist **36**(1 Suppl): S127-30.
Wolff, J. (1892). Das Gesetz der Transformation der Knochen. Berlin, Hirschwald.
Wronski, T. J. and E. R. Morey-Holton (1987). "Skeletal response to simulated weightlessness: a comparison of suspension techniques." Aviat Space Environ Med **58**(1): 63-8.
Wronski, T. J. and E. R. Morey (1983). "Effect of spaceflight on periosteal bone formation in rats." Am J Physiol **244**(3): R305-9.

Wu, R. (1999). Human Readaptation to Normal Gravity Following Short-Term Simulated Martian Gravity Exposure and the Effects of Countermeasures. Aeronautics and Astronautics. Cambridge, MA, Massachusetts Institute of Technology. **Master's**.

Yoshikawa, T., S. Mori, et al. (1994). "The effects of muscle fatigue on bone strain." J Exp Biol **188**: 217-33.

Youdas, J. W., B. J. Kotajarvi, et al. (2005). "Partial weight-bearing gait using conventional assistive devices." Arch Phys Med Rehabil **86**(3): 394-8.

Youm, T., K. J. Koval, et al. (1999). "Do all hip fractures result from a fall?" Am J Orthop **28**(3): 190-4.

Young, L. R. (1999). "Artificial gravity considerations for a mars exploration mission." Ann N Y Acad Sci **871**: 367-78.

Young, L. R. (2003). Artificial Gravity. Encyclopedia of Space Science and Technology. New York, John Wiley and Sons, Inc. **1:** 138-151.

Yuganov, Y. (1972). Artificial gravitation and physiology (Artificial gravitational environment for maintaining physiological processes and astronaut workability during prolonged space flight) Space Medicine: Reports on Artificial Gravitation and Space Suits NASA**:** 1-5.

Yuganov, Y. and M. Yemelyanov (1972). "The problem of artificial gravitation from the viewpoint of experimental physiology (Physiological weightlessness threshold parameters and generation of artificial gravity during manned space flight) " Space Biol. and Med **6**(3): 69-74.

Yuganov, Y. and M. Yemelyanov (1975). Problem of artificial gravity from the point of view of experimental physiolog. Weightlessness: Med. and Biol. Res. NASA**:** 351-357

Zangemeister, W. H., M. V. Bulgheroni, et al. (1991). "Normal gait is differentially influenced by the otoliths." J Biomed Eng **13**(6): 451-8.

Zerahn, B., A. O. Munk, et al. (2006). "Bone mineral density in the proximal tibia and calcaneus before and after arthroscopic reconstruction of the anterior cruciate ligament." Arthroscopy **22**(3): 265-9.

Zerath, E. (1998). "Effects of microgravity on bone and calcium homeostasis." Adv Space Res **21**(8-9): 1049-58.

Zumwalt, A. C., M. Hamrick, et al. (2006). "Force plate for measuring the ground reaction forces in small animal locomotion." J Biomech **39**(15): 2877-81.

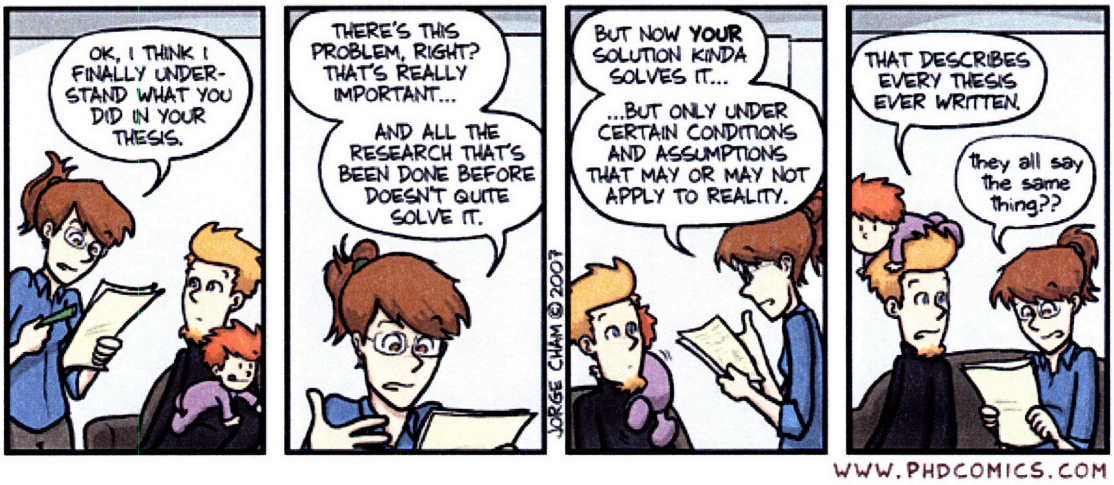

From: "Piled Higher and Deeper" by Jorge Cham, with permission

www.phdcomics.com

Appendix A

Mars Gravity Biosatellite

A.1 Program Summary

With NASA's direct leadership of the International Space Station coming to an end and exploration class missions looming large on the horizon, a demonstrated need exists for free-flyer platforms on which to conduct supporting science. Furthermore, as clearly demonstrated in the National Academies report *Rising above the Gathering Storm* and elsewhere, the US is falling critically behind in inspiring and educating students for careers in science, technology, engineering, and mathematics (STEM) fields.

Since 2001, the Mars Gravity Biosatellite program has engaged over 500 students, from high school through graduate studies. Together with advisors in academia, government, and industry, this team has made significant progress in designing, modeling, prototyping, and managing the development of a new free-flyer spacecraft. Our novel satellite platform will offer an uncrewed laboratory for artificial gravity research, hosting up to 15 mice for missions up to 5 weeks in duration, and returning the payload safely to Earth for analysis.

The science planned for the first flight of the biosatellite offers the first real glimpse into the effects of Martian gravity levels on mammalian physiology. Data in this regime may be important to the mitigation of the effects of micro-gravity in extended-duration, low Earth orbit operations. It will be critical to eventual human

operations in a Martian gravity environment where the duration of reduced gravity exposures will reach periods of over a year. Furthermore, the understanding of these deconditioning processes may provide enhanced understanding of diseases on Earth, such as osteoporosis.

The initial payload manifested for the vehicle will launch 15 mice into LEO for a five-week flight. In a spin-stabilized mode, the satellite will provide artificial gravity at 0.38-g, simulating the accelerations found on the surface of Mars. After 35 days of data collection, the satellite will reenter the Earth's atmosphere. A mid-air recovery will be conducted over the Utah Test and Training Range, and the vehicle will be returned to laboratory facilities to allow for further scientific investigations. This research will be the first of its kind and the longest self-contained biosatellite flight in history.

As the first study of mammalian physiology in partial gravity, the inaugural flight of the biosatellite will focus on broad, hypothesis-driven investigations. This peer-reviewed research will include characterization of musculoskeletal degradation, alterations of vestibular reflexes, and downregulation of the immune response. Beyond basic science, Mars Gravity represents a uniquely affordable platform for quantifying risks and testing hypotheses related to NASA's exploration vision. Sized for launch on the SpaceX Falcon I, total mission costs are estimated at under $40M, including launch.

This profile makes the spacecraft not only a desirable and unique American capability, but an amazing educational enterprise. Current efforts represent a core collaboration between MIT and the Georgia Institute of Technology. MIT spearheads Science, Payload, Bus, and Systems Engineering efforts, while Georgia Tech takes the lead on Entry, Descent, and Landing (EDL) development.

This program is both an affordable and meaningful investment in the future that will:

1. Help establish whether Mars-level artificial gravity can serve as an effective countermeasure for mammals against the physiological deterioration that accompanies long-duration spaceflight in microgravity.

2. Validate a low-mass artificial gravity spacecraft and life support system to support future missions.

3. Educate and excite students about real-world aerospace and biomedical endeavors, providing a core training ground for the next generation of STEM professionals.

A.2 Satellite Design

The Mars Gravity Biosatellite design is comprised of four main hardware elements:

- PAYLOAD provides life support to 15 mice for 5 weeks of flight, plus up to an additional week pre-flight time with appropriate ground support equipment (GSE). This element houses the main flight computer, and collects, stores, and processes science and life support system data for transmission by the spacecraft bus. The Payload is incorporated into the entry vehicle and is returned post-flight.

- ENTRY, DESCENT, & LANDING (EDL) protects the payload through atmospheric reentry, slows the vehicle during descent, and facilitates mid-air recovery.

- BUS provides basic functionality of power, thermal control, attitude determination and control, propulsion, and communications. The Bus separates from the entry vehicle following reorientation and burn maneuvers and is largely destroyed during reentry.

- YOUR NAME INTO SPACE (YNIS) consists of personal and corporate logos and other images placed on the spacecraft interior and exterior, as well as cameras arranged to image these external graphics for revenue generation.

Total launch mass, including margin, is specified at 625 kg wet mass, with up to 200 kg payload mass recovered post-flight.

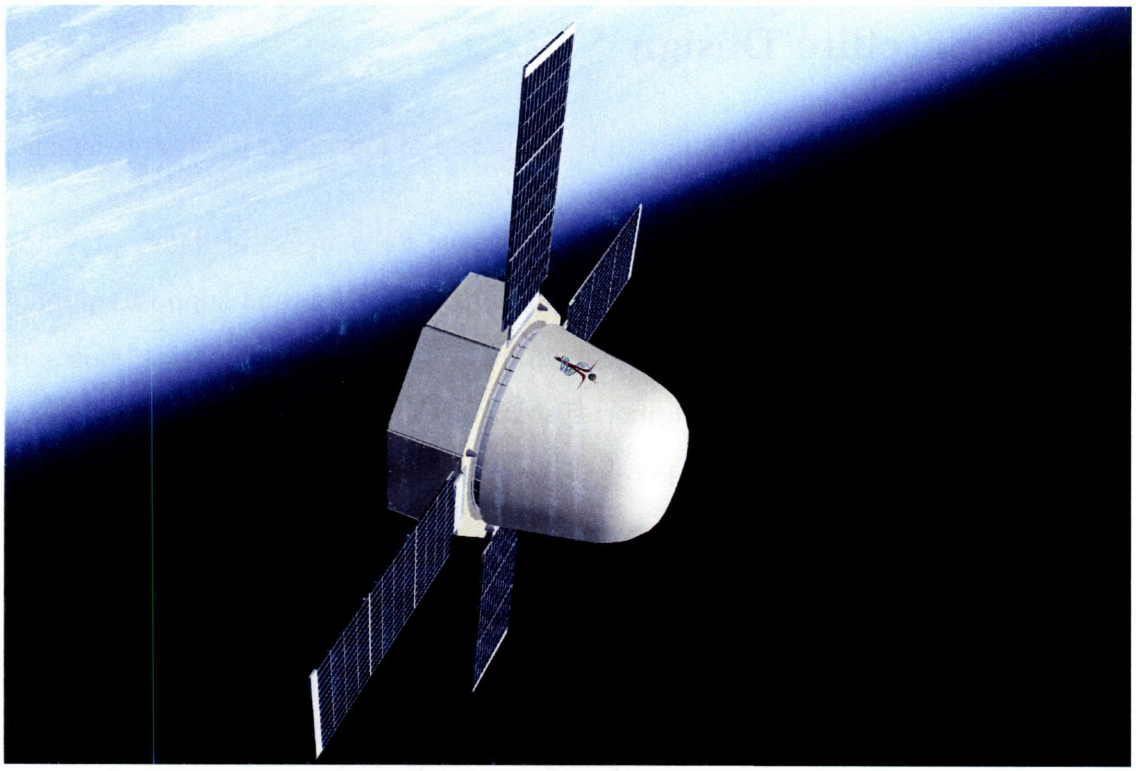

Figure A-1: Artist's conception of the Mars Gravity Biosatellite in low Earth orbit. *(Image Credit: Mars Gravity)*

A.3 Baseline Mission Operations

Baseline mission operations begin with integration of flight hardware elements at a central facility of the mission's lead industrial partner. Following integrated testing, the system will be shipped to the launch site for animal load-in, final testing, fueling, and launch vehicle integration. The Mars Gravity Biosatellite is planned as a primary payload on a domestic expendible launch vehicle, with baseline set as the SpaceX Falcon I.

The Payload has been designed to support animals for up to 7 days from integration to launch, with GSE for power, data, and atmospheric processing throughout this time. No provision has been made for on-pad exchange of specimens.

At launch, the vehicle will be placed in a 370 km, 41 ° inclination, circular LEO trajectory. The spacecraft is sun-pointing, with the heatshield providing some degree of thermal protection for the payload. Power is provided throughout the main flight phases by solar arrays and secondary batteries. After initial 3-axis-stabilized pointing maneuvers using a hydrazine monopropellant system, the vehicle will spin up to approximately 32 rpm, providing 0.38-g of artificial gravity outwards against the curved floors of the specimen chambers. Once the vehicle is checked out and stabilized, the exterior YNIS cameras will acquire images for our donors, and the communication subsystem will downlink them to the ground.

Over the next 5 weeks, the vehicle will operate largely autonomously, with no planned orbital maintenance or attitude control maneuvers. Thermal energy from the payload will be rejected to the cold backplate of the bus, via the Lightband separation system. S-band communication with commercial ground stations will occur at least once every 8.5 hours to provide adequate monitoring of the system and animals, as well as downlink of telemetry, images, and video footage. Software patches will be uploaded as needed. Data will be distributed via secure internet protocols to a Mission Control Center at MIT and other distributed users.

On mission day 35, a command from the ground will be used to initialize the reentry sequence. Hydrazine thrusters will be used to spin down, reorient, and spin up

the vehicle for its reentry burn. The bus will be separated from the reentry vehicle, deorbiting separately from the reentry vehicle to burn up over the Pacific Ocean. An ablative heatshield will protect the reentry vehicle through entry. Primary batteries will provide power for life support, data collection, and tracking systems. A supersonic drogue chute will decelerate and stabilize the vehicle through the transonic flight region, then deploy the main parafoil. Helicopters will execute a mid-air recovery at the Utah Test and Training Range, then safely fly the payload to a Recovery Operations Center based at a local military installation or university. Within 2 hours of recovery, the vehicle will be safed, animal habitats will be extracted, and mice will be delivered to a team of PIs for in vivo measurements, followed by dissection. Primary PIs will have immediate access to core science samples, and remaining specimens will be preserved for use through a Biospecimen Sharing Program.

A.4 Science

A.4.1 Motivation

As detailed in Chapter 2, evidence from numerous flight and ground studies has identified skeletal degradation, muscle atrophy, and deconditioning of neurovestibular pathways as major challenges facing life in a microgravity environment. Surprisingly, nearly all flight physiology research to date has focused solely on the questions of health in LEO and the effects of microgravity. The prospect of a human presence on the Moon and Mars raises yet another set of medical uncertainties regarding how the body will respond to the partial-g environments of living and working beyond LEO. The basic questions of "how much gravity is sufficient to prevent deconditioning?" and "how will long-duration exposure to partial gravity levels affect basic physiological processes?" remain unanswered.

Particularly with the Centrifuge Accommodation Module (CAM) no longer scheduled to fly and crew time and up/down mass sharply limited by ISS assembly schedules, NASA has no capability to address these questions. A free-flying biosatellite

would provide a much-desired interim opportunity for collecting spaceflight data, and would offer options for flying a variety of future science missions that cannot or will not be conducted on the ISS.

Partial gravity investigations further offer insights into developing artificial gravity architectures, offering evidence as to whether such a system would need to be designed at a scale and rate of rotation that can support full 1-g activities. If 0.38-g is highly protective of physiological processes, relative to microgravity operations, the development costs of a rotating system could be sharply reduced.

A.4.2 Design of Flight Experiments

Fifteen skeletally mature BALB/cByJ female mice will be flown for a duration of 5 weeks. This strain was selected due to its robust skeletal responses to unloading. Females utilize fewer consumables, allowing for a larger number of animals and greater statistical power from the cohort. The cohort size and flight duration provide scientific margin on the expected statistical results for representative skeletal parameters.

The Mars Gravity Biosatellite program is intended to provide a broad snapshot of the physiological issues and opportunities provided by a 0.38-g artificial gravity environment. Rather than focusing narrowly on a particular physiological system, the current dearth of any data regarding partial gravity effects justifies a wider perspective for our investigations.

A prioritized list of science objectives has been developed in collaboration with the program's External Science Advisory Panel. On the basis of available resources and instrumentation, these priorities have been narrowed to the following:

In a suitable mammalian model, quantify the extent of the following effects seen as a result of extended exposure to Mars-equivalent levels of artificial gravity, as compared to both microgravity and 1-g physiology, wherever possible:

Bone Demineralization

Hypothesis 1. Bone loss and increased fracture risk in the weight-bearing areas of the skeleton is expected relative to 1-g controls, with greater losses in the

trabecular compartment and at sites of muscle insertion. Biomarkers indicating both a reduction in bone formation and an increase in bone remodeling are expected.

Hypothesis 2. Bone preservation in the weight-bearing areas of the skeleton is expected relative to previous flight trends and hindlimb suspension models.

Muscle Atrophy

Hypothesis 3. Skeletal muscle atrophy is expected relative to 1-g controls, with greater losses in postural extensor muscles, and a shift in myosin expression towards faster isoforms.

Hypothesis 4. Extensor muscle preservation is expected relative to previous flight trends and hindlimb suspension models.

Neurovestibular Adaptation

Hypothesis 5. Reduction of the tonic gravitational input is expected to cause an increase in utricular sensitivity, compared to 1-g controls, as demonstrated by plasticity of neural connections, functional responses to linear accelerations, and reductions in complex sensorimotor task performance.

Hypothesis 6. The chronically rotating environment of the spacecraft is expected to cause a decrease in semicircular canal sensitivity, compared to non-rotating 1-g controls, as demonstrated by plasticity of neural connections, functional responses to angular accelerations, and reductions in complex sensorimotor task performance.

Immune Suppression

Hypothesis 7. Compromise of immune responses is expected relative to 1-g controls, as measured by splenocyte, bone marrow, and peripheral leukocyte counts and activity, as well as atrophy of lymphoid organs.

Planned ground investigations include vivarium, suspension, flight habitat, and rotational controls, designed to clarify the contributions of various elements of the flight environment.

A.5 Team

Teams of graduate and undergraduate students have both accomplished and led the majority of work to this point, progressing the program to a Preliminary Design Review (PDR). An initial team of MIT, the University of Washington, and the University of Queensland has evolved to a collaboration between MIT and the Georgia Institute of Technology.

Typically, over 80% of the students are volunteers, donating between six and twenty hours per week during the school year, and over forty hours per week during summer and January holidays. Students range in experience and age, from high school volunteers to graduate students. Faculty and industry advisors play a significant role in mentoring students.

Following PDR, the program plans to transition from a predominantly student effort to one that embraces a collaborative role for industry partners. Partnerships with payload, bus, and EDL hardware providers will be explored to support high quality flight hardware production in a manner that continues to provide meaningful roles for student workforce development.

A request for information (RFI) was released in Spring 2007 to begin selection of a partner for Bus development and Systems Integration. Final definition of that partnership is expected following PDR, with a Delta PDR to be conducted when that commercial component is at the appropriate level of development.

Selection of Payload and EDL partners will follow PDR.

Flight science principal investigators (PIs) will be selected by two peer-reviewed solicitations. The first will identify a cohort of 8-12 Primary PIs, spanning the fields of bone, muscle, neurovestibular, and immune biology. After appropriate protocols have been developed to meet the full needs of this primary team, a second Biospecimen

Sharing Program (BSP) solicitation will be released to identify BSP PIs who can make full use of the remaining tissues.

Appendix B

MIT Animal Care and Use Committee Protocol

MASSACHUSETTS INSTITUTE OF TECHNOLOGY
COMMITTEE ON ANIMAL CARE
BLDG. 16-408
CAMBRIDGE, MA 02139
Phone 617.253-9436/Fax 617 258-8257

NOTICE OF COMMITTEE REVIEW

Approval Date:	12 February 2007
Protocol #:	0906-104-09
Protocol Title:	Skeletal Responses to Partial Weightbearing in Mice
Principal Investigator:	Dava Newman
Department:	AA
Funding Agency:	No changes
Grant #:	No changes

___x___ Expedited Addendum: Add 97 mice

The above-named proposal will be listed on the minutes of the 1 March 2007 meeting of the Committee on Animal Care as an expedited review. This is to inform you of the following:

__X__ Approval with the provisions below

The PI is responsible for assurance that study personnel:

1. Understand CAC policy on all aspects of animal experimentation described within the protocol.
2. Identify animals with contact information and the correct CAC protocol number at the room, rack, and cage level.
3. Will submit any changes in experimental methods for CAC review prior to implementation.
4. Route all animal purchases or gift requests through the DCM Animal Purchasing officer.

***If this protocol addendum involves the use of radioactive, chemical or biological hazards in animals, work cannot begin until:**

1. **PI has received and signed a completed "Required Protection/Control" form generated by DCM and EHS/WIBR.**
2. **Study personnel have discussed the study with and been oriented by the DCM Hazards Coordinator (Dr. Mary Patterson) or designee.**

The following additional provisions and/or suggestions have been made by the CAC:

This institution has an Animal Welfare Assurance on file with the Office for Laboratory Animal Welfare. The Assurance number is A-3125-01.

Chair, CAC

Director, Office of Sponsored Programs/Grants Management

Investigator:						previous number:			
date rec'd:			date apprv'd:			CAC:	I	Ib	II
biohaz.	radio.	surg.	radionuc.	nuc.	other:	USDA:		C	D

Application/Protocol for the Use of Animals at MIT and the Whitehead Institute

Note: This form is used for the Initial Protocol Application as well as for the 3 year renewal.

Instructions

1. Please complete this form using Word. When possible, use simple terms that will be clear to reviewers without a scientific background.
2. Please do **not** substitute reprints or attach copies of other printed materials in lieu of explanation in each section.
3. Answer all questions in Sections 1 through 10 or indicate "N/A" where not applicable. Complete appropriate details for specific procedures in The Supplement. Discard Supplement pages not relevant to your project before you submit protocol to the CAC.
4. Refer to the CAC website or the Laboratory Animal User's Handbook (produced by DCM) or CAC guidelines on general procedures, drug doses, acceptable methods of euthanasia, etc.

Renewal Info.

Original three year protocol number:	> N/A
Date of original CAC approval:	> N/A
Your application for the use of animals at MIT and the Whitehead Institute was originally approved by the CAC on the date above and is now due for three-year renewal. Do you wish to renew? **yes or no**	> N/A

If **no**, please fill out Sections 1. A., 1. D., and 10. and return this form to the CAC so we can terminate your protocol.

If **yes**, complete each section. Please review your original protocol or the last annual renewal and any addenda submitted to the CAC so that you will be sure to include any changes since then. Please discard any Supplement sections that are not relevant to your research.

Please Note: Animal orders will be held on protocols that are overdue for renewal

Section 1
General Information

Principal Investigator: Professor Dava Newman

Department: Aeronautics & Astronautics

Contact person for this protocol: Erika Brown Wagner

Address, office extension, lab extension, fax number, home phone number and e-mail address:

MIT Room 37-219
77 Massachusetts Avenue
Cambridge, MA 02139
(617) 258-9730 (office)
(617) 258-8111 (fax)
(617) 251-6714 (home)
erika@mit.edu

Title of protocol: Skeletal Responses to Partial Weightbearing in Mice

Will any aspect of the experimental study (course) or animal husbandry be conducted at another institution? **yes or no**	> no
If **yes**, where?	
Was the proposal approved by the IACUC of that institution? **yes or no**	>

If **yes**, please attach the IACUC approval notification (or most recent approval letter on annual renewals) from the other institution

Section 2
Funding Information

Funding agency : NASA	Grant Number: NRA-03-OBPR-03

If verification of approval by the MIT Office of Sponsored Programs is required, indicate address of contact person at granting agency: David R. Liskowsky, Ph.D

Full street address, city, state, zip code:
Fundamental Space Biology Division
Mail Code UF
NASA Headquarters
Washington, DC 20546-0001

Date grant submitted:	> July 15, 2003
Is this a grant renewal? **yes or no**	> No
Date grant begins	> January 1, 2004
Date grant ends	> December 31, 2006
Does the information in this form agree with the animal use section of the grant application? **yes or no.** If no, explain.	> Yes
Has this research been subject to peer review? **yes or no**	> Yes
If **yes**, by what authority?	Dr. Emily Holton NASA Ames Research Center

If **no**, please attach Department Head's letter of approval documenting review of the protocol and confirming the scientific merit of this research proposal.
A peer review letter from the Department Head should be updated every three years.

(If the PI is the Department Head, please provide approval from a knowledgeable person outside the Department.)

Section 3
Purpose/Justification of Research or Teaching Proposal

Write a brief description of the specific aims of your research justifying scientific merit and the need to use animals (use lay terms):

After more than three decades of space life sciences research, the domain of partial gravity physiology remains almost wholly unexplored. Yet, in preparing for human missions to the surface of Mars, understanding the continuum of gravitational biology, and examining lower intensity artificial gravity as a countermeasure to microgravity deconditioning, understanding the effects of loading environments between microgravity and 1-g is essential.

The adaptive physiological processes in response to such reduced loads are expected to resemble some scaled version of those seen in microgravity spaceflight conditions. The dramatic and enduring responses of the musculoskeletal system make it a particularly critical focus for research. Thus the following objectives center on meeting this need:

1) Develop and validate a system capable of supporting mice in a variety of partial weight-bearing environments to elucidate the effects of such loading on bone mineral metabolism, morphology and strength.

2) Characterize in depth the spatial and temporal musculoskeletal effects of 1 to 35 days of Mars-analog weight-bearing.

3) Examine the effects of partial weight-bearing on the time course of readaptation to normal physiologic loads.

These experiments leverage techniques from biochemistry, histology, histomorphometry, and biomechanics to provide a detailed portrait of the adaptive process at both cellular and structural levels.

This research effort will provide insights to fundamental gravitational biology, as well as to countermeasure development. It will produce targeted data for design of future experiments aboard the International Space Station Centrifuge Accommodation Module (CAM), and the ground model will serve as a novel control for musculoskeletal work aboard both the CAM and free-flying biosatellites.

Which of the following best describes the proposed work (please check all which apply):

> causes more than momentary unrelieved pain

>√ requires survival surgery

> requires withholding food/water for training

> requires a method of euthanasia that must be scientifically justified (e.g. cervical dislocation or decapitation)

>√ requires prolonged physical restraint

> requires a single, non-survival procedure

> none of the above

Section 4
Search for Alternatives

Investigators are required to annually conduct a literature search to document their consideration of alternative models and methods. A well designed literature search strategy should justify the choice of animal model and the methods selected to minimize pain and distress. The Animal Welfare Information Center of the National Agricultural Library http://www.nal.usda.gov/awic offers assistance and database search services for alternative models and methods. Most procedures can easily be identified as likely to cause pain and stress such as surgery, despite use of general anesthesia, and post operative recovery, despite use of analgesics. The potential for other procedures to cause pain and distress may not be as obvious but could be reasonably expected to be painful or stressful, such as water or food deprivation, prolonged physical restraint, adjuvant injections, tumor models, infectious disease models, and toxicology models. CAC approved euthanasia methods, routine handling and injections other than adjuvants are not considered to cause pain or distress.

Name of database(s) searched > PubMed / MEDLINE

Date of last literature search > June 2003

Years covered by search > 1966-2003

List the keywords used in the search. Keywords should be selected on their potential to identify published work that is similar to that proposed and the availability or lack of alternative models (lower species, non-animal systems). Keywords should include procedures likely to cause pain and distress (tumors, craniotomy, vascular cut down, adjuvant use, water or food deprivation for training motivation etc) and methods that will minimize pain and distress (anesthesia, analgesia, use of humane endpoints for euthanasia such as body condition scoring).

- mice
- bone
- skeletal
- hindlimb unloading
- suspension
- tetracycline
- BALB/c
- female
- spaceflight
- partial gravity
- restraint
- strain gauge
- pair feeding

Conclusions from Search for Alternatives. Please justify the choice of animal model as the best model available to address the scientific hypothesis. Explain why a lower species (phylogenetically) or non-animal system would not be suitable.

The animal model chosen for the proposed study is that planned for use in the Mars Gravity Biosatellite mission, toward which this research is targeted. Because the mission aims to contribute to understanding of systemic human adaptations to reduced gravity, a mammalian animal model is required. While human and primate studies are prohibitively mass intensive and expensive for the Mars Gravity program, rodent models provide a reasonable alternative for studying mammalian physiology and allow for extensive post-mortem tissue analysis.

Aboard Apollo, Skylab, Space Shuttle, and the Cosmos biosatellite series, our literature reviews have catalogued over 265 experiments with rats, around 12 with mice, and only 2 with pocket mice.[44] While the extensive previous microgravity studies with rats and much larger tissue samples make *Rattus norvegicus* an ideal animal model for the mission, severe spacecraft constraints on mass budget have pushed us towards the smaller *Mus musculus*.

Additionally, the large and rapidly growing knowledge base of mouse/human genetic homology has opened up valuable tool for extrapolation to human physiology. Emerging technologies in medical imaging and genetic studies are extending laboratory capabilities with mice. Micro-Computer Tomography (m-CT) – with in vitro resolution on the order of 10 mm, and in vivo resolution around 50 mm – also enables post-flight or post-experimental microstructural evaluation of skeletal demineralization.[7,57,58]

The National Research Council Space Science Board recommended that spaceflight "rodent models should include mice, given their smaller size and the availability of genetic variants and transgenic animals. Adult animals should be used."[46] Thus far, only two flights – STS-90 and STS-108 – have flown mice, and in both cases, the cohort was comprised of growing young animals (~6-8 weeks). Slowly but surely, however, ground studies are beginning to rely more heavily on the mouse model, in a trend that we anticipate will be felt on board the Shuttle and ISS in the future, and we have focused our research accordingly.

One comprehensive tail suspension study is the cross-strain comparison by Judex et al.[25] Compared with age-matched controls, 16-week old BALB/cByJ mice undergoing 3 weeks of tail suspension showed significant suppression of bone formation, leading to a highly significant reduction in trabecular bone volume. The effect sizes seen in BALB mice were significantly larger than seen in either the B6 or C3H mice also under study, allowing for more powerful statistical analyses. Additionally, BALB/c and BALB/c-derived mice are among the most commonly used inbred research strains, making them a valuable data source for the broader science community and subject to minimal intra-species variability.[70] While there is no indication of gender differences in response to suspension of young, growing BALB/cJ mice [68] a number of laboratories have indicated that females better withstand the stresses of suspension. In keeping with the extensive analysis by Judex et al.[25] that showed that 16-week old BALB/cByJ mice undergoing suspension showed significant suppression of bone formation rates, we have selected a cohort of 16-week old, virgin BALB/cByJ females (Jackson Laboratories, Bar Harbor, ME) for this proposed research effort.

Explain how use of the proposed animal model will add to work previously reported.

The novelty of this experiment is the use of a passive partial weight-bearing platform. One other lab has used a more complex system with full hindlimb unloading and partial forelimb unloading in growing rats.[6] Our system will allow for the first in-depth characterization of the temporal and spatial adaptation due to partial weight-bearing in mice and will provide a new perspective on the incremental role of gravity in musculoskeletal adaptation, helping to tailor designs for future flight research and providing ground controls for such work.

Please list proposed methods to minimize pain and distress. Include drug names and doses for anesthetics. For analgesics, include drug names, doses and when they will be given. If drugs can not be used for scientific reasons, provide rationale. For models associated with debilitation (tumor induction, infections, significant inflammation etc), provide objective criteria for humane endpoints that will result in euthanasia.

No explicit measures for pain or distress reduction are planned during periods of suspension, since analgesia or anesthesia is unnecessary and would interfere with the musculoskeletal loading patterns experienced by the animal.

For strain gauge implementation, PIXImus densitometry, and periorbital blood collection, animals will be given a pre-surgical aspirin analgesia (25 mg/kg i.p.) and anesthetized with using a mixture of ketamine (120 mg/kg) and xylazine (10 mg/kg), injected intraperitoneally in saline dilution.

For fitting of the spandex "jackets", animals will be lightly anesthetized with pentobarbital sodium (40 mg/kg i.p.). Gauze padding may be used to help animals adapt to load-bearing points on the jackets.

Endpoint criteria are described in detail below.

Section 5
Rationale for Species and Numbers

Animal species to be used (indicate strain when appropriate):

Animal Species A: > BALB/cByJ mice (*Mus musculus*)
Animal Species B: >
Animal Species C: >
Animal Species D: >

Estimate required number of **each** species to purchase:

first year	> 72
second year	> 186
Third year	> 90
Total	**> 348**

Estimate number of **each** species bred in-house:

first year	> 0
second year	> 0
Third year	> 0
Total	**> 0**

Estimate required number of **each** species to house at MIT or the Whitehead Institute (please circle) from purchasing and breeding:

first year	> 72
second year	> 186
Third year	> 90
Total	**> 348**

Anticipated sex ratio for primates:

Note: Purchasing female primates allows for higher success in social housing. Investigators are encouraged to purchase primates in established pairs. (Used to estimate risks associated with Q fever)

> % female
> % male

Anticipated sex ratio for sheep:

> % female
> % male

Appropriateness of the species: Please specify why **each** species was chosen.

Only one species is planned for use in this protocol. For justification, please see Section 4: Search for Alternatives.

Appropriateness of the numbers: Please specify study groups and size of each group for each species. Group sizes range from 8 to 15 animals, depending on the goals and nature of the specific aim.

Study Name	# of Groups	Max. Exp't. Duration	Total # of Animals in Group
Aim 1a	4	15 wks	8
Aim 1b	2	14 d	16
Aim 1c	6	14 d	48
Aim 2a	12	42 d	96
Aim 2b	6	42 d	90
Aim 3a	6	28 d	90

Have statistical analyses been applied to determine the least number of animals required? Explain.

Because no data yet exists on partial unloading in mice, the precise number of animals needed to achieve statistical significance for this proposal is a subject of great debate. In particular, while Aim 2a looks primarily at broad indices and trends, Aim 2b seeks to quantify differences between Mars-analog suspended and control animals and requires greater statistical power for meaningful conclusions.

Statistical power calculations using representative means and standard deviations from adult female BALB/cByJ mice [25] suggest that only 3 to 7 animals are needed to achieve a significance of α=0.05 and β=0.20 in traditional tail suspension for a variety of common metrics of skeletal adaptation. However, a linear change in the magnitude of such effects with increased weight-bearing would suggest that changes under Mars-analog loading may be only 62% as large as those seen in full unloading, while other modeling efforts within the skeletal research community suggest that they may be as low as 40% of those values.[27,60,72] This would sharply reduce the power of a given study.

Conversely, whereas full hindlimb unloading is highly sensitive to even transient reloading,[25,67] we believe that our partial loading scenario will reduce this sensitivity, and thereby further decrease inter-animal variability, strengthening our statistical power. Furthermore, recent research into the skeletal changes of adult rats undergoing hindlimb unloading suggests that reductions in bone formation are still apparent after 35 days of suspension, unlike the return to steady state observed after 14 days in younger animals.[1] Differences between suspended animals and controls for both femoral and soleus masses for were approximately 30-35% larger after 5 weeks of suspension than after 3 weeks. This data indicates that longer experiments may provide an opportunity for larger effect sizes in the musculoskeletal research domain, further strengthening the power of our longer studies, compared to the 3-week data we are using for our calculations.

Bearing this in mind, we will assume 25% smaller variances and an effect size 50% of those seen in full tail suspension as a representative baseline for Aim 2b. With these constraints and the representative Judex data[25] for representative means and standard deviations, our calculations suggest group sizes between 7 and 15 animals to achieve statistically significant results in a variety of structural and histomorphometric indices, including trabecular number and bone formation rate. Therefore, we will initially size the Aim 2b studies at 15 animals per group and will utilize data from our pilot studies and Aim 2a to refine these estimates and to derive a more appropriate final cohort size.

Has the proposed research been designed to use a larger number of animals as a means of reducing the number of procedures on each animal? No

Section 6
Investigator Qualifications

Personnel[1]
List all personnel on protocol
Indicate name, years of experience, project responsibilities, method of training[2], date of CAC orientation and type of anticipated training:

- Prof. Dava Newman, MIT
  - Animal experience: None
  - Project responsibilities: Principal Investigator
  - Date of CAC orientation: None
  - Type of anticipated training: none

- Dr. Mary Bouxsein, BIDMC Orthopedic Biomechanics Laboratory
  - Animal experience: 6 years of extensive research in musculoskeletal biomechanics (rats, mice, rabbits, and monkeys)
  - Project responsibilities: Co-Investigator
  - Date of CAC orientation: N/A
  - Type of anticipated training: none

- Erika Wagner, MIT (formerly Erika Brown)
  - Animal experience: 1 year with basic animal handling training, MIT DCM
  - Project responsibilities: graduate student responsible for animal procedures and care
  - Date of CAC orientation: 7/26/02
  - Type of anticipated training: periorbital & intracardiac bleeding, post-mortem tissue harvesting, strain gage implantation. The latter will be obtained in the lab of Prof. Stefan Judex at SUNY Stony Brook. See attached letter of invitation.

- Following acceptance of the grant, other research assistants will go through appropriate orientation and will be added to the protocol.

[1] CAC orientation of all personnel is required including students, technical staff, and principal investigators. Please call the CAC office at 253-9436 to arrange orientation, Call DCM at 253-9439 to arrange individual training, or assistance with animal handling and research techniques. An advanced degree (MS, DVM, PhD, MD) does not substitute for practical training or experience

[2] All training descriptions refer to species listed on this protocol

Section 7
General Procedures[3]

Summarize sequentially all animal procedures, time intervals between procedures, techniques and disposition of all species. Include special husbandry requirements (e.g., diet, housing), equipment to be used. Describe the end point of the experimental use of the animal, the duration of use and the final disposition.

Use lay terms when possible and reserve details for The Supplement. (Section 9)

Study Groups

This protocol is intended to cover a series of six studies, including development and validation of a new technique for supporting partial weight-bearing in adult mice, and its use in characterizing the skeletal changes induced by prolonged exposure to a Martian-analog loading environment (approximately 38% normal Earth loads), with and without reloading under normal weight-bearing conditions.

Populations for each study will consist of experimental suspension groups (SUSP) and a control group that is harnessed but fully weight-bearing (CON). All study animals will be mature virgin females between 15 and 30 weeks of age.

Objective 1: System Validation

- **Aim 1a.** Develop a Load Titration Unit to support a range of passive partial weight-bearing environments for adult mice.
- **Aim 1b.** Validate the Load Titration Unit through characterization of the surface strains induced in the ulna and tibia by 10%, 40%, and 70% weight-bearing.
- **Aim 1c.** Monitor systemic stress responses in suspended animals and controls.

Objective 2: Mars-Analog Characterization

- **Aim 2a.** Characterize in brief the time course of histological, histomorphometric and biochemical changes induced by 1, 3, 7, 14, 21 and 35 days of 40% weight-bearing. Identify critical time points and potential mechanisms to be investigated in Aim 2b.
- **Aim 2b.** Characterize in depth the structural, material, histological, histomorphometric and biochemical response to 1, 2, and 5 weeks of 40% weight-bearing, as compared with pair-fed controls.

Objective 3: Response to Reloading

- **Aim 3a.** Characterize the effects of 1, 2, or 4 week of normal weight-bearing (i.e. reloading), following 2 weeks of either 10% or 40% weight-bearing.

	2004				*2005*				*2006*			
Specific Aim	*Q1*	*Q2*	*Q3*	*Q4*	*Q1*	*Q2*	*Q3*	*Q4*	*Q1*	*Q2*	*Q3*	*Q4*
1a – System Development	■	■	■									
1b – System Validation			■									
1c – Stress Validation				■								
2a – Mars-Analog Temporal Characterization					■	■						
2b – Mars-Analog Physiological Characterization							■	■				
3a – Response to Reloading									■	■		

[3] Please refer to DCM Handbook or CAC guidelines on anesthetics and analgesics, polyclonal and monoclonal antibody production, neoplasia and ascites production, survival surgical procedures in rodents and/or in rabbits and higher mammals, maintenance of fluid homeostasis in rodents, methods of euthanasia, hazard control in the animal research facility, and select zoonoses of laboratory animals. Call the CAC office (253-9436) if you need a copy of any of these guidelines.

Study Environment

Accommodations:

Over the last two decades, various passive models of partial weight-bearing have been used in human locomotion and energetics research.[9,11,15,16,47-54] This habitats designed under this protocol will draw on the design elements developed in that field, coupling them with lessons learned over three decades of rodent suspension. They will draw on the expertise of Dr. Newman (MIT) in suspension rig design and partial gravity physiology as well as that of Dr. Bouxsein (OBL) in skeletal biology and biomechanics.

Design requirements specify that the Load Titration Unit (LTU) must:

- Support adult mice (16-36g) in hypodynamic loading for periods of up to 5 weeks;
- Be tunable to within +/- 5% of a desired hypokinetic stimulus between 10% and 80% weight-bearing;
- Provide an environment that is not significantly more stressful than controls, as measured by body mass changes, corticosteroid levels, and other markers of systemic stress;
- Support normal movement, cleaning, and feeding; and
- Allow for full recovery to facilitate reloading studies.

In order to help preserve normal gait characteristics and loading patterns, we have opted for a full-body suspension design, rather than the traditional tail suspension model used in hindlimb unloading. While back suspension with attached aluminum braces proved early on to be a stressful procedure for growing rats,[38,76] Musacchia and colleagues made repeated successful use of a fabric harness model in their studies of muscular hypokinesia and hypodynamia in growing rats.[40,41,42,69] Furthermore, adult mice do not present problems of rapid growth, which necessitate refitting harnesses throughout the experiment, and their lower body masses allow for better adaptation to suspension than in their rat counterparts.

Animals will be singly housed in specially developed Load Titration Unit habitats, derived from designs utilized at NASA Ames Research Center and Cornell University[38]. The cage is a rectangular structure constructed out of rigid plastic. The actual spring-loaded suspension mechanisms will be modeled after the MIT Partial Gravity Simulator and the Harvard suspension system,[23,48] with appropriate modifications for animal use, as shown below.

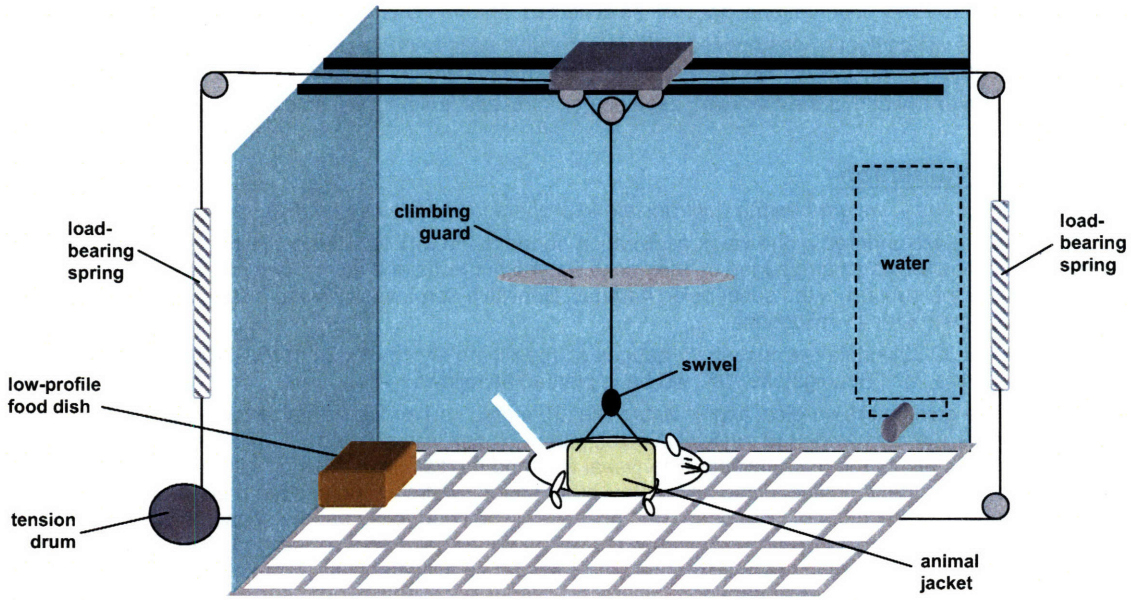

Springs and other potentially hazardous components will be located outside of the animal living space to prevent pinching or other injury. Prior to introduction into the DCM facilities, all designs will subject to review and approval by Dr. Mark Whary.

Custom spandex "jackets" (Lomir Inc., Malone, NY) will be placed on the animals and secured dorsally with Velcro. A four-point distributed load harness will join this garment to a swiveled tether, allowing for 360 degrees of rotation. The tether will be guarded by a plastic disk to prevent the mouse from climbing the line and will in turn be anchored to a line and pulley system that is free to move along a track down the center axis of the cage, as in other suspension systems. Tension will be provided by taking up slack onto a fixed drum, and passive damping of locomotor forces will be provided by a pair of load-bearing springs. Stops placed along the sides of the cage will restrict the animals from bearing weight on their habitat walls.

To maintain consistent body position and avoid the reloading opportunity provided by piles of bedding, a plastic grid floor will be used over an absorbent paper to allow for passive removal of waste products. Wooden dowels will be provided as needed as enhancements to discourage the mice from chewing through the exposed flooring grid.

The cages will be cleansed with quatricide on a weekly basis, and the bedding material below the floor will be changed at that time. New chew bars will be provided to the animals as needed to enhancements to discourage the mice from chewing on the plastic floor grating. Daily inspection of the hardware will allow for rapid replacement of components as needed.

Populations for each study will consist of experimental suspension groups (SUSP) and control groups that are harnessed but fully weight-bearing (CON). Standard laboratory chow will be made available *ad libitum* at floor level for the suspended mice. However, because many skeletal parameters of interest are highly weight-dependent and suspended animals often reduce their food intake in the early days of unloading, CON animals will be fed according to the mean daily consumption of their SUSP group. Food and water supplies will be placed near ground level to ensure easy access.

IF IT CAN BE ACCOMMODATED IN THE MIT DCM FACILITIES, local temperature will be maintained between 24.5° and 26°C to minimize the basal metabolic costs of thermoregulation for the singly housed animals.[38]

Aim 1a – System Development Pilot Studies

Throughout the hardware development process, it will be necessary to adjust the fit and function of the unit to better meet the needs of our animal population. To this end, we will utilize mice in a number of short pilot observations to ensure the safety and success of more in depth experiments later. We anticipate using no more than 8 mice over the course of these pilots. Only observational data will be collected, and no invasive procedures will be used.

As needed, animals will be lightly anesthetized with pentobarbital sodium (40 mg/kg i.p.), fitted with a spandex "jacket" (Lomir Inc., Malone, NY), and individually housed in one of the experimental habitats for up to 7d of observation.

At 30 weeks of age or the end of the hardware development process, animals will be sacrificed by CO2 euthanasia.

Aim 1b – System Validation

Hypothesis: Reductions in weight-bearing will translate to proportionally reduced peak dynamic strains.

Animals in this study will undergo a one-week acclimation period to the MIT facilities. After this period, the animals will be equipped with single-axis strain gauges on their contralateral humerus and tibia in order to characterize the loading environment under the support of the suspension harness. Sensitive non-invasive force plate platforms, as used in gait analysis may also be utilized in validation.

As described in [26,32,39] single element strain gauges of approximately 1mm x 2mm (EA-06-015LA-120, Measurements Group, Inc., Basingstoke, UK) will be implanted as follows:

The animals will be given a pre-surgical aspirin analgesia (25 mg/kg i.p.) and anesthetized with using a mixture of ketamine (120 mg/kg) and xylazine (10 mg/kg), injected intraperitoneally in saline dilution. Under aseptic conditions, the anterio-medial aspect of the metaphyseal-diaphyseal tibia and medial ulnar midshaft will be exposed with minimal musculoskeletal disruption. A scalpel blade and diethyl ether cotton swabs will be used to prepare attachment fields on the periosteal surface of each bone. Cyanoacrylate adhesive will be used to secure the sensor in place. The site will be wrapped in gauze to prevent infection and lead wires will be will be secured with "second skin" to the posterior aspect of the limb. As evidenced in the Judex lab, animals should be fully ambulatory within 2-4 h. A 2d healing period will follow to minimize animal stress and pain.

After their surgical sites have healed, all animals will be lightly anesthetized with pentobarbital sodium (40 mg/kg i.p.), fitted with a spandex "jacket" (Lomir Inc., Malone, NY), and individually housed in one of the experimental habitats for

a 5d acclimation period. Following acclimation, each of the suspension animals will be clipped onto a Load Titration Unit (LTU) tether. By positioning the LTU above a laboratory scale, adjustments will be made to provide the proper level of partial weight-bearing (initially 40% of normal). CON animals will remain harnessed but fully weight-bearing. (n=8 mice per group)

Continuous strain gauge data will be collected for 3d and stored locally to a laptop hard drive using LabView software. Once stability of the measurements is ensured, suspension animals will receive 1d each of 10%, 40%, and 70% loading, in a randomized order. This data will be analyzed to determine the principle surface strains of each loading environment.

On a daily basis, animals will be inspected for body sores, body condition, hydration level, food and water consumption, and body mass. In order to avoid undue weight-bearing, which could alter the outcome of the experiment, animals will be weighed by brief full suspension on a modified scale (final apparatus to be approved by Dr. Mark Whary of the DCM).

At the end of the trial suspension period, animals will be sacrificed by CO2 euthanasia.

Aim 1c –Stress Validation

Hypothesis: *One week of adaptation to the harness prior to unloading will provide sufficient opportunity for the animal to adjust to the housing environment, and partial suspension will not cause a significant increase in systemic stress.*

Because only the animals of Aim 1b will be subject to surgical stresses, and we are interested in obtaining information about the systemic stress response due strictly to the Load Titration Unit and harnesses, a second validation study will be run at 10%, 40%, and 70% unloading to monitor this response.

Animals will be acclimated to the MIT facilities, spandex harness, and LTU habitat as above. Following acclimation, each of the suspension animals will be clipped onto a Load Titration Unit (LTU) tether. By positioning the LTU above a laboratory scale, adjustments will be made to provide the proper level of partial weight-bearing (either 10%, 40%, or 70% of normal, n=8 mice per group). CON animals will remain harnessed but fully weight-bearing and will be pair-fed as described above.

For one week of suspension, animals will be inspected for body sores, body condition, hydration level, food and water consumption, and body mass as described above.

At the end of the trial suspension period, animals will be sacrificed by isoflurane inhalation to avoid rapid escalation of stress hormone levels. Blood will be collected by intracardiac puncture and used to measure serum cortiocosterone levels. Adrenal glands will be harvested as an additional metric of systemic stress.

Aim 2a – Mars-Analog Temporal Characterization

Hypothesis: Reductions in the dynamic loading environment will cause decrements in osteoblastic activity, resulting in a decrease in bone mass and other structural properties, so as to normalize strains within the bone. The mechanisms driving the temporal response to partial unloading will operate with similar time constants to that seen in earlier research with full hindlimb unloading, but with gains proportional to the strain magnitudes of the loading environment.

This key Aim provides a detailed temporal characterization of the musculoskeletal response to unloading. Under this Aim, staggered sacrifices will allow for characterization of the relative timelines of these resorptive and formative processes in adult mice, as indicated by histomorphometry and serum biochemistry. These results will also provide an indication of the key adaptive transitions, which will become the focus of Aim 2b.

Adult female BALB/c mice (n=8/group) will be randomly assigned to either SUSP or CON conditions for 1, 3, 7, 14, 21 or 35 day-long studies. As above, CON mice will be placed in harnesses but retain full loading. As in Aims 1b and 1c, animals will be inspected and on a daily basis.

To examine bone formation rates, tetracycline, calcein and demeclocycline labels (15 mg/kg in 100 µl saline) will be injected intraperitonially at the time of suspension, 7d prior to sacrifice, and 2d prior to sacrifice in each of the 3 longer protocols. These non-toxic, non-radioactive markers are standard to the field and are the best agents available for this purpose. No side effects or enduring discomfort are expected.

In vivo bone density measurements will be performed using peripheral dual-energy x-ray absorbtiometry (pDXA, PIXImus, GE-Lunar Corp.) at baseline and sacrifice in the 15, 25, and 35 day groups. Animals will be anesthetized prior to the procedure with an i.p. injection of ketamine (120 mg/kg) and xylazine (10 mg/kg). During the baseline measurement, a periorbital blood draw will also be collected (300 ul/mouse). Group serum will be pooled as necessary for various analyses.

At the appropriate timepoint, animals will be sacrificed by CO2 euthanasia. Blood will be collected a second time via intracardiac puncture following sacrifice for analysis of serum markers of bone turnover (osteocalcin, c-telopeptide, bone-specific alkaline phosphatase, and osteoprotegrin) and systemic stress. Gastrocnemius, soleus, and extensor digitorum longus (EDL) will be harvested and weighed to assess muscle mass. Tibias and femurs will be collected for histological and histomorphometric analysis.

Aim 2b – Full Physiological Characterization

Hypothesis: Reductions in the dynamic loading environment will cause changes predominantly in the higher (structural) levels of skeletal composition, rather than in the lower (material) levels.

Groups of 15 adult female BALB/c mice will be randomly assigned to either SUSP or CON cages for one of three experimental durations to be selected on the basis of the experiments carried out in Aim 2a (Baseline = 7, 14, and 35 days).

Health inspections, PIXImus bone density measurements, and sacrifice will follow the procedures outlined in Aim 2a. Following sacrifices, intracardiac bleeding, coupled with muscle mass, imaging, material analysis, biomechanical testing and histology, will provide an extensive musculoskeletal characterization.

Aim 3a – Reloading Characterization

Hypothesis: In accordance with mechanostat theory, the rate of skeletal recovery following reloading will be dependent upon the difference between the unloading and loading environments, such that larger changes induce greater formation rates.

This Aim will draw on the results of Year 1 and 2 studies to appropriately size cohorts and suggest optimal time increments for stepwise unloading. The SUSP groups will be unloaded for 14 days each at either 10% or 40% weight-bearing, followed by either 1, 2, or 4 weeks at full weight-bearing.

Health inspections, PIXImus bone density measurements, tetracycline injections and and sacrifice will follow the procedures outlined in Aim 2a. Periorbital blood draws (300 ul/mouse) will be made at the ends of weeks 1, 3, and 5 for analysis of serum markers of bone turnover. Following sacrifices, intracardiac bleeding, coupled with muscle mass, imaging, and histology, will provide the necessary characterization for this Aim.

Health Evaluation & Endpoints

Previous research suggests that our experimental environment will create no serious health problems for SUSP animals. Over 800 tail suspension experiments are currently in publication, and there is great support for that model for hindlimb unloading.[38] Experiments of 3-5 weeks are not uncommon, and the model has been used for studies longer than 2 months. Musacchia and colleagues published numerous papers utilizing harness suspension more similar to our model, again, with no serious health concerns.[40,41,42,69] The harnesses we will be using are commercial lab materials with extensive research heritage. Strain gauges used in Aim 1c have been used in previous mouse studies, [26,32,39] and Dr. Stefan Judex at SUNY Stony Brook, who has extensive experience in such work, will train the researchers for this portion of the protocol. (See attached letter)

The novelty of this experiment is the partial weight-bearing scenario, and we believe that this loading paradigm will actually pose even less stress for the mice. They will maintain at least partial loading on all four limbs and should be able to maintain nearly normal use of their habitat environment, rather than locomoting only with their forelimbs. As adaptation is typically rapid and readily apparent, animals not demonstrating reasonable adaptation to the system within 4 four days of suspension will be excluded from the study and euthanized.

The primary indicator of animal health will be body mass, and food and water consumption, each monitored daily. In traditional hindlimb unloading studies, the onset of suspension prompts a substantial temporary weight loss (in the range of 10-15%);[2,38] around one week after suspension, however, weight gain returns to control levels. Moreover, stress parameters and mass-adjusted food intake are restored to normal levels in the same time frame upon return to full weight-bearing.

The proposed studies will allow for temporary adult weight losses of up to 15% during the first few days of suspension without termination; body weights during this period will be reported twice weekly to DCM veterinary staff. We do not, however, expect to see substantial prolonged weight loss, as rodents exposed to full hindlimb suspension have not shown such changes in prior studies. Adult body weights below initial values observed after the first 5 days of suspension will be reported to DCM veterinary staff for consideration.

Control animals that are being pair-fed to match their suspended counterparts will also be subject to some weight loss due to these dietary restrictions. Again, the proposed studies will allow for temporary adult weight losses of up to 15% during the first few days without termination; body weights during this period will be reported twice weekly to DCM veterinary staff. Adult body weights below initial values observed after the first 5 days of suspension will be reported to DCM veterinary staff for consideration.

Daily visual inspections will monitor adult animals for abnormal appearance or posture; extreme, persistent lethargy; vocalization; and piloerection. Any of these conditions will be reported to DCM veterinary staff for evaluation. Animals deemed to be in poor condition will be euthanized.

Dehydration will be carefully monitored, particularly in the first 48 hours of suspension. Animals exhibiting signs of dehydration (recessed eyes, skin elasticity) will be offered moist chow or feeding by dropper. If the situation persists, DCM veterinary staff will be contacted for decisions regarding euthanasia. Observed conditions associated with anemia (footpad pallor), diarrhea (moist feces), or injury (skin lesions, etc.) will also be reported to veterinary staff.

During daily weighing sessions, animals will be inspected for body sores or other adverse effects of harnessing. Gauze padding and antibiotic cream will be applied to any open sores. Lesions persisting for more than 3 days will serve as an experimental endpoint for that animal.

Which of these procedures have not been performed in this laboratory before?

To our knowledge, suspension for reduction of weightbearing and strain gauge implantation in mice have not been performed in this laboratory before.

Are any of these procedures considered pilot experiments? **yes or no** > yes

If **yes**, which ones: Aim 1a

If prolonged restraint is needed, please describe method, frequency and duration of restraint: Suspension technique and device described in detail above.

If applicable, list building and room numbers within your lab where animal manipulations take place. No answer is necessary if you use procedure areas located within the animal facilities.

Is there a potential[4] for the development of pain, suffering, or morbidity? **yes or no** > yes

If **yes**, describe the expected nature of the pain, suffering, or morbidity and the procedures which may be responsible

Strain gauge implantation – potential for post-surgical discomfort, infection, failure for surgical sites to heal

Suspension – potential for harness sores, decreased food intake

Early pair feeding – potential for forced decreased food intake and weight loss

Describe criteria for appropriate intervention

Detailed above

Frequency and duration of observations:

Daily health inspections will be conducted, comprised of direct observations, body weight measurements, and quantification of food and water consumption. It is anticipated that this process will take approximately 5-10 minutes per animal.

Methods of analgesia to prevent or relieve pain and suffering (pharmacological methods including agents, dosage, frequency of administration, and nonpharmacologic methods, e.g., cage padding, bandaging, application of cold, etc.):

For strain gauge implementation, PIXImus densitometry, and periorbital blood collection, animals will be given a pre-surgical aspirin analgesia (25 mg/kg i.p.) and anesthetized with using a mixture of ketamine (120 mg/kg) and xylazine (10 mg/kg), injected intraperitoneally in saline dilution.

For fitting of the spandex "jackets", animals will be lightly anesthetized with pentobarbital sodium (40 mg/kg i.p.). Gauze padding may be used to help animals adapt to load-bearing points on the jackets.

[4] All procedures such as surgery, ascites production, tumor induction, transgenic experiments, injections of adjuvant, prolonged restraint, etc. have inherent risk of medical problems

What is the duration of survival?

Total duration of survival is equal to the sum of the acclimation period and the suspension period, plus reloading periods in Aim 3a, totaling between 8 and 42 days. Animals used in the Aim 1a pilot studies may be kept for up to 15 weeks, but will only undergo experiments less than 7 days in length.

What is/are the method(s) of euthanasia for each species?
Please provide specific agents and doses as appropriate.

In all experiments except Aim 1b, animals will be euthanized via carbon dioxide immersion, using standard laboratory facilities. In Aim 1b, to avoid the rapid escalation of stress hormones often seen with CO2 euthanasia, isoflurane inhalation will be utilized.

Cervical dislocation or decapitation without anesthesia as the methods of euthanasia are not approved without scientific justification. If appropriate, please justify.

Are you using toe clips, ear tags, tattoos or ear punches for animal identification? **yes or no** > no

If **yes**, please indicate which method you are using and specify:
age of animal at time of procedure, species of animal, type of anesthesia

Section 8
Hazards Affecting Animals, Personnel & the Environment

Are rodent or human cells or cell lines to be used in animals? **yes or no** > no

If yes, complete Supplement D and attach

Are radionuclides to be used? **yes or no** no

If **yes**, indicate name of isotope(s), RPO protocol number and complete and attach appropriate Supplement (A –I) that best describes isotope use in animals:

Are hazardous chemical and/or microbial agents to be used? **yes or no** > no

If **yes**, indicate name of agent(s), complete and attach Supplement B:

If any of the above uses pose any risk (or if you are uncertain of the risk) if humans come in contact with the animals, their tissues or their caging and waste (bedding), complete an Application to Use Hazardous Materials (Supplement I) and send to DCM, Bldg. 16-829 independently of this application to the CAC.

Fill in date sent:

Recombinant DNA

Are transgenic/knock-out animals used or produced in the experiment? **yes or no** > no

If **yes**, fill out the Transgenic/Knock-Out Animals Supplement F in this protocol

Does material being injected into the animal contain recombinant RNA or DNA? **yes or no** > no

If **yes** to either of the above, obtain approval from the Biosafety Office, tel. (617)253-1740 and supply Recombinant DNA protocol number

If safety of animals and/or personnel may be compromised, is this reflected in your Departmental Safety Plan? **yes or no** > N/A

If **no**, contact the Biosafety Office, tel. 253-1740.

For users of materials/substances potentially hazardous to human health: have new personnel been educated about potential health risks associated with radiation, biologics, or chemicals? **yes or no** > N/A

If **no**, contact the appropriate office for training:
- **Radiation Hazards**: Radiation Protection Committee and Office, Bldg.16-268, tel. 253-2180
- **Biologics Hazards**: Biosafety Office, tel. 253-1740, Bldg. 56-255
- **Chemical Hazards**: Industrial Hygiene Office, tel. 253-2596, Bldg. 56-253
- **Zoonotic risks**: Division of Comparative Medicine, Bldg. 16-825A, tel. 253-9435.

Occupational Health Assessment: <u>All personnel</u> on this protocol with **<u>any animal contact</u>** are required to have an occupational health questionnaire evaluated by an EMS physician or nurse.

Questionnaires can be submitted either: 1) **electronically** on the CAC Website: http://tute.mit.edu:8001/comp-med/restrict/cac/forms.htm 2) on **paper** by filling out a printed version obtained from the CAC website or the administrative office then sent directly to: MIT Medical Employee and Occupational Health Office (EOHS: E23-180), or 3) in **person** by scheduling an appointment with a clinician in the EOHS (Jackie Sherry RN, CS, 617.253.8552: E23-180).

Has everyone that is listed on this protocol submitted a health questionnaire? **no**
yes or no If no, provide explanation.

Only Erika Wagner who will be working with the animals has submitted the questionnaire (name at time of submission was Erika Brown). Other research assistants will go through appropriate orientation and will be added to the protocol following acceptance of the grant.

Are there any occupational health issues that have developed for any protocol participant since a questionnaire was first submitted? **yes or no_ no**

If yes, have these health issues been evaluated by EMS? **yes or no**

For personnel in contact with non-human primates, list the name of each protocol participant along with the date of the most recent TB screen by MIT Medical (must be current within 1 year). Protocol approval and renewal are contingent on strict compliance by all participants – "pending" is not satisfactory. >

Information about safety and health measures such as immunizations and protection against explosion and fire is available through DCM, EMS, the Safety Office, and the Medical Department.

Section 9
List of Supplemental Forms

Supplements must be completed for the following procedures, see supplement to complete details of procedures. Select appropriate sections from the following and indicate your selection:

> √ A. Surgical Procedures, including Survival Tissue Harvest
> B. Immunization and Antibody Harvest, including Hybridoma
> C. Chemical, Microbial, Physical Agent Administration
> D. Use of Rodent or Human Cells or Cell Lines (Other Than Hybridoma)
> √ E. Device Implantation
> F. Transgenic/Knock-Out Animals
> G. Behavioral Training Techniques
> H. Teaching Proposal
> I. Application to Use Hazardous Materials in Vivo

Section 10
Signatures

Person preparing this form date

Principal Investigator date

Please allow 4 weeks for the processing of this protocol

The Committee on Animal Care meets on the first Thursday of every month (except August and December). Protocols should be submitted at least two weeks before a CAC Meeting.

Please Note: A substantial change in protocol, an increase in the number of animals used, a change in the animal species used, or a change of personnel will necessitate an addendum to or re-submission of this form. The principal investigator must sign approval for such changes before they will be reviewed by the committee.

References

1. Allen MR, Bloomfield SA. Hindlimb unloading has a greater effect on cortical compared with cancellous bone in mature female rats. J Appl Physiol. 2003 Feb; 94(2): 642-50.
2. Amblard D, Lafage-Proust MH, Laib A, Thomas T, Ruegsegger P, Alexandre C, Vico L. Tail suspension induces bone loss in skeletally mature mice in the C57BL/6J strain but not in the C3H/HeJ strain.J Bone Miner Res. 2003 Mar;18(3):561-9..
3. Beamer WG, Donahue LR, Rosen CJ, Baylink DJ. Genetic variability in adult bone density among inbred strains of mice. Bone. 1996 May; 18(5): 397-403.
4. Bloomfield SA, Allen MR, Hogan HA, Delp MD. Site- and compartment-specific changes in bone with hindlimb unloading in mature adult rats. Bone. 2002 Jul; 31(1): 149-57.
5. Colleran PN, Wilkerson MK, Bloomfield SA, Suva LJ, Turner RT, Delp MD. Alterations in skeletal perfusion with simulated microgravity: a possible mechanism for bone remodeling. J Appl Physiol 2000 Sep; 89(3): 1046-54.
6. Daphtary M, Schultheis L, Lee JJ, Rastogi S, Ruff CB. Effects Of Dynamic Loading On Bone Structural Properties Under Conditions Of 50% Weight-bearing. Poster Presented at the Biomedical Engineering Society Conference, Durham, NC, 4-7 Oct 2001.
7. David VN, et al. Longitudinal Survey of Trabecular Bone Architecture Deterioration in the Hindlimb Unloaded Female Rat Model Using 3D Micro-Computed Tomography. 2001 ASBMR Conference, Presentation F165.
8. Dehority W, Halloran BP, Bikle DD, Curren T, Kostenuik PJ, Wronski TJ, Shen Y, Rabkin B, Bouraoui A, Morey-Holton E. Bone and hormonal changes induced by skeletal unloading in the mature male rat. Am J Physiol 1999 Jan; 276(1 Pt 1): E62-9.
9. Duddy JH. The simulation of weightlessness using water immersion techniques: an annotated bibliography. Hum. Factors. 1969; 11: 507-40.
10. Farley CT and Macmahon TA. Energetics of walking and running: insights from simulated reduced-gravity experiments. Journal of Applied Physiology. 1992; 73, 2709-2712.
11. Flynn TW, Canavan PK, Cavanagh PR, and Chiang JH. Plantar pressure reduction in an incremental weight-bearing system. Phys Ther. 1997; 77: 410-416.
12. Fosse G. The radiodensity of skeletal parts in animals growing and living in a constant artificially increased gravitational field. Growth. 1971 Mar; 35(1): 33-53.
13. Giangregorio L, Blimkie CJ. Skeletal adaptations to alterations in weight-bearing activity: a comparison of models of disuse osteoporosis. Sports Med. 2002; 32(7): 459-76.
14. Globus RK, Bilke DD, Morey-Holton E. The Temporal Response of Bone to Unloading. Endocrinology. 1986; 114: 2264-2270.
15. Griffin TM, Tolani NA, and Kram R. Walking in simulated reduced gravity: mechanical energy fluctuations and exchange. J Appl Physiol. 1999; 86: 383-390.
16. He JP, Kram R, and McMahon TA. Mechanics of running under simulated low gravity. Journal of Applied Physiology. 1991; 71, 863-870.

17. Hellmich Ch, Ulm FJ. Are mineralized tissues open crystal foams reinforced by crosslinked collagen? Some energy arguments. J Biomech. 2002 Sep; 35(9): 1199-1212.
18. Hemmersbach R, Voormanns R, Hader DP. Graviresponses in Paramecium biaurelia under different accelerations: studies on the ground and in space. J Exp Biol. 1996, Oct; 199(10): 2199-205.
19. Hewes DE. Reduced-gravity simulators for studies of man's mobility in space and on the moon. Hum. Factors. 1969; 11: 419-32.
20. Hoffman SJ, Kaplan DI, Eds. Human Exploration of Mars: The Reference Mission of the NASA Mars Exploration Study Team. NASA Special Publication 6107. 1997.
21. Holick MF. Perspective on the impact of weightlessness on calcium and bone metabolism. Bone. 1998 May; 22(5 Suppl): 105S-111S.
22. Ivanenko YP, Grasso R, Macellari V, Lacquaniti F. Control of foot trajectory in human locomotion: role of ground contact forces in simulated reduced gravity. J Neurophysiol. 2002 Jun; 87(6): 3070-89.
23. Jackson DK, Newman DJ. Adaptive effects of spaceflight as revealed by short-term partial weight suspension. Aviat Space Environ Med. 2000 Sep;71(9 Suppl):A151-60.
24. Johnston RS, Dietlein LF, and Berry CA. Biomedical Results of Apollo (SP-368), National Aeronautics and Space Administration, Lyndon B. Johnson Space Center, Houston, Texas, 1975.
25. Judex S, Donahue LR, Rubin C. Genetic predisposition to low bone mass is paralleled by an enhanced sensitivity to signals anabolic to the skeleton. FASEB J. 2002 Aug; 16(10): 1280-2.
26. Judex S, Gross TS, Zernicke RF. Strain gradients correlate with sites of exercise-induced bone-forming surfaces in the adult skeleton. J Bone Miner Res. 1997 Oct;12(10):1737-45.
27. Keller TS, Strauss AM. Predicting skeletal adaptation in altered gravity environments. J Br Interplanet Soc. 1993 Mar; 46(3): 87-96.
28. Kiss JZ, Edelmann RE. Spaceflight experiments with Arabidopsis starch-deficient mutants support a statolith-based model for graviperception. Adv Space Res. 1999; 24(6): 755-62.
29. Laurinavicius R, Svegzdiene D, Gaina V. Force sensitivity of plant gravisensing. Adv Space Res. 2001; 27(5): 899-906.
30. LeBlanc A, Schneider V, Shackelford LL, West S, Oganov V, Bakulin A, Voronin L. Bone mineral and lean tissue loss after long duration spaceflight. J Bone Miner Res. 1996; 11: S323.
31. Leblanc A, Shackelford L, Schneider V. Future Human Bone Research in Space. Bone. 1998 May; 22(5 Suppl):113S–116S.
32. Lee KC, Maxwell A, Lanyon LE. Validation of a technique for studying functional adaptation of the mouse ulna in response to mechanical loading. Bone. 2002 Sep; 31(3): 407-12.
33. Li XJ, Jee WS, Chow SY, Woodbury DM. Adaptation of cancellous bone to aging and immobilization in the rat: a single photon absorptiometry and histomorphometry study. Anat. Rec. 1990; 227: 12–24.
34. Looker AC. Updated data on proximal femur bone mineral levels of US adults. Osteoporos Int. 1998; 8: 468-89.
35. Lyndon B. Johnson Space Center. Spacelab Life Sciences 1: First Space Laboratory Dedicated to Life Sciences Research. National Aeronautics and Space Administration NP 120, August 1989.
36. Margaria R, Cavagna GA. Human locomotion in subgravity. Aerosp. Med. 1964; 35: 1141.
37. Morey ER. Spaceflight and bone turnover: Correlation of a new rat model of weightlessness. Bioscience. 1979; 29: 168-72.
38. Morey-Holton ER, Globus RK. Invited review: Hindlimb unloading rodent model: technical aspects. J Appl Physiol. 2002; 92: 1367–1377.
39. Mosley JR, March BM, Lynch J, Lanyon LE. Strain magnitude related changes in whole bone architecture in growing rats. Bone. 1997 Mar; 20(3): 191-8.
40. Musacchia XJ, Deavers DR. A new rat model for studies of hypokinesia and antiorthostasis. Physiologist. 1980 Dec;23(Suppl 6):S91-2.
41. Musacchia XJ. An assessment of suspension systems: models that reproduce responses to weightlessness. Physiologist. 1992 Feb;35(1 Suppl):S92-5.
42. Musacchia XJ, Steffen JM, Fell RD, Dombrowski MJ. Skeletal muscle response to spaceflight, whole body suspension, and recovery in rats. J Appl Physiol. 1990 Dec; 69(6):2248-53.
43. NASA Critical Path Roadmap (BCPR) Baseline Document: A Risk Reduction and Management Approach for Human Space Flight, Revision D. April 2003. < http://criticalpath.jsc.nasa.gov/>. [July 10, 2003].
44. NASA Life Sciences Data Archive. Last Updated: Oct. 20, 2000. <http://lsda.jsc.nasa.gov/>. [Sept. 7, 2001- Feb. 22, 2002].
45. NASA Strategic Plan. Last Updated: February 2003. <http://www.plans.nasa.gov>. [July 10, 2003].
46. National Research Council, Space Science Board. A Strategy for Research in Space Biology and Medicine in the New Century. Washington, D.C.: National Academy Press, 1998, 276 pp. <http://www.nationalacademies.org/ssb/csbmmenu.htm>. [July 1, 2003].
47. Newman DJ, A Submersible Partial Gravity Simulator for Lunar and Martian Locomotion, International Design for Extreme Environments Assembly (IDEEA), Houston, TX, November 1991.

48. Newman DJ. Human locomotion and energetics in simulated partial gravity. Massachusetts Institute of Technology. Department of Aeronautics and Astronautics. Doctoral dissertation, 1992.
49. Newman DJ, Biodynamics Modeling of Human Movement, World Congress on Computational Medicine, Public Health, and Biotechnology, Women in Mathematical Modeling: A Showcase, Austin, TX, April 1994.
50. Newman DJ, Modeling Reduced Gravity Human Locomotion, Advances in Mathematical Modeling of Biological Processes, D. Kirschner, ed., International Journal of Applied Science and Computation, June 1996; 3(1): 91-101.
51. Newman DJ, Life in Extreme Environments: How Will Humans Perform on Mars? ASGSB Gravitational and Space Biology Bulletin, June 2000; 13(2): 35-47.
52. Newman DJ and HL Alexander, Human Locomotion and Workload for Simulated Lunar and Martian Environments, Acta Astronautica, 1993; 29(8): 613-620.
53. Newman DJ, Alexander HL, and Webbon BW. Energetics and mechanics for partial gravity locomotion. Aviation, Space and Environmental Medicine. 1994; 65, 815-823.
54. Newman DJ, Jackson DK and JJ Bloomberg, Altered Astronaut Lower-Limb and Mass Center Kinematics in Downward Jumping Following Space Flight, Exp Brain Res, 1997; 117: 30-42.
55. Newman DJ, Schultz KU and JL Rochlis, Closed Loop, Estimator Based Model of Human Posture Following Reduced Gravity Exposure, AIAA Journal of Guidance, Control, and Dynamics, 1996; 19(5): 1102-1108.
56. Oganov VS, Grigoriev AI, Voronin LI, Rakmanov AS, Bakulin AV, Schneider VS, LeBlanc A. Bone mineral density in cosmonauts after 4.5–6 month long flights aboard orbital station Mir. Aerospace Environ Med. 1992; 26: 20 –24.
57. Paulus MJ. Small Animal microCT Instrumentation for Evaluation of Bone Density Loss in a Microgravity Environment. White Paper, The Oak Ridge National Laboratory. October 26, 2000.
58. Paulus MJ, Gleason SS, Easterly ME. A review of high-resolution X-ray computed tomography and other imaging modalities for small animal research. Lab Anim (NY). 2001 Mar; 30(3): 36-45.
59. Pavy-Le Traon A, et al. Cardiovascular and hormonal changes induced by a simulation of a lunar mission. Aviat Space Environ Med. 1997 Sep; 68(9 Pt 1): 829-37.
60. Peterman MM, Hamel AJ, Cavanagh PR, Piazza SJ, Sharkey NA. In vitro modeling of human tibial strains during exercise in micro-gravity. J Biomech. 2001 May; 34(5): 693-8.
61. Rambaut PC, Johnston RS. Prolonged weightlessness and calcium loss in man. Acta Astronaut. 1979; 6:1113–1122.
62. Rambaut PC, Leach CS, Johnson PC. Calcium and phosphorus change of the Apollo 17 crew members. Nutr Metab. 1975; 18(2): 62-9.
63. Roberts JF. Walking responses under lunar and low-gravity conditions. AMRL-TDR-63-112. Aerospace Medical Research Laboratory. Wright-Patterson AFB. Ohio. 1963.
64. Robling AG, Duijvelaar KM, Geevers JV, Ohashi N, and Turner CH. Modulation of Appositional and Longitudinal Bone Growth in the Rat Ulna by Applied Static and Dynamic Force. Bone. 29 (2) August 2001:105–113
65. Ruff CB, Beck TJ, Newman DJ, Oden ZM, Schaffner G, LeBlanc A, Shackelford L and N Rianon, Skeletal Structural Consequences of Reduced Gravity Environments, Proceedings of the First Biennial Space Biomedical Investigators' Workshop, League City, TX, January 1999.
66. Seminara JL, Shavelson RJ. Lunar simulation. Hum. Factors. 1969; 11: 451-62.
67. Simske SJ, Ferguson VL, Bateman TA. Mice and Osteoporosis Research. In Press. 2003.
68. Simske SJ, Luttges MW, Allen KA, Gayles EC. The role of sex and genotype on antiorthostatic suspension effects on the mouse peripheral skeleton. Aviat Space Environ Med. 1994 Feb; 65(2): 123-33.
69. Steffen JM, Fell RD, Musacchia XJ. Physiological responses during whole body suspension of adult rats. Physiologist. 1987 Feb;30(1 Suppl):S94-5.
70. The Jackson Laboratory. Inbred Strains of Mice: BALB. Mouse Genome Informatics Web Site. Bar Harbor, Maine. <http://www.informatics.jax.org>. [July 8 2003].
71. Turner CH, Forwood MR, Otter MW. Mechanotransduction in bone: do bone cells act as sensors of fluid flow? FASEB J. 1994 Aug; 8(11): 875-8.
72. Turner CH. Three rules for bone adaptation to mechanical stimuli. Bone. 1998 Nov; 23(5): 399-407.
73. Turner RT. Invited review: what do we know about the effects of spaceflight on bone? J Appl Physiol. 2000 Aug; 89(2): 840-7.
74. Vico L, Lafage-Proust MH, Alexandre C. Effects of gravitational changes on the bone system in vitro and in vivo. Bone. 1998 May; 22(5 Suppl): 95S-100S.
75. Whole Genome Homology Map: human on mouse background. Mouse Genome Informatics Web Site, The Jackson Laboratory, Bar Harbor, Maine. <http://www.informatics.jax.org>. [Feb. 23, 2002].
76. Wronski TJ, Morey-Holton ER. Skeletal response to simulated weightlessness: a comparison of suspension techniques. Aviat Space Environ Med. 1987 Jan; 58(1):63-8.
77. Zerath E. Effects of microgravity on bone and calcium homeostasis. Adv Space Res. 1998; 21(8-9): 1049-58.

Surgical Procedures

Details of Surgery

Describe details of surgery including preparation of animal such as fasting (if applicable), surgical approach, intraoperative manipulations, and methods of closure (type of suture or wound clip to close each tissue layer as applicable - muscle wall, subcutaneous tissue and skin). If multiple surgeries on individual animals are part of the experimental design describe each procedure and the time interval between procedures.

Under aseptic conditions, the anterio-medial aspect of the metaphyseal-diaphyseal tibia and/or medial ulnar midshaft will be exposed with minimal musculoskeletal disruption. A scalpel blade will be used to remove residual tissues and periosteal surface to prepare for gage seating. A cotton swab dipped in <0.5 ml of chloroform will be used to cleanse the site and the back of the gage of fatty acids, and a second swab of water will follow to prevent dehydration or unnecessary exposure. A suture will be advanced behind the posterior surface of the tibia to support the bone during gage placement, taking care to minimize damage to surrounding musculature. Cyanoacrylate adhesive and steady pressure will be used to secure the sensor in place. The site will be wrapped in Tegaderm "second skin" and gauze to prevent infection (Judex, Gross & Zernicke, 1997). Lead wires will be tunneled under the loose skin of the back with the aid of a removable sterile plastic tube, and exteriorized out of reach of chewing by the animals. The small inlet and outlet incisions will be closed with cyanoacrylate adhesive. The procedure is expected to take less than 30 minutes, and as evidenced in the Judex lab and our own, animals should be fully ambulatory within 1-4 h. Data will be collected within 48 hours of surgery, followed by euthanasia via carbon dioxide immersion.

Animal Species to be Used

Animal species and number of animals to have surgical procedure before the next annual or three-year protocol renewal:

BALB/cByJ mice – approximately 23 in the next year

Rationale for Multiple Survival Surgeries

If more than one survival surgical procedure is proposed, PHS Policy and the "Guide" require investigators to provide scientific justification to the CAC. Considerations that multiple survival procedures would reduce the number of animals used or reduce costs are not sufficient justification. Provide scientific rationale for multiple survival surgical procedures on individual animals.

Personnel

If survival surgery, these names must match survival surgery column in Section 6

Name of surgeon:	Lab and home phone numbers:
Erika Wagner	X-4-0529, 617.251.6714
Nicholas Granzella	X8-5794,

Name of anesthetist if different:	Lab and home phone numbers:

Personnel responsible for postoperative care if different:	Lab and home phone numbers:

Room address (if investigator's lab) or name of DCM facility and room where surgery will be performed:

68S procedure room

Anesthesia

Premedication (include doses in mg/kg, volume of injection(s), and route of administration):

pre-surgical buprenorphine analgesia (0.1 mg/kg subcutaneous)

Anesthesia drug and starting dose. For injectables, provide dose in mg/kg, volume of injection(s), and route of administration. For isoflurane, indicate if a vaporizer or bell jar will be used and scavenging method.

Inhalational isoflurane via chamber at 1-4% to effect (Hrapkiewicz et al., 1998)

How will depth of anesthesia be monitored?

Anesthesia will be monitored with testing of rear foot reflexes before surgery, and observation of respiratory patterns and responsiveness to manipulations throughout the procedure.

Verification of Aseptic Technique

It is required that Aseptic technique be used in all survival surgical procedures. All the aspects of aseptic technique listed below must be addressed. Give rationale if you wish to be exempt from any of these.

List or **bold all methods** used for instrument sterilization: Autoclave/ **ethylene oxide / glass bead sterilizer** / commercially supplied sterile instruments / other methods (describe in detail what other method(s) are used)

List or **bold all methods** used for implanted materials: Autoclave**/ ethylene oxide** / glass bead sterilizer / commercially supplied sterile materials / other methods (describe in detail what other method(s) are used)

List or **bold all methods** used for surgical site preparation: **Clipping hair with #40 blade / cleaning the skin to be incised with several cycles of povidine iodine or Betadine scrub or chlorhexidine scrub followed by alcohol rinse and application of Betadine solution or chlorhexidine solution** / other methods (describe in detail what other method(s) are used)

List or **bold all methods** used for maintaining the aseptic/sterile field*: **Sterile drapes / sterile gloves / face mask** / sterile surgical gown / surgeon's hat / other methods (describe in detail what other method(s) are used)

***Due to visibility problems related to small body size and relative risk of contamination, the use of drapes, gowns and hats may not be practical for some forms of rodent surgery. NIH Guidelines for Aseptic Surgery on Rodents are posted on the CAC website at https://web.mit.edu/comp-med/Restrict/CAC/overview.htm**

Postoperative Procedures, Analgesia Plan and Maintenance of Medical Records

Procedures known to cause postoperative pain in humans should be considered painful to animals. Analgesia should be routinely administered before anesthetic recovery and continued postoperatively based on the relative invasiveness of the procedure and evaluation of each animal for signs of pain. For example, a thoracotomy is considered sufficiently painful that analgesia should be given for several days irrespective of what appears to be a comfortable postoperative animal. If analgesia will interfere with your research objectives, you must provide scientific justification.

Note that the analgesia regimen (drug name, dose, route and timing of administration) from the perioperative period through the post-operative monitoring period (defined as when healing is complete – typically 7 to 14 days) must be performed on schedule as approved by the CAC unless veterinary consultation changes the treatment plan.

Selection of an analgesic should be based on species and the potential for postoperative pain based on the invasiveness of the surgery. Drugs of choice include buprenorphine, morphine, fentanyl (available as patch for larger species), carprofen and ketoprofen (injectable drugs with systemic effects) and lidocaine or bupivicaine (longer acting lidocaine) for regional analgesia such as for a thoracotomy. Consult the Laboratory Animal Users Handbook and the veterinarian for your animal colony for advice on drug selection, dosage, potential side effects, and duration of pre-emptive analgesia.

Rodents, birds, amphibians, reptiles and similar species should have DCM-issued white surgery cards posted on their cage with appropriate documentation to alert the veterinary staff to the date and type of surgery performed. These cage cards should also list ensuing postoperative monitoring entries as needed until healing is complete (7-14 days on average). DCM postoperative care forms for rabbits, ferrets, livestock, nonhuman primates, cats and dogs, including preemptive analgesia, must be completed at the time of surgery with monitoring forms kept in the animal room. Surgery cage cards or DCM-issued surgery forms must remain with the animal until sutures or wound clips are removed and postoperative complications have been resolved.

How often will animal be monitored and how will potential complications such as pain be treated during the first 24 hours? Describe how pain is monitored and preempted (or treated if observed) including drug name, dose in mg/kg, route and timing of administration (supply details even if described elsewhere in the protocol). Pre-emptive dosing with an analgesics during surgery prep is optimal to achieve blood levels before anesthesia wears off. Continued dosing should be based on assessment of each animal for signs of pain.

Pre-surgical buprenorphine will be given for analgesia (0.1 mg/kg subcutaneous). After gage implantation, animals will be monitored until anesthesia wears off and they are fully mobile

Follow-up will occur a minimum of twice daily for vocalizations, signs of limping or favoring the contralateral limb. Further buprenorphine will be provided up to three times daily, as necessitated.

During the second 24 hours:

Observation will occur a minimum of twice daily for vocalizations, signs of limping or favoring the contralateral limb. Further buprenorphine will be provided up to three times daily, as necessitated.

List any additional follow-up care until healing is judged complete including when you expect to remove skin sutures or wound clips:

Rationale for Multiple Survival Surgeries

If more than one survival surgical procedure is proposed, PHS Policy and the "Guide" require investigators to provide scientific justification to the CAC. Considerations that multiple survival procedures would reduce the number of animals used or reduce costs are not sufficient justification. Provide scientific rationale for multiple survival surgical procedures on individual animals.

If additional surgery beyond what is described above becomes necessary in the future for scientific reasons, submit the Addendum to Request Additional Major Survival Surgical Procedures, available on the CAC website under Forms.

Device Implantation

Animal Species to be Used

Animal species (indicate strain when appropriate):
BALB/cByJ mice

Description of implantation device:
Single-axis strain gauge, approximately 1mm x 2mm with waterproofed leadwires
(e.g. EA-06-015LA-120, Measurements Group, Inc., Basingstoke, UK)

What purpose does the implant serve?
Gathers data on the surface strain environment of the tibia and/or ulna for validation of partial weight-bearing system and correlation with tissue measurements

Site of implantation:
Anterio-medial aspect of the metaphyseal-diaphyseal tibia and/or medial ulnar midshaft

Procedure of implantation (also described in Supplement A):
Under aseptic conditions, the anterio-medial aspect of the metaphyseal-diaphyseal tibia and/or medial ulnar midshaft will be exposed with minimal musculoskeletal disruption. A scalpel blade and cotton swabs of minimal quantities (<0.5 ml) of chloroform, then water, will be used to prepare attachment fields on the periosteal surface of each bone. Cyanoacrylate adhesive will be used to secure the sensor in place. The site will be wrapped in gauze to prevent infection and lead wires will be will be secured with "second skin" to the posterior aspect of the limb (Judex, Gross & Zernicke, 1997). These leads will be tunneled under the loose skin on the animals hind-quarters and exteriorized near the nape of the neck, or further posteriorly as jackets will allow. Entrance and exit sites will be closed with application of cyanoacrylate adhesive to prevent movement of wires and minimize risk of infection. Post-surgical buprenorphine analgesia (0.1 mg/kg subcutaneous) will be provided up to three times daily as required. As evidenced in the Judex lab and our own, animals should be fully ambulatory within 1-4 h. All data will be collected within 48 hours of implantation, and animals will be sacrificed by CO2 immersion.

Procedure for removal of implant (also described in Supplement A):
N/A

How long will implant be maintained? If prolonged implantation is necessary, what methods will be used to avoid tissue infection, inflammation, erosion, or accidental removal of the implant?

Up to 48 hours. Site will be wrapped in gauze and secured with "second skin" coating. Lead wires will be secured to prevent accidental removal.

Monitoring for untoward effects consequent to implantation is necessary. Describe observational regimen and interventions including antibiotics, analgesics, and/or euthanasia (describe drugs, doses, methods).

Animals will be observed at least twice daily following implantation. Post-surgical buprenorphine analgesia (0.1 mg/kg subcutaneous) will be provided up to three times daily as required. All data will be collected within 48 hours of implantation, and animals will be sacrificed by CO2 immersion.

Appendix C

Partial Weight Suspension Habitat: Detailed Design

The detailed design in this appendix was developed in conjunction with Nicholas Granzella, Matt Theis, Travis Samuel, Viviana Serra, and Adam Yock. All measurements are given in English units for ordering and manufacturing convenience.

C.1 Habitat Structure

As described in Chapter 4, the walls of the PWS habitats were made from four 12" x 12" sheets of polycarbonate, 0.1875" thick. Two grooves designed to hold the 5"-wide aluminum support channel were cut into the upper edges of two sheets using a band saw, as shown in Figure C-1, and filed smooth. Using acrylic solvent, these two end sheets were joined with two side sheets to form a 12.1875" x 12.1875" open box (Figure 4-1).

Four L-brackets for mounting water bottle brackets were installed on one of the grooved walls, using four 0.1875" holes (Figure C-1). An additional 0.5" hole was drilled lower on the wall to accommodate the nozzle of the water bottle. Support of the water bottle via the L-brackets was accomplished with two 9" lengths of wire.

The configuration of the walls created a square area 11.8125" on a side within the cage. PVC perforated sheet was cut to fit with a band saw, and the edges were

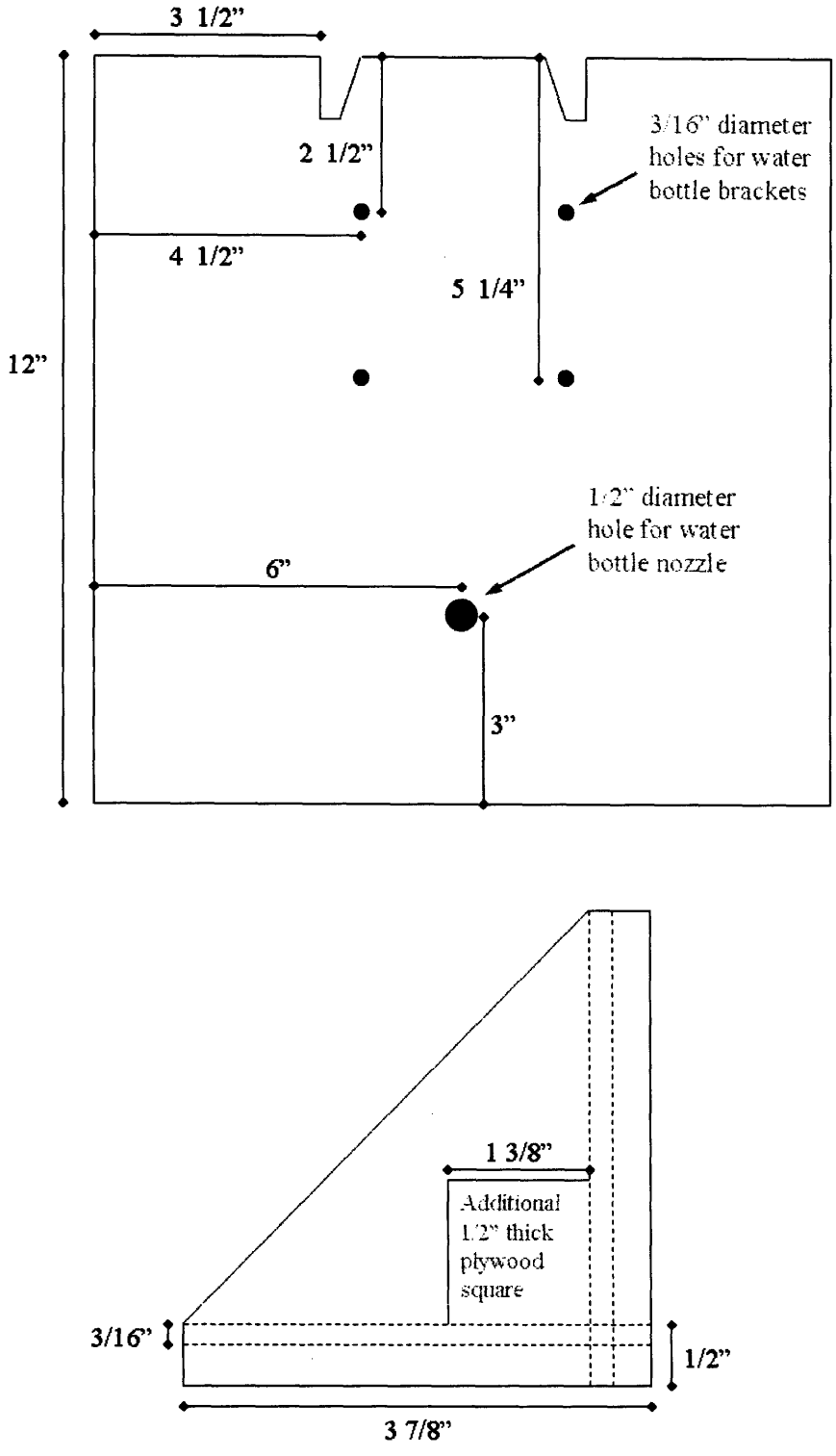

Figure C-1: Schematic of PWS habitat wall and feet. Not drawn to relative scale.

sanded smooth. Four feet were cut from 0.5" plywood to support the floor of each cage (Figure C-1). Two grooves 0.1875" wide were cut for the polycarbonate walls using a table saw set to 0.25" depth.

The lids of the cages were made from perforated PVC sheet 12.1875" long and roughly 3.594" wide, attached to the polycarbonate walls with 2" wide plastic hinges.

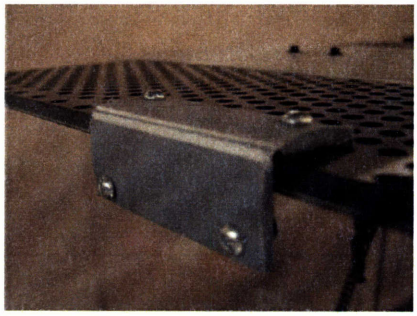

Figure C-2: A flexible plastic hinge between the PVC ceiling and polycarbonate wall allowed for easy installation and cleaning.

C.2 Aluminum Support Channel

Across the top of each cage was a 15" long U-shaped aluminum channel, from which the transit rod and associated hardware were supported. Two 0.125" wide slots, 2.75" long, were milled along the center of this channel to allow for flexible mounting of the hardware underneath. Through holes were drilled were drilled as needed for wires, breadboards, and cable ties for the flexure system, briefly described in Section 4.2.2.

Two 1" x 1" x 1.5" aluminum blocks (Figure C-3, A) were milled to provide a stable support for one end of the flexure/transit rod system. Two 4-40 screws ran through the adjustment slots in the aluminum support channel to hold these in place.

Two 1" x 0.75" x 0.125" plates (Figure C-3, B) were milled to clamp the flexure to these larger blocks, once again using 4-40 screws.

On the other end of the flexures, another plate (Figure C-3, B) clamped to a T-shaped fixure (Figure C-3, C), supporting both the flexure and transit rod (Figure C-4). A 4-40 set screw held the 0.125" diameter steel rod firmly in place. Of the 4.5"

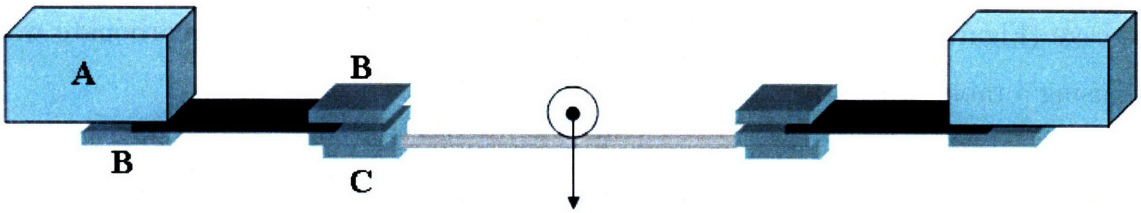

Figure C-3: Schematic of transit rod and fixtures. Large blocks (A) provide a stable point of attachment. Small plates (B) clamp the flexure in place. T-shaped fixtures (C) hold both the flexure and the transit rod.

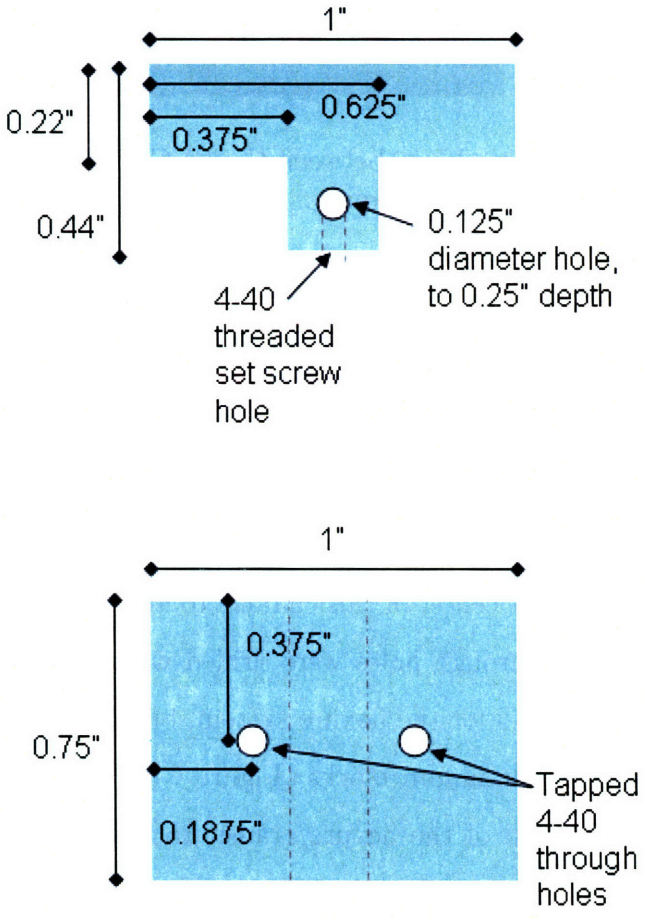

Figure C-4: T-shaped aluminum fixture for flexure and transit rod (Figure C-3, part C).

long rod, approximately 0.25" was held in each T-shaped fixure, leaving a remaining span of approximately 4".

Note: for applications without the flexures, this system could be simplified greatly to hold the transit rod in a fixed position. Stops may be necessary to prevent the animals from rearing up and bearing weight against the end walls.

C.3 Suspension Hardware

A wheel was machined from a 0.75" nylon rod to provide low-friction motion along the transit rod. After the outer radius was reduced to 0.6120", a central hole was drilled using a 0.234" bit followed by a 0.25" ream. A V-shaped groove was then cut along the edge of the wheel to a depth of 0.125". Bearings were press fit into the nylon wheels. Steel rod 0.125" in diameter and 0.5" in length was sanded on a lathe to an appropriate slip-fit with the bearing.

The suspension tether consisted of an integrated system of bead chain, splicing links, fishing swivels, hooks, a hollow spacer rod, and a plastic-coated low-modulus spring (k$\approx$ 1.6 N/m), assembled as shown in Figure C-5.

The forelimb jackets were made primarily from moleskin, athletic tape, and velcro (Figure C-5). Fabrication steps were as follows:

1. Remove a length of athletic tape from the roll, 5" per jacket. Fold the piece in half so that the adhesive sides adhere to one another.

2. Using the dimensions in Figure C-5, cut a 0.625" x 2.125" rectangle out of the athletic tape.

3. Cut out a 0.625" x 1.625" rectangle from the moleskin. Remove the smooth backing and place the adhesive side down onto the athletic tape rectangle, leaving 0.25" of athletic tape on each side for the soft velcro strips.

4. Cut two 0.25" pieces of soft velcro ("loop" side). Remove backings and place them on the exposed ends of the athletic tape (moleskin and velcro should be on the same side).

5. Using the left side of Figure C-5 as a template, trace and cut out the jacket. Take care to remove all rough edges and any threads left by the cutting.

6. Similarly, trace and cut pieces of moleskin and rough velcro ("hook" side) for the tab on the right of Figure C-5. Remove the backings of both the moleskin and velcro, and adhere.

7. Using a stiff needle and thread, attach a metal eye hook to the center of the tab created in step 6. Make several strong stitches.

When putting the mice into suspension, care was taken to keep the jacket and tail loop approximately level so that the weight of the mouse was distributed evenly between fore- and hindlimbs. In order to prevent the mice from climbing up the harnesses, small plastic lids from mailing tubes (3.125" diameter) were integrated into the harness assembly below the spring, as seen in Figure 4-2.

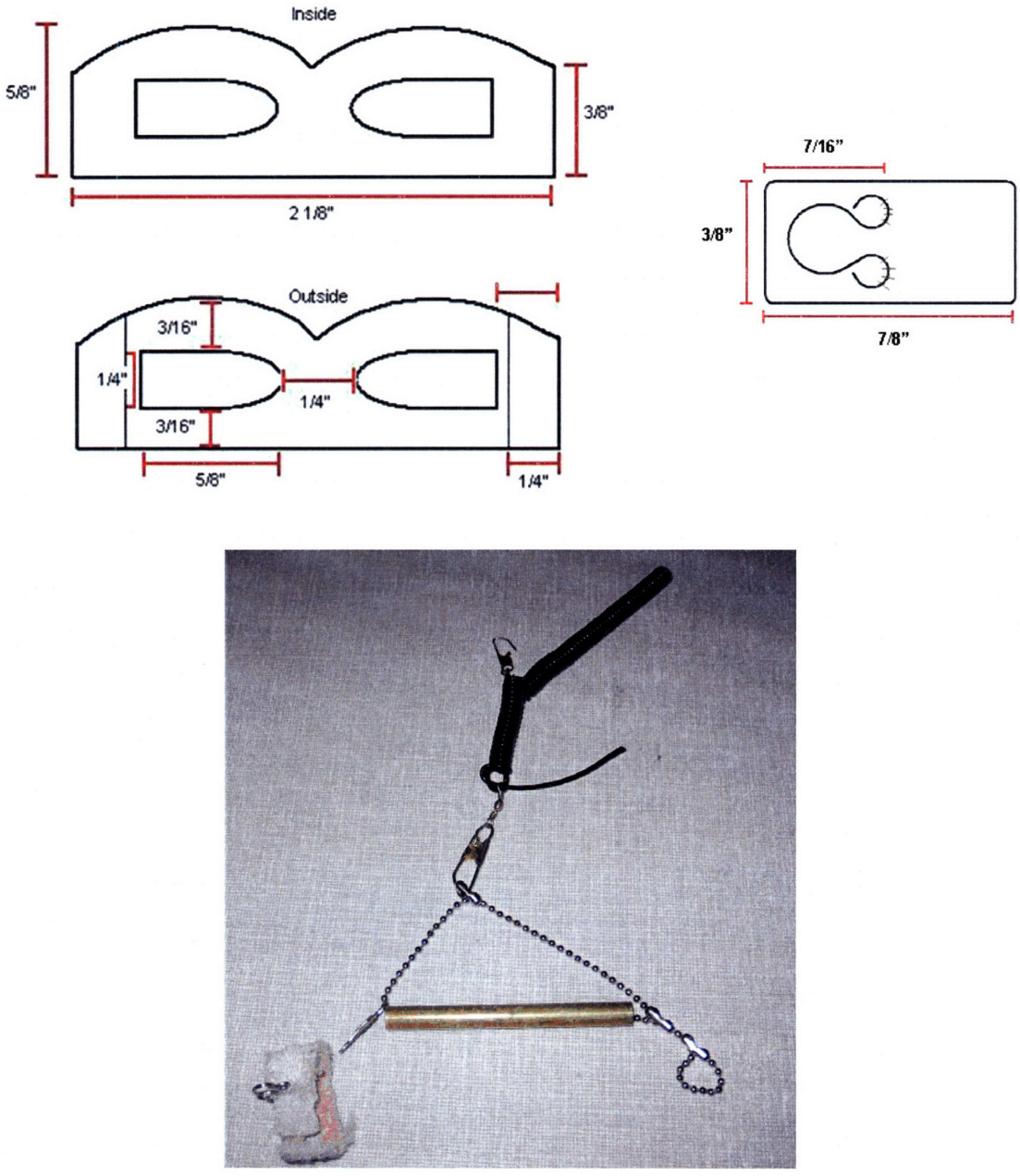

Figure C-5: Schematic for custom jackets, and photograph of suspension tether with integrated spacer rod, hooks, and swivels. The forelimb jacket was attached to the bead chain via a front latching hook. Athletic tape was wrapped through the rear bead chain loop and around the base of the mouse's tail to support its hindquarters. Line tension was adjusted by engaging variable lengths of the suspension spring.

Appendix D

Study Populations

Due to logistical constraints, the musculoskeletal study effort was conducted in a series of five three-week experiments, as outlined in the table below. Numbers of indicate those that completed a study of those that began it to give a sense for attrition rates:

Month	SUSP	JACK	AGE	BASE	NOTES
OCT	M, n=5	M, n=3 of 4	A, n=7		
NOV	M, n=4 of 5	M, n=2 of 4	A, n=3 of 4		Baseline serum collection led to eye infections and high losses
JAN	L, n=5	L, n=4	A, n=5	B, n=8	
FEB	L, n=3 of 5	L, n=3	A, n=5		
APR		M, n=3 of 5 L, n=4			Extra JACKET animals to accommodate earlier losses

Appendix E

MATLAB Code

The following MATLAB code was adapted from John Muller at the Beth Israel Deaconess Orthopedic Biomechanics Lab.

E.1 correct_lvdt

```
function correct_lvdt

% CORRECT_LVDT v0.4
% Copyright (C) 2004-2006  John A. Muller
% Email:  john.muller@alum.rpi.edu
%
% This program is free software; you can redistribute it and/or modify
% it under the terms of the GNU General Public License as published by
% the Free Software Foundation; either version 2 of the License, or
% any later version.
%
% This program is distributed in the hope that it will be useful,
% but WITHOUT ANY WARRANTY; without even the implied warranty of
% MERCHANTABILITY or FITNESS FOR A PARTICULAR PURPOSE.  See the
% GNU General Public License for more details.
%
% The full text of the GNU General Public License is included in the
% program folder as file "license.txt"
```

```
%
% You should have received a copy of the GNU General Public License along
% with this program; if not, write to the Free Software Foundation, Inc.,
% 51 Franklin Street, Fifth Floor, Boston, MA 02110-1301 USA.

sample_conf = struct([]);
sample_conf(1).source_pathname = pwd;
[filename, sample_conf] = jam_getfiles(sample_conf);

for j = 1:length(filename)
    rawfile = fullfile(sample_conf(1).source_pathname,filename{j});
    newfilename = [filename{j}(1:end-4),'_corrected',filename{j}(end-3:end)];
    newfile = fullfile(sample_conf(1).dest_pathname,newfilename);
    f = importdata(rawfile);

    fidin = fopen(rawfile);
    fidout = fopen(newfile,'a+');
    for k = 1 : 7
        header{k} = fgets(fidin);
    end
    for i = 1 : 7
        fprintf(fidout,'%s',header{i});
    end
    fclose(fidin);
    fclose(fidout);

    [m,n] = size(f.data);
    offset_time = 0 - f.data(1,1);
    f.data(:,1) = f.data(:,1) + offset_time;
    offset = 0 - f.data(1,2);
    f.data(:,2) = f.data(:,2) + offset;
    offset2 = 0 - f.data(1,3);
    f.data(:,3) = f.data(:,3) + offset2;

    figure(j);
    hold on;
```

```
    plot(f.data(:,2),f.data(:,3),'b');
    [dataset] = jam_correct_displacement(sample_conf, f)
    dlmwrite(newfile,dataset(1).data,'delimiter',',','newline','pc','precision',
    '%.4f','-append');
    plot(dataset(1).data(:,2),dataset(1).data(:,3),'g');
    title(filename{j});
    hold off;
    orient landscape;
    pause; close(j);
    clear f m n offset newfile dataset
end

function [filename, sample_conf] = jam_getfiles(sample_conf)
[filename, sample_conf(1).source_pathname, filterindex] = uigetfile({'*.*',...
  'All Files (*.*)'}, 'Choose Files To Smooth','MultiSelect', 'on');
if isequal(filename,0) || isequal(sample_conf(1).source_pathname,0), disp('User
   pressed cancel'), return,
else disp(['Source Directory: ', sample_conf(1).source_pathname]), end

sample_conf(1).dest_pathname = uigetdir(sample_conf(1).source_pathname, 'Choose
  Output Directory');
if isequal(sample_conf(1).dest_pathname,0), disp('User Failed To Choose
Destination Directory'), return
else disp(['Output Directory: ', sample_conf(1).dest_pathname]), end

function [dataset] = jam_correct_displacement(sample_conf, dataset)
d = dataset(1).data(:,2);
t = dataset(1).data(:,1);
rate = ((d(end-100) - d(100))/(t(end-100) - t(100)));
dataset(1).data(:,2) = ((t*rate));
```

E.2 vert_comp_0_main

```
function vert_comp_0_main(bonetype)

%
```

```
% vert_comp_0_main(bonetype)
%
%   VERT_COMP_0_MAIN Backbone script for general mechanical test analysis.
%       VERT_COMP_0_MAIN(bonetype) runs a generic vertebral compression or
%       femur three-point-bend analysis on user-specified data sets.
%
%       The script will prompt for data sets, which must be comma-separated
%       values, with columns 1-3 being time, displacement, and force in
%       that order.  Data is plotted for the user, who is asked to choose
%       three points, in this order:
%
%           (1) linear region lower bound
%           (2) linear region upper bound
%           (3) failure point
%
%       The script then asks the user for a filename to save interim
%       workspace variables.  The script then analyzes the data, creates
%       new figures with salient points onboard, prints them to PDF (in the
%       output directory previously chosen) and saves data to an
%       excel-style spreadsheet.
%
%       Bonetype should be either 'vert' or 'femur'.
%
%

%       Mechanical Analysis v1.0
%       Copyright (C) 2004-2007  John A. Muller
%       Email:  john.muller@alum.rpi.edu
%
%   vert_comp_0_main and mechanical_analysis v0.2 Copyright 2004-2007 John A.
% Muller


tic;
sample_conf = struct([]); dataset = struct([]);
close all;
```

```
sample_conf(1).num_header_lines = 8;
sample_conf(1).first_data_point = 1;
sample_conf(1).smoothing_factor = 1;        % ignore this - EBW Apr07
sample_conf(1).begin_point = 1;
sample_conf(1).offset_yield_factor = 0.002; % 0.002 = 0.2% offset

sample_conf(1).slope_yield_factor = 0.95;
% 0.95 = secant line at 95% of original stiffness, rotated about x-intercept

sample_conf(1).support_span = 6.00; % 9 mm outside span - 3 mm rod diameter


[filename, sample_conf] = vert_comp_1_getfiles(sample_conf);

if iscell(filename) && exist(sample_conf(1).dest_pathname)
    for i = 1 : length(filename)
        full_filename = fullfile(sample_conf(1).source_pathname,...
         filename{i});
        [dataset] = vert_comp_2_getdata(full_filename, sample_conf,...
         dataset, i);
        [dataset] = vert_comp_35_choose_range(sample_conf, dataset, i);
        destname = strcat(filename{i}(1:end-3),'pdf');
        full_dest_filename = fullfile(sample_conf(1).dest_pathname,
         destname);

    end
    sample_conf =  vert_comp_37_save_file(sample_conf, dataset); clear i

    switch bonetype
        case 'vert'
            for i = 1 : length(dataset)
                [dataset] = vert_comp_4_modulus_yield_b(sample_conf,...
                 dataset, i);
                destname = strcat(filename{i}(1:end-3),'pdf');
                full_dest_filename =
                 fullfile(sample_conf(1).dest_pathname,...
```

```
                destname);
                vert_comp_5_plot(sample_conf, dataset, i, ...
                 full_dest_filename);
            end
            sample_conf =  vert_comp_37_save_file(sample_conf, dataset); clear i
            vert_comp_6_write_output(sample_conf, dataset)
        case 'femur'
            for i = 1 : length(dataset)
                [dataset] = femur_bend_4_moment(sample_conf, dataset, i);
                destname = strcat(filename{i}(1:end-3),'pdf');
                full_dest_filename =
                 fullfile(sample_conf(1).dest_pathname, destname);
                femur_bend_5_plot_force(sample_conf, dataset, i,...
                 full_dest_filename);
            end
            sample_conf =  vert_comp_37_save_file(sample_conf, dataset); clear i
            femur_bend_6_write_output(sample_conf, dataset)
    end
end

toc;
```

E.3 vert_comp_1_getfiles

```
function [filename, sample_conf] = vert_comp_1_getfiles(sample_conf)

[filename, sample_conf(1).source_pathname, filterindex] = uigetfile({'*.*',...
  'All Files (*.*)'}, 'Choose Files To Analyze','MultiSelect', 'on');
if isequal(filename,0) || isequal(sample_conf(1).source_pathname,0),...
 disp('User pressed cancel'), return,
else disp(['Source Directory: ', sample_conf(1).source_pathname]), end

sample_conf(1).dest_pathname = uigetdir(sample_conf(1).source_pathname,...
 'Choose Output Directory');
if isequal(sample_conf(1).dest_pathname,0), disp('User Failed To Choose
 Destination Directory'), return
```

```
else disp(['Output Directory: ', sample_conf(1).dest_pathname]), end
```

E.4 vert_comp_2_getdata

```
function [dataset] = vert_comp_2_getdata(filename, sample_conf, dataset, i);

[header] = textread(filename,'%q',11,'delimiter',',','headerlines',1,'endofline',...
'\r\n');
[temp_data] = textread(filename,'','delimiter',',','headerlines',...
sample_conf(1).num_header_lines,'endofline','\r\n');
dataset(i).sample_name = header{8};
dataset(i).time = (temp_data(sample_conf(1).first_data_point:end,1));
dataset(i).displacement = (temp_data(sample_conf(1).first_data_point:end,2));
dataset(i).force = (temp_data(sample_conf(1).first_data_point:end,3));
```

E.5 vert_comp_3_smoothdata

```
function [dataset] = vert_comp_3_smoothdata(sample_conf, dataset,i)

f = dataset(i).force;
d = dataset(i).displacement;
s = sample_conf(1).smoothing_factor;

for j = sample_conf(1).smoothing_factor:min(length(f), length(d));
    dataset(i).force(j) = sum(f(j-s+1:j))/s;
    dataset(i).displacement(j) = sum(d(j-s+1:j))/s;
end
```

E.6 femur_bend_4_moment

```
function [dataset] = femur_bend_4_moment(sample_conf, dataset, i)

dataset(i).moment = ((dataset(i).force)*((sample_conf(1).support_span)/4));

tempdata_x =
```

```
(dataset(i).displacement(dataset(i).linear_range_low_index:dataset(i)
.linear_range_high_index));
tempdata_y =
(dataset(i).moment(dataset(i).linear_range_low_index:
dataset(i).linear_range_high_index));
[p,s] = polyfit(tempdata_x, tempdata_y, 1); m = p(1); b = p(2);
dataset(i).x_intercept = (-b/m);

dataset(i).stiffness = m;       % N
dataset(i).offset_y_intercept = b;
dataset(i).slope_y_intercept = -(sample_conf(1).slope_yield_factor * m *
dataset(i).x_intercept);

% For force-displacement alternative
tempdata2_x =
(dataset(i).displacement(dataset(i).linear_range_low_index:dataset(i)
.linear_range_high_index));
tempdata2_y =
(dataset(i).force(dataset(i).linear_range_low_index:
dataset(i).linear_range_high_index));
[p2,s2] = polyfit(tempdata2_x, tempdata2_y, 1); m2 = p2(1); b2 = p2(2);
dataset(i).x_intercept2 = (-b2/m2);
dataset(i).Fd_stiffness = m2       % N/mm
dataset(i).bending_rigidity = m2*(sample_conf(1).support_span)^3/48;


k = dataset(i).linear_range_high_index;
dataset(i).offset_y = 0;
while dataset(i).moment(k) > dataset(i).offset_y && k <
length(dataset(i).displacement) && k < (dataset(i).failure_point_index)
    k = k + 1;
    dataset(i).offset_y = ((m * dataset(i).displacement(k)) - (-b*(1 +
    sample_conf(1).offset_yield_factor)));
end
dataset(i).offset_yield_point_index = k;
```

```
j = dataset(i).linear_range_high_index;
dataset(i).slope_y = 0;
while dataset(i).moment(j) > dataset(i).slope_y && j <
length(dataset(i).displacement) && j < (dataset(i).failure_point_index)
    j = j + 1;
    dataset(i).slope_y = (((sample_conf(1).slope_yield_factor * m) *
    (dataset(i).displacement(j))) + (dataset(i).slope_y_intercept));
end
dataset(i).slope_yield_point_index = j;

dataset(i).displacement_offset_yield = dataset(i).displacement(k);
dataset(i).moment_offset_yield = dataset(i).moment(k);

dataset(i).displacement_slope_yield = dataset(i).displacement(j);
dataset(i).moment_slope_yield = dataset(i).moment(j);

[dataset(i).moment_ultimate, dataset(i).ultimate_index] =
max(dataset(i).moment);      % Determine ultimate moment
dataset(i).displacement_ultimate =
dataset(i).displacement(dataset(i).ultimate_index);
% Determine displacement that corresponds to ultimate moment

dataset(i).moment_to_offset_yield =
dataset(i).moment(1:dataset(i).offset_yield_point_index);
dataset(i).displacement_to_offset_yield =
dataset(i).displacement(1:dataset(i).offset_yield_point_index);

dataset(i).moment_to_slope_yield =
dataset(i).moment(1:dataset(i).slope_yield_point_index);
dataset(i).displacement_to_slope_yield =
dataset(i).displacement(1:dataset(i).slope_yield_point_index);

dataset(i).moment_to_failure =
dataset(i).moment(1:dataset(i).failure_point_index);
dataset(i).displacement_to_failure =
dataset(i).displacement(1:dataset(i).failure_point_index);
```

```
dataset(i).post_offset_yield_displacement =
dataset(i).displacement_to_failure(end) -
dataset(i).displacement_to_offset_yield(end);
dataset(i).post_slope_yield_displacement =
dataset(i).displacement_to_failure(end) -
dataset(i).displacement_to_slope_yield(end);

dataset(i).strain_energy_to_offset_yield =
trapz(dataset(i).displacement_to_offset_yield,
dataset(i).moment_to_offset_yield);
dataset(i).strain_energy_to_slope_yield =
trapz(dataset(i).displacement_to_slope_yield,
dataset(i).moment_to_slope_yield);
dataset(i).strain_energy_to_failure =
trapz(dataset(i).displacement_to_failure,
dataset(i).moment_to_failure);
dataset(i).post_offset_yield_energy = dataset(i).strain_energy_to_failure -
dataset(i).strain_energy_to_offset_yield;
dataset(i).post_slope_yield_energy = dataset(i).strain_energy_to_failure -
dataset(i).strain_energy_to_slope_yield;
```

E.7 femur_bend_5_plot

```
function femur_bend_5_plot(sample_conf, dataset, i, full_dest_filename)

figure(10*i + 4);
set(gcf,'position',[260 260 1120 840]); hold on; box on; grid on;

plot(dataset(i).displacement(1:end), dataset(i).force(1:end), 'b-',...
'linewidth', 1); v = axis; v(1) = 0 ; v(3) = 0;


line_1_y = [0 0.99*v(4)]; line_1_x = ((line_1_y - dataset(i).offset_y_intercept)
/ (dataset(i).stiffness));
```

```
line_2_y = line_1_y; line_2_x = ((line_2_y - dataset(i).slope_y_intercept)
/ ((sample_conf(1).slope_yield_factor) * (dataset(i).stiffness)));
text(1.005*dataset(i).displacement_slope_yield,dataset(i)
.moment_slope_yield,...
 ([' \leftarrow Yield (', num2str(sample_conf(1).slope_yield_factor),...
  ' Slope Method)']),'background', 'none', 'fontsize', 12);
text(0.985*dataset(i).displacement(dataset(i).linear_range_low_index),...
dataset(i).moment(dataset(i).linear_range_low_index), ...
    (['Linear Section Lower Bound \rightarrow ']),'background', 'none',...
     'fontsize', 6, 'horizontalalignment', 'right');
text(0.985*dataset(i).displacement(dataset(i).linear_range_high_index),...
dataset(i).moment(dataset(i).linear_range_high_index), ...
    (['Linear Section Upper Bound \rightarrow ']),'background', 'none',...
    'fontsize', 6, 'horizontalalignment', 'right');
text(1.005*dataset(i).displacement(dataset(i).failure_point_index),...
dataset(i).moment(dataset(i).failure_point_index), ...
    ([' \leftarrow Failure Point']),'background', 'none', 'fontsize', 12);
text(1.005*line_2_x(2),0.995*line_2_y(2), (['\leftarrow 0.95 Secant
Stiffness']),'background', 'none', 'fontsize', 12);
line(line_2_x, line_2_y, 'color', 'black');

plot(dataset(i).displacement_slope_yield,...
 dataset(i).moment_slope_yield,'ro','markersize', 3, 'linewidth', 0.5);
plot(dataset(i).displacement(dataset(i).failure_point_index),...
dataset(i).moment(dataset(i).failure_point_index),'r*','markersize',...
5, linewidth', 0.5);


title(strcat(['Force vs. Crosshead Displacement -- ', dataset(i).sample_name]),
'fontweight', 'bold','interpreter','none');
ylabel('Force (N)', 'fontweight', 'bold');

xlabel('Crosshead Displacement (mm)', 'fontweight', 'bold');
num2str(dataset(i).post_slope_yield_displacement), ' mm'])};

axis(v);
```

```
orient landscape;
hold off;
pause;
print(gcf, '-dpdf', full_dest_filename); close;
close;
```

E.8 femur_bend_6_write_output

```
function femur_bend_6_write_output(sample_conf, output)

%WRITE_OUTPUT
%     WRITE_OUTPUT(OUTPUT) takes the cell structure OUTPUT and writes it
%  to an Excel worksheet.
%
%     Cells can be text or numerical information.
%

% WRITE_OUTPUT v0.2
% This function written by John Muller
% Orthopaedic Biomechanics Laboratory
% Beth Israel Deaconess Medical Center
% A Teaching Hospital Of Harvard Medical School
% Boston, MA, USA
% Copyright 2005
% Modified by Erika Wagner, MIT, 2007

warning off MATLAB:xlswrite:AddSheet
filename = strcat(['output_',datestr(now,30),'.xls']);
out_file = fullfile(sample_conf(1).dest_pathname, filename);
for i = 1 : length(output)
    out(i,1) = {output(i).sample_name};
    out(i,2) = {output(i).moment_offset_yield};
    out(i,3) = {output(i).displacement_offset_yield};
    out(i,4) = {output(i).moment_slope_yield};
    out(i,5) = {output(i).displacement_slope_yield};
    out(i,6) = {output(i).Fd_stiffness};
```

```
    out(i,7) = {output(i).bending_rigidity};
    out(i,8) = {output(i).moment_ultimate};
    out(i,9) = {output(i).displacement_ultimate};
    out(i,10) = {output(i).strain_energy_to_failure};
    out(i,11) = {output(i).post_offset_yield_displacement};
    out(i,12) = {output(i).post_offset_yield_energy};
    out(i,13) = {output(i).post_slope_yield_displacement};
    out(i,14) = {output(i).post_slope_yield_energy};
end
header_row = {'Specimen', 'Moment at Yield (Offset Method) [N*mm]',...
'Displacement at Yield (Offset Method) [mm]', 'Moment at Yield (Slope
Method)  [N*mm]','Displacement at Yield (Slope Method) [mm]',
'Stiffness [N/mm]',...
'Bending Rigidity [N*mm^2]', 'Ultimate Moment [N*mm]', 'Crosshead
Displacement At Failure [mm]', ...
    'Bending Energy To Failure [N*mm^2]', 'Post-Yield Crosshead Displacement
    (Offset Method) [mm]', 'Post-Yield Bending Energy (Offset Method)
    [N*mm^2]', 'Post-Yield Crosshead Displacement (Slope Method) [mm]',
    'Post-Yield Bending Energy (Slope Method) [N*mm^2]'};
xlswrite(out_file, header_row, 'Sheet1', 'A1');
xlswrite(out_file, out, 'Sheet1', 'A2');

confirmation = (['Output written in Excel workbook ',out_file]);
disp(confirmation);
```

E.9 Force plate output filter and analysis

```
%Acquisition freq in Hz
acqfreq=200

XAMTI=data(:,1);
YAMTI=data(:,2);
ZAMTI=data(:,3);
specgram(XAMTI,[],acqfreq);
specgram(YAMTI,[],acqfreq);
specgram(ZAMTI,[],acqfreq);
```

```
%2nd   order filter, corner freq 25Hz
[b,a]=butter(2,25/(acqfreq/2));
filtXAMTI=filtfilt(b,a,XAMTI);
filtYAMTI=filtfilt(b,a,YAMTI);
filtZAMTI=filtfilt(b,a,ZAMTI);
specgram(filtXAMTI,[],200);
specgram(filtYAMTI,[],200);
specgram(filtZAMTI,[],200);

figure
plot(spectrum(XAMTI))
hold on
plot(spectrum(filtXAMTI),'r')
title('X Spectrum')

figure
plot(spectrum(YAMTI))
hold on
plot(spectrum(filtYAMTI),'r')
title('Y Spectrum')

figure
plot(spectrum(ZAMTI))
hold on
plot(spectrum(filtZAMTI),'r')
title('Z Spectrum')

Butterworth Filter
% Acquisition freq in Hz
acqfreq=200

RF1=data (:,1);
RF2=data (:,2);
RF3=data (:,3);
```

```
%2nd order filter, corner freq  25Hz
[b,a]=butter(2,(25/(acqfreq/2)));
filtRF1=filter(b,a,RF1);
filtRF2=filter(b,a,RF2);
filtRF3=filter(b,a,RF3);
```

Appendix F

Data by Group

Group means and standard deviations for all major variables are included below for reference. A complete data set is on file at the MIT Man-Vehicle Laboratory.

Variable names are given in accordance with the following convention:

Ct Cortical

Tb Trabecular

Vx Voxel-based calculation

TRI Triangularization-based calculation

DT Distance transformation-based calculation

BA Bone area

TA Total area

MA Medullary area

Thick, Th Thickness

TV Tissue volume

BV Bone volume

Thresh Threshhold

ConnD Connectivity density

SMI Structural model index

N Number

Sp Spacing

DA Degree of anisotropy

Mean1 Estimated voxel values of full volume of interest

Mean2 Estimated voxel values of bone volume

CM Center of mass

I Areal moment of inertia

pMOI Polar moment of inertia

Df Distal femoral metaphysis

Tib Proximal tibial metaphysis

IxxCy

Angle

H1 Shortest vector of the MIL tensor

H2 Intermediate vector of the MIL tensor

H3 Longest vector of the MIL tensor

O Osteoid

Ob Osteoblast

Oc Osteoclast

BS Bone surface

ES Eroded surface

MS Mineralizing surface

BFR Bone formation rate

MAR Mineral apposition rate

AP Anterior-posterior

Displ Displacement

BendEn Bending energy

Fail At failure

PostY Post-yield

Gastr Gastrocnemius mass

Norm Normalized to final body mass

Mass_n Full body mass on day n

Food_n Food usage on day n

		BASELINE		AGE		JACKET_M		MARS		JACKET_L		LUNAR	
Femoral Midshaft MicroCT	CtBA	0.866	(0.078)	0.901	(0.054)	0.869	(0.045)	0.786	(0.047)	0.855	(0.051)	0.830	(0.066)
	CtTA	1.549	(0.087)	1.560	(0.088)	1.553	(0.094)	1.462	(0.102)	1.538	(0.104)	1.510	(0.107)
	CtMA	0.683	(0.083)	0.659	(0.080)	0.684	(0.058)	0.676	(0.069)	0.683	(0.066)	0.680	(0.075)
	CtBA/TA	55.940	(4.479)	57.841	(3.512)	55.984	(1.562)	53.834	(2.194)	55.627	(1.962)	55.028	(3.112)
	CtMA/TA	44.060	(4.479)	42.159	(3.512)	44.016	(1.562)	46.166	(2.194)	44.373	(1.962)	44.972	(3.112)
	CtThick	223.750	(16.456)	238.300	(13.468)	230.750	(5.312)	212.444	(8.918)	225.818	(8.424)	216.875	(12.287)
	CtMean2	1231.196	(20.524)	1268.930	(14.504)	1261.885	(13.029)	1251.248	(11.991)	1269.430	(11.203)	1264.461	(15.421)
	CMx	0.740	(0.115)	0.733	(0.090)	0.724	(0.115)	0.730	(0.123)	0.692	(0.092)	0.706	(0.092)
	CMy	0.792	(0.083)	0.822	(0.078)	0.825	(0.088)	0.799	(0.115)	0.834	(0.105)	0.826	(0.085)
	Ixx	0.161	(0.036)	0.180	(0.033)	0.177	(0.039)	0.148	(0.046)	0.180	(0.043)	0.169	(0.037)
	Iyy	0.146	(0.043)	0.149	(0.035)	0.141	(0.036)	0.129	(0.038)	0.134	(0.028)	0.129	(0.028)
	Ixy	-0.038	(0.014)	-0.023	(0.037)	-0.019	(0.033)	-0.023	(0.017)	-0.031	(0.020)	0.001	(0.040)
	pMOI	0.307	(0.037)	0.329	(0.033)	0.319	(0.037)	0.276	(0.039)	0.313	(0.040)	0.298	(0.041)
	IxxCy	0.219	(0.029)	0.236	(0.024)	0.230	(0.029)	0.201	(0.036)	0.231	(0.033)	0.221	(0.030)
	IyyCx	0.204	(0.031)	0.215	(0.027)	0.205	(0.025)	0.187	(0.030)	0.199	(0.023)	0.192	(0.026)
	Imax	0.205	(0.027)	0.218	(0.022)	0.210	(0.027)	0.183	(0.030)	0.208	(0.028)	0.197	(0.029)
	Imin	0.102	(0.011)	0.111	(0.012)	0.109	(0.011)	0.093	(0.010)	0.105	(0.014)	0.101	(0.013)
	Angle	50.497	(21.828)	26.919	(54.384)	23.781	(60.368)	52.961	(31.671)	43.363	(47.466)	-8.851	(65.573)
	ImaxCmax	0.246	(0.024)	0.259	(0.019)	0.250	(0.021)	0.223	(0.025)	0.248	(0.023)	0.237	(0.025)
	IminCmin	0.174	(0.017)	0.189	(0.015)	0.183	(0.013)	0.160	(0.014)	0.178	(0.016)	0.170	(0.017)
	Area	0.849	(0.077)	0.901	(0.054)	0.869	(0.045)	0.786	(0.047)	0.855	(0.051)	0.830	(0.066)
Distal Femoral Metaphysis MicroCT	DfThresh	10172.143	(580.975)	10026.050	(375.847)	9415.000	(406.345)	8713.250	(532.936)	9122.900	(464.234)	8599.000	(440.854)
	DfCtThick	166.571	(9.658)	167.100	(8.062)	158.600	(7.470)	134.000	(6.459)				
	DfVxTV	1.625	(0.138)	1.812	(0.183)	1.991	(0.162)	1.971	(0.201)	1.966	(0.219)	2.060	(0.168)
	DfVxBV	0.382	(0.060)	0.343	(0.051)	0.360	(0.046)	0.283	(0.071)	0.354	(0.049)	0.340	(0.058)
	DfVxBV/TV	0.235	(0.030)	0.190	(0.026)	0.181	(0.016)	0.143	(0.032)	0.180	(0.019)	0.165	(0.025)
	DfConnD	207.118	(23.889)	137.349	(19.161)	145.838	(18.735)	124.288	(26.287)	143.331	(22.756)	143.332	(20.478)
	DfTRISMI	1.309	(0.300)	1.621	(0.265)	1.788	(0.222)	2.144	(0.404)	1.790	(0.222)	1.920	(0.341)
	DfDTTbN	5.236	(0.291)	4.468	(0.297)	4.473	(0.183)	4.375	(0.291)	4.461	(0.229)	4.499	(0.231)
	DfDTTbTh	0.055	(0.003)	0.054	(0.002)	0.053	(0.003)	0.048	(0.002)	0.052	(0.002)	0.049	(0.002)
	DfDTTbSp	0.183	(0.012)	0.218	(0.018)	0.217	(0.010)	0.222	(0.015)	0.218	(0.013)	0.213	(0.013)
	DfMean1	304.302	(41.672)	265.323	(29.454)	232.460	(28.542)	193.375	(36.473)	217.340	(29.037)	193.582	(26.973)
	DfMean2	930.365	(32.155)	948.055	(24.656)	908.737	(28.399)	873.478	(35.978)	888.108	(29.968)	854.459	(28.431)
	DfTRITV	1.588	(0.136)	1.773	(0.181)	1.950	(0.160)	1.931	(0.199)	1.926	(0.217)	2.019	(0.167)
	DfTRIBV	0.369	(0.061)	0.329	(0.052)	0.344	(0.046)	0.265	(0.071)	0.337	(0.049)	0.322	(0.059)
	DfTRIBV/TV	0.232	(0.031)	0.186	(0.027)	0.176	(0.017)	0.137	(0.033)	0.176	(0.020)	0.160	(0.026)
	DfTRIBS	15.829	(1.711)	14.558	(2.040)	15.733	(1.746)	13.630	(2.700)	15.431	(2.125)	15.861	(2.253)
	DfTRIBS/BV	43.253	(2.972)	44.405	(2.194)	45.954	(2.480)	52.269	(3.780)	45.846	(2.148)	49.639	(3.133)
	DfTRITbN	4.992	(0.398)	4.109	(0.442)	4.031	(0.266)	3.528	(0.574)	4.010	(0.355)	3.928	(0.450)
	DfTRITbTh	0.046	(0.003)	0.045	(0.002)	0.044	(0.002)	0.038	(0.003)	0.044	(0.002)	0.040	(0.002)
	DfTRITbSp	0.155	(0.019)	0.201	(0.030)	0.205	(0.017)	0.251	(0.047)	0.208	(0.025)	0.217	(0.034)
	DfTRIDA	1.627	(0.102)	1.527	(0.102)	1.486	(0.067)	1.450	(0.086)	1.501	(0.054)	1.472	(0.090)
	DfTRI|H1|	0.170	(0.016)	0.210	(0.027)	0.214	(0.015)	0.253	(0.043)	0.217	(0.021)	0.225	(0.030)
	DfTRI|H2|	0.275	(0.016)	0.319	(0.030)	0.318	(0.014)	0.364	(0.045)	0.326	(0.029)	0.329	(0.029)
	DfTRI|H3|	0.193	(0.017)	0.241	(0.030)	0.242	(0.019)	0.280	(0.045)	0.240	(0.024)	0.246	(0.035)
	DfTRIH1x	0.108	(0.038)	0.113	(0.113)	0.097	(0.138)	0.036	(0.149)	0.054	(0.127)	-0.008	(0.191)

		BASELINE		AGE		JACKET_M		MARS		JACKET_L		LUNAR	
Distal Femoral Metaphysis MicroCT	DfTRIH1y	-0.120	(0.043)	-0.104	(0.095)	-0.126	(0.068)	-0.157	(0.149)	-0.159	(0.072)	-0.060	(0.130)
	DfTRIH1z	-0.008	(0.013)	-0.002	(0.022)	-0.005	(0.021)	0.001	(0.034)	-0.006	(0.014)	-0.001	(0.031)
	DfTRIH2x	0.026	(0.027)	0.024	(0.039)	0.030	(0.021)	0.047	(0.026)	0.020	(0.018)	0.043	(0.037)
	DfTRIH2y	-0.005	(0.020)	-0.009	(0.048)	0.009	(0.029)	0.001	(0.033)	0.001	(0.027)	0.026	(0.037)
	DfTRIH2z	0.112	(0.268)	0.215	(0.234)	0.314	(0.014)	0.359	(0.046)	0.324	(0.029)	0.322	(0.027)
	DfTRIH3x	-0.043	(0.145)	-0.031	(0.160)	-0.079	(0.145)	-0.163	(0.177)	-0.115	(0.161)	-0.117	(0.097)
	DfTRIH3y	0.005	(0.141)	0.073	(0.166)	0.062	(0.184)	-0.087	(0.141)	-0.004	(0.154)	0.057	(0.200)
	DfTRIH3z	0.006	(0.025)	-0.006	(0.046)	0.007	(0.028)	0.014	(0.031)	0.001	(0.023)	0.002	(0.047)
	DfCMx	1.005	(0.136)	1.072	(0.094)	1.045	(0.077)	1.019	(0.176)				
	DfCMy	1.106	(0.114)	1.209	(0.157)	1.178	(0.103)	1.157	(0.098)				
	DfIxx	0.427	(0.091)	0.451	(0.084)	0.459	(0.086)	0.347	(0.104)				
	DfIyy	0.313	(0.067)	0.333	(0.096)	0.336	(0.081)	0.292	(0.093)				
	DfIxy	-0.103	(0.044)	-0.021	(0.107)	-0.096	(0.046)	-0.049	(0.039)				
	DfpMOI	0.741	(0.098)	0.784	(0.085)	0.795	(0.086)	0.639	(0.084)				
	DfIxxCy	0.401	(0.054)	0.416	(0.039)	0.411	(0.042)	0.322	(0.056)				
	DfIyyCx	0.347	(0.044)	0.354	(0.065)	0.354	(0.050)	0.293	(0.058)				
	DfImax	0.506	(0.075)	0.532	(0.062)	0.534	(0.059)	0.424	(0.065)				
	DfImin	0.235	(0.024)	0.252	(0.028)	0.261	(0.029)	0.214	(0.021)				
	DfAngle	58.676	(16.727)	29.661	(65.587)	61.307	(18.704)	33.665	(56.042)				
	DfImaxCmax	0.432	(0.048)	0.448	(0.039)	0.441	(0.036)	0.362	(0.036)				
	DfIminCmin	0.290	(0.023)	0.298	(0.027)	0.297	(0.025)	0.239	(0.021)				
	DfArea	1.130	(0.108)	1.142	(0.071)	1.099	(0.080)	0.920	(0.068)				
Proximal Tibial Metaphysis MicroCT	TibThresh	6600.429	(327.452)	6394.667	(463.595)	6266.200	(355.058)	5991.667	(305.258)				
	TibVxTV	1.951	(0.169)	1.989	(0.240)	2.101	(0.290)	2.201	(0.221)				
	TibVxBV	0.275	(0.029)	0.222	(0.048)	0.240	(0.033)	0.213	(0.030)				
	TibVxBVTV	0.142	(0.019)	0.112	(0.022)	0.116	(0.021)	0.098	(0.018)				
	TibConnD	119.958	(14.566)	70.463	(26.217)	83.706	(22.748)	59.308	(19.681)				
	TibTRISMI	2.278	(0.160)	2.591	(0.270)	2.579	(0.237)	2.692	(0.222)				
	TibDTTbN	4.446	(0.319)	3.932	(0.303)	4.109	(0.363)	4.008	(0.227)				
	TibDTTbTh	0.049	(0.001)	0.049	(0.002)	0.048	(0.002)	0.046	(0.002)				
	TibDTTbSp	0.230	(0.021)	0.258	(0.021)	0.245	(0.022)	0.250	(0.014)				
	TibMean1	198.184	(26.565)	162.912	(42.085)	151.335	(32.955)	138.424	(20.469)				
	TibMean2	850.167	(34.773)	851.192	(42.132)	855.337	(23.593)	807.432	(38.086)				
	TibTRITV	1.885	(0.170)	1.925	(0.236)	2.038	(0.288)	2.138	(0.219)				
	TibTRIBV	0.247	(0.027)	0.197	(0.045)	0.212	(0.032)	0.186	(0.029)				
	TibTRIBVTV	0.132	(0.018)	0.102	(0.021)	0.106	(0.021)	0.088	(0.018)				
	TibTRIBS	12.424	(1.341)	9.893	(1.795)	11.017	(1.420)	10.291	(1.226)				
	TibTRIBSBV	50.353	(2.103)	50.735	(3.000)	52.077	(2.423)	55.580	(4.170)				
	TibTRITbN	3.309	(0.360)	2.575	(0.427)	2.737	(0.443)	2.428	(0.363)				
	TibTRITbTh	0.040	(0.002)	0.040	(0.002)	0.038	(0.002)	0.036	(0.003)				
	TibTRITbSp	0.266	(0.040)	0.358	(0.063)	0.335	(0.064)	0.384	(0.063)				
	TibTRIDA	1.698	(0.083)	1.692	(0.092)	1.706	(0.081)	1.731	(0.094)				
	TibTRI|H1|	0.250	(0.037)	0.331	(0.056)	0.309	(0.050)	0.344	(0.049)				
	TibTRI|H2|	0.423	(0.046)	0.558	(0.083)	0.530	(0.110)	0.597	(0.097)				
	TibTRI|H3|	0.303	(0.035)	0.381	(0.055)	0.358	(0.057)	0.407	(0.061)				
	TibTRIH1x	-0.004	(0.020)	-0.008	(0.065)	0.001	(0.033)	-0.018	(0.054)				

		BASELINE		AGE		JACKET_M		MARS		JACKET_L		LUNAR	
Proximal Tibial Metaphysis MicroCT	TibTRIH1y	-0.008	(0.010)	-0.022	(0.020)	-0.017	(0.009)	-0.025	(0.031)				
	TibTRIH1z	0.249	(0.037)	0.324	(0.055)	0.307	(0.050)	0.337	(0.052)				
	TibTRIH2x	-0.011	(0.030)	-0.003	(0.034)	-0.021	(0.058)	-0.024	(0.058)				
	TibTRIH2y	-0.305	(0.316)	-0.554	(0.085)	-0.330	(0.471)	-0.455	(0.411)				
	TibTRIH2z	-0.005	(0.023)	-0.037	(0.034)	-0.008	(0.036)	-0.026	(0.059)				
	TibTRIH3x	-0.301	(0.035)	-0.374	(0.054)	-0.242	(0.295)	-0.400	(0.065)				
	TibTRIH3y	0.009	(0.020)	0.005	(0.021)	0.027	(0.030)	0.014	(0.036)				
	TibTRIH3z	-0.004	(0.023)	-0.011	(0.074)	0.000	(0.038)	-0.020	(0.066)				
Proximal Tibial Histology	BV/TV	13.695	(2.083)	7.627	(1.277)	6.028	(2.932)	5.414	(1.402)				
	TbTh	49.418	(4.334)	39.545	(4.742)	36.102	(9.588)	33.537	(3.361)				
	TbSp	316.808	(52.060)	484.679	(64.829)	621.277	(184.020)	610.570	(135.870)				
	TbN	2.771	(0.361)	1.930	(0.229)	1.621	(0.463)	1.604	(0.312)				
	MS/BS	18.585	(4.102)	17.722	(6.803)	10.624	(4.281)	11.186	(2.911)				
	BFR/BS	169.718	(62.127)	105.502	(88.159)	46.914	(44.547)	43.382	(16.693)				
	BFR/BV	731.545	(217.835)	441.212	(356.496)	200.540	(168.551)	263.087	(98.463)				
	BFR/TV	96.047	(28.454)	32.799	(20.350)	17.891	(20.993)	12.028	(3.819)				
	MAR	2.487	(0.567)	1.415	(0.635)	1.034	(0.580)	1.099	(0.227)				
	OS/BS	3.187	(1.599)	2.083	(0.287)	2.093	(0.580)	1.483	(0.424)				
	ObS/BS	24.166	(5.425)	12.922	(4.710)	9.842	(0.668)	10.762	(2.208)				
	ES/BS	1.099	(0.550)	0.952	(0.204)	1.125	(0.277)	0.950	(0.176)				
	OcS/BS	0.654	(0.305)	0.816	(0.082)	0.688	(0.235)	0.582	(0.186)				
	OTh	6.783	(1.038)	4.727	(0.595)	3.732	(0.522)	4.465	(1.474)				
	NOb/BS	14.711	(4.719)	7.289	(2.864)	5.428	(0.110)	5.995	(1.051)				
	NOc/BS	0.484	(0.207)	0.590	(0.073)	0.633	(0.114)	0.458	(0.172)				
Whole Femur Biomechanical Properties	Length	14.234	(0.459)	14.921	(0.305)	14.970	(0.277)	14.559	(0.448)	14.726	(0.435)	14.983	(0.504)
	AP Diameter	1.146	(0.034)	1.167	(0.038)	1.163	(0.026)	1.151	(0.062)	1.142	(0.038)	1.169	(0.039)
	YieldMoment	15.695	(5.557)	17.327	(4.501)	11.111	(4.391)	13.054	(1.210)	9.973	(5.741)	14.108	(3.735)
	YieldDispl	0.117	(0.031)	0.111	(0.034)	0.088	(0.027)	0.101	(0.015)	0.097	(0.034)	0.086	(0.021)
	Stiffness	125.855	(12.101)	136.053	(10.126)	113.759	(19.205)	114.697	(13.863)	116.957	(25.977)	129.892	(11.547)
	Bending Rigidity	566.346	(54.455)	612.236	(45.568)	511.914	(86.424)	516.137	(62.382)	526.305	(116.895)	584.516	(51.960)
	Young's Modulus	5611.947	(598.129)	5584.611	(580.812)	4641.472	(580.421)	5480.992	(702.874)	5024.281	(1086.889)	5870.174	(825.418)
	Ultimate Moment	26.103	(3.593)	29.099	(3.903)	22.938	(5.885)	21.202	(3.379)	22.493	(7.465)	24.666	(4.194)
	FailDispl	0.300	(0.050)	0.284	(0.035)	0.281	(0.048)	0.275	(0.036)	0.265	(0.049)	0.238	(0.031)
	FailBendEn	6.233	(1.898)	6.379	(1.701)	6.255	(1.943)	6.221	(2.240)	5.706	(2.605)	5.783	(1.515)
	PostYDispl	0.246	(0.115)	0.220	(0.067)	0.302	(0.086)	0.295	(0.101)	0.288	(0.100)	0.244	(0.082)
	PostYBendEn	5.453	(2.157)	5.512	(1.707)	5.813	(1.857)	5.673	(2.220)	5.348	(2.496)	5.195	(1.668)
Gastrocnemius Mass	Gastr_R	0.108	(0.009)	0.119	(0.007)	0.114	(0.006)	0.092	(0.011)	0.115	(0.009)	0.104	(0.013)
	Gastr_L	0.110	(0.006)	0.119	(0.005)	0.114	(0.012)	0.090	(0.009)	0.116	(0.007)	0.102	(0.013)
	GastrAvg	0.108	(0.007)	0.119	(0.006)	0.114	(0.009)	0.091	(0.009)	0.116	(0.007)	0.103	(0.012)
	GastrNorm	0.006	(0.000)	0.005	(0.000)	0.005	(0.000)	0.005	(0.000)	0.005	(0.000)	0.005	(0.001)
Daily Body Mass	Mass_0	19.929	(1.129)	20.700	(0.868)	21.075	(1.460)	20.378	(1.363)	20.400	(1.354)	20.538	(1.436)
	Mass_1			20.855	(1.062)	20.925	(1.227)	20.011	(1.230)	20.500	(1.554)	20.188	(1.331)
	Mass_2			20.900	(0.981)	20.825	(1.329)	19.756	(1.223)	20.209	(1.530)	20.088	(1.445)
	Mass_3			20.960	(1.086)	20.288	(1.440)	19.356	(1.149)	19.982	(1.249)	19.725	(1.296)
	Mass_4			21.145	(1.074)	20.438	(1.068)	19.311	(1.080)	19.282	(1.056)	19.375	(1.382)
	Mass_5			21.100	(1.077)	20.175	(0.942)	19.311	(0.971)	19.091	(0.922)	19.488	(1.429)

		BASELINE	AGE		JACKET_M		MARS		JACKET_L		LUNAR	
Daily Body Mass	Mass_6		21.130	(0.982)	20.550	(0.873)	19.033	(1.025)	18.564	(0.766)	19.225	(1.420)
	Mass_7		21.185	(0.939)	20.688	(1.097)	19.344	(1.028)	17.991	(1.074)	19.675	(1.276)
	Mass_8		21.240	(1.057)	20.913	(1.278)	19.389	(1.059)	18.800	(1.282)	19.575	(1.280)
	Mass_9		21.315	(1.084)	21.013	(1.255)	19.367	(1.048)	18.773	(1.193)	19.550	(1.086)
	Mass_10		21.350	(1.074)	20.938	(1.276)	19.289	(1.130)	19.355	(1.160)	19.888	(1.163)
	Mass_11		21.305	(1.101)	21.263	(1.392)	19.444	(1.123)	18.800	(1.381)	19.863	(1.201)
	Mass_12		21.395	(1.269)	21.600	(1.539)	19.400	(1.147)	19.509	(1.439)	20.038	(1.297)
	Mass_13		21.370	(1.327)	21.838	(1.802)	19.456	(1.265)	19.409	(1.744)	19.875	(1.234)
	Mass_14		21.515	(1.327)	22.038	(1.778)	19.356	(1.133)	20.136	(1.697)	20.000	(1.378)
	Mass_15		21.480	(1.253)	22.300	(1.757)	19.322	(1.183)	20.536	(1.500)	19.988	(1.494)
	Mass_16		21.490	(1.126)	22.400	(1.747)	19.533	(1.002)	20.300	(1.802)	19.963	(1.485)
	Mass_17		21.505	(1.109)	22.663	(1.737)	19.222	(1.133)	20.745	(1.334)	19.788	(1.366)
	Mass_18		21.760	(1.184)	22.800	(1.503)	19.289	(0.947)	21.118	(1.272)	19.725	(1.429)
	Mass_19		21.670	(1.029)	22.825	(1.422)	19.467	(0.953)	21.536	(1.491)	19.763	(1.416)
	Mass_20		21.590	(1.319)	22.813	(1.575)	19.644	(1.070)	21.764	(1.318)	19.463	(2.270)
	Mass_21		21.777	(1.102)	22.160	(1.146)	19.033	(0.643)	22.145	(1.473)	19.913	(1.720)
Daily Food Usage	Food_1				6.000	(0.962)	6.178	(0.873)	5.391	(0.470)	5.338	(1.193)
	Food_2				5.250	(0.053)	5.267	(0.292)	5.018	(0.366)	5.100	(1.090)
	Food_3				5.500	(0.000)	5.478	(0.665)	5.309	(1.044)	5.338	(1.461)
	Food_4				6.950	(1.122)	7.044	(1.295)	5.355	(0.522)	5.300	(1.235)
	Food_5				6.400	(0.214)	6.456	(0.629)	5.036	(0.731)	5.513	(0.794)
	Food_6				8.000	(0.855)	8.111	(1.412)	5.845	(0.627)	5.988	(1.079)
	Food_7				8.000	(0.748)	8.078	(1.052)	7.464	(0.992)	7.225	(1.241)
	Food_8				7.350	(0.481)	7.400	(0.853)	6.482	(0.209)	6.350	(0.481)
	Food_9				8.200	(0.748)	8.289	(1.054)	6.845	(0.627)	6.813	(1.469)
	Food_10				7.550	(0.909)	7.600	(1.195)	6.818	(0.366)	6.988	(0.846)
	Food_11				8.200	(0.748)	8.067	(1.277)	7.364	(0.992)	7.125	(1.131)
	Food_12				8.050	(0.802)	8.144	(1.395)	7.445	(0.627)	7.213	(0.970)
	Food_13				8.550	(0.695)	8.633	(1.012)	7.209	(1.044)	7.088	(1.156)
	Food_14				9.200	(0.748)	9.300	(1.357)	7.300	(0.574)	7.200	(1.263)
	Food_15				8.950	(0.481)	9.000	(1.298)	7.382	(0.783)	7.275	(1.217)
	Food_16				9.300	(0.107)	9.300	(0.950)	8.118	(0.366)	8.025	(1.127)
	Food_17				8.400	(1.390)	8.533	(1.697)	7.591	(0.104)	7.563	(1.391)
	Food_18				7.500	(0.748)	7.589	(1.589)	7.973	(1.462)	7.750	(1.865)
	Food_19				8.600	(0.748)	8.656	(1.094)	8.300	(1.149)	8.138	(1.432)
	Food_20				8.150	(2.085)	8.367	(2.615)	7.327	(1.410)	6.886	(1.670)